RECONSTRUCTION OF RECENT AND PALAEO SEA ICE CONDITIONS IN THE BARENTS SEA

by

Alba Navarro Rodríguez

A thesis submitted to Plymouth University in partial fulfilment of the degree of

DOCTOR OF PHILOSOPHY

Petroleum and Environmental Geochemistry Group

School of Geography, Earth and Environmental Sciences

Plymouth University

April 2014

Reconstruction of Recent and Palaeo Sea Ice Conditions in the Barents Sea

By
Alba Navarro-Rodríguez

ABSTRACT

IP_{25} is a highly branched isoprenoid alkene derived from certain Arctic sea ice diatoms that, when detected in marine sediments, has been used as a proxy for past Arctic sea ice over the last decade. In the current study, the structure of this biomarker was determined following large-scale extraction from sediment material collected from the Canadian Arctic. After purification, the structure of IP_{25} was confirmed by NMR spectroscopy as being the same as that of a laboratory standard. The purified IP_{25} was subsequently used to obtain a quantitative (GC-MS) instrumental response factor that could be used to improve the future quantification of IP_{25} and would help to produce a robust database.

IP_{25}, other highly branched isoprenoid (HBI) lipids and some other phytoplanktonic lipids (sterols) were analysed to provide modern and past sediment-based sea ice reconstructions for the Barents Sea. First, a surface sediment study was conducted and biomarker distributions were compared to satellite sea ice records. The occurrence of IP_{25} was consistent with the presence/absence of seasonal sea ice but there was also evidence of lateral transport of IP_{25} and other biomarkers in sediments from the southern Barents Sea. In contrast to some previous studies, abundances of IP_{25}, and of those combined with other biomarkers, including sterols, did not show strong quantitative relationships to sea ice concentration.
The surface study was used to relate biomarker distributions to recent sea ice and oceanographic conditions and apply this information to long-term sediment records in the eastern and western Barents Sea covering ca. 2 kyr and 11 kyr (Holocene) respectively. IP_{25} concentrations for the former were found to be very variable and were used to identify the period with maximum sea ice cover occurring from ca. 900 - 400 cal. yr BP where the highest abundances of IP_{25} and IRD were observed. Similarly, biomarker results from the eastern Barents Sea provided evidence for a dynamic advance of the marginal sea ice zone potentially situated at ca. 78° N (maximum extent) during ca 9.4 – 5.9 cal. kyr BP, to late Holocene and modern day maximum MIZ advance ca. 75° N.

Replicate analysis of various biomarkers in individual push-cores collected from a box core obtained from Rijpfjorden (north Svalbard) demonstrated some variability between cores. Variability in individual biomarker concentrations was lowest for HBI lipids and greatest for sterols. These data are consistent with a selective and relatively minor source of the former. In contrast, the somewhat more generic origins of sedimentary sterols likely explain the greater variability in their distributions between cores

Finally, the strong abundance relationship between IP_{25} and a structurally related di-unsaturated HBI ($C_{25:2}$) was confirmed in all sediments, similar to that found between two tri-unsaturated HBIs, consistent with co-production by certain marine phytoplankton. The progressive use of novel HBIs with two or three degrees of unsaturation (e.g. $C_{25:2}$ and $C_{25:3}$) could provide further valuable insights into environmental conditions.

List of contents

List of Figures

List of Tables

Acknowledgements

I would like to thank my supervisors Prof. Simon Belt and Dr. Thomas Brown for their guidance, wisdom, patience and support throughout my PhD studies. Also thanks to Dr. Jochen Knies (NGU, Trondheim) and Dr. Katrine Husum (University of Tromsø) for sharing their knowledge with me.

I would also like to thank the technicians in Plymouth University (Dr. Andy Fisher, Andy Arnold, Andrew Tonkin) for their excellent technical assistance and patience showed to me over the years.

It was a great pleasure to once become part of the Biogeochemistry Research Centre when I first arrived of Plymouth, being a student of Dr. Charlotte Braungardt and Dr. Miranda Keith-Roach who had to deal with my terrible English and who showed me endless patience, support, knowledge and friendship. It was great news to have to move back (the light side) where I enjoyed office with the best secretary team anyone could wish for: Dave Bocadillo de Atún and Kato, and the crazy Holliester, Bret and Vanessa with whom I shared really good times, beer, music and laughs.

It has been a pleasure to be part of the Petroleum and Environmental Geochemistry Group, thanks to Paul Sutton and his advice and little talks in the JSV; Adilou (which always has been telling me "actually you're right" even when I wasn't!) and Wieb (surfer woman), and the PhD students that I had the chance to meet: Mike Jabanandro, Hayley, Crocs and Blasa (long record colleague from Valencia) which whom I shared great adventures in Plymouth la nuite.

Also to mention the people I met over the PhD time and which whom I spent so many good times, all the PhD students of the CASE project: Miky, Sarah, Johan, Christian, Lord Frazer, and especially Theo Tiranicus which whom I had the pleasure to travel with on many occasions and cruise until the tires fall off!, and the very good friends I made on the way in Plymouth (Sebas, Estela and Gertru) which whom I shared many many "Farras" in Plymouth! Not to forget my old friend Olga sharing friendship since we were little kids! and recently thanks to George, for supporting me and put some good music in my head, "we can't possibly go out like that" Manushka!

Finally I am eternally grateful to my family, which have always been by my side supporting me in every decision I had to make, and have nourished my mind with love and a whole life of good memories.

AUTHOR'S DECLARATION

At no time during the registration for the degree of Doctor of Philosophy has the author been registered for any other University award without prior agreement of the Graduate Committee.

Work submitted for this research degree at the Plymouth University has not formed part of any other degree either at Plymouth University or at another establishment.

This study was financed with the aid of a research studentship from the European Community's 7th Framework Programme FP7 2007/2013, Marie-Curie Actions, under Grant Agreement No.238111

A programme of advanced study was undertaken, with relevant scientific seminars and conferences attended, at which work was often presented.

Word count of main body of thesis: 51.577

Signed ……

Alba Navarro Rodriguez

Date: April 2014

Conference presentations and publications

Conferences attended:

11th International Conference on Palaeoceanography (ICP) Barcelona, Spain, 1-6 September 2013. Poster presentation

BOGS meeting 2013. Plymouth University, Plymouth **U.K**., 10-11 of July 2013. Oral presentation

4th Annual Biogeochemistry Centre Conference. University of Plymouth, Plymouth, **U.K.**, 17 December 2012. Oral presentation.

22nd V.M. Goldschmidt Conference 2012, Montreal, **Canada,** 24-29 June 2012. Poster presentation.

EGU General Assembly 2012, Vienna, **Austria**, 23-27 April 2012. Poster presentation.

3rd Annual Biogeochemistry Centre Conference. University of Plymouth, Plymouth, **U.K.**, 9 December 2011. Oral presentation.

UK Arctic Science Conference. University of Leeds, **U.K.,** 14-16 September 2011. Poster presentation.

2nd Annual Biogeochemistry Centre Conference. University of Plymouth, Plymouth, **U.K.**, 17 December 2010. Oral presentation.

Publications:

Berben, S.M.P., Husum, K., **Navarro-Rodriguez, A**., Belt, S.T., Aagaard-Sørensen, S., (in prep.), Atlantic water inflow and sea ice distribution in the northern Barents Sea: A Holocene paleoceanographic evolution.

Navarro-Rodriguez, A., Belt, S.T., Knies, J. and Brown, T.A. (2013) Mapping recent sea ice conditions in the Barents Sea using the proxy biomarker IP_{25}: Implications for palaeo sea ice reconstructions. ***Quaternary Science Reviews 79***, 26-39.

Belt, S.T., Brown, T.A., Ampel, L., Cabedo-Sanz. P., Fahl, K., Kocis, J.J., Massé, G., **Navarro-Rodriguez, A.**, Ruan, J. and Xu, Y. (2013) An inter-laboratory investigation of the Arctic sea ice biomarker proxy IP_{25} in marine sediments: key outcomes and recommendations. ***Clim. Past Discuss. 9***, 5263-5298.

Belt, S.T., Brown T.A., Cabedo Sanz, P. and **Navarro Rodriguez, A.** (2012) Structural confirmation of the sea ice biomarker IP_{25} found in Arctic marine sediments. ***Environmental Chemistry Letters 10***, 189-192.

Belt, S.T., Brown, T.A., **Navarro Rodriguez, A.**, Cabedo Sanz, P., Tonkin, A. and Ingle, R. (2012). A reproducible method for the extraction, identification and quantification of the Arctic sea ice proxy IP_{25} from marine sediments. ***Analytical Methods 4***, 705-713.

List of common abbreviations

BP	Before present
BSTFA	Bis-trimethylsilyl trifluoroacetamide
CAA	Canadian Arctic Archipelago
DIP_{25}	Ratio between diene II and IP_{25}
ESC	East Spitsbergen current
GC-MS	Gas Chromatography- Mass Spectrometry
HTM	Holocene thermal maximum
HBI	Highly branched isoprenoid
HPLC	High performance liquid chromatography
IPCC	Intergovernmental Panel on Climate Change
IRD	Ice-rafted debris
IP_{25}	Ice proxy with 25 carbon atoms
MIZ	Marginal ice zone
MOC	Marine organic carbon
MSIE	Maximum sea ice extent
NAC	North Atlantic Current
NMR	Nuclear Magnetic Resonance
NSIDC	National Snow and Ice Data Center
P_BIP_{25}	Index (brassicasterol and IP_{25})
SIM	Selected ion Monitoring
THE	Total hexane extract
TIC	Total ion Current
TOC	Total organic carbon
TOE	Total organic extract
TPD	Transpolar Drift
WSC	West Spitsbergen Current

Dedicated to my parents Jose & Rosario
and to my grandparents Rafael & Victoria

Le voyage est ton père, quand tu te seras
trouvé, tu renteras, et la terre sera ta mère.
Proverb tuareg

CHAPTER ONE

1 Introduction

1.1 Sea ice

Arctic sea ice plays an important role in climate regulation on Earth. Sea ice influences global heat and moisture exchange between the oceans and the atmosphere, provides a mechanism for the transportation of cold water masses into the Atlantic and also influences water column stratification and the thermohaline circulation in the Atlantic Ocean (Thomas, 2012). The Arctic sea ice has suffered and important reduction over the last decades, being especially pronounced in the summer months. If values of the sea ice extension for September 1979 and 2012 are compared, a reduction of ca. 3.6 million km^2 of sea ice (NSIDC; http://nsidc.org/; accessed January 2014) is observed. This drastic retreat is likely to have an anthropogenic contribution (Kinnard et al., 2011) and is especially unexpected since modelled orbital summer insolation decreased from the Holocene (ca. last 11 kyr) towards modern times, which contradicts the general cooling trend (Laskar et al., 2004). The sea ice loss is additionally linked to a subsequent decrease of multi-year sea ice (perennial) and increases in first year sea ice (seasonal, a single year growth), which is gradually transforming the Arctic region in a an area more sensitive to climatic changes (Polyak et al., 2010). Multi-year sea ice characterises the Arctic Ocean, being continuously moved and transported across the Arctic Ocean towards the North Atlantic through the Fram Strait via the Transpolar Drift (TPD) moving along East Greenland (Figure 1.1) (Rudels, 2009). First year sea ice is also formed during winter in the Barents Sea, extending southwards to ca. 75° N each year and retreating seasonally to ca. 80° N, (NSIDC; 2014). The boundary between areas covered by first year sea ice and those with open water (i.e. the sea ice edge) is ecologically important (Falk-Petersen et al., 2000) and provides a unique and dynamic

habitat, influencing not only the ice edge flora and fauna, but also the underlying water column and sediments (Wassmann et al., 2006). This biologically productive region is often referred to as the marginal ice zone (MIZ).

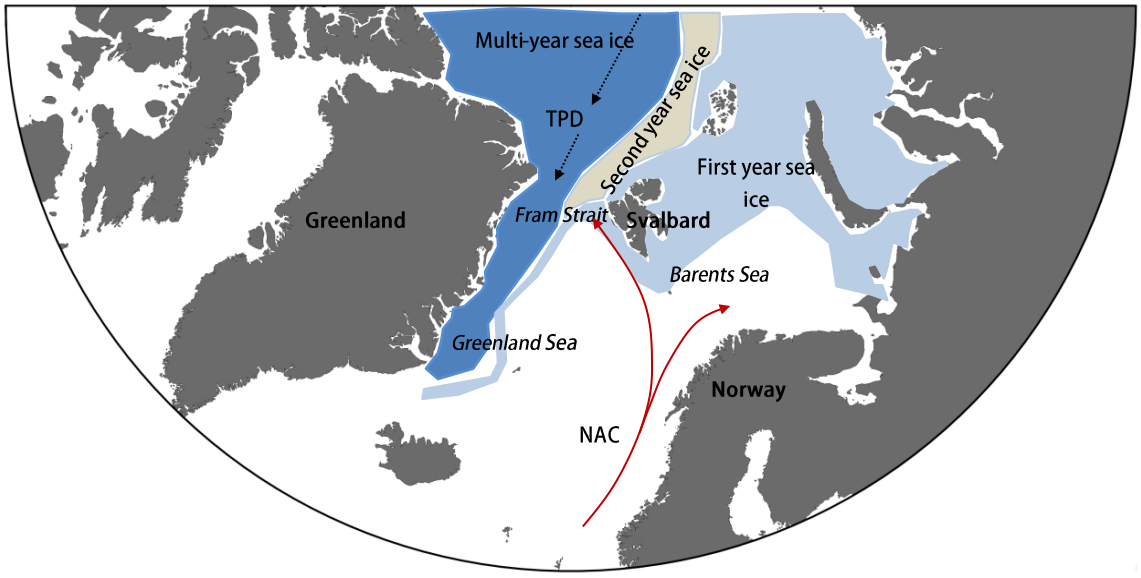

Figure 1.1 Schematic distribution of sea ice in the North Atlantic. Red arrows represent) Atlantic water, North Atlantic Current (NAC) and dashed arrows represent the Transpolar Drift (TPD).

A main concern is the impact that the rapid sea ice retreat during the last decades could also have on the distribution of flora and fauna on the Arctic region. This has been already considered by Wassmann et al. (2011), who concluded that more and reliable data and studies especially regarding phytoplankton primary producers are necessary from the Arctic region to evaluate and better understand any effect that the pronounce loss of sea ice could have, or might have, imprinted on the ecosystem.

1.2 Microfossils / proxies for palaeo-sea ice reconstructions

In recent decades, the characteristics and variability of sea ice cover have been determined in detail via satellite passive microwave measurements since the launch of

Nimbus-5 in 1972 (e.g. Comiso et al., 1997; Parkinson, 2008). In contrast, longer-term sea ice reconstructions prior to historical observations (ca 1750 AD; Divine and Dick, 2006) have been based mainly on sediment-based micropalaeontological studies, including assemblages of dinoflagellate cysts, the species composition of foraminifera, mineralogical and sedimentological data and various other geochemical proxies as discussed by de Vernal and co-workers (2013).

1.2.1 Dinoflagellates

Dinoflagellates are unicellular protists (20-200 µm) with the majority of the species present in the marine environment. Dinoflagellates often present two flagella which provide them certain mobility to migrate up and down the water column to adapt to changes in salinity, temperature and nutrients. Together with coccolithophores and diatoms, dinoflagellates constitute the major source of primary production in the oceans. The fossils recorded in sediments from dinoflagellates are very resistant organic walled cysts, termed dinocysts. These represent a fraction (ca. 10-20 %) of the original dinoflagellate population due to the fact that they are only produced by some species during a particular point in their life cycle (reproduction). Dinoflagellates are highly diversified in polar and sub-polar areas (Vernal and Rochon, 2011). Their cysts are commonly used to interpret past sea ice and oceanographic conditions in the Nordic Seas. For example, *Operculodium centrocarpum* is the predominant species in the Nordic Seas and dominates the underlying sediment where warmest water masses occur (Matthiessen et al., 2001), while *Islandinium minutum* dominates assemblages underlying cold ice-covered polar water masses (Rochon et al., 1999).

The recently updated dinocyst data base (de Vernal et al., 2013) and the application of transfer functions has provided great utility for the reconstruction of certain parameters

such as sea surface temperature and salinities (SST and SSS respectively) and sea ice coverage for the Arctic region.

1.2.2 Calcareous and siliceous microfossils

Foraminifera are planktic and benthic protists which build a calcareous shell that reflects the conditions of the water masses that they inhabit. The variety of species is quite low in the northern latitudes, being dominated by a few species (e.g. *Neogloboquadrina pachyderma* (sin.) is dominant in recent and past planktic foraminiferal assemblages from the Arctic region (Eynaud, 2011)). However, morphological changes and geochemical information from the carbonate shell, such as their stable isotopic signature ($\delta^{13}C$, $\delta^{18}O$), or Mg/Ca ratio, provide useful paleoceanographic information including the possibility to reconstruct SSTs. A limitation of this proxy is that the calcareous shell is not always well preserved (Archer and Maier-Reimer, 1994). This was suggested by Steinsund and Hald (1994) to be due to CO_2-rich, denser water masses formed of the sea ice. Therefore the shell degradation represents a limiting aspect in the use of this microfossil and, as a result, the preservation of the calcareous shells is often assessed. Foraminifera have been commonly used in the North Atlantic Ocean to reconstruct paleoceanographic conditions (Ślubowska-Woldengen et al., 2008) through an extensive compilation of sediment records.

Siliceous microfossils are characteristic of diatoms. Diatoms are photosynthetic microalgae which are enclosed in a cell wall made of silica (2 µm- 2 mm) called the frustule which can exist in both marine and lacustrine environments but is restricted to the photic zone (generally planktonic) (Crosta and Koç, 2007). Studies of diatoms in sediments have been carried out as a complementary tool for paleoceanographic

reconstructions (Collins et al., 2013; Weckström et al., 2013), but the silica skeleton is not always well preserved in sediments.

1.2.3 Ice-rafted debris

Ice-rafted debris (IRD) is a useful tool to reconstruct sea ice characteristics from marine sediments. The size and shape of these terrigenous particles are occasionally used to gather shore distal settings (Forwick and Vorren 2009). For example large particles are occasionally transported by icebergs and smaller particles by rafted sea ice. The composition of these particles found in marine sediments can also be related to the mineralogical coastal composition (glaciers), tracking the movement of drift sea ice and icebergs (Andrews and Eberl, 2012; Müller and Knies, 2013).

1.2.4 Highly Branched isoprenoid biomarkers

Other types of proxies are geochemical compounds, mainly derived from primary producers, such as diatoms. A highly branched isoprenoid alkene (Ice Proxy with 25 carbon atoms, "IP_{25}") (Figure 1.2) was proposed as a proxy for sea ice (Belt et al., 2007) and its presence in marine sediments has provided the basis for several palaeo sea ice reconstructions across the Arctic for the last decade (e.g. Massé et al., 2008; Andrews et al., 2009; Müller et al., 2009; Belt et al., 2010; Vare et al., 2010; Müller et al., 2012; Belt and Müller, 2013). A key attribute of the IP_{25} biomarker is that is most likely biosynthesized selectively by a limited number of sea ice diatoms during the spring bloom conditions (Brown et al., 2011) and is thus considered to be highly specific as a sea ice proxy (Belt et al., 2007). IP_{25} has also been detected in marine sediments up to at least 2.2 Ma (Stein and Fahl, 2013), making it particularly suitable for palaeo sea ice reconstructions.

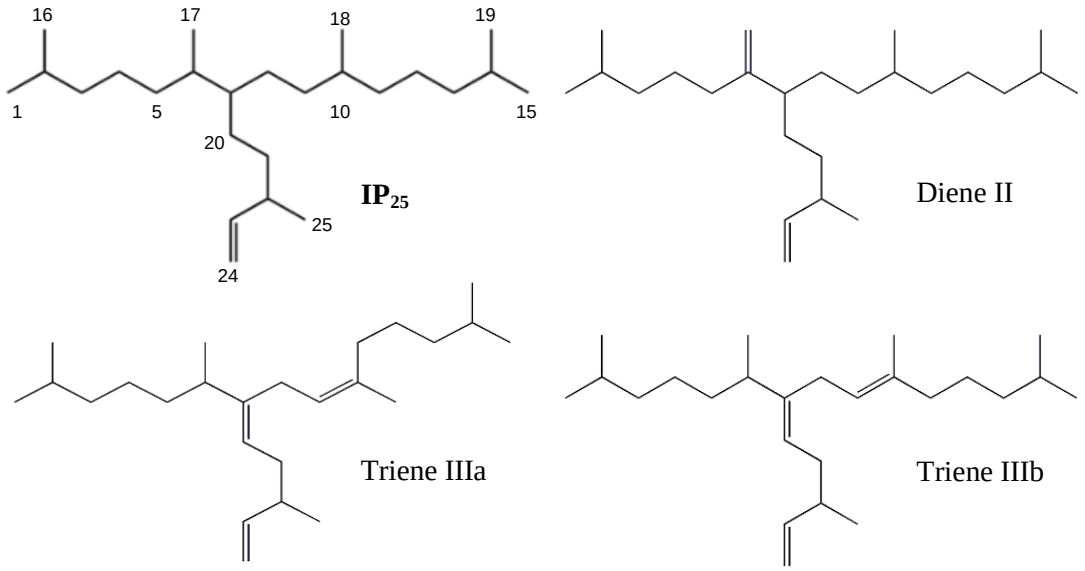

Figure 1.2 Structures of the highly branched isoprenoid alkenes biomarkers (HBIs); IP_{25}, diene II and trienes IIIa and IIIb.

In addition to IP_{25}, marine diatoms are known to produce other C_{25} HBIs with between two to six double bounds (Rowland and Robson, 1990). It was first identified by Rowland et al. (2001) that the main parameter affecting the distribution of these C_{25} alkenes in cultured diatoms of *Haslea ostrearia* was temperature, i.e. increased number of unsaturations with temperature and, consistent with this observation, is the production of IP_{25} by Arctic sea ice diatoms. One of these HBIs of special interest is a di-unsaturated C_{25} which was first reported in sea ice diatoms from the Antarctic, (Nichols et al., 1988) and later identified in diatoms and sediments from the Antarctic by Johns et al. (1999) and shown to be diene II (Figure 1.2). The specific sources of this lipid in the environment are unknown, although it has been observed in cultures of *H. ostrearia* (Masse, 2003). HBI have been used for climatic reconstructions (in the absence of IP_{25}) in other studies in the Antarctic (Massé et al., 2011; Collins et al., 2013) and in combination to IP_{25} in some Arctic regions e.g. (Vare et al., 2009; Fahl and Stein,

2012; Cabedo-Sanz et al., 2013; Xiao et al., 2013). It was reported by Massé et al. (2011) and further by Cabedo-Sanz et al. (2013) to be highly associated with IP_{25} when measured in sediments from the Canadian Arctic Archipelago (CAA) and North Iceland. Their relationship to a common source was also supported from the heavy and distinctive ^{13}C isotopic signature of both IP_{25} and diene II (Belt et al., 2008) ($\delta^{13}C$ = -19‰ to -21 ‰) and, consistent from a sea ice origin, in contrast to lighter isotopic signatures for phytoplanktonic lipids e.g. ($\delta^{13}C$ = -35 ‰ to -40 ‰). Despite the good correlations of diene II to IP_{25} (and thus a sea ice origin), other closely isomer (with the double bond in C5-6 position) have been found in more temperate regions such as the Caspian Sea (Belt et al., 1994) and the Mediterranean Sea (Grossi et al., 2004). More recently, Brown (2011) found diene II in sea urchin (*Echinus esculentus*) sample from a region of the West Coast of England. These findings suggest that $C_{25:2}$ lipids are sometimes also produced under warmer conditions and the environmental parameters and microorganisms that produce it are not fully understood.

Amongst the most common natural HBI hydrocarbons found in marine waters and sediments, are also the C_{25} tri-unsaturated HBIs, which were first reported in cultures of *H. ostrearia* (Volkman et al., 1994) and the structures identified later (Belt et al., 1996). Other tri-unsaturated isomers were isolated and identified in the planktonic diatom *Rhizosolenia* genus (Belt et al., 2002). In the case of the microphytobenthic diatom genus *Pleurosigma,* two stereoisomers of $C_{25:3}$ (triene Z and E) with the double bonds in C7-20 and C9-10 positions (Belt et al., 2000; Belt et al., 2001) were identified. These two trienes, herein referred to as triene IIIa and IIIb (Figure 1.2), were also found in phytoplankton (Massé et al., 2011) and sediment samples (Barbara et al., 2010; Denis et al., 2010; Massé et al., 2011) from the Antarctic. As such, their presence in the environment is considered to represent a phytoplankton signature. In the Arctic Ocean

have also been found in surface samples (Xiao et al., 2013) as well as in long core sediment records (Stein and Fahl, 2013). In all cases these have been interpreted as a signature of phytoplankton primary production.

In addition to HBI biomarkers, other geochemical proxies (steroidal lipids), considered to be broadly of phytoplanktonic origin, are often used to gather complementary information to IP_{25} based sea ice reconstructions, providing a signature of biological production. Previous studies showed that distributions of 24-methylenecholesterol followed profiles similar to IP_{25} or diene II in the coast of Norway (Andfjord) (e.g. Knies, 2005; Cabedo-Sanz et al., 2013). This could suggest that this lipid biomarker also has a sea ice source, but this C_{28} sterol has been identified in many diatoms and dinoflagellate species, which all can be an important constituents of phytoplankton (Volkman, 1986). Therefore, this suggestion is most likely to be a localised production limited to particular environmental areas. Similarly brassicasterol is a steroidal lipid considered to be a general biomarker indicator of phytoplankton which is derived from numerous algal groups (e.g. Volkman, 1986; Volkman et al., 1998), dinoflagellates and coccolithophores. Müller et al. (2011) suggested that brassicasterol could be interpreted as a general phytoplanktonic biomarker. Nevertheless, this biomarker has also recently been observed in sea ice samples (Belt et al., 2013b) and specific attributions related to source production are therefore uncertain. In all cases steroidal lipids provide additional information to identify phytoplankton production, in addition to sea ice reconstructions which, for example, helps in the identification of seasonal sea ice conditions.

1.2.5 Other geochemical proxies

Finally, other proxies exist to estimate past climatic conditions in the Northern latitudes. $U^{K'}_{37}$ uses the relative distribution of alkenones from coccolithophores to reconstruct sea

surface temperatures (SSTs) for tropical regions (Brassell et al., 1986), where these microorganisms exhibit a wide variety of species. However the variety of coccolithopher is very poor and often not adequate for the description of hydrographic conditions (Solignac et al., 2008) in the Arctic. Despite this, for some localised environments (eastern Fram Strait) it still provides successful data (Rueda et al., 2013). SSTs are also produced by the TEX_{86} index (TetraEther indeX, tetraethers with 86 carbons) reconstructed from glycerol dialkyl glycerol tetraethers (GDGTs) which are membrane lipids of Archaea and Bacteria from soil and aquatic environments. The TEX_{86} approach was originally calibrated for temperate regions (Schouten et al., 2002). It was shown that the number of rings in the lipid structures was dependent to temperature (Schouten et al., 2008, Kim et al., 2008) and later, its application was expanded to Polar regions by changing their relative distribution (Kim et al., 2008, Kim et al., 2010). However the TEX_{86} application for colder regions was still weak correlated to modern SST and other approaches, including OH-GDGTs (Fietz et al., 2013) and regional calibrations (Ho et al., 2014), have been undertaken to produce better SST reconstructions.

1.3 The present study

The application of IP_{25} as a sea ice proxy has gradually increased in the Arctic, reflected by the increasing number of publications conducted during the last decade. However this approach can present potential limitations, mainly related to the interpretation process of the results. Certain cases of ambiguous interpretations can arise from IP_{25} measurements, for example, absence of IP_{25} could equally be interpreted as open water conditions (absence of sea ice), or similarly, heavy sea ice cover (permanent, multi-year sea ice type, which difficult light penetration allowing bloom conditions). The

ambiguous result can easily be resolved by conducting multi-proxy analysis, for example carrying analysis of indicatives of primary production (e.g. sterols), which would help to distinguish from this two scenarios i.e. when sterols are present, it could be generally interpreted as open water conditions, and when they are absent (in addition to IP_{25}) it could be interpreted as heavy sea ice conditions that restricts any primary production. The other limitation of IP_{25} identified so far is that it only provides reliable qualitative measurements of sea ice conditions, i.e. presence or absence of seasonal sea ice, whilst the quantitative side of it is still being studied. Regardless of these limitations, IP_{25} has become a powerful tool for modern and palaeo sea ice reconstructions and further investigation and establishment of the analytical procedure was required. In order to create a robust IP_{25} database was necessary to investigate and establish the analytical procedure from which different laboratories can benefit from, as it was demonstrated by Belt et al. (2013a) which also identified and proposed recommendations to common problems. Previous to the inter-laboratory assessment, the structure of IP_{25} in marine sediments (extracted) was confirmed by GC-MS and NMR analysis to be the same as for the synthetic IP_{25}. Further method development in the extraction process and additional IP_{25} calibrations for analytical quantification were conducted in order to carry out IP_{25} measurements for modern and old sediment material from the Barents Sea. In order to complement the IP_{25} interpretations of sea ice conditions, these were contextualised with other proxy records, which were introduced earlier in section 1.2.

During the last decade many IP_{25}-based studies have been carried out in the Arctic region (Andrews et al., 2009; Müller et al., 2009; Vare et al., 2009; Vare et al., 2010; Müller et al., 2011; Muller et al., 2012). The continued successful utility of IP_{25} in

palaeoclimate for the description of sea ice conditions incentivized further investigations into the analytical methods and methodology. These were carried out in (Chapter 2-3). Therefore, the isolation and purification of IP_{25} from natural sources and its comparison to the synthesised compound (mass spectra) and characterisation (NMR spectra ^{1}H ^{13}C) in Arctic sediments was necessary to produce a reference compound with the purpose of improving the analytical procedures e.g. (laboratory methods and instrumental methods, specifically GC-MS calibration. After the analytical development, IP_{25} measurements were carried out in sediment material from the Arctic region (Figure 4.1), which combined a suite of surface sediments (red dots), two gravity cores (green stars) and a multicore (yellow star).

Therefore the aims of the study described here were to:

i) Isolate and purify IP_{25} from marine sediments for calibration purposes and improvement of the analytical procedure (Chapter 2-3).

ii) Test the use of IP_{25} as a sea ice proxy for the Barents Sea through comparison of sedimentary abundances with satellite records of sea ice, and potentially identify any particularity in the biological production signal imprinted in the sediment material by the study, alongside other biomarkers (Chapter 4).

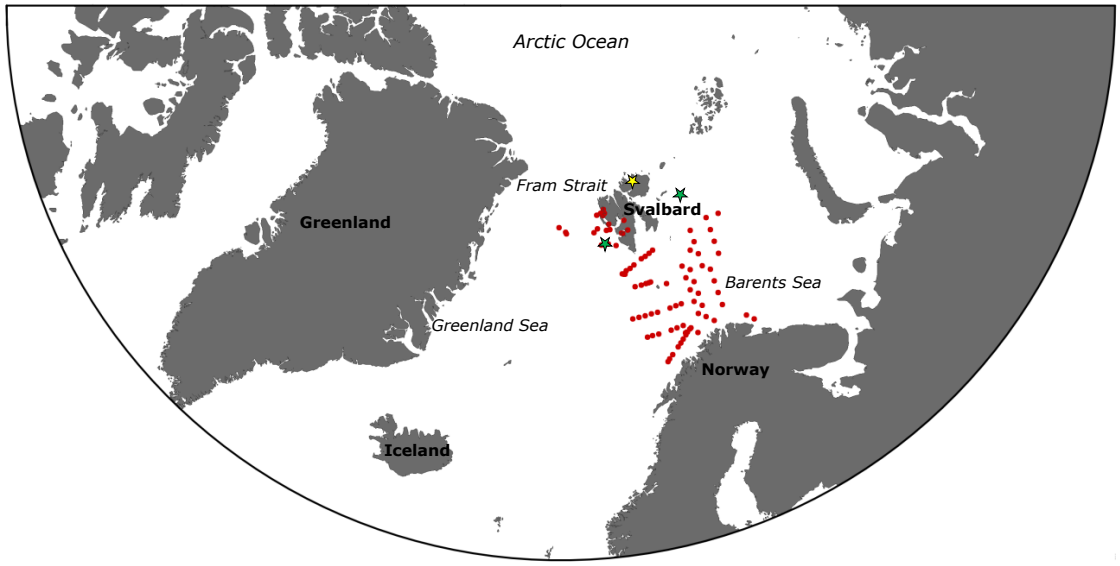

Figure 1.3. Location of the sediment material analysed in this study. Red dots correspond to surface sediment samples (Mareano); green stars correspond with long-cores NP05-70-GC (on the west of Svalbard) and push core HH11-134BC (on the east of Svalbard). Yellow star represents the location of multicores taken from Rijpfjorden (north Svalbard).

iii) Investigate the use of a combined biomarkers approach to better define sea ice conditions (Chapter 4).

iv) Apply the use of IP_{25} for sea ice reconstructions covering longer time-scales (e.g. the Holocene) in the Barents Sea (Chapter 5-6).

v) Examine the reproducibility of biomarkers in a series of nearby sediment material and its implication on the production of robust datasets (Chapter 7).

These aims are described below and related to the specific chapters:

Chapter 2: *Methodology;* describes the laboratory procedure development and detailed methods adopted for the analysis of IP_{25} and other biomarker sterols.

Chapter 3: *Extraction and isolation of IP_{25}*; describes the isolation and purification of IP_{25} from marine sediments for calibration purposes.

Chapter 4: *An investigation of IP_{25} and other biomarkers in surface sediment from the Barents Sea;* Determination of IP_{25} concentrations in surface material from the Barents

Sea and comparison to what extent this distribution resembles the known sea ice concentrations observed by satellite records. Qualitative and quantitative applications of IP_{25} as a sea ice indicator. This study presented the foundation which upon to base further down core sediment studies in the same region.

Chapter 5: *Palaeo-sea ice reconstructions over the last ca. 3800 years in the western Barents Sea;* describes the sea ice conditions of the western Barents Sea for the last 3500 years based on interpretation of biomarker data.

Chapter 6 *Palaeo-sea ice reconstructions over the last 10.5 kyr in the eastern Barents Sea;* describes the sea ice conditions of the eastern Barents Sea for the Holocene based on interpretation of biomarker data.

Chapter 7: *Reproducibility of biomarker analysis within box core sediments study*; Testing IP_{25} reproducibility in a series of multicores.

Chapter 8: *Conclusions.* Summarises the conclusions derived from the work presented here, and identifies potential areas for future studies.

CHAPTER TWO

2 Method development and laboratory procedure

2.1 Introduction

The content of this chapter describes the general laboratory procedure and analytical methods adopted in this study including chemical identification, quantification and instrumental methods. All the analyses were carried out on marine sediment samples, distributed over the Arctic region. Any additional procedures are also described in this chapter.

2.2 General methodology

2.2.1 Storage and freeze drying

All sediment analysed followed the same storage procedure. After collection from the seabed sediment cores were sliced and placed into plastic bags. After the sectioning, sediments were kept in the freezer under dark conditions. Part of the sediments analysed here were freeze dried in other laboratories. For the sediment samples freeze-dried in our laboratory, a Thermo Savant Modulyo D freeze dryer Thermo, USA; -45º C; 0.2 mbar for 24 - 48 hours. Gentle homogenization of the sediment material previous weighting was necessary in some cases in a grinding bowl.

2.2.2 Internal standards for lipid quantification

Addition of the following standards prior to extraction was used to allow quantification of the analytes; 9-octyl-8-heptadecene (9-OHD) and 7-hexylnonadecane (7-HND), both 10µL; 10µg mL^{-1}; Figure 2.1 a, b) were added to the sediment samples for quantification of the lipid HBIs and 5α-androstan-3β-ol (10µL; 10µg mL^{-1}; Figure 2.1 c) was added to the sediment for quantification of the sterols.

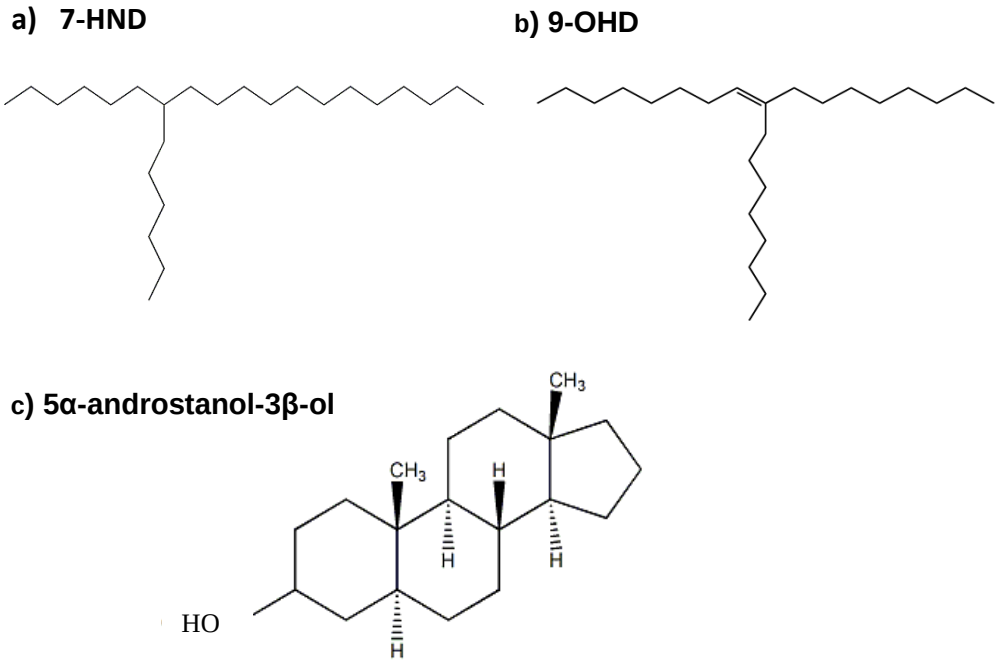

Figure 2.1 Structure of the internal standards used for biomarker identification and quantification; a) 7-HND; b) 9-OHD; c) 5α-androstanol-3β-ol

2.2.3 Total organic extracts

Total organic extracts were recovered as follows. Sediments were placed in glass vials and extracted with dichloromethane/methanol (2:1 v/v) using a sufficient volume to cover the sediments (e.g. 3 mL for ca. 1g of sediment). The vials were sealed with polypropylene screw caps, ultrasonicated (15 min; 30°C) and centrifuged (2500 rpm; 1 min). Supernatant solvent was pipetted and placed in a clean glass vial. This procedure was repeated 2 times (2:1 *v/v* 1.5 mL total extractant volume) to allow a better recovery of the compounds.

2.2.4 Lipid separation by silica column chromatography

TOEs were dried under a nitrogen (N_2) gas stream at room temperature. The resulting dried TOEs were re-dissolved in 1 mL hexane and ultrasonicated (5 min) prior to partial

purification using open column chromatography (SiO_2). The columns were prepared in pasteur pipettes, (150 mm and 3 mL capacity) by plugging DCM-extracted cotton wool and filling the pipette with ca. 0.5 mg SiO_2 (60 - 200 µm Fisher, UK). Conditioning of the column with ca. 6 mL hexane was necessary to homogenize the stationary phase, after which the sample was introduced and eluted with hexane (ca. 6 mL) for the collection of the lipid fraction, followed by an elution with hexane/methylacetate; (80:20 *v/v*; 6 mL) for the collection of the steroidal lipid fraction (Müller et al., 2011) (Figure 2.2). The solvent volume necessary for the complete elution of the internal standards and IP_{25} was tested (4 mL) (Figure 2.3 a) by reproducing the extraction procedure from a sediment sample with known IP_{25} concentrations and collecting individual fractions every 0.5 mL. The solvent was evaporated under a slow stream of N_2 at room temperature. The effect that longer exposition of the total hexane extract (THE) to N_2 stream could have on IP_{25} and IS abundances was tested. Sediments extracts THE, of known IP_{25} concentrations, were exposed to 5; 10; 20 and 30 min N_2 stream. Duplicates were carried out for the sample data displaying error bars (Figure 2.3 b). While IP_{25} abundances at 20 min appeared to be under the limit of detection < (3S/N), decreased abundances were found for the extracts exposed to longer periods of N_2 stream. This solvent evaporation step was then carried out making sure not to exceed the recommended 5 min N_2 exposure after the total dryness of the THE in order to avoid any loss of analytes or IS. THE dried lipidic fraction was recovered with 2x (50 µL of hexane) with a 50 µL syringe SGE and transferred to a 2 mL glass vial for GC-MS analysis and cramped with teflon cramps septa. In some cases, the identification of IP_{25} and other HBIs was dificulted due to either low concentration or the presence of abundant co-elutant compounds (e.g. sulfur). In such cases, further extraction and or separation methods (described in section 2.3) were added to the general procedure.

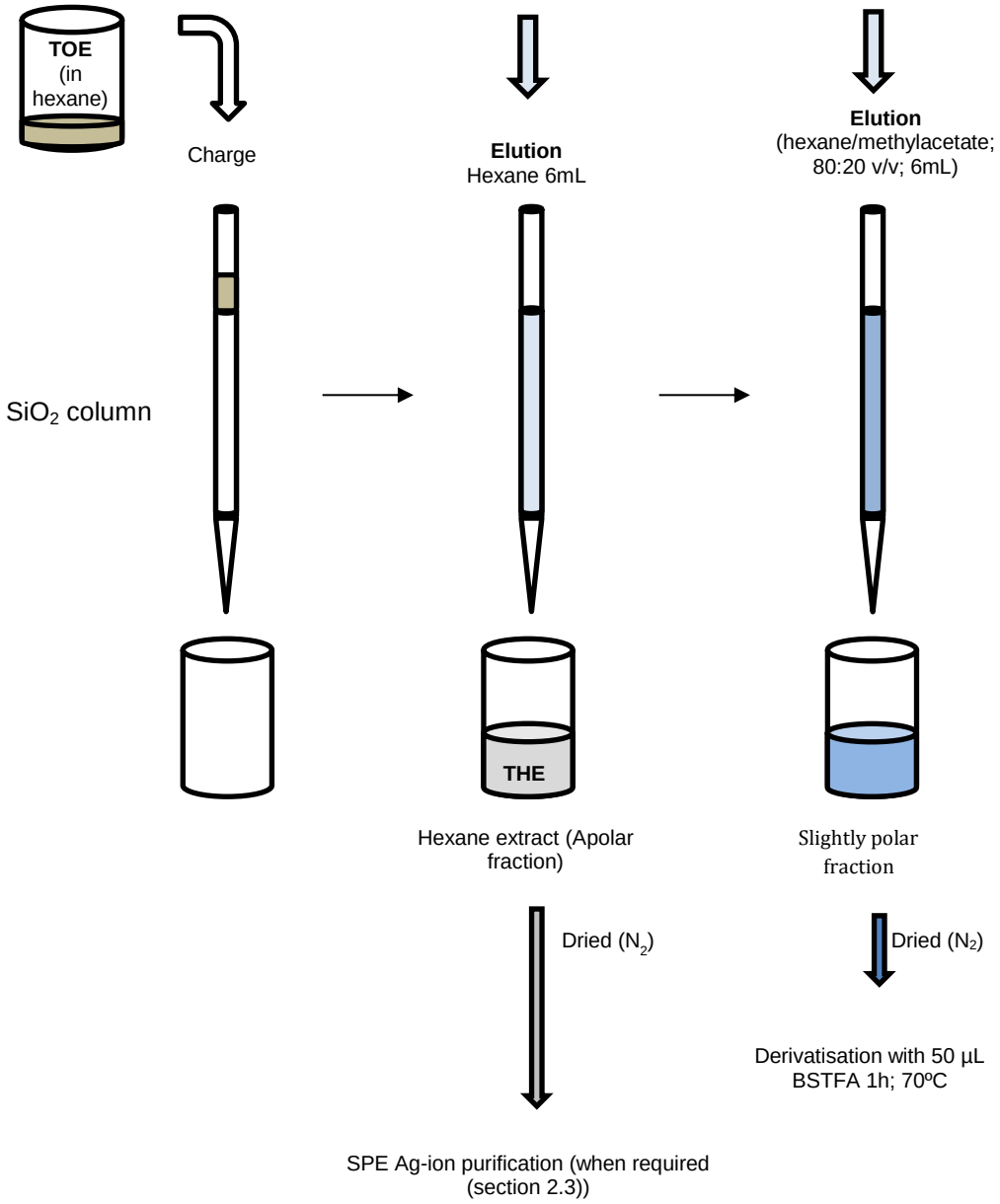

Figure 2.2 Schematic representation of the procedure adopted for the purification with SiO_2 open column chromatography of the total organic extracts (TOE) from marine sediments. Apolar fraction containing IP_{25} was collected with 6mL of Hexane and slightly polar fraction containing sterols was collected with a mixture 80:20 v/v hexane/methylacetate).

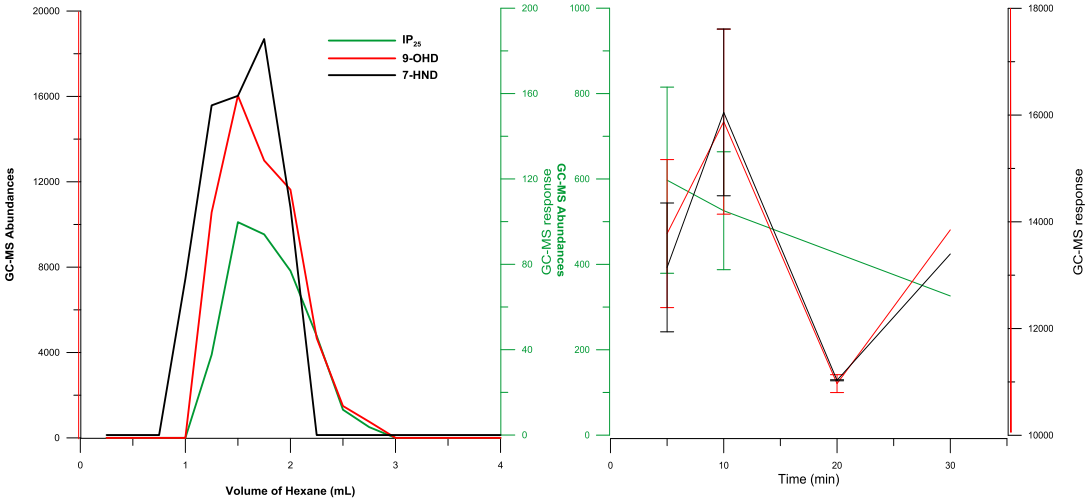

Figure 2.3 a) Graph representing the volume of elutant required for complete elution of IP_{25} and IS for the purification with SiO_2 open column chromatography of a total organic extract (TOE). Peak areas of IP_{25}, 9-OHD and 7-HND on the Y axis and volume (mL) on the X axis. b) Sediment extracts (THE) from sediment D37 from the Canadian Arctic Archipelago (CAA) exposed to different times under nitrogen stream 5; 10; 20 and 30 min.

2.2.5 Derivatisation

Fractions containing the steroidal lipidic fraction were dried under N_2 and silylated with BSTFA (50 µL; 70° C; 1 h) prior to analysis by GC-MS, to provide higher volatility to the compounds that were going to be analysed with a 95-5 % dimethylpolisiloxane/phenil, apolar capillary column. The excess of silyl agent was retained in the final volume with DCM in the 2 mL glass vials for analysis, in order to prevent reversal of the reaction.

2.2.6 Gas chromatography-mass spectrometry

All partially purified extracts were analysed by GC-MS using an Agilent 7890A GC fitted with an Agilent HP-5ms column (30 m x 0.25 mm x 0.25 µm) coupled to a 5975 series mass selective detector (MSD). The injection volume was 1 µL with auto-splitless injection (300° C inlet temperature). The GC oven temperature program was (40 - 300°

C; 10° C min^{-1}) followed by an isothermal interval (300° C; 10 min). Helium was the carrier gas with a constant flow rate (1 mL min^{-1}). The ionization potential was set at 70 eV. Total ion current (TIC; *m/z* 50 – 500 Daltons) technique was used for identification whereas selected ion monitoring (SIM; -0.3 + 0.7 *m/z* for selected ions) was used for quantification of the analytes after separation in the capillary column. Data was processed with the Agilent Chemstation software.

2.2.7 Identification and quantification of biomarkers

2.2.7.1 HBIs

Identification of HBIs isolated from marine sediments was established by comparison of the respective mass spectra with those of authentic compounds kept in the laboratory. Individual lipids were identified from the mass spectra, molecular ion and fragmentation pathways (Figures 2.4; 2.5) and retention indices (IP_{25}: 2086; diene II: 2085; triene IIIa: 2045; triene IIIb: 2092) calculated using Equation 1. *Ri* corresponds to retention index and Rt to the retention time on GC-MS (HP – 5ms column type) (Brown, 2011) in comparison to C_{20} and C_{21} alkanes.

$$Ri = \frac{Rt^{HBIs} - Rt^{nC_{20}}}{Rt^{nC_{21}} - Rt^{nC_{20}}/100} + 2000$$

(Eq. 1)

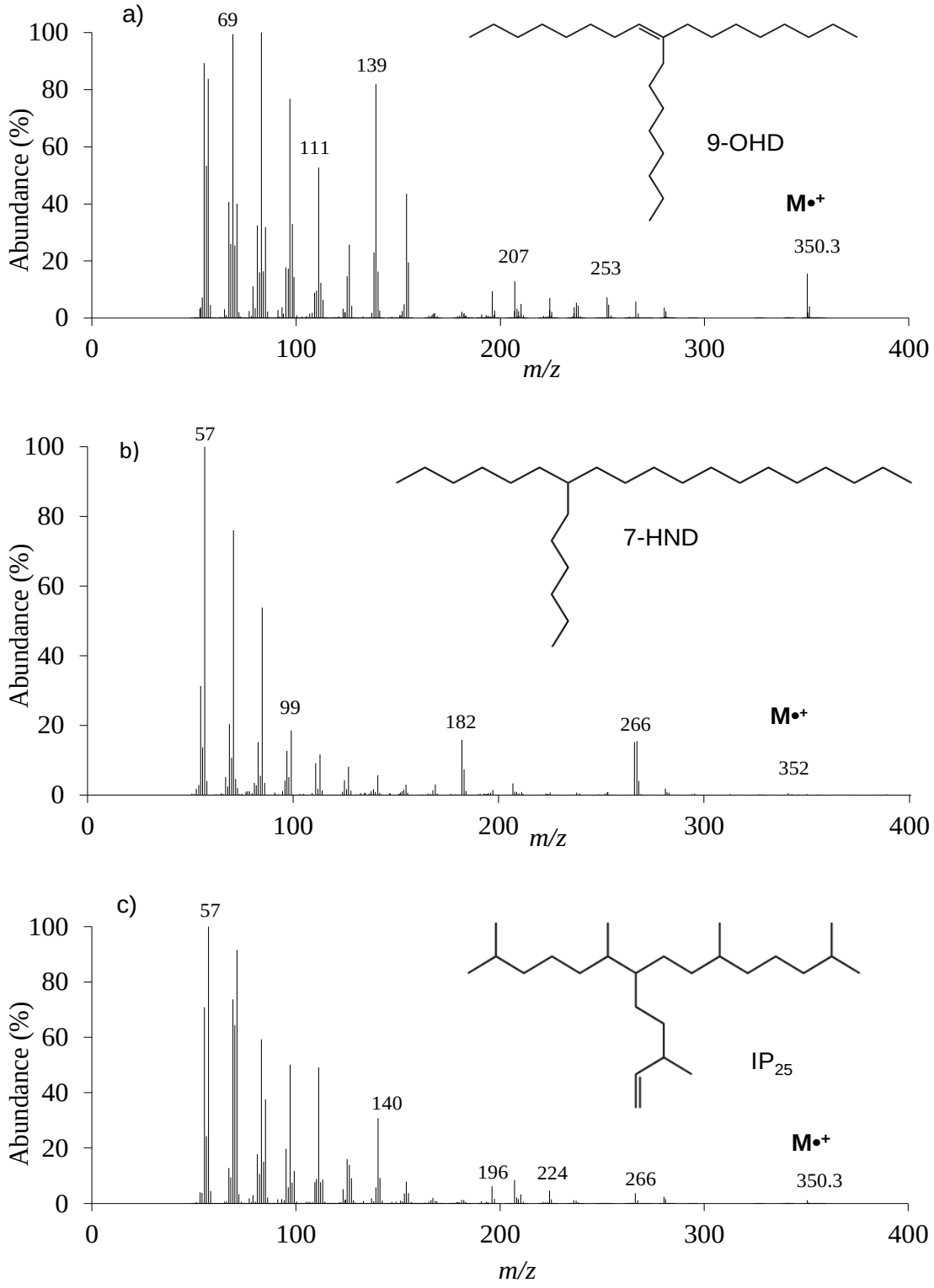

Figure 2.4 Background subtracted mass spectra and structures of the two internal standards a) 9-OHD (9-octyl-8-heptadecene); b) 7-HND (7-hexylnonadecane) and c) highly branched isoprenoid IP_{25}. Molecular ions indicated with $M\bullet^{+}$.

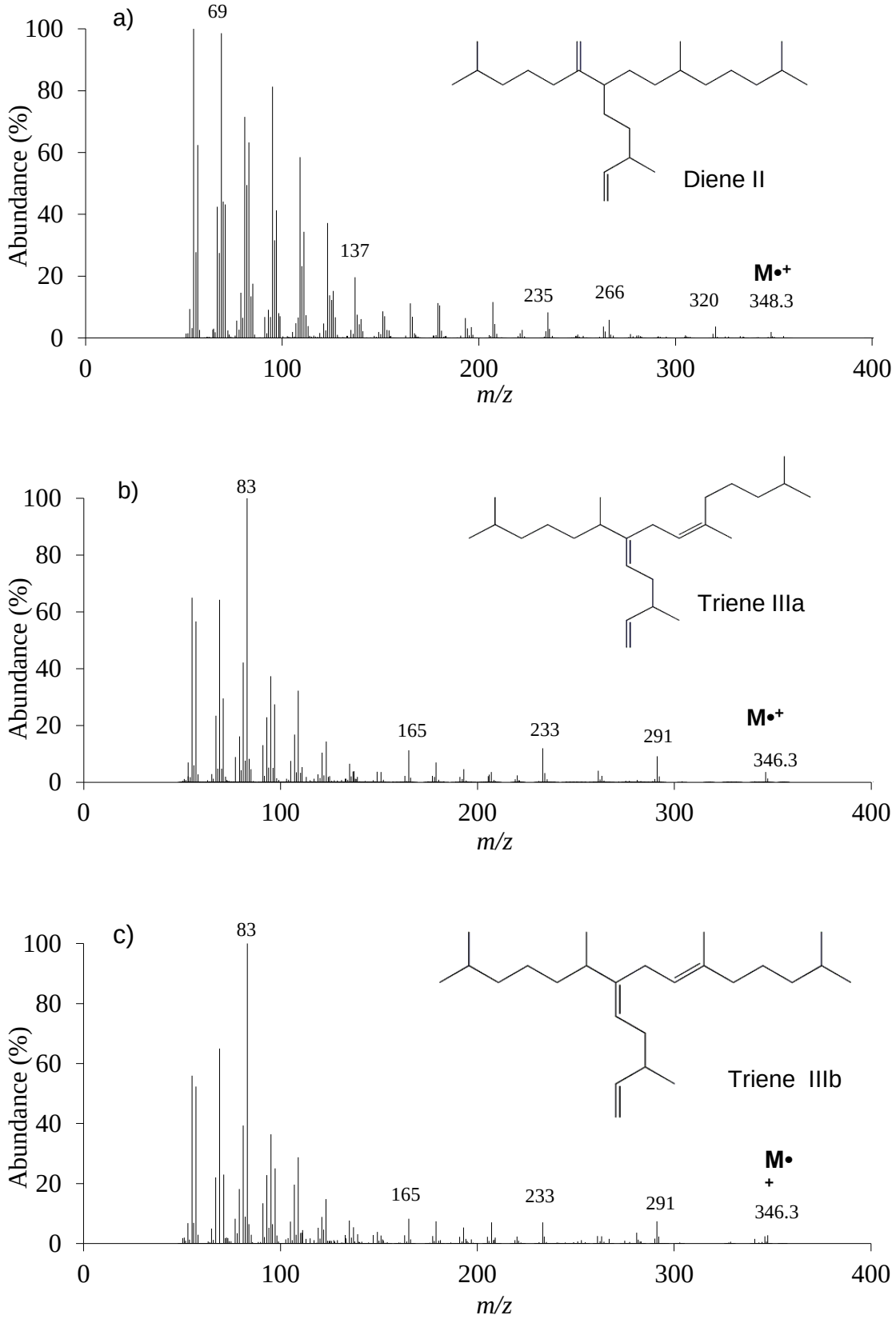

Figure 2.5 Background subtracted mass spectra and structures of the authentic compounds, highly branched isoprenoid alkenes described in the current study; a) diene II; b) triene IIIa; c) triene IIIb. Molecular ions indicated with $M^{\bullet+}$.

Quantification of HBIs was achieved by manual integration (Chemstation, version C.03.00 software) of the signal intensities obtained by the GC-MS in SIM mode for the molecular ions (IP_{25}: *m/z* 350.3; diene II: *m/z* 348.3; trienes IIIa and IIIb: *m/z* 346.3) (Figure 2.6). The sensitivity of the analysis is highly increased by measuring selected ions in SIM rather than TIC mode as a characteristic of this technique. Additionally, SIM mode allows identification of possible co-elutant compounds.

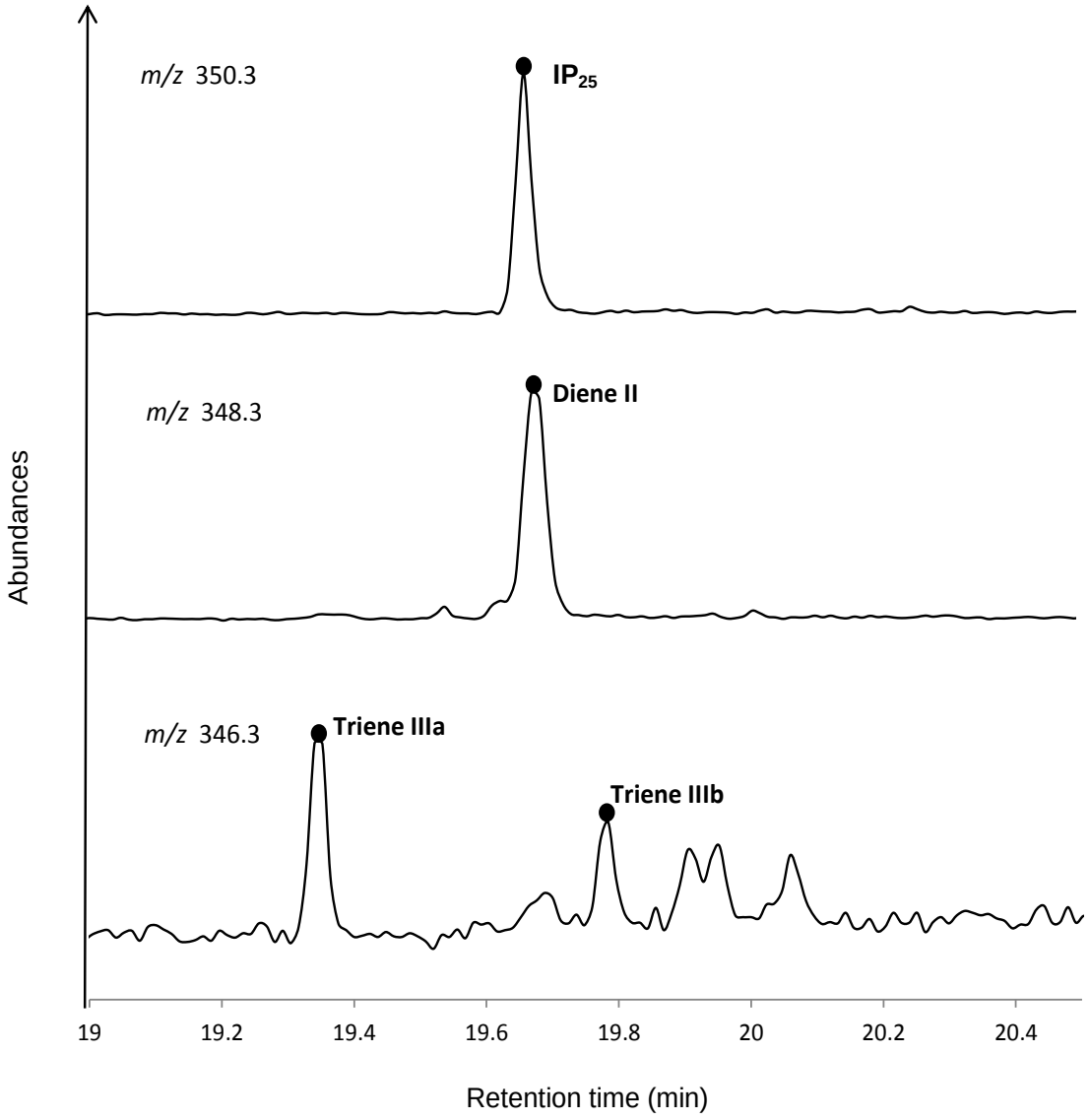

Figure 2.6 Partial GC-MS chromatogram in SIM mode (*m/z* 350.3, 348.3, 346.3) of the reference marine sediment extract from the Canadian Arctic Archipelago (CAA) St 428 after SiO_2 open column chromatography purification. The figure shows the elution order of the lipids.

Quantification of the biomarkers was carried out using Equation 2.

$$IP_{25}(\mu g\ \ g\ sed^{-1}) = \frac{\left(\frac{Pa}{P_{IS}}\right)\ x\ RF}{Ms}\ x\ M_{IS}(\mu g)$$

(Eq. 2)

Briefly, *Pa* and P_{IS} refers to peak area of the analyte and internal standard, respectively; *Ms* refers to the mass (g) of sediment extracted and M_{IS} to the mass of internal standard added to the samples for quantification purposes, typically 0.1µg. The RF is a response factor, a value added to account for differences in the fragmentation (spectral responses) caused by electronic ionization of the molecules (IS and HBIs) in the mass selective detector MSD which was observed to fluctuate over time (Chapter 3). The response factor is the ratio between abundances of the internal standard and the analyte of interest. Since the quantification of analytes were carried out in SIM mode, the RF therefore depend on the mass spectral response of the selected ion from the internal standard.

The novel internal standard (9-OHD) is a C_{25} hydrocarbon with one double bond and a molecular mass of 350.3 (i.e. the same as IP_{25}). 9-OHD was proposed as a new internal standard for IP_{25} quantification (substituting 7-HND) since they are closer structurally (both have one unsaturation). Similar structures result in similar extraction efficiencies through the analytical procedure which would effectively mirror any effect that IP_{25} could have through the extraction process, aiming to obtain more accurate quantifications. Both analyte and internal standard have the same molecular mass *m/z* of 350.3 but different molecular structures, therefore differences in the bond energies between carbons will result in different fragmentation when ionized in the MSD. Figure 2.7 represents the different instrumental responses of the IS and IP_{25} in TIC and SIM

mode for a sample of equal concentrations. Especially it shows the differences that the selection of specific ions in SIM (molecular ion or characteristic fragments e.g. *m/z* 99) have on the GC-MS signal (Table 2.1). In addition, by using a high *m/z* (350.3) for the identification of the analyte of interest, smaller *m/z* product of the fragmentation of co-elutant compounds contributing to the spectrum are avoided e.g. *m/z* 99.

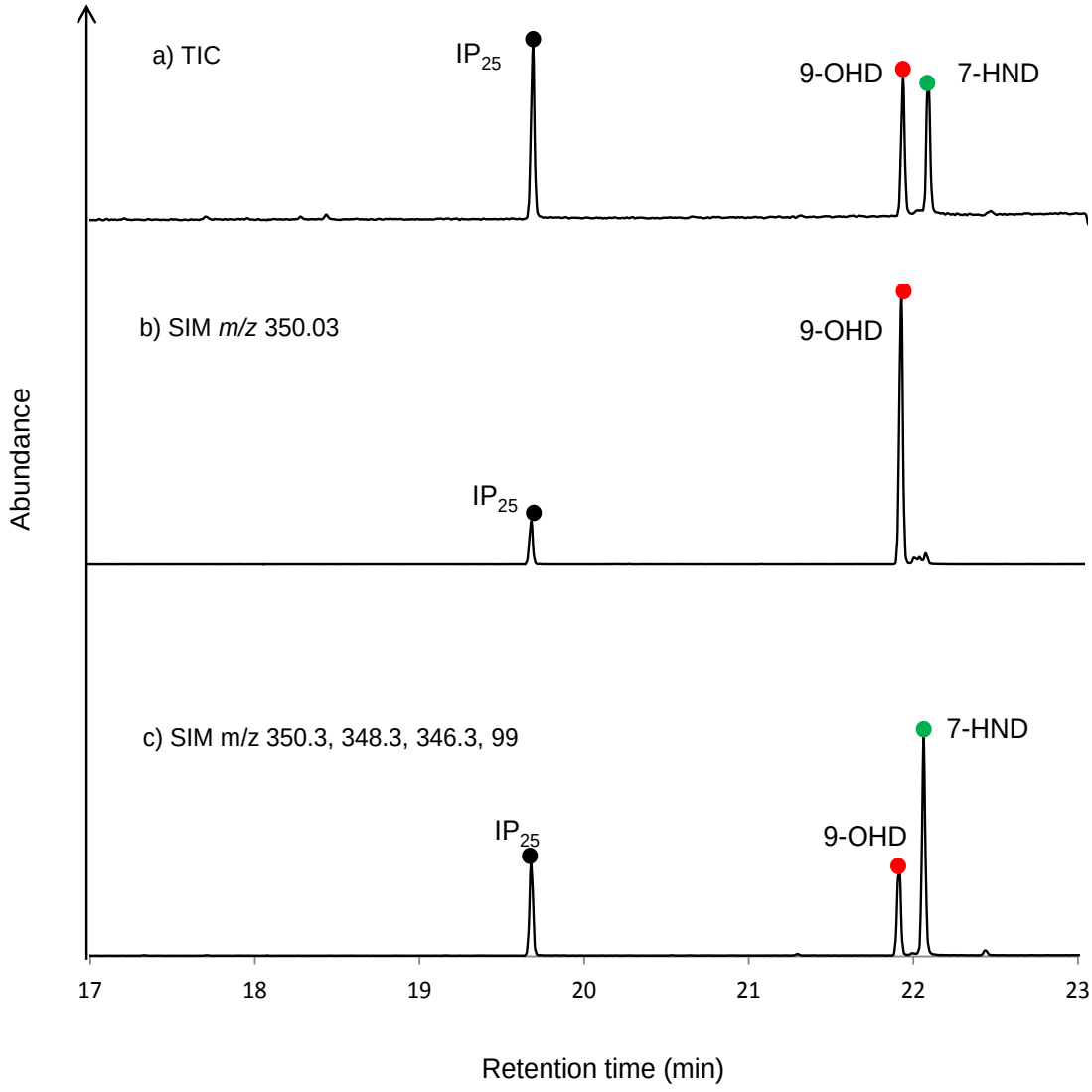

Figure 2.7 Partial chromatogram from a calibration of equal concentrations (1 µg mL^{-1}) of IP_{25} and the respective internal standards 9-OHD, 7-HND. Black dot corresponds to IP_{25}, red dot to 9-OHD and green dot to 7-HND a) TIC chromatogram b) SIM *m/z* 350.3 c) SIM *m/z* 350.3; 348.3; 346.3; 99.

In order to see the difference numerically, the relative abundance of the ion *m/z* 350.3 obtained from the spectral response selected for quantification of IP_{25} is shown in Table 2.1, being almost by a factor of 5.

Table 2.1 Relative abundances of the internal standards 9-OHD and 7-HND and IP_{25} subtracted from spectral responses. Relative abundances correspond to the percentage of the selected ion with respect to the rest of the fragment ions of the molecule in the mass spectra.

Compound	***Relative ion abundances (%)(350.3) to base peak***
IP_{25}	1.47
9-OHD	10.4

The calculation for the quantification of IP_{25} is described in Table 2.2. For the calculation of the response factor for IP_{25} was necessary its previous extraction and concentration from marine sediment (detailed in Chapter 3).

Table 2.2 Calculation steps and data required for the quantification of HBI in marine sediments. Peak areas correspond to the chromatogram in Figure 2.6; grams of dry sediment = 1.01. MIS =0.01 µg. ***RF **** for IP_{25} detailed in Chapter 3.HBIs expressed in (µg g^{-1}).

HBI	***Pa (HBI)***	***Pa (IS) 9-OHD***	***RF****	$\frac{\frac{Pa\ (HBI)}{Pa\ IS}}{g\ sediment} xRf$	$\frac{\frac{Pa\ (HBI)}{Pa\ IS}}{g\ sediment} xRfx\ M_{IS}$
IP_{25}	20827	6544	**5.03***	15.8500	0.1585
Diene II	38664	6544	11.29	66.0444	0.6604
Triene IIIa	5982	6544	1	1.6472	0.0165
Triene IIIb	3100	6544	1	0.8536	0.0085

The calculation of the RF of the rest of HBIs was conducted with authentic compounds kept in the laboratory (diene II and trienes IIIa and IIIb). RF were calculated from individual calibration curves, of diene II, trienes IIIa and IIIb (0.0001 $mgmL^{-1}$; 0.0002 $mgmL^{-1}$; 0.0004 $mgmL^{-1}$; 0.0006 $mgmL^{-1}$; 0.0008 $mgmL^{-1}$; 0.001 $mgmL^{-1}$; R^2= 0.99;

R^2= 0.99; R^2=0.99) against the internal standard (9-OHD) of equal concentrations proceeding similarly to Figure 3.2 in Chapter 3.

Data was routinely normalised to total organic carbon (TOC) (Equation 3), in an attempt to compensate for any differences in regional environmental processes most likely to be reflected in fluctuations of the TOC values e.g. surface sediment study (Chapter 4). TOC per weight of sediment (%) was determined using ca. 100 mg of freeze-dried sediment which was digested in HCl (1 mL; 18 h) to remove any inorganic carbonate. Analyses were conducted by Andrew Tonkin (Plymouth University) with a Carlo Erba EA 1110 elemental analyser for carbon, nitrogen and hydrogen.

$$HBI\ (\mu g\ g^{-1}\ TOC) = \frac{HBI\ (\mu g\ g^{-1})}{TOC\ (wt.\%)} \quad \text{(Eq. 3)}$$

In some cases, biomarker concentrations were expressed as fluxes (Equation 4) in order to compensate for differences in the compactation of the sediment material and sedimentation rates in down core analysis. For the calculation of the fluxes was necessary to count with an age model that provides sediment accumulations rates (A_{sed}) and dry bulk densities (DBDs; Equation 5). Water content (*Wc*) was determined from the wet (*Wm*) and dry (*Dm*) sediment masses before and after freeze-drying (Equation 6). A constant density for sediment particles (2.65 g cm^{-3}) and for sea water (1.025 g cm^{-3}) was assumed.

$$\boldsymbol{HBI\ flux}\ (\mu g\ cm^{-2} kyr^{-1}) = \boldsymbol{IP_{25}}\ (\mu g\ g^{-1}) \times \boldsymbol{DBD}\ (g\ cm^{-3}) \times \boldsymbol{A_{sed}} (cm\ kyr^{-1}) \quad \text{(Eq. 4)}$$

$$DBD\ (\ gcm^{-3}) = \frac{Dm}{(Wc/1.025) + (Dm/2.065)}$$

(Eq. 5)

$$Wc\ =\ Wm - Dm$$

(Eq. 6)

Approximately each 15 sediment samples, a reference sediment material from Franklin Bay in the Canadian Arctic Archipelago (ca. 1g) of known biomarker concentrations was also extracted in order to check the extraction procedure and calculate the reproducibility of the analytical procedure.

2.2.7.2 Sterols

Identification of sterols isolated from marine sediments was achieved by comparison of the derivatised trimethyl silyl ethers (TMS) mass spectra in TIC chromatograms with authentic compounds (brassicasterol Table 2.3). Elution order and retention time were compared to that of authentic compounds in (column HP-5ms) (Brown, 2011) and further verification of molecular ions and fragmentation pathways was conducted with spectra of the TIC chromatograms for samples abundant in sterols, (Table 2.3; Figures 2.8, 2.9, 2.10) and with spectra of authentic compounds in (Brown, 2011) and NIST bibliography (dinosterol).

Table 2.3 Identification of derivatised sterols (TMS ethers) analysed in this study and the selected ions in SIM *m/z*. The relative abundances correspond to the SIM ions in the mass spectrum.

Sterol	IUPAC Name	Common name	SIM (*m/z*)	Relative abundances SIM (%)
SI	24-Methylcholesta-5,22*E*-dien-3β-oI	Brassicasterol	470	21
SII	Ergosta-5, 24(28)-dien-3β-ol	24-Methylenecholesterol	470	14
SIII	Cholest-5,24-dien-3β-ol	Desmosterol	343	33
SIV	24-Ethylcholesta-5,22E-dien-3β-ol	β-Sitosterol	396	37
SV	24-Methylcholest-5-en-3β-ol	Campesterol	382	67
SVI	4α,23,24-trimethyl-5α-cholest-22E-en-3β-ol	Dinosterol	500	3
SVII	5α-Androstan-3 β-ol	Androstanol	333	58

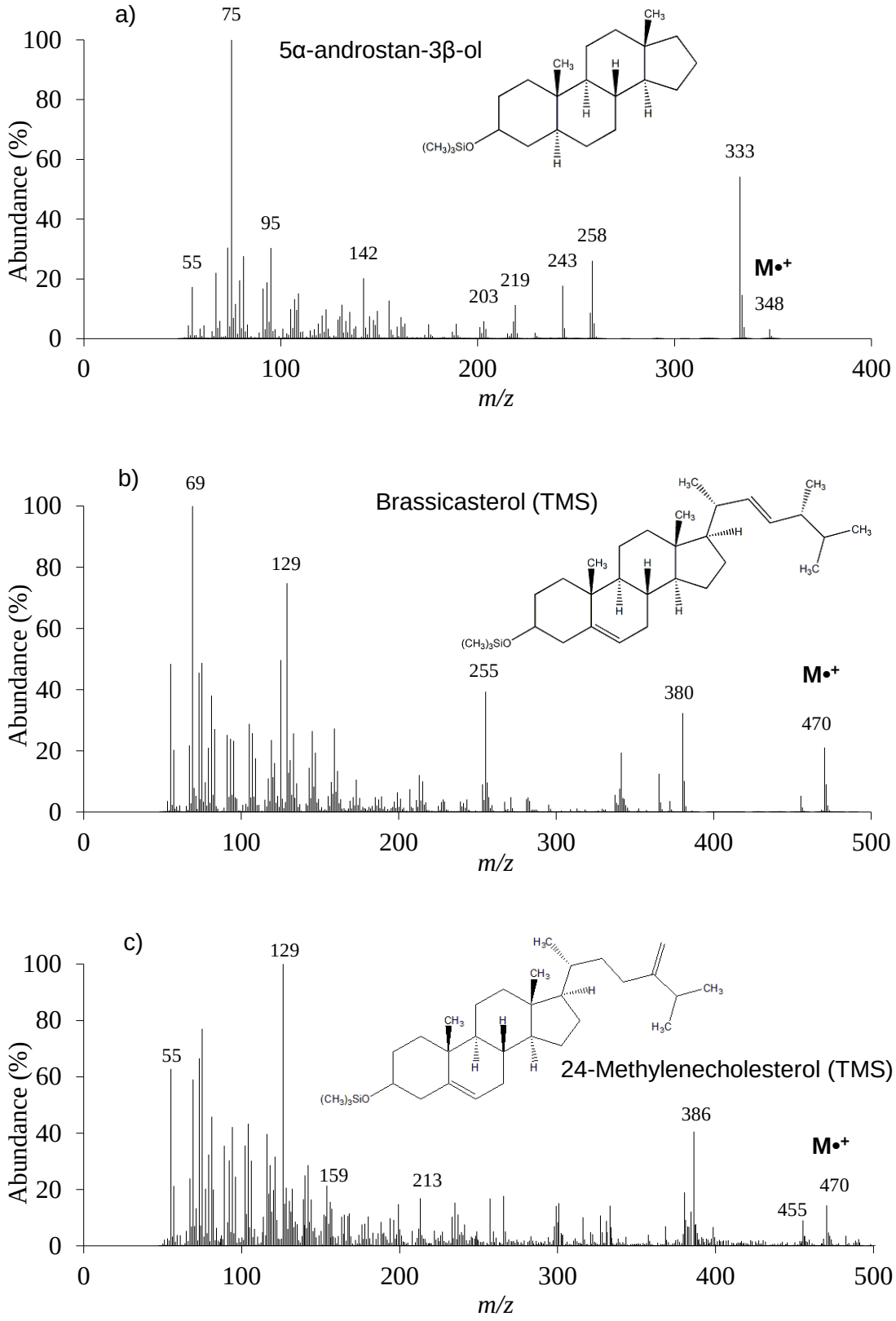

Figure 2.8 Background subtracted mass spectra and structures of the trimethylsilyl (TMS) internal standard a) 5α-androstan-3β-ol, **SVII**; and (TMS) sterol ethers described in this study: b) 24-Methylcholesta-5,22E-dien-β3-ol (brassicasterol, **SI**), c) 24-Methylcholesta-5,24(28)-dien-3β-ol (24-methylenecholesterol). Molecular ions indicated with $M^{\bullet+}$.

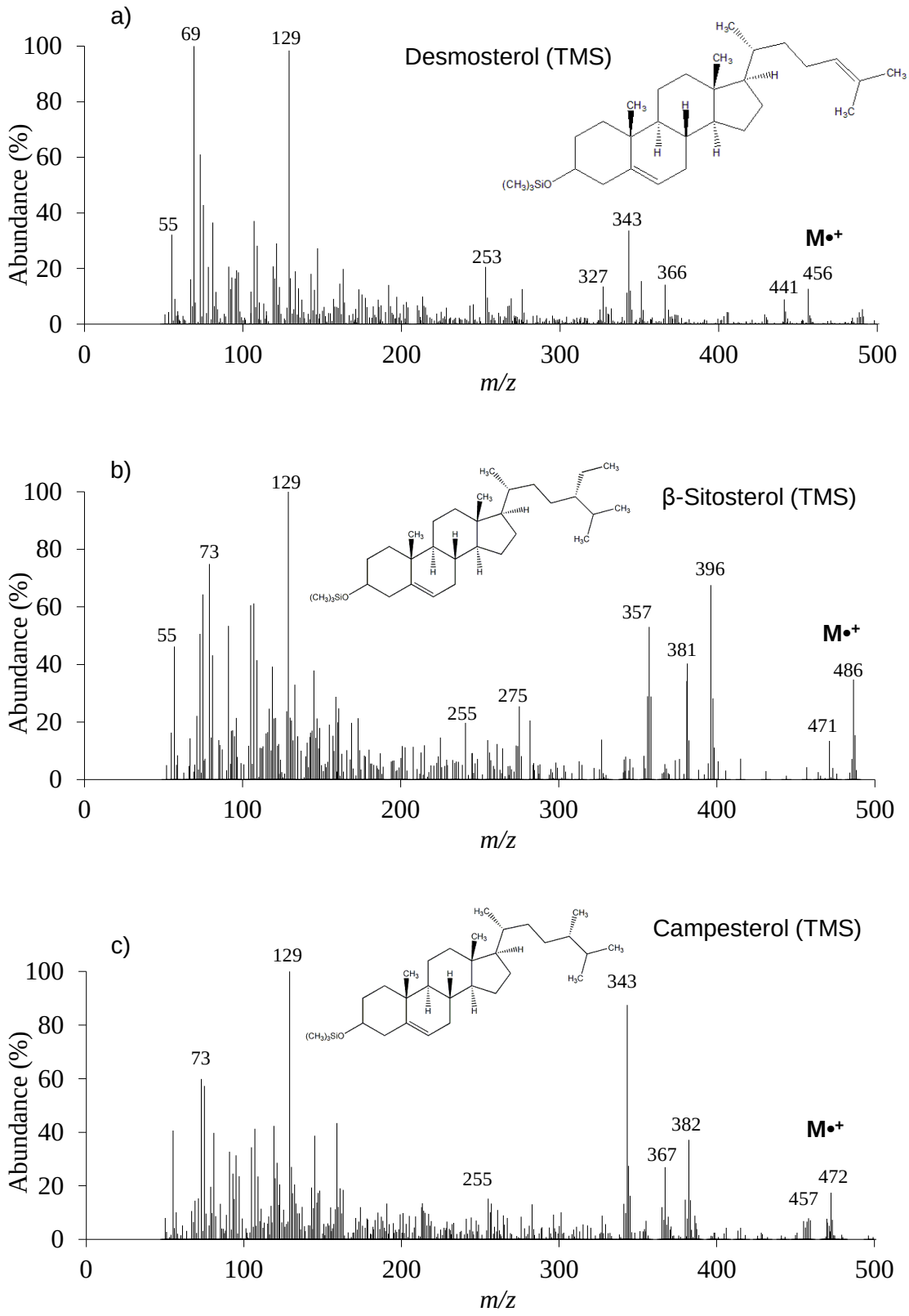

Figure 2.9 Background subtracted mass spectra and structures of the trimethylsilyl (TMS) sterol ethers described in this study: a) Cholest-5,24-dien-3β-ol (desmosterol, **SIII**), b) 24-Ethylcholest-5-en-3β-ol (β-sitosterol, **SIV**), c) 24-Methyelcholest-5-en-3β-ol (campesterol, **SV**). Molecular ions indicated with $M\bullet^{+}$.

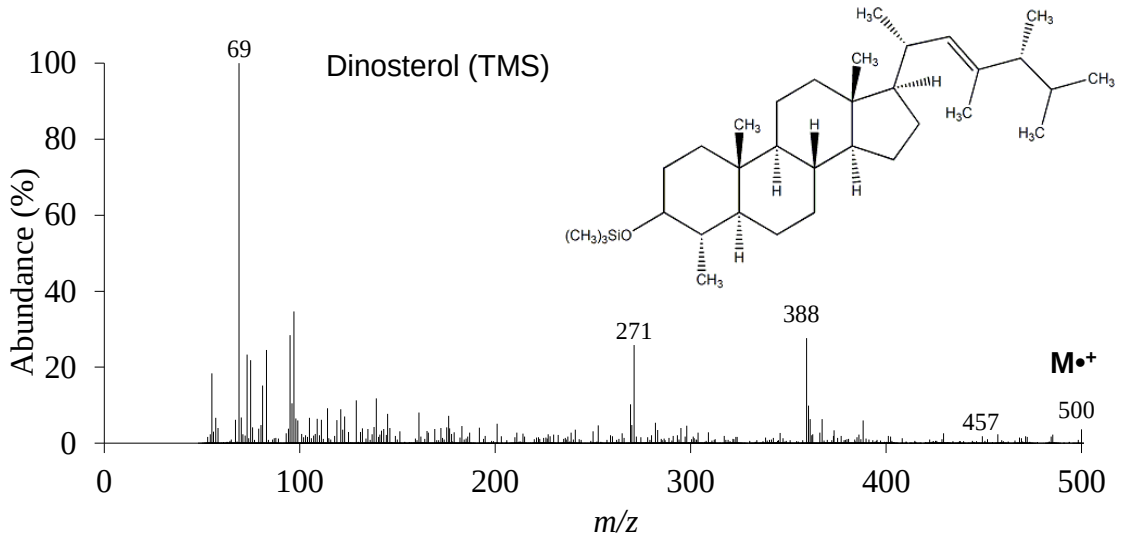

Figure 2.10 Background subtracted mass spectra and structure of the trimethylsilyl (TMS) sterol ether described in this study: a) 4α,23,24-trimethyl-5α-cholest-22E-en-3β-ol (dinosterol, **SVI**). Molecular ions indicated with $M\bullet^{+}$.

Quantification of sterols was achieved by manual integration (Chemstation, version C.03.00 software) of the signal intensities obtained by the GC-MS in SIM mode for the TMS molecular ions (brassicasterol and 24-methylenecholesterol: *m/z* 470) (Figure 2.8). For the rest of sterols, signal intensities were obtained in SIM mode of selected ion fragments (desmosterol: *m/z* 343; campesterol: *m/z* 382; β-sitosterol: *m/z* 396) and molecular mass of dinosterol: *m/z* 500 (Figures 2.9; 2.10) and relative values were calculated (Table 2.4) due to unavailable authentic compounds which made it not possible to calculate the respective response factors. Quantification of the sterols was achieved with equation 7. Relative elution order of the sterols analysed here are shown in Figure 2.11, which is the partial chromatogram of a sediment extract from the CAA.

Equation 7

$$Sterol\ (\mu g\ g^{-1}) = \frac{\frac{Pa\ (sterols)}{Pa\ IS}}{g\ sediment}\ x\ Rf\ x\ M_{IS}$$

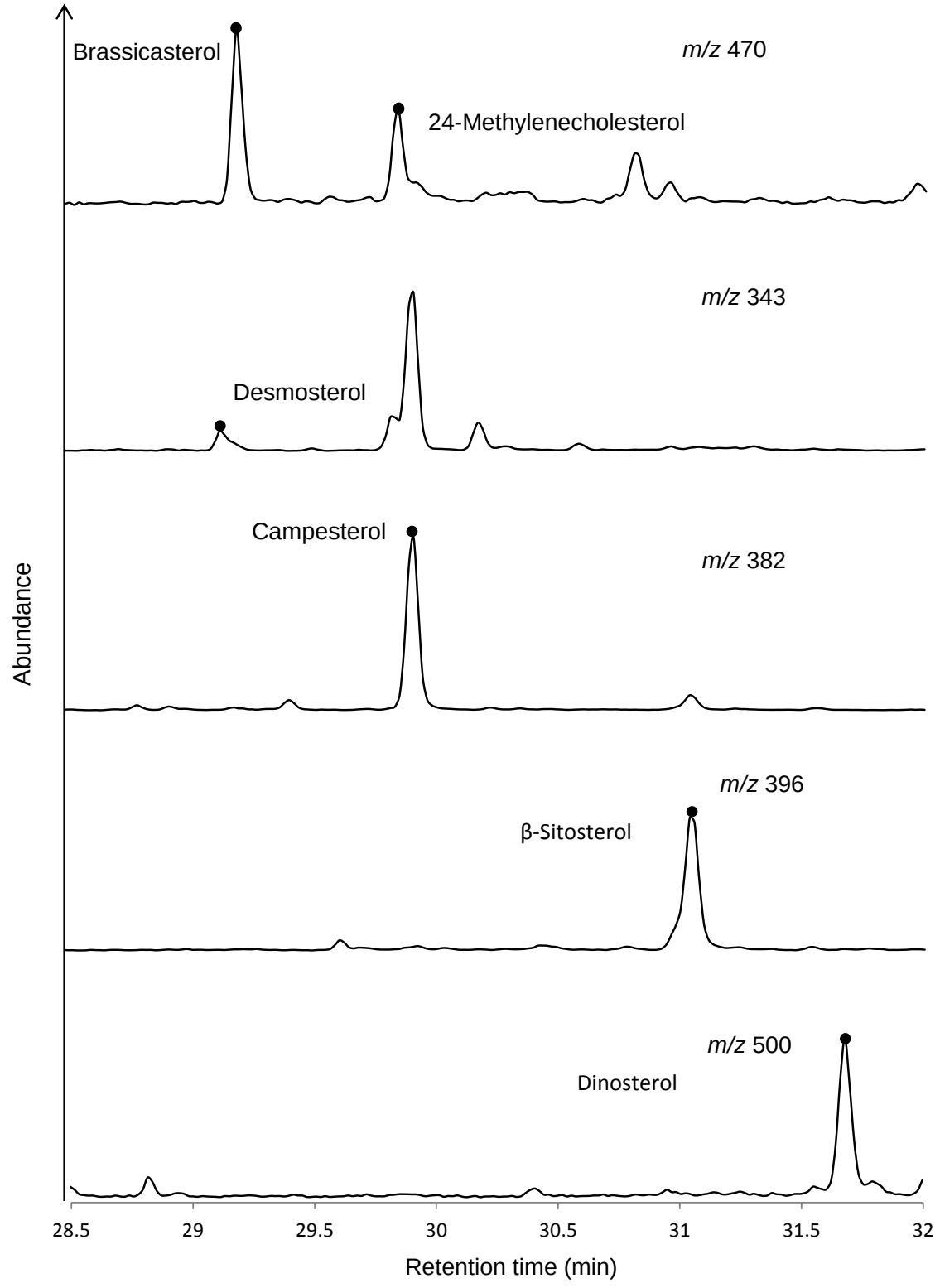

Fig 2.11 Partial GC-MS chromatograms (SIM *m/z* 470, 343, 382, 396, 500) of the reference sediment from Franklin Bay, Canadian Arctic Archipelago (CAA) St 428 showing the relative elution order of the the trimethylsilyl (TMS) sterol ethers studied here.

Calculation of the response factor for TMS brassicasterol was obtained from calibration curves of (0.0004 mg mL^{-1}; 0.0006 mg mL^{-1}; 0.0008 mg mL^{-1}; 0.001 mg mL^{-1}; 0.002 mg mL^{-1}; 0.004 mg mL^{-1} R^2= 0.99) against the TMS internal standard (5α-androstanol-3β-ol) of equal concentrations.

Table 2.4 Calculation steps and data required for the quantification of sterols in a reference marine sediment. Peak areas correspond to the chromatogram Figure 2.9 (g of dry sediment =). MIS =0.01 µg. Sterol concentrations expressed in (µg g^{-1}).

HBI	*Pa (sterols)*	*Pa (IS) Androstanol*	*RF**	$\frac{Pa\ (sterols)}{\frac{Pa\ IS}{g\ sediment}}$	$\frac{Pa\ (sterols)}{\frac{Pa\ IS}{g\ sediment}} xRfx\ M_{IS}$
SI	122966	1976390	32	0.086	0.276
SII	56127	1976390	32	0.039	0.126
SIII	129203	1976390	-	0.091	-
SIV	887590.5	1976390	-	0.623	-
SV	603915	1976390	-	0.424	-
SVI	59438.5	1976390	-	0.042	-

Sterol concentrations were also routinely normalised to TOC (Equation 3) and occasionally expressed as fluxes for down core analysis (Equation 6).

2.3 Additional methodology

Additional methodology was required in some cases when the identification of IP_{25} was difficult, due either to low concentrations or co-eluting compounds. In some cases, undesired highly abundant compounds were also extracted which prevented concentration of the samples. The most common and identified compound (NIST SM Search 2.0) in this study was elemental sulfur (*m/z* 256, 98% match spectrum probability) (Figure 2.12) which in some cases was visible as large crystals in the TOEs. Elemental sulfur has a very similar elution time to IP_{25} and is not removed through the general extraction and purification method.

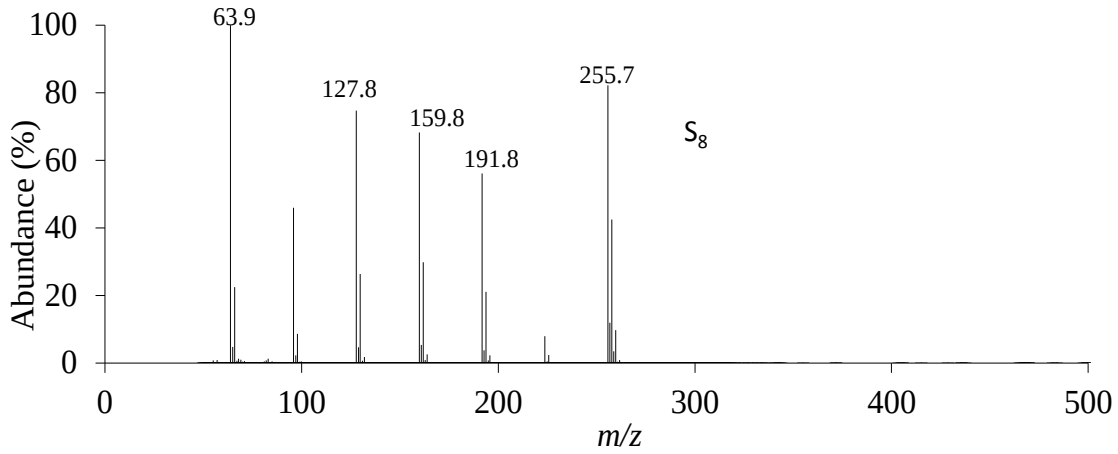

Figure 2.12 Mass spectrum of sulfur obtained from environmental sample.

2.3.1 Sulfur removal

Sulfur removal was conducted following the method described in Jensen et al. (1977), slightly modified for the purposes of this study. This procedure is a non-destructive method to remove sulfur from natural samples following the reaction below. Preparation of the following stock solution was required: tetrabutylamonium hydrogen sulphate (TBA- sulphite reagent) 3.39 g was weighted in an Erlenmeyer flask, followed by the addition of 100 mL of high purity water (HPW) and the subsequent addition of 25 g of sodium sulfite. Solutions were shaken vigorously until dissolution (all reagents were Merck analytical grade).

$$(TBA^{+})_2SO_3^{\,2} + S_{(s)} \quad \rightleftharpoons \quad 2TBA^{+} + S_2O_3^{\,2-}$$

The TOE from the marine sediments was dried in a 7 mL glass vial, was re-dissolved with 1 mL hexane. After which 1 mL of TBA sulphite reagent (previously prepared) and 1 mL of 2-propanol were then added. The vial was capped with an aluminium lined propylene screw cap and shaken for 1 min in a vortex followed by the addition of 3 mL

of HPW and shaken again vigorously. The sample was then centrifuged (2500 rpm; 2 min). The distinction of the two phases was visible, aqueous phase underneath, and organic phase (hexane) above. The hexane layer was decanted by pipetting carefully to another 7 mL neutral glass vial. This process was repeated 2 more times to allow complete removal of sulfur. The hexane fraction was then evaporated with a slow stream of N_2 at 25º C. Samples were then ready for the continuation of the general extraction process.

An investigation of the possible differences in HBI concentrations before and after removal of elemental sulfur was carried out (Cabedo-Sanz, 2013). A sediment with known presence of sulfur was re-analysed after sulfur removal, to see if the overload of the detector with the elemental sulfur could interfere or diminish the detection of the desired analytes i.e. IP_{25} and diene II (*m/z* 350.3, 348.3) with very similar retention times. Results showed less than 10% loss for IP_{25} and diene II and up to 6% and 20% increase for triene IIIa and IIIb respectively. These results are comparable to the analytical reproducibility of the reference sediment calculated here which is very similar (15%; Chapter 7).

2.3.2 Solid phase extraction (silver ion)

In some cases where the identification of IP_{25} by GC-MS was complicated, due to either low concentrations of the biomarker or unknown co-elutant / high background noise, a further purification of the samples was required. Samples were purified using silver ion solid-phase extraction cartridges (SPE) Agilent Supelco ® Ag-Ion. The cartridges are formed by a stationary phase containing silica gel (irregularly shaped) and an active matrix, which in this case, was benzenesulfonic acid bonded polymerically to the silica gel and coated with Ag-Ion. The interactions taking place are between the negative

density charge of the double bound (π) and the silver ion cationic charge. A schematic figure of this interaction is shown in Figure 2.13.

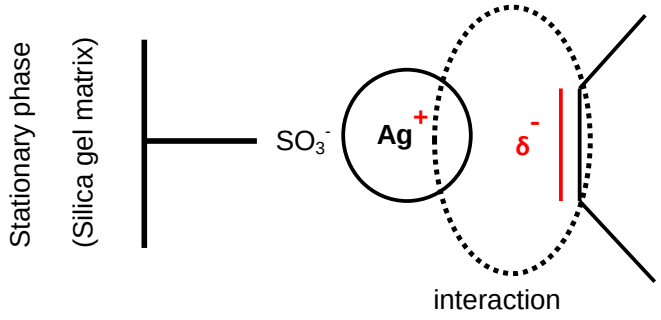

Figure 2.13 Schematic figure of the interactions occurring into the cartridges (SPE) Agilent Supelco ® Ag-Ion between the stationary phase and a double bond

Various purification methods were developed according to the needs of the analysis. The first method was developed to obtain IP_{25} and the internal standard 9-OHD in a unique (monounsaturated) fraction. For this method (Figure 2.14), the eluents used for conditioning were 5 column volumes of acetone, followed by 5 column volumes of hexane. The samples (partially purified hexane extracts, THE) were introduced into the cartridges (Supelco discovery ® Ag-Ion) diluted in ca. 100 µL hexane. Elution with 6 column volumes of hexane followed by 6 of DCM allowed collection of the saturated hydrocarbons. A mixture of 95/5 % DCM/acetone; (10 column volumes) recovered the unsaturated fraction containing (IP_{25} and 9-OHD), recovering the rest of the unsaturated compounds with 5 column volumes of acetone. The DCM/acetone fraction was then dried under N_2 and diluted in hexane (ca. 20 µL in Chromacol 300 µL vials) for analysis by GC-MS in high sensitivity instrumental method (detailed in section 2.4)

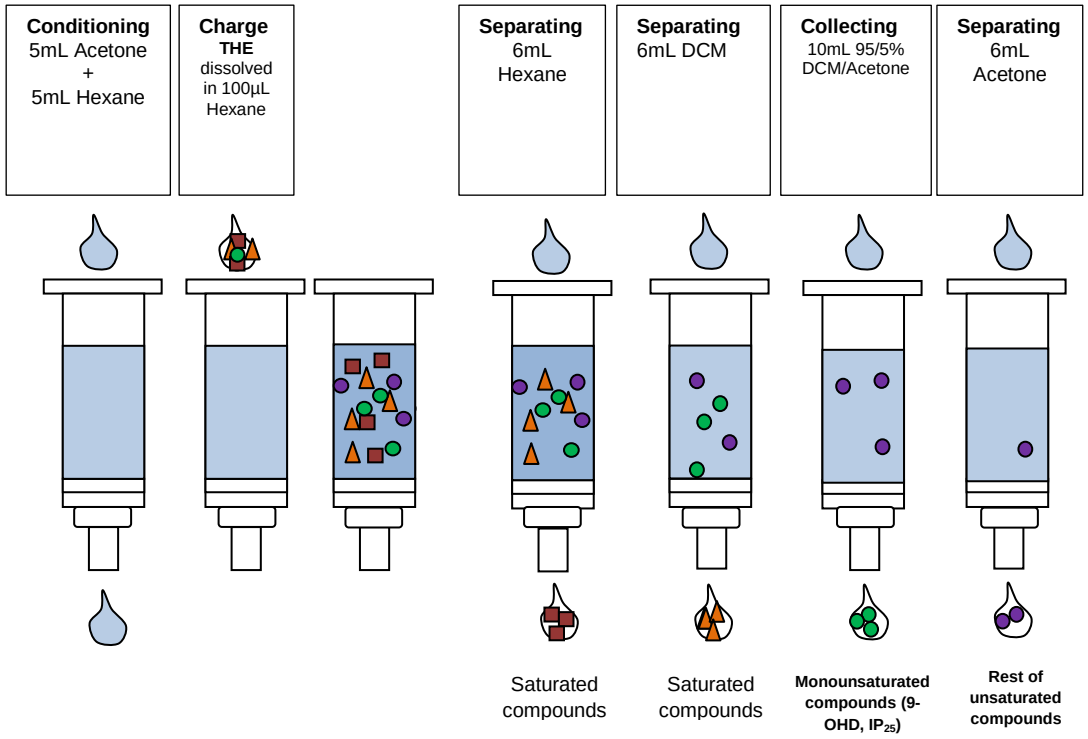

Figure 2.14 Schematic figure of the solid phase extraction procedure with silver ion cartridges. Elution of IP_{25} was conducted with 95/5 % DCM/acetone.

After the Ag-Ion purification, the abundance of the total ion current in the chromatograms clearly diminished (Figure 2.15; red line). A chromatogram of a sediment sample extracted with the normal procedure (SiO_2 partial purification), and the same sample processed with silver ion cartridges are shown in Figure 2.16 b. The identification of the *m/z* 350.3 peak at the specific retention time in the sample purified with Ag-ion SPE was clearly observed, which was visible after the removal of other compounds (alkanes) increasing the abundance of the base line. In addition to the extraction method (laboratory), an instrumental method was developed (GC-MS), changing the settings in the injection mode and in the MSD to increase sensibility of the detection of IP_{25}, see section 2.4.

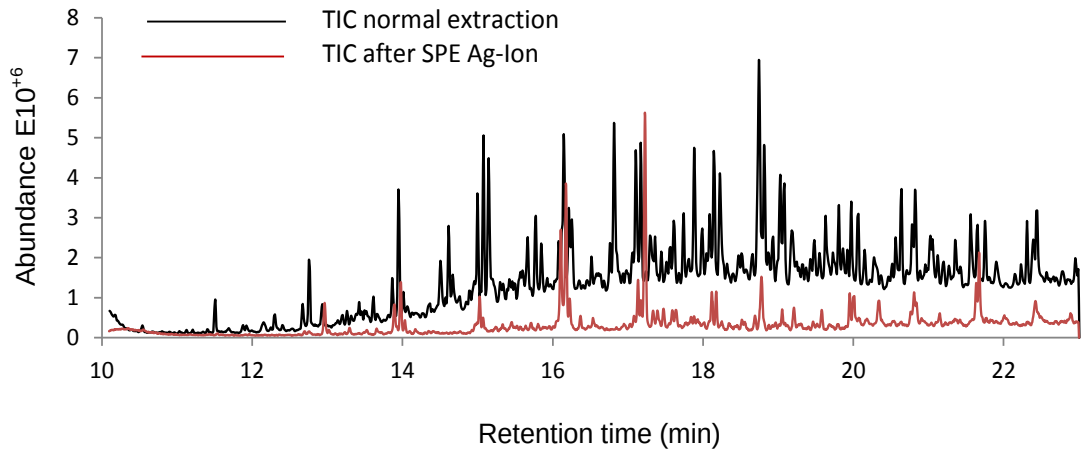

Figure 2.15 Environmental sample extracted and purified with SiO_2 open column chromatography. TIC chromatogram before and after silver ion purification.

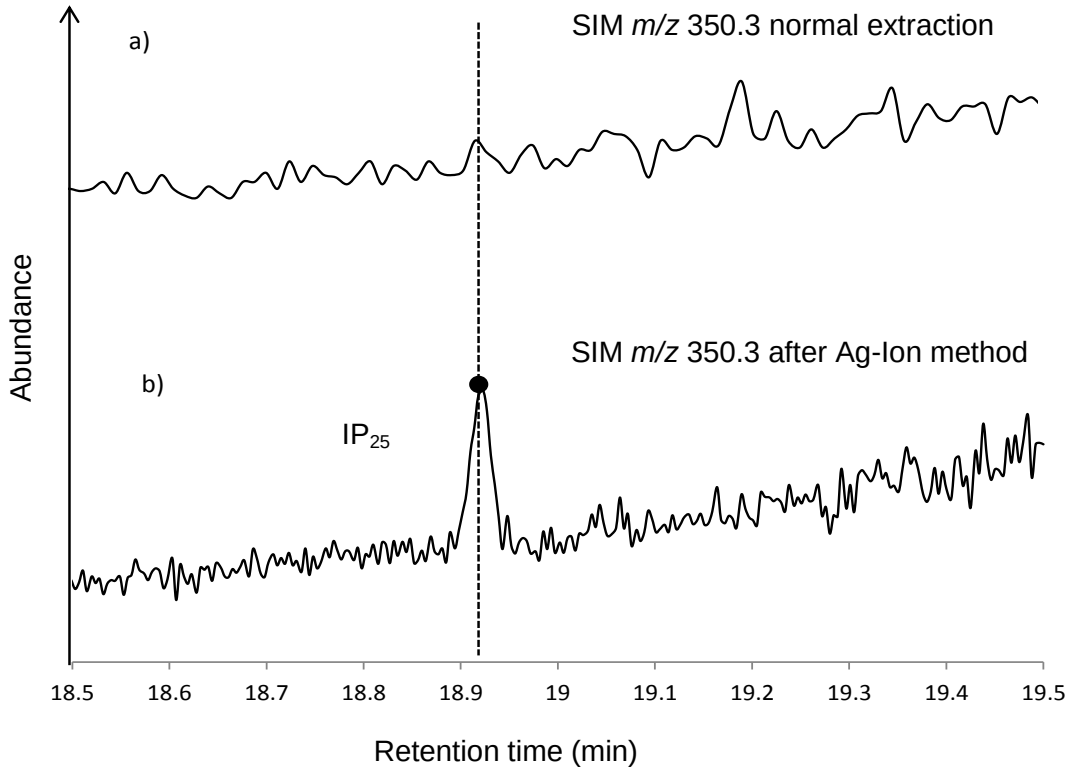

Figure 2.16 Partial chromatogram (SIM *m/z* 350.3) for a sediment sample where IP_{25} was not detectable with normal extraction method a); and after the solid phase extraction Ag-ion purification (DCM/Acetone) with High Sensitivity instrumental method b), see section 2.4.

A variation in the eluents used in the SPE method was made to collect a wider range of unsaturated compounds in the same fraction (IP_{25}, 9-OHD, diene II and trienes IIIa and IIIb) (Figure 2.17). The cartridges were replaced by Ag-Ion columns made in the

laboratory, since the Ag-Ion stationary phase was cheaper and more reliable than the cartridges. Therefore ca. 500 mg of stationary phase was placed into a pipette pasteur previously plugged with DCM cleaned cotton wool (proceeding similarly to the SiO_2 columns). For this purpose 5 mL of acetone and 5 mL of DCM were used for the conditioning. The sample, partial purified hexane extracts, was diluted in ca. 100 µL of DCM and introduced in the column. The separation was conducted with 6 mL of DCM (to collect saturated compounds) and 6 mL of acetone (to collect the unsaturated compounds).

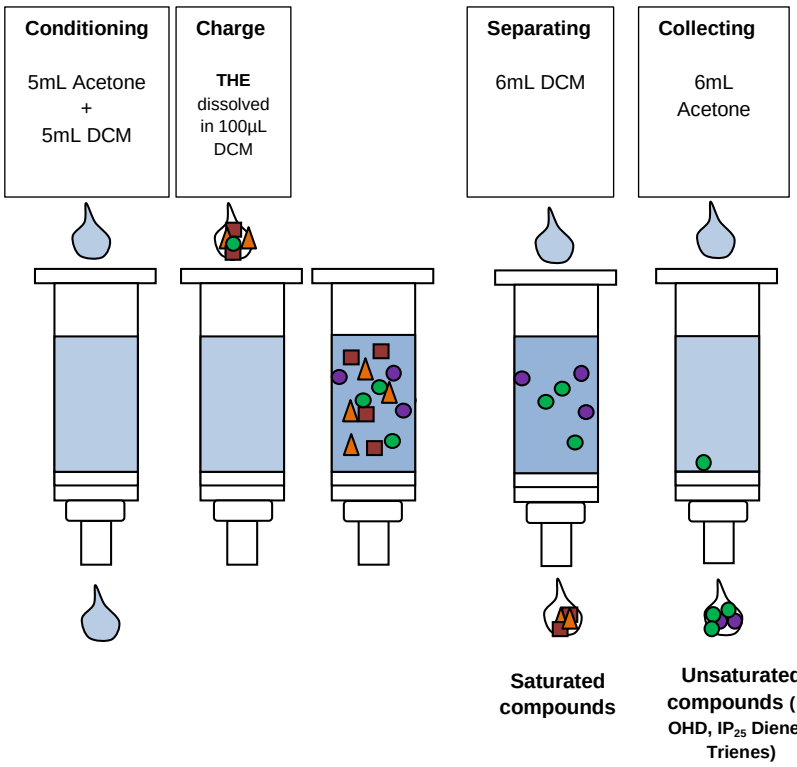

Figure 2.17 Schematic figure of the solid phase extraction procedure with silver ion cartridges. Elution of IP_{25} was conducted with 6 mL acetone.

Samples were dried under N_2 stream and diluted into 20 µL hexane in Chromacol 300 µL vials for GC-MS analysis in high sensitivity method. A chromatogram of a sediment sample treated with this method is shown in Figure 2.18.

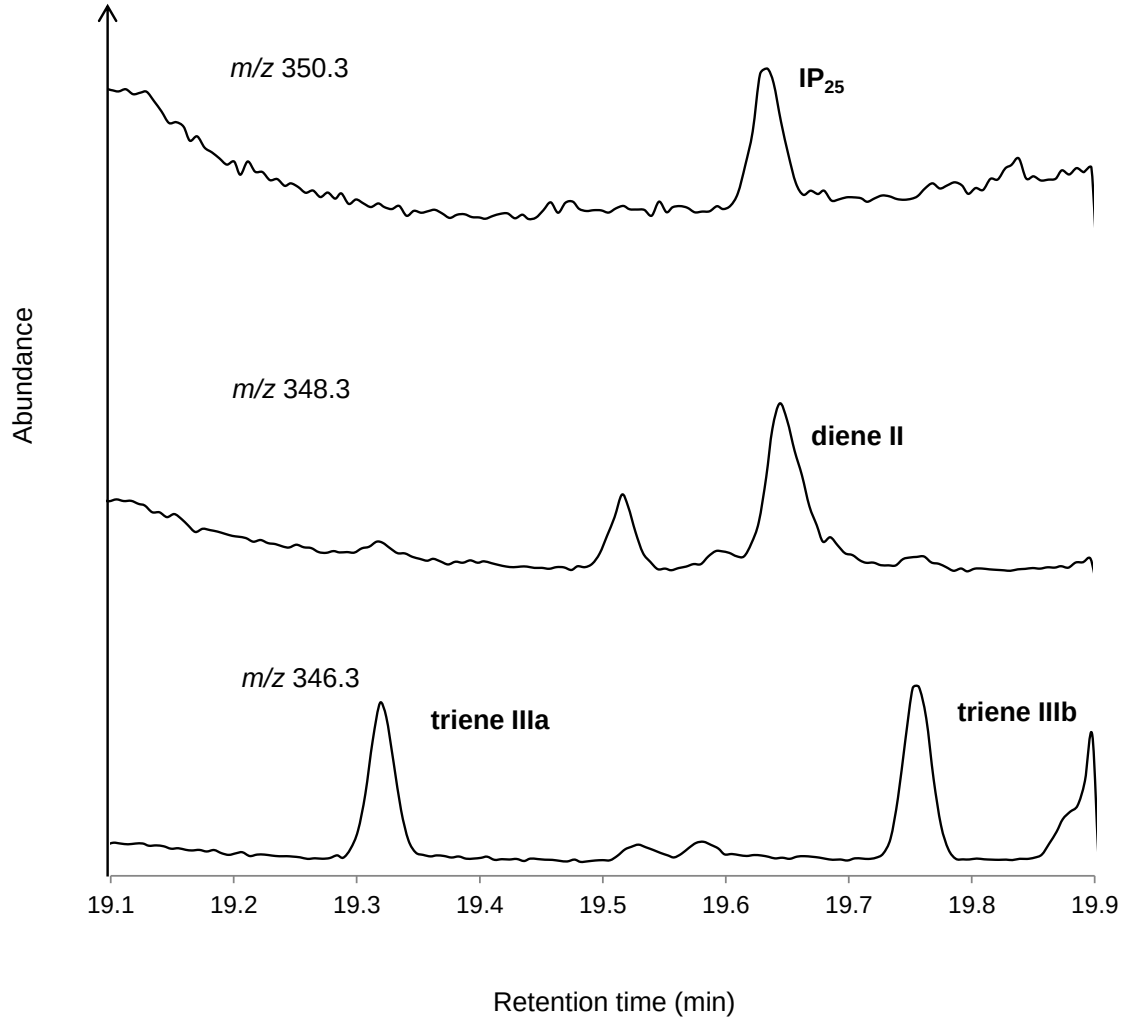

Figure 2.18 Partial SIM chromatograms for the HBI (window elution) after the Ag Ion purification method collecting all HBIs in the acetone fraction e.g. Mareano bulk extraction sample HH11-134-BC (Chapter 5).

A further development was conducted to obtain an optimum separation of the compounds achieved with the most economic option. The amount of stationary phase was reduced to ca. 100 mg (Figure 2.19). The conditioning was conducted with 5 mL of acetone followed by 5 ml of hexane. The sample was introduced to the column diluted in ca 100 µL of hexane. Elution with 1 mL of hexane was followed by elution with 2 mL of acetone to recover the unsaturated fraction containing (IP_{25}, 9-OHD, diene II and trienes IIIa and IIIb). Chromatograms of the acetone fraction and concentrations of

HBIs before and after this Ag-Ion purification method showed good recovery of the compounds of interest (Cabedo-Sanz 2013).

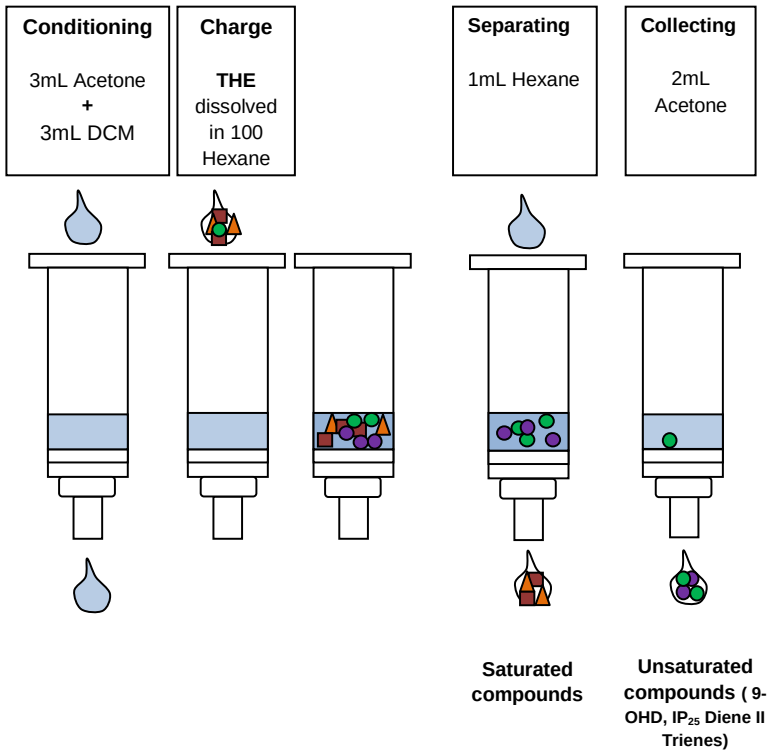

Figure 2.19 Schematic figure of the solid phase extraction procedure with 100 mg silver ion solid phase. Elution of IP_{25} was conducted with 2 mL acetone.

2.4 GC-MS instrumental method development

In order to increase the sensitivity of the detection of IP_{25}, a new instrumental method was developed. HBI SIM-SCAN regular was the method developed for normal extraction enabling to obtain a first vision of the composition of the extract in TIC and SIM for identification of analytes of interest. When the analytes of interest were not detectable in this method, another method (HBI SIM-SCAN high sensitivity) was used which included some new features in the inlet and MSD (Table 2.5) in order to allow a more efficient detection.

Table 2.5 Main settings for the various methods developed in the GC-MS and detailed inlet settings. RF* had to be calibrated over time, see Chapter 3.

MAIN FEATURES (GC-MS)			
Method	**HBI SIM-SCAN REGULAR**	**HBI SIM-SCAN IP_{25} HIGH SENSITIVITY**	**HBI SIM-SCAN IP_{25} HIGH SENSITIVITY (I)**
Function	Routine HBI detection	Increased sensitivity for IP_{25} only	Increased sensitivity for IP_{25} only
Mass range (*m/z*)	50-500	50-500 (18-20 min =90-360)	90-360
SIM ions (*m/z*)	350.3, 348.3 346.3, 99	350.3	350.3
Total run time	36 min	36 min	36 min
GC Temperature profile	40 °C – 300 °C at 10 °C min^{-1} (10 min isothermal)	40 °C – 300 °C at 10 °C min^{-1} (10 min isothermal)	40 °C – 300 °C at 10 °C min^{-1} (10 min isothermal)
Detection time	10-26 min	10-25 min	18.5-19.5 min
RF*	5.03	4.72	4.72
INLET (SPLITLESS)			
Injection	1µL	1µL	1µL
(Temperature and pressure)	300 °C 0.4874 bar	300 °C 0.3972 bar	300 °C 0.3972 bar
Purge flow	100 mL min^{-1} 0.5 min	100 mL min^{-1} 0.35 min	100 mL min^{-1} 0.35 min
Total flow	104 mL min^{-1}	104 mL min^{-1}	104 mL min^{-1}
Gas saver	3 mL min^{-1}	3 mL min^{-1}	3 mL min^{-1}
Injection pulse pressure	-	25 psi 0.35 min	25 psi 0.35 min

The injection was conducted in auto-splitless mode which is designed for low volume and concentration of samples to allow the maximum volume of the mixture sample and carrier solvent to get introduced into the column by avoiding the split vent which removes most of the sample volume. 1 µL of sample is introduced into the inlet (300 °C, 7.0699 psi). The purge flow to split vent was set up at 100 mL min^{-1} for 0.5 min. For the high sensitivity method, an injection pulse pressure was included with the

purpose of allowing rapid transport of the volatilised sample from the inlet in the column.

2.5 Combined biomarker indices

2.5.1 PIP_{25} index

Calculation of P_BIP_{25} values was performed according to the method of Müller et al. (2011) using equation 8, where IP_{25} and P represent the concentrations of IP_{25} and the phytoplankton biomarker respectively. The *c* term is included to compensate for the significantly higher concentrations of the phytoplankton biomarkers compared to IP_{25} and corresponds to the ratio of the mean concentrations of the two biomarkers across all sediments under study (Müller et al., 2011).

$$PIP_{25} = IP_{25} / (IP_{25} + (P \times c)) \quad \text{(Eq. 8)}$$

2.5.2 DIP_{25}

DIP_{25} ratios were calculated as previously described in Cabedo-Sanz et al. (2013) Equation 9, where Pa corresponds to peak area. In order to evaluate the potential relationship between diene II and IP_{25} (DIP_{25}), relative abundances (GC-MS responses) were obtained by integration of the peaks corresponding to the molecular ions from the SIM chromatograms. Further ratios were calculated with the available lipid biomarkers trienes *IIIa* and *IIIb* (Chapter 5). The correlation between the trienes *IIIa* and *IIIb* was calculated in the same way as the DIP_{25} (Table 5.3) and relative abundances of the molecular ions (*m/z* 346.3) of both trienes were plotted together. For the calculation of ratios, peak areas were used rather than concentrations of the biomarkers. This was due to the fact that for the calculation of concentrations requires an instrument specific

response and this might vary between MS instruments. Results were normalized, where all peak areas were divided by the maximum value of one of the parameters plotted.

$$DIP_{25} = \frac{P_A\ diene\ II}{P_A\ IP_{25}}$$

(Eq. 9)

CHAPTER THREE

3 Extraction and isolation of IP_{25}

3.1 Introduction

This chapter contains the description of the isolation of the highly branched isoprenoid (HBI) monoene alkene IP_{25} from marine sediments. Additional purification, identification (GC-MS) and structural characterisation by ^{1}H and ^{13}C NMR spectroscopy were conducted.

The aim of this work was to obtain IP_{25} in enough quantities for calibration purposes replacing the tedious synthesis process from its related diene (Belt et al., 2007). To achieve this goal, a pilot experiment was conducted. Marine sediments from the Canadian Arctic Archipelago, see Belt et al. (2012a) were chosen for this experiment previously knowing that IP_{25} was present, besides being in reasonable concentrations (Belt et al., 2010; Vare et al., 2009), and appropriate for extraction, making sure to obtain a good extraction yield. For this purpose, a series of 4 soxhlet systems was arranged. After proving the success of the pilot experiment, a large scale extraction was carried out, details of the procedures are explained in this section.

Once the structural determination was confirmed via comparison with that of the synthetic compound, a calibration with the extract (IP_{25}) purified from natural sources was carried out. From this calibration were determined the response factor values for the quantification of IP_{25}.

3.1 Extraction procedure

3.1.1 Pilot experiment

Four soxhlet systems (Figure 3.1) were connected in a fume cupboard for the extraction of the marine sediment material. Ca. 50 grams was placed in each paper thimble and topped gently with DCM-cleaned cotton wool. Soxhlet borosilicate glass tubes were then half filled with hexane and sediment extracted (50 º C; 24 h).

Figure 3.1 Soxhlet system used for the extraction of IP_{25} from sediment material from the Canadian Arctic Archipelago (CAA).

3.1.2 Large scale experiment

Proving successfully this pilot method of extraction of IP_{25} from marine sediments, it was developed a series of bulk extractions of ca. 3 kg sediment per batch (ca. 16 kg total) (Figure 3.2). Sediment was placed in a 10L rounded bottomed flask with a stirring device to which 5 L of hexane were added (72 h / 50 ºC) for the extraction. The remaining sediment, after decanting the hexane suspension, was rinsed 3 times with hexane for a better collection of the organic extracts, and vacuum pressure filtered using Buchner filtration.

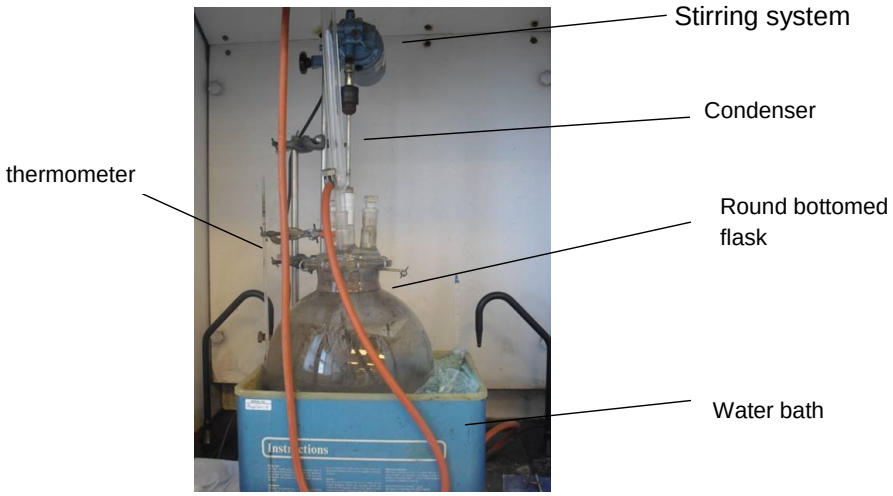

Figure 3.2 Large scale sediment extraction of IP_{25} from marine sediments from the Canadian Arctic Archipelago (CAA).

3.2 Purification

Total organic extracts from individual experiments were dried in a rota-evaporator (Büchi; 25 ºC), combined and transferred to glass vials after which several purification steps were conducted.

3.2.1 SiO_2 and Ag-Ion chromatography

Once the extracts were collected, purification with open silica columns (SiO_2) (Chapter 2 section 2.2.4) was carried out (ca. 1 mg of the total extracts per column). Further purification process using (SPE) cartridges (Supelco® Discovery Ag-Ion 750 mg 6 mL) was also conducted to obtain higher purity for calibration purposes. The conditioning of the columns was conducted with acetone/DCM (5 column volumes), of each solvent followed by the introduction of the sample (diluted in DCM, 0.5 mL) and eluted with 5 column volumes of DCM and acetone collecting the saturated and unsaturated different fractions respectively in different 7 mL vials. At this point checking the purity achieved

so far, was checked by GC-MS (instrumental setting described in Chapter 2, Table 2.5) as a result it was decided to add other purification steps, using high performance liquid chromatography (HPLC) due to some impurities still being present in the sample.

3.2.2 HPLC chromatography

The instrument used was an Agilent 1100 series high performance liquid chromatography (HPLC) system fitted with a Varian ChromSpher 5 Lipids (250 x 4.6 mm ID) Ag-Ion column. Specific HPLC gradient conditions were: 100% DCM (0-5 min), 100% DCM to 100% acetone (5-10 min), 100% acetone (10-15 min). Before the application of this method to the organic extracts, it was tested with a small fraction. The elution of IP_{25} within the mobile phase gradient was determined by collecting manually individual fractions at 1 min intervals. Each minute fraction was analysed by gas chromatography – mass spectrometry (GC-MS), revealing that IP_{25} was eluted between 100% DCM and 95:5 DCM: acetone. The individual fractions of interest containing IP_{25} were combined together for GC-MS analysis. The process is described in Figure 3.3.

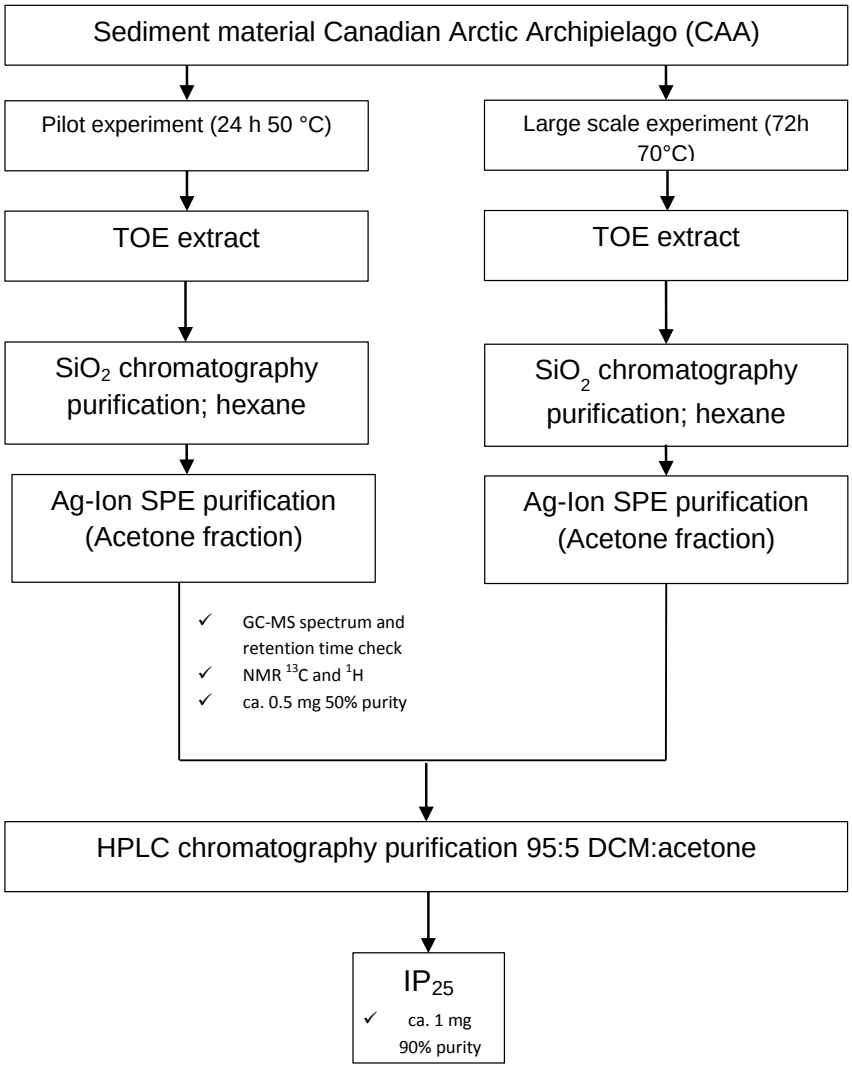

Figure 3.3 Diagram representing the laboratory procedure and analytical techniques used carried out for the isolation and purification and characterisation of IP_{25} from marine sediments

3.3 Structural confirmation

The mass spectra obtained for the compound IP_{25} synthesized under natural conditions by diatoms and extracted from marine sediments was the same that the spectrum of IP_{25} synthesised in the laboratory (from the relative diene). This is described in more detail in Belt et al. (2007), Figure 3.4.

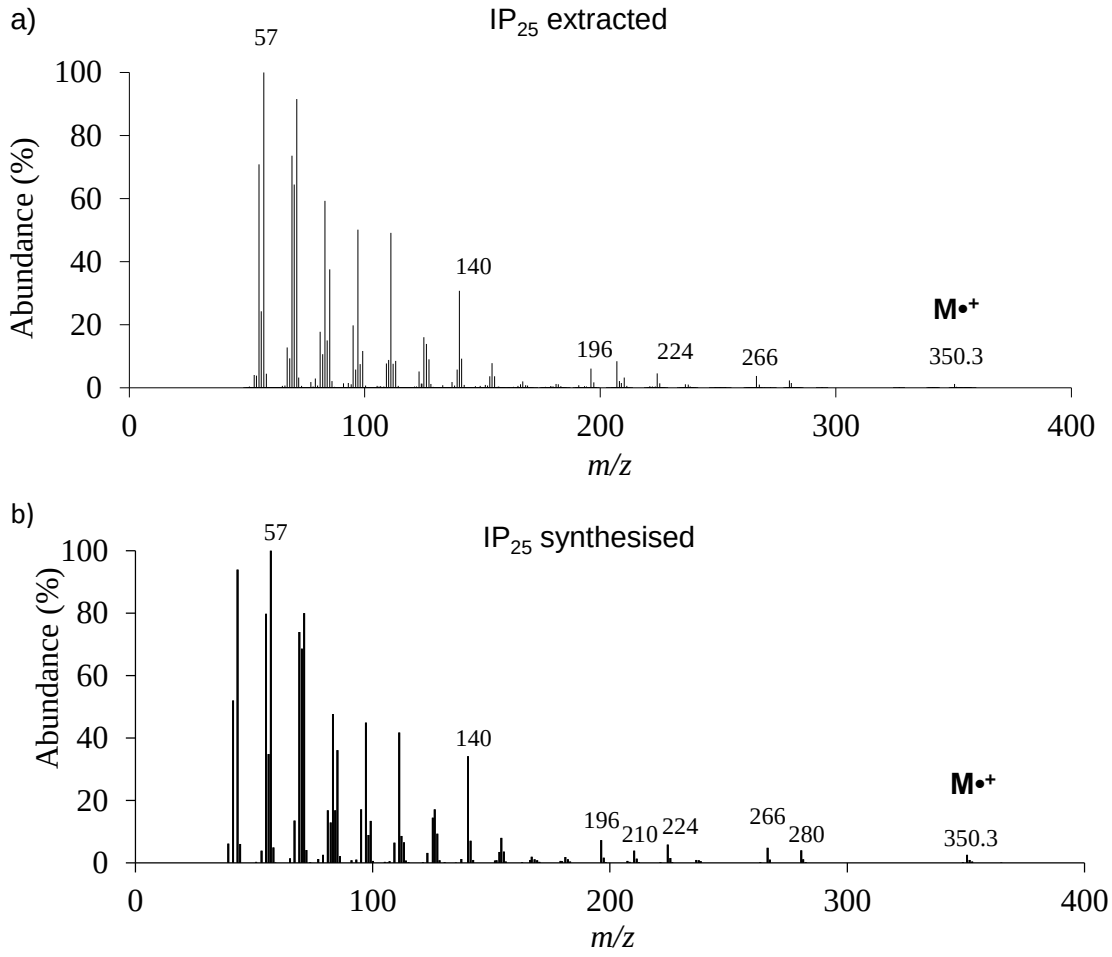

Figure 3.4 Mass spectra for IP_{25} extracted from marine sediments a) and b) synthesised in the laboratory.

3.4 Characterisation by NMR spectroscopy

The purity of IP_{25} was determined by ^{1}H and ^{13}C NMR spectroscopy (JEOL ECP-400 NMR spectrometer). The results revealed that the approximate purity of the compound was between 50-90 %, depending on the original sediment. Chemical shifts were measured relative to those of the solvent ($CDCl_3$; ^{1}H: 7.24 ppm; ^{13}C: 77.0 ppm; Table 3.1. NMR) analysis and interpretation was carried out by Prof. Simon T. Belt.

Table 3.1 ^{1}H ^{13}C NMR spectral data for IP_{25} isolated from the Canadian Arctic Archipelago marine sediments.

Carbon number	Carbon shift (/ ppm)	Proton number	Proton shift (/ ppm)
1 (16) [a]	22.71 , 22.78	1, 15, 16, 19	0.85 (12H, d, J = 7.3Hz)
2[b]	28.03, 28.06	17	0.74 (3H, d, J = 6.9Hz)
3	39.44	18	0.82 (3H, d, J = 6.9Hz)
4	25.61	23	5.67 (1H, ddd, J=17.6, 10.3, 7.7 Hz)
5	35.48	24	4.91 (2H, m)
6	34.36	25	0.96 (3H, d, J = 6.9Hz)
7	42.70		
8	29.76		
9	34.96		
10	33.22		
11	37.47		
12	24.80		
13	39.44		
14[b]	28.03, 28.06		
15 (19)[a]	22.71. 22.78		
17	15.52		
18	19.83		
20	29.76		
21	34.44		
22	38.22		
23	145.11		
24	112.32		
25	20.45		

3.5 Calibration

Calculation of the RF was conducted by measuring the abundance of the HBI molecular ions (*m/z* 350.3; 348.3; 346.3) against the abundance of (*m/z* 350.3 of the internal standard 9-OHD) at increasing concentrations on a calibration curve (Figure 3.5). They were also measured using different instrumental methods which imply different settings on the MSD (Chapter 2) in order to investigate the impact of the instrumental changes on the respective response factors.

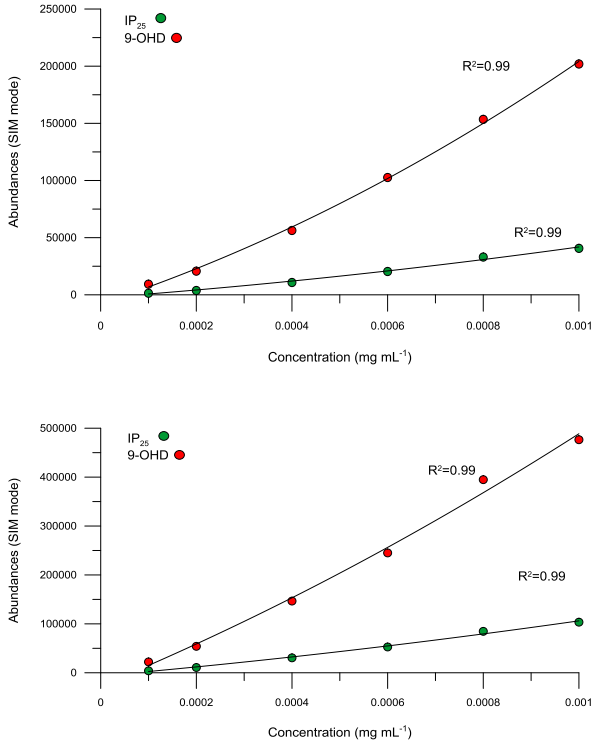

Figure 3.5 Calibration of 9-OHD and IP_{25} for the corresponding concentrations mg mL^{-1}. Peak areas in SIM mode of the ion *m/z* 350.3 for: a) the standard method (50-500) and b) the high sensitivity method (scan range (90-360).

Slight changes were observed in the RF for IP_{25} and 9-OHD obtained from the two instrumental methods i.e. Standard method (RF= 5.03 ± 0.28) and High Sensitivity method (RF= 4.72 ± 0.14). These results showed that individual instrumental methods need to be calibrated in order to provide accurate quantification. The calculation of the RF was performed by obtaining the mean of the RF calculated for individual concentrations of the calibration curve. By proceeding this way, the variation of the RF with respect to different concentrations was assessed, showing little variation. However, it an RF increase was observed for the lowest calibration point (close to the limit of detection) with respect to the other calibration points, and it was decided to exclude it from the mean RF calculation (Table 3.2).

The response factor was similarly calculated using both instrumental methods for the other HBIs of interest i.e. diene II (*m/z* 348.3) and trienes IIIa and IIIb (*m/z* 346.3)

against the abundance of *m/z* 350.3 of the internal standard 9-OHD at increasing known concentrations on a calibration curve.

The response factor was re-calculated after a period of time for IP_{25}, observing certain fluctuations, from which it was calculated more regularly (Table 3.2 and Table 3.3), including both instrumental methods and HBI lipids. Routinely calibrations of the instrument were highly recommended in order to report changes in the sensibility of the MSD detector.

Table 3.2 Response factor for IP_{25} and 9-OHD are indicated for the instrumental methods (Standard and High sensitivity) in SIM mode for different periods (2011-2013).* values excluded

Date	October 2011	January 2013	July 2013	December 2011	January 2013	July 2013
GC-MS Method	Standard	Standard	Standard	High-sensitivity	High-sensitivity	High-sensitivity
Concentration (mg mL^{-1})	RF	RF	RF	RF	RF	RF
0.0001	6.26*	7.47*	nd	5.35*	nd	nd
0.0002	5.38	7.23	5.26	4.94	5.15	5.57
0.0004	5.19	6.97	5.65	4.78	5.34	6.05
0.0006	5.01	6.65	4.99	4.63	4.96	5.32
0.0008	4.63	6.73	5.16	4.65	5.42	5.55
0.001	4.96	6.54	5.07	4.60	5.48	5.7
Average	**5.03**	**6.82**	**5.22**	**4.72**	**5.27**	**5.64**
SD	0.28	0.28	0.26	0.14	0.21	0.27
RSD (%)	5.54	4.10	4.89	2.94	3.99	4.76

Table 3.3 Response factor calculations for diene II and 9-OHD, and for trienes IIIa and IIIb and 9-OHD (Cabedo-Sanz, 2013). Calibrations were conducted in October 2011; January and July 2013.

Date	October 2011	January 2013	July 2013	December 2011	January 2013	July 2013
GC-MS Method	Standard	Standard	Standard	High-sensitivity	High-sensitivity	High-sensitivity
Diene II concentration (mg mL^{-1})	RF	RF	RF	RF	RF	RF
0.0001	nd	14.49	8.92	nd	15.69	7.24
0.0002	11.89	14.28	8.50	nd	15.71	7.66
0.0004	nd	nd	nd	nd	nd	nd
0.0005	11.05	nd	nd	nd	nd	nd
0.0006	nd	15.33	9.73	nd	13.77	7.84
0.0008	11.07	15.46	9.09	nd	13.56	7.86
0.001	11.14	14.01	9.70	nd	13.12	8.19
Average	**11.29**	**14.71**	**9.19**	nd	**14.37**	**7.76**
SD	0.40	0.65	0.53	nd	1.15	0.22
RSD (%)	3.57	4.40	5.73	nd	7.98	2.81
Date	October 2011	January 2013	July 2013	December 2011	January 2013	July 2013
GC-MS Method	Standard	Standard	Standard	High-sensitivity	High-sensitivity	High-sensitivity
Triene IIIa and IIIb concentration (mg mL^{-1})	RF	RF	RF	RF	RF	RF
0.0001	nd	1.58	1.00	nd	1.61	0.96
0.0002	nd	1.68	0.97	nd	1.66	0.94
0.0004	nd	1.71	1.00	nd	1.64	0.88
0.0006	nd	1.89	1.02	nd	1.64	0.93
0.0008	nd	2.01	1.00	nd	1.68	0.95
0.001	nd	2.05	1.22	nd	1.69	1.06
Average	nd	**1.82**	**1.04**	nd	**1.65**	**0.95**
SD	nd	0.19	0.09	nd	0.03	0.06
RSD (%)	nd	10.47	8.93	nd	1.71	6.39

3.6 Results and discussion

The extraction of IP_{25} from marine sediments (environmental samples) was successfully conducted providing structural determination of the compound with previously obtained spectra from the synthesized compound. Further characterisation techniques (^{1}H and ^{13}C NMR spectroscopy) confirmed the structure. This work represented an improvement in the analytical and instrumental procedure for IP_{25} analysis, which in future will provide more reliable data. The isolated and purified IP_{25} was kept for calibration purposes.

From the calibration study it was concluded that the RF was sensitive to time, and instrumental calibrations were recommended to be conducted approximately every 4 months.

CHAPTER FOUR

4 An investigation of IP_{25} and other biomarkers in surface sediments from the Barents Sea

4.1 Introduction

Recent sea ice / open water conditions in Arctic marine systems can be determined by satellite data. Complementary analysis of biomarkers in surface sediments potentially facilitates the subsequent comparison and calibration with satellite records, thus improving the reliability of interpretations of biomarker-based proxy data with regard to environmental and climatic conditions. The outcomes of this calibrated approach can then be applied to longer timescales, up to and including, the present interglacial, for example, in order to derive oceanographic and sea ice conditions in the past.

One important region for carrying out sea ice reconstruction studies is the Barents Sea since it is particularly sensitive to reductions in sea ice cover during polar amplification of global warming (IPCC, 2007). Further, the Barents Sea has attracted a considerable number of investigations studying the relationships between Arctic food webs and sea ice cover (e.g. Falk-Petersen et al., 2000; Reigstad et al., 2008; Wexels Riser et al., 2008), not least since this is one of the most productive regions of the Arctic (Wassmann et al., 2006). Previously, the Marine AREal Database for NOrwegian Waters (MAREANO) programme (2005 - 2010) was undertaken to provide a comprehensive map of the physical, chemical and biological characteristics of the sea bed for the Western Barents Sea (Knies, 2009; Thorsnes, 2009) and a range of biological proxy data (e.g. dinocysts assemblages; Grøsfjeld et al., 2009; Solignac et al., 2009), organic matter composition (Knies and Martinez, 2009), hydrocarbon distributions (Boitsov et al., 2009) and mineralogical data (Vogt and Knies, 2009) were

compiled. The availability of a comprehensive suite of samples with an array of complementary background data, therefore, presented an excellent opportunity to contribute to this programme further and, in particular, compile specific biomarker data that could be used to perform sea ice reconstructions and compare these outcomes with known sea ice characteristics (recent decades), with the overall aim of improving our understanding of the calibration aspects of current biomarker-based sea ice proxies. In modern times, approximately 60% of the Barents Sea is covered with sea ice during peak coverage in March-April (Loeng and Drinkwater, 2007) and this figure provides a useful foundation upon which to examine the ability for specific biomarkers (and combinations of these) to accurately represent known sea ice conditions so that quantitative palaeo sea ice reconstructions might be made with greater confidence.

The objectives of the current study were:

1. To follow a previously published approach comparing surface biomarker data with recent sea ice observations by:
    a) Establishing the spatial distribution of the sea ice diatom biomarker IP_{25} in a large number (ca. 100) of contemporary surface sediments from the Barents Sea.
    b) Comparing these IP_{25} biomarker data with the known position of the maximum sea ice extent in recent decades derived from satellite data.
    c) Determining the corresponding brassicasterol, 24-methylenecholesterol and dinosterol concentrations in surface sediments and use these alongside the IP_{25} contents to investigate the applicability of the P_BIP_{25} index to provide more detailed and quantitative sea ice conditions.
2. To develop this approach further using other biomarkers by:

a) Determining surface sediment abundances for other HBI lipid biomarkers.
b) Comparing other biomarker and biomarker combinations with modern satellite records to investigate potential improvements to the biomarker-sea ice relationship.
c) Carrying out analyses between biomarkers which might reveal further underlying relationships between lipids, similar to those previously identified between diene II and IP_{25} ratio (Cabedo-Sanz et al., 2013).

4.2 Environmental conditions of the study area

The Barents Sea is one of the most productive of the Arctic Seas (Wassmann et al., 2006) located between the north Norwegian coast and the Svalbard archipelago. The Barents Sea is a relatively shallow continental shelf with an average depth of 230 m although the bathymetry is rather variable. Shallow banks of less than 50 m are found in Spitsbergenbanken (Spitsbergen Bank) and in the south-eastern region, while deeper troughs such as the Bear Island Trough are also found with depths up to 500 m (Loeng, 1991).

A detailed description of the oceanic circulation of the region can be found in Loeng (1991). The North Atlantic Drift carries warm and saline Atlantic water (AW) northwards. One of its main branches is the West Spitsbergen Current (WSC) (Figure 4.1), which is defined by temperatures, (>2ºC) and salinities, (>34.9). Separated by the polar front, colder (<0°C), less saline (<34.4) and ice-covered Arctic waters (ArW) cross the northern Barents Sea and join the East Spitsbergen Current (ESC) (Figure 4.1). The ESC flows southward along the SE coast of Spitsbergen and transports cold water from the Arctic Ocean, which mixes with ambient water, including fresh water outflow

from fjords, before continuing northward along the continental shelf off Spitsbergen. The density barrier separates the warm, saline AW from the relatively cold, fresh ArW on the shelf. The frontal region prevents intrusions of warm AW into the shelf and fjord region during winter.

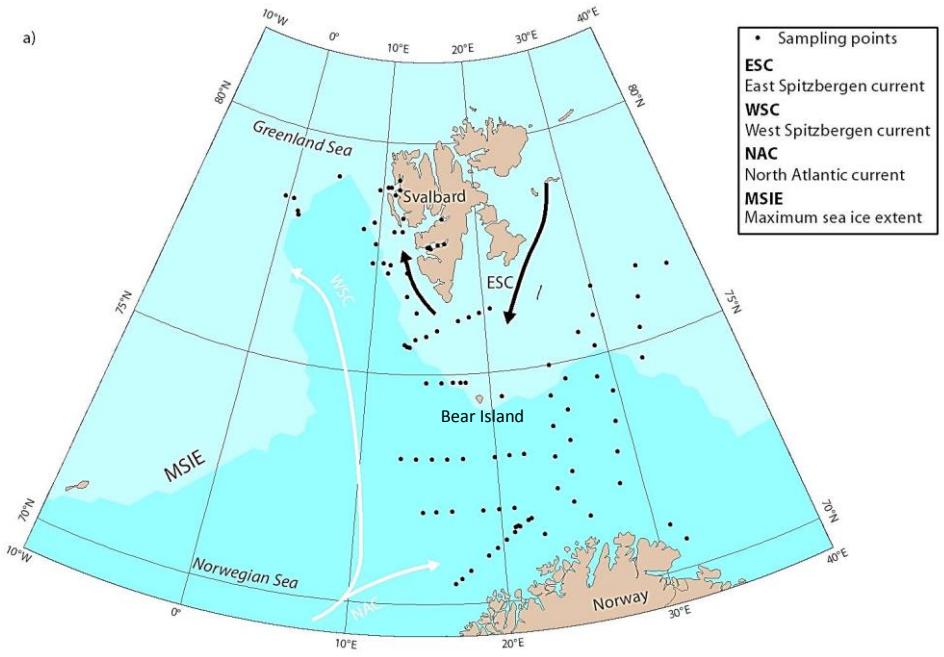

Figure 4.1 Map of the region of the Barents Sea described in the current study: (a) key oceanographic currents and sampling locations *(repeated).*

During winter (January-March), the ice edge in the Barents Sea achieves its maximum southward extent and corresponds to the marginal ice zone (MIZ), where the ice edge is most frequently located during spring. During the winter months of the sampling year (2004), the south and west coasts of Spitsbergen were regularly covered by drift ice. Sea ice coverage is susceptible to global climate changes on Earth and this is reflected by high inter-annual variability of sea ice extent of hundreds of kilometres (Vinje, 2001; Divine and Dick, 2006). The reduction in sea ice within the Barents Sea in recent decades has been attributed to increased heat transport as a result of the strengthening and warming of Atlantic waters and this, in turn, controls the position of the ice edge in

the western region (Årthun et al., 2012). The dynamism in sea ice will determine the distribution of the flora and fauna that inhabit it. The MIZ has a complicated zonal structure in terms of primary production, where generally, diatom bio volume was observed to increase from a transect south (sea ice free) to north (MIZ) at least for May 1993 in the central Barents Sea. The total bio volume including (flagellates, dinoflagellates and picoplankton) for the ice free region was comparable to the biovolume (characterised by diatoms) in the sea ice areas (Wassmann et al., 1999). The vernal bloom was observed to occur at the south of the MIZ and extend north-southwards to the sea ice free areas of the Atlantic which ceased in June. The temperature under sea ice is highly stable below -1.7 °C. Waters with temperatures higher than this will produce the melting of the sea ice with the loss of the algae attached (Wassmann et al., 2006). In the Barents Sea, the inflow of warm current of the North Atlantic under sea ice surface in occasions can result in rapid melts of the marginal ice zone clearing off the remaining algae within hours (Wassmann et al., 2006) with no suitable bloom conditions (Falk-Petersen et al., 2000), highlighting the high variability in primary production in the Barents Sea.

4.3 Methods

4.3.1 Description of sediment material

In total, 93 surface sediment samples were collected and analysed from a broad range of locations within the Barents Sea (Figure 4.1) using box cores and multicores. The majority (86) of the surface sediment samples (0-1 cm) were collected in from 2001 to 2004 (Boitsov et al., 2009; Knies and Martinez, 2009) and later included as part of the MAREANO program (2005- 2010) (Thorsnes, 2009) which provided fundamental physical, chemical and biological characteristics of the sea bed of the Western Barents

Sea (Knies, 2009). Additional multicores and gravity cores (x7) were obtained in 2011 aboard the RV *Helmer Hanssen* as part of the Changing Arctic and Sub-Arctic Environment International Training Network research project, from which further surface material was obtained and these were stored frozen (-20ºC) prior to being freeze-dried for extraction and analysis. From the 93 surface sediments analysed here, 93 where analysed for IP_{25} and a subsequent extraction was conducted for 88 of the available sediment for the sterols. Finally, some data reported previously by Müller et al. (2011) obtained from sediment samples from the northern North Atlantic were also considered, especially when making comparisons between PIP_{25} data and mean sea ice concentrations.

For the extended biomarker analysis, section (4.4.6), sample availability limited the number of samples to 58.

4.3.2 Representations of individual biomarker data and spatial distribution

Biomarker concentrations were presented and interpreted as point location representations using ArcGIS (ArcGIS 10 service pack 3) and Ocean Data View software (ODV; Version 4.5; Schlitzer, 2012). The latter approach, which uses the same primary data as used for the ArcGIS representations, extrapolates individual biomarker concentrations to provide potentially useful estimates of data for areas where samples were not measured and results in a continuous estimation of concentrations and gradients for the region under study. It is useful, therefore, as a conceptual model that predicts spatial variations in concentrations and this can be useful when the study region has independently defined regions, as is the case here with a sea ice margin, but has the potential limitation of oversimplifying trends or concealing more localised phenomena.

4.3.3 Sea ice data

Satellite records for Arctic sea ice extent derived from Nimbus-7 SSMR and DMSP SSM/I passive microwave data (Fetterer et al., 2002) were taken from the National Snow and Ice Data Center (NSIDC). In order to decide on an appropriate time interval from which to compile the sea ice records, some assessment of sedimentation rates for the Barents Sea was carried out and these were assumed to be fairly representative for the entire region. Since sedimentation rates are typically in the region (0.7 - 1.1) ± 0.4 mm yr^{-1} for the Barents Sea (e.g. Zaborska et al., 2008; Maiti et al., 2010), but can be both lower and higher than this range (e.g. 1.16 ± 0.11 mm yr-1; Vare et al., 2010), it was decided to use a 20 year time-interval for the sea ice compilations. In practice, however, the outcomes from 10 and 15 year analyses showed little in the way of variation. Polyline shapefiles of sea ice extent for the 20 year period 1983-2002 (NSIDC) were used to generate a maximum sea ice extent (hereafter referred to as the MSIE; Figure 4.1) for this interval. Additional estimates of mean spring (March-May) sea ice concentrations (± 5%) for the region within the MSIE boundary were obtained for the interval 1983-2002 from the UK Met Office Hadley Centre database (HadISST) (Rayner et al., 2003). This method was also used to re-calculate the estimates of sea ice concentrations for locations described previously by Müller et al. (2011) who used data from the NSIDC. In practice, however, only 8 out of the 38 values reported by Müller et al. (2011) were different between the two methods and these differences were never more than 10%.

4.3.4 Biomarker analysis

Biomarker analysis was conducted as described in Chapter 2 including the purification of extracts using silver ion solid phase extraction methods. HBIs (IP_{25}, diene II and

trienes IIIa and IIIb) and sterol biomarkers (brassicasterol and 24-methylenecholesterol and dinosterol) were analysed.

4.4 Results and discussion

4.4.1 Individual biomarker distribution

Of the 93 surface sediments analysed in the current study, the sea ice biomarker IP_{25} was detected in 51 samples and was absent or, at least, below the limit of detection in the remaining 42. When present, the concentrations of IP_{25} ranged from 0.03 – 0.74 µg g^{-1} TOC (0.05 – 1.78 µg g^{-1} MOC; Table A.1 in Appendix) consistent with values found in samples analysed by Müller et al. (2011) from some nearby locations (west Svalbard). In general, there was an approximate north-south division between samples containing IP_{25} compared to those where it was absent, although there was a much more consistent classification according to the position of each sampling location relative to the MSIE (Figure 4.1 b). Thus, of the 59 samples containing IP_{25} (51 from the current work and 8 in the study by Müller et al. (2011), 47 were from locations within the MSIE for the period 1983-2002 (Figure 4.1 b) and a further two samples were within close proximity of this boundary (76°-78° N; 5°-10° E). Finally, IP_{25} was also detected in 10 samples that were somewhat remote from the MSIE and were located at ca. 72°-73° N; 13°-22° E (Figure 4.1 b).

In contrast to the IP_{25} distributions, the more general sterols analysed here showed rather different patterns. For example, brassicasterol was detected in sediments from across the entire study area (with the exception of a single sample point located near to the Norwegian coast) (Figure 4.1 c) and was present with a much greater range of concentrations (ca. 6.87 - 909 µg g^{-1} TOC; 13.15-1477 µg g^{-1} MOC) compared to IP_{25}.

24-methylenecholesterol however, was only present in 55 of the 88 samples, (Table A.1 in Appendix). The highest concentrations were generally found within the MSIE to the North Eastern Barents Sea (ca. 11.42 - 61.41 µg g^{-1} TOC; Figure 4.1 d) but high concentrations were also found for discrete locations, one in the vicinity of the MSIE and another on the north coast of Norway. 24-methylenecholesterol was also present in 5 of the 13 samples located on the Bear Island Trough (0.85 - 3.22 µg g^{-1} TOC).

Lastly, dinosterol was found in 62 of the 88 samples. This sterol shows a non-specific production over the Barents Sea (Figure 4.1 e) where overall abundances were quite homogeneous across the study area. It was detected in 10 of 13 samples in the Bear Island Trough. Slightly higher values were found along the MSIE.

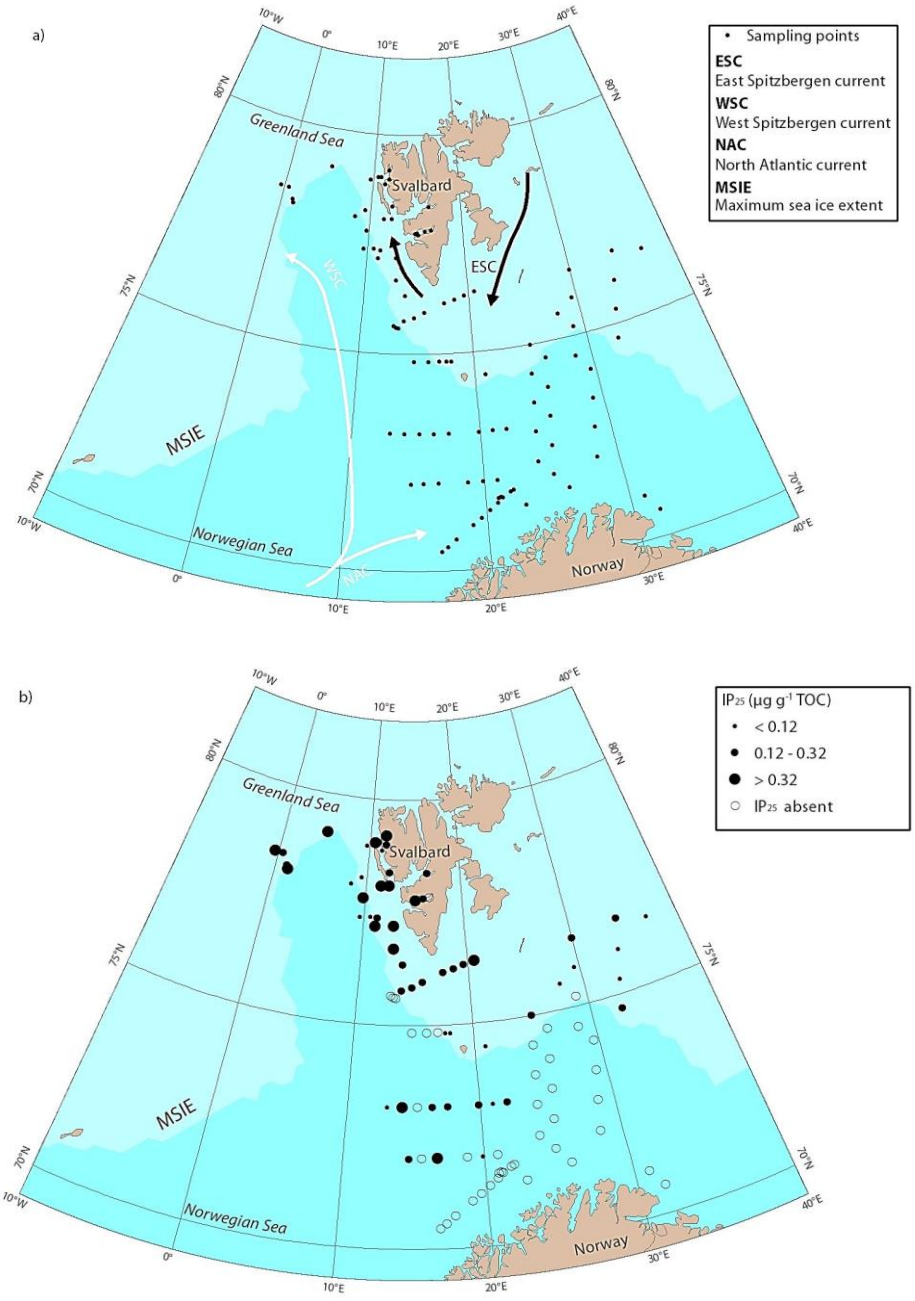

Figure 4.1 Maps of the region of the Barents Sea described in the current study: (a) key oceanographic currents and sampling locations (b) occurrences and concentration ranges of IP_{25}. The maximum sea ice extent (MSIE) for the period 1983-2002 is also indicated;, *(continued on the next page)*

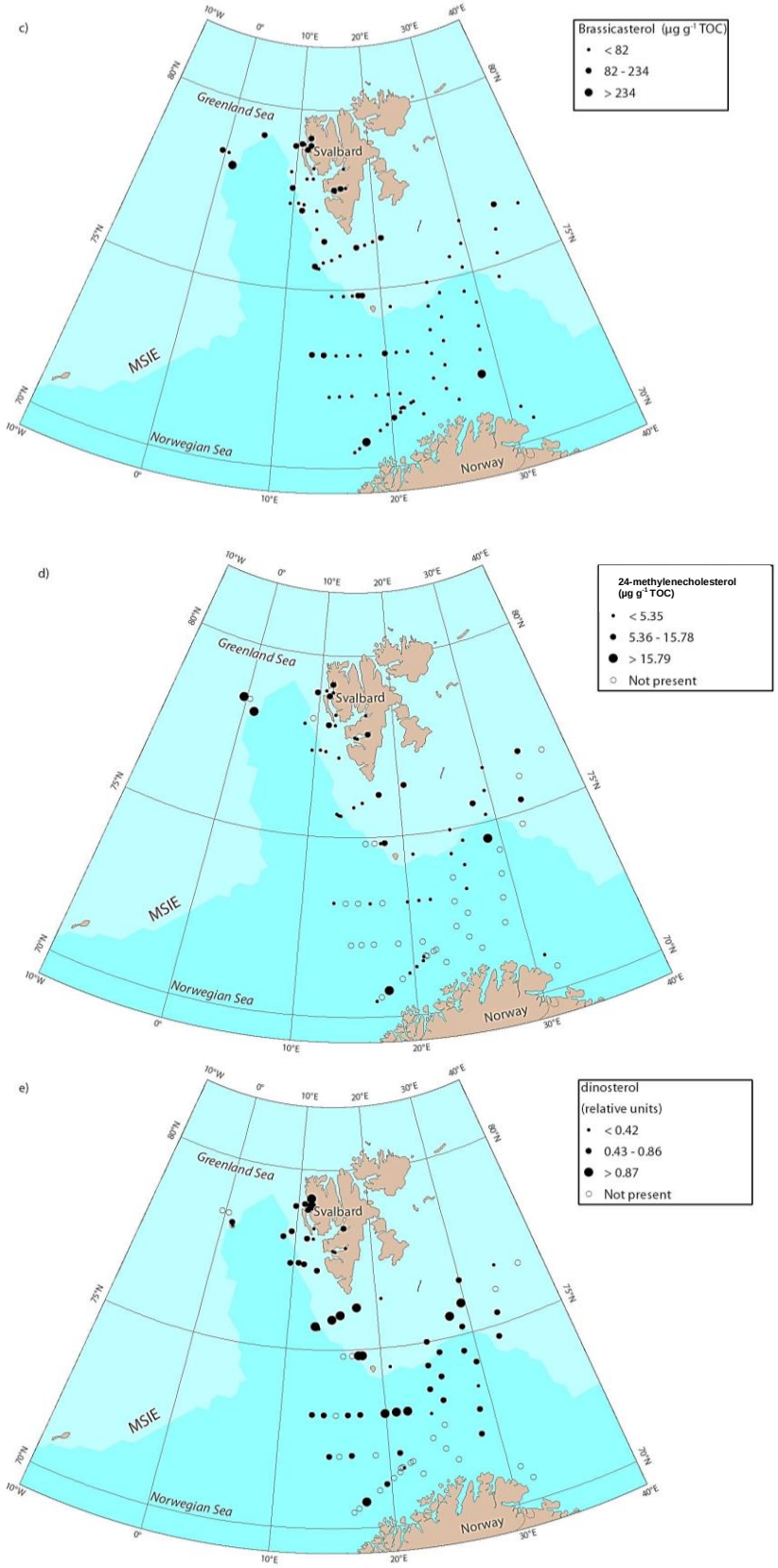

Figure 4.1.Maps of the region of the Barents Sea described in the current study: (c) occurrences and concentration ranges of brassicasterol (d) occurrences and concentration ranges of 24-methylenecholesterol; (e) occurrences and concentration ranges of dinosterol (in relative units). MSIE indicated for the period 1983-2002.

4.4.2 Assessment of marine/ total organic carbon influence on biomarker distributions in the Barents Sea

At the beginning of the biomarker data interpretation, the idea of the possible influences of variable primary production, sediment accumulation and burial rates was considered by normalising biomarker concentrations to organic carbon content, especially as TOC is known to be somewhat variable in the Barents Sea. This is, in part, because of the strong productivity association with the MIZ (Knies, 2009), which provides a suitable habitat for a wide range of microorganisms (Thomas, 2012), but also because vertical particulate organic carbon (POC) export is thought to be relatively weak in the Atlantic region of the Barents Sea compared to regions of the MIZ where pelagic-benthic coupling is stronger (Wassmann et al., 2006; Maiti et al., 2010). Further, the potential influence of alternative methods of normalising sedimentary concentrations using total versus marine organic matter was considered. Significant differences between the two approaches could potentially have materialised, especially since the contribution of MOC to TOC has also been shown to be variable in the Barents Sea sediments (Knies and Martinez, 2009), likely as a result of differential productivity and input of terrigenous material.

In practice, although the ranges of TOC- versus MOC-normalised concentrations were slightly different (necessarily), the distributions in concentrations across the study area were largely unaffected by the method of choice (Figure 4.2 a, b). As such, since the dataset of TOC values was larger and previous TOC-normalised data were also available for comparison purposes, the biomarker interpretations were based on TOC-normalised concentration data.

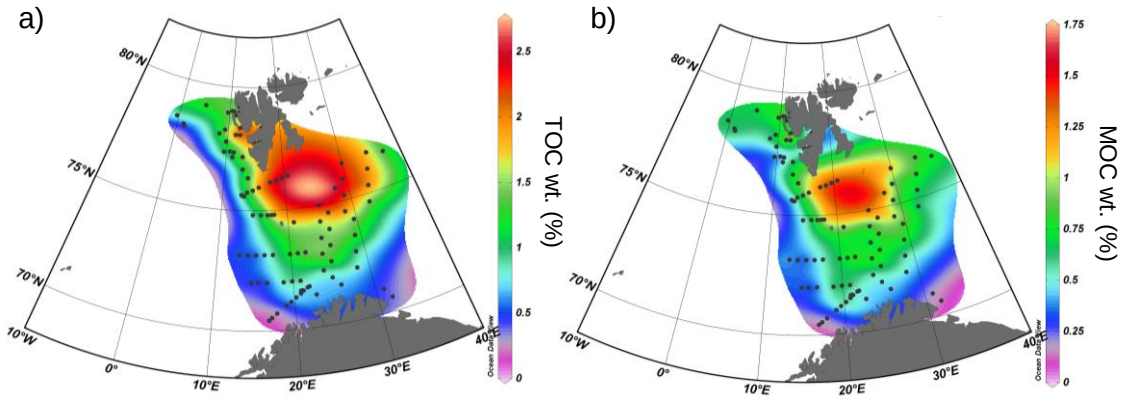

Figure 4.2 Total organic carbon (TOC) and marine organic carbon (MOC) in wt. (%) for the Barents Sea. Data obtained from (Knies and Martinez 2009).

4.4.3 Distributions of IP_{25} and sterols described by sea ice conditions

4.4.3.1 Point locations

When comparing the concentrations and distributions of the sea ice biomarker IP_{25} with the MSIE for the 20-year period 1983-2002 (NSIDC), a clear relationship between the two was identified (Figure 4.1 b), providing further evidence of the potential for IP_{25} to be used as a reliable sea ice proxy in the Arctic. Thus, of the 59 sample locations where IP_{25} was detected (or had been reported previously; Müller et al. (2011)), 47 were within the MSIE and two further locations were within close proximity to this boundary. In contrast, IP_{25} was absent in 42 samples that represented locations for which no sea ice has been observed in the same 20-year interval (NSIDC). Exceptionally, IP_{25} was absent in only two samples from sites that have had at least partial sea ice cover (647; north east Barents Sea and St21; western Barents Sea) and these represented locations that are extremely close to the MSIE and may, therefore, have only experienced infrequent sea ice occurrence. A further sample with no IP_{25} and a very low brassicasterol concentration (10.5 µg g^{-1} TOC) (1254; Table A.1 Appendix) was collected from the innermost part of Van Mijenfjorden in Svalbard, a location for which extremely low numbers of dinocysts had been reported previously (Grøsfjeld et al., 2009), possibly

reflecting low nutrient levels. This, in turn, may have resulted from severe sea ice conditions during the spring, followed by a rapid melt in the summer, leading to very low productivity in sea ice and the pelagic environment

The occurrence of IP_{25} in virtually all sediments from locations within the boundary of the MSIE was also consistent with the outcomes of previous analyses of dinocyst assemblages from a sub-set of the same sample locations, namely the identification of (variable) seasonal sea ice cover (Solignac et al., 2009). Specifically, Solignac et al. (2009) observed the dominance of *Islandinium minutum*, which is related to Arctic waters, in two transects south of Svalbard (74°-76° N) and within the MSIE where IP_{25} was also detected. Further, *I. minutum* was generally identified as the major dinocyst species west of Spitsbergen (Grøsfjeld et al., 2009), coincident with the highest concentrations of IP_{25} observed here (77°-79° N; 10°-16° E). As such, both sets of proxy data indicate the strong influence of Arctic waters and the occurrence of spring sea ice in this region.

Of the 47 sample locations within (or near to) the MSIE where IP_{25} was detected, two regions could be identified broadly according to IP_{25} concentrations (Figure 4.1 b), possibly suggesting different sea ice conditions between two seasonal ice-edge regimes. Currently, the factors that control IP_{25} production and transfer to sediments are not fully understood which prevents detailed quantitative assessments from being carried out on the basis of IP_{25} concentrations alone. It is noted, however, that for sample locations on the eastern side of Svalbard, IP_{25} concentrations were relatively low (ca. 0.06 - 0.22 µg g^{-1} TOC; mean 0.13 µg g^{-1} TOC; n=9) or, at least, lower than for sites to the immediate south and west of Svalbard. Spring sea ice extent is more variable in extension on an annual basis for the eastern Barents Sea compared to the western region of Svalbard (NSIDC) mainly due to the close proximity of the Svalbard Archipelago on the western

marginal sea ice which together with the influences of the inflowing Atlantic waters (Årthun et al., 2012) limits the sea ice extension. This increased variability in the position of the maximum ice edge potentially results in a smaller number of months per year of sea ice cover over a fixed (e.g. 20-yr) interval. As such, it is possible that less frequent spring sea ice occurrences may contribute to the observation of lower IP_{25} concentrations in the eastern region, although uncertainties in the sedimentation rates prevent this suggestion being tested more quantitatively. Higher concentrations of IP_{25} (0.03 – 0.74 µg g^{-1} TOC; mean 0.23 µg g^{-1} TOC; n=30) were found to the west and immediate south of Svalbard (Figure 4.1 b) consistently with samples from Müller et al. (2011) (0.17 - 0.85 µg g^{-1} TOC; mean 0.53 µg g^{-1} TOC; n=8) Table A1. For the south of Svalbard, in particular Storfjorden, winter / spring sea ice extent is more consistent on an annual basis, possibly resulting in a higher frequency of spring algal blooms during which IP_{25} is produced (Brown et al., 2011). This could be the reason of the high concentrations of IP_{25} found here. For West Svalbard, in turn, the sea ice concentrations are consistently very low (5-10% sea ice concentrations) due to the path of the warmer Atlantic waters. In contrast, three sample locations further south of Svalbard and in close proximity to the MSIE (St 20, 1239, 1241; Table A.1 in Appendix) had very low IP_{25} concentrations (0.03 – 0.11 µg g^{-1} TOC), potentially as a result of the greater variability of the ice edge in this region.

Alternatively, variations in IP_{25} concentrations within the boundary of the MSIE may better reflect post-production influences, with relative depletions resulting from removal processes such as degradation (water column and the sediment interface), scavenging of organic matter (OM) by heterotrophs or weaker pelagic-benthic coupling, in general. As such, this study reinforces the notion that while the occurrence of IP_{25} provides an excellent qualitative proxy for past sea ice, quantitative interpretations need to be

treated with caution and should be considered alongside other proxy data. A more quantitative analysis of the relationship between sea ice and biomarker concentrations is described in section 4.4.4.2.

In contrast to $IP_{25,}$ distributions of sterols showed different results. Firstly, in comparison to the relatively localised occurrence of IP_{25}, brassicasterol was present in virtually all sediments and the distribution of concentrations (Figure 4.1 c) showed little, if any, relationship to either sea ice cover or the position of the MSIE. Instead, this biomarker, which is generally considered to be representative of open water phytoplankton (Müller et al., 2011), was distributed in sediments representing both seasonally ice-covered and ice-free conditions over the entire study area, with the exception of one location off the north coast of Norway. Within the region covered by the MSIE boundary, brassicasterol concentrations were within the range 9.6 – 686 µg g^{-1} TOC (mean 86.2 µg g^{-1} TOC) being especially abundant in the western margin of Svalbard in comparison to the eastern margin. Equivalent values for permanently open water conditions were between 0 – 909 µg g^{-1} TOC (mean 77.34 µg g^{-1} TOC). These data suggest that brassicasterol can be considered as a non-specific indicator for either of these two regional divisions (i.e. seasonally sea ice covered or open water conditions) in the Barents Sea and that for the sea ice cover region, brassicasterol concentrations could be enhanced by ecological parameters such as terrestrial and freshwater input in the west margin of Svalbard as derived from TOC values (Figure 4.2 a).

24-methylenecholesterol was also present in sea ice covered areas as in ice free regions (Figure 4.1 d), showing lower concentrations than brassicasterol. The mean 24-methylenecholesterol concentration within the MSIE was 7.53 and 3.46 µg g^{-1}TOC for the region outside the MSIE (annually open water conditions). The higher value within the MSIE might indicate that production of this sterol may be more favoured under sea

ice conditions or at least, produced by sea ice algae in addition to phytoplankton. Indeed previous studies have suggested that the production of the sterol 24-methylenecholesterol (in localised areas) could be associated with sea ice conditions (Knies, 2005; Cabedo-Sanz et al., 2013).

The occurrence of dinosterol (Figure 4.3 e) suggests that its production is rather homogeneous for the study area if compared with previous sterols. Dinosterol mean abundances for the area covered by the MSIE were 0.61, and 0.38 relative units for the area out of the MSIE, and no preference by any ecological parameter (sea ice, water masses) was observed.

4.4.3.2 Spatial biomarker distributions

When the (point location) IP_{25} and sterol concentrations were re-examined as broader spatial representations (ODV; Figure 4.3 a, c, d), the trends identified from the point location analyses were confirmed and more detailed distribution patterns were also identified. For example, the regions of highest concentrations of IP_{25} were shown to be within the boundary defined by the MSIE and to the west and south of Svalbard (ca. 0.32 – 0.85 µg g^{-1} TOC; Figure 4.3 a), while the lowest concentrations (0.03 – 0.06 µg g^{-1} TOC; Figure 4.3 b) were found for locations near to the MSIE in the south and for the sites within the boundary of the MSIE in the east. Further, the majority of locations south of the MSIE had IP_{25} concentrations less than 0.042 µg g^{-1} TOC, which corresponds to the analytical limit of detection, and is consistent with the failure to detect IP_{25} in the majority of sediment extracts from this area.

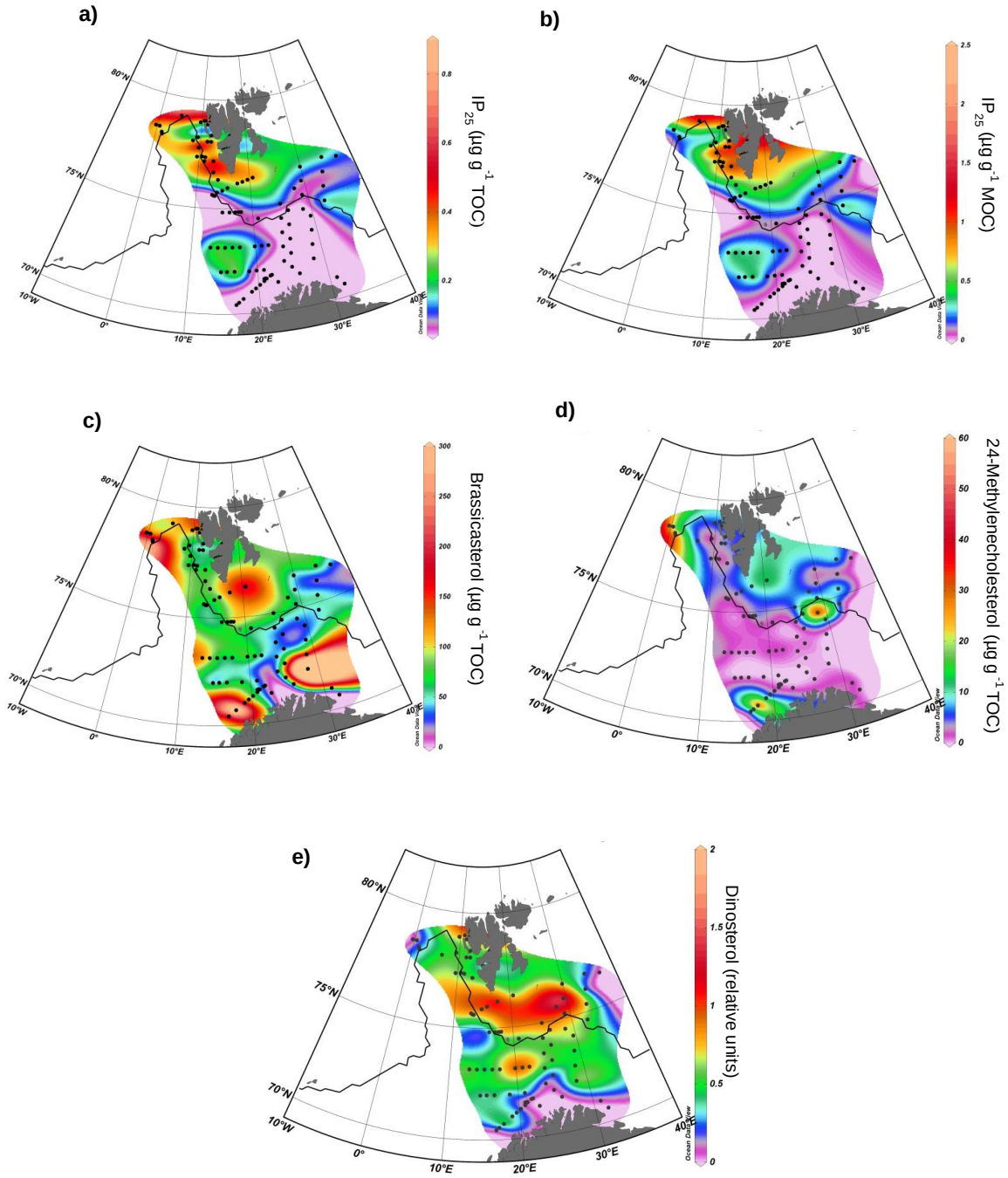

Figure 4.3 Distributions of individual biomarker concentrations and other organic geochemical parameters derived from analysis of 101 surface sediments from the Barents Sea: (a) the sea ice biomarker IP_{25} TOC normalised; (b) the sea ice diatom biomarker IP_{25} MOC normalised; (c) brassicasterol. Maps are generated with Ocean Data View (ODV) software (v.4) using the Diva Gridding Algorithm. The maximum winter sea ice extent MWSIE for March and April (1983-2002) is represented by the continuous black line (calculated from NSIDC records).

Exceptionally, a region of relatively low-mid range concentrations of IP_{25} was also identified within the south-west of the study area (72°-73° N and 13°-22° E), consistent with the detection of IP_{25} in 10 samples from this region (a more detailed discussion of this will be given in section 4.5).

In direct contrast to these IP_{25} concentration data, the distributions of brassicasterol (Figure 4.3 c) were not at all closely defined by the MSIE and, indeed, ranges and mean concentrations of brassicasterol from locations within the MSIE were not significantly different from those representing ice-free locations. Instead, brassicasterol distributions were found to be influenced more by other regional influences on primary production, which is consistent with the biosynthesis of this biomarker by a wide range of algal sources (e.g.Volkman, 1986; Volkman et al., 1998). The more general production of brassicasterol likely also explains its significantly higher abundance in sediments compared to IP_{25} which, in contrast, is thought to be produced selectively by a small number of diatom species living in sea ice (Belt et al., 2007; Brown et al., 2011). Within the spatial heterogeneity of the brassicasterol distributions, however, two relatively high concentration regions could be identified that can be attributed to distinct events; the first of which was on the north Norwegian coast where phytoplanktic blooms have been detected in summer months (MODIS-Aqua 8-2011) and a second, to the south of Svalbard, where high biological productivity occurs within the MIZ (Knies and Martinez, 2009). In contrast, the reduced brassicasterol concentrations for some parts of the north coast of Norway/ central south and east north Barents Sea presumably reflect influences other than sea ice on the production of this biomarker and such factors may also impact on the outcomes of other individual biomarkers or the outcomes of combined biomarker indices such as the PIP_{25} index (discussed later).

24-methylenecholesterol concentrations (Figure 4.3 d), showed highest values along the MSIE to the northwest of Svalbard and in coastal areas of north Norway, while lower concentrations were generally found for areas of no ice cover. Dinosterol distribution was not closely defined by the MSIE (Figure 4.3 e) although in contrast to the other two sterols there was a relatively homogeneous distribution of dinosterol for the Barents Sea. Similar to brassicasterol, however, dinosterol concentrations were low in the central south Barents Sea.

No specificity or localised association to environmental conditions (e.g. sea ice water masses) was found for the sterols. In conclusion, sterols did not show any source-specific relationship.

4.4.4 Assessment and application of the PIP_{25} index for quantitative sea ice reconstructions

In order to extend the qualitative aspects of the biomarker distributions further and, with the specific aim of identifying whether the outcomes could be made more quantitative, a method proposed recently by Müller et al. (2011) which combines the individual sea ice diatom (IP_{25}) and phytoplankton (brassicasterol) biomarkers together into a single index (P_BIP_{25}) was adopted, resulting in more detailed descriptions of past sea ice conditions. Although the outcomes of this initial study were reasonably convincing, Müller et al. (2011) also recommended that a more extensive set of samples covering a wider spatial range would be needed in order to assess the full potential of this novel approach. Nevertheless, the principles behind the P_BIP_{25} index are reasonably clear and, on the basis of their initial findings, Müller et al. (2011) suggested that individual P_BIP_{25} values had the potential to identify discrete oceanographic or sea ice scenarios. In addition, the PIP_{25} approach was investigated using different sterols, phytoplankton

biomarkers such as dinosterol (Müller et al., 2011; Stoynova et al., 2013) and 24-methylenecholesterol (Table A.2 in Appendix). The subsequent indices calculated here are described in Table 4.1.

Table 4.1 PIP_{25} indices and *c* terms. *c= 0.0018 corresponds to the dataset in the present study n=101; **c=0.0068 corresponds to the dataset including the samples from Müller et al. (2001)) n=121. (P) phytoplankton biomarker origin, (SI) sea ice biomarker.

P LIPID	**SI**	***C* term**	**INDEX**
Brassicasterol	**IP_{25}**	0.0018*	P_BIP_{25}
Brassicasterol	**IP_{25}**	0.0068**	P_BIP_{25}
24-methylenecholesterol	**IP_{25}**	0.022	$P_{24M}IP_{25}$
dinosterol	**IP_{25}**	0.242	$P_DIP_{25.}$

Thus, high (0.75 – 1.0) P_BIP_{25} values were suggested as representing extensive sea ice conditions (IP_{25} is favoured relative to phytoplankton biomarkers), mid-range values (0.50 - 0.75) indicated MIZ or seasonal ice cover (conditions favour both types of biomarker), while P_BIP_{25} values less than ca. 0.5 represent infrequent or ice-free conditions (IP_{25} is low or absent). It was also accepted, however, that the boundaries between these classifications should also be considered with some flexibility.

Firstly, the individual IP_{25} and brassicasterol data measured in the current study were combined, together with those reported by Müller et al. (2011) for the same region (8 sample locations), to obtain P_BIP_{25} data for the Barents Sea. In doing so, it was noticed that the ranges in concentration of IP_{25} and brassicasterol measured as part of the current study (0 - 0.60 µg g^{-1} TOC and 10 - 157 µg g^{-1} TOC, respectively) were consistent with those from Müller et al. (2011) (0.17 - 0.85 µg $^{-1}$g TOC and 63 - 234 µg g^{-1} TOC, respectively) where there was overlap between sampling regions (i.e. West Svalbard). Further, although 93 sediments were analysed for IP_{25} in the current study, there was

insufficient material from five locations to also analyse for brassicasterol and, for one sample location, both IP_{25} and brassicasterol were below the limit of detection.

The outcomes of the spatial representation of the P_BIP_{25} data are in reasonable agreement with those derived from the IP_{25} data alone and, in addition, provide potentially more detailed insights into the sea ice conditions. Firstly, for locations which experienced sea ice cover during (at least part of) the 1983 – 2002 sampling period (i.e. those generally north of the MSIE), P_BIP_{25} values were consistently in the range ca. 0.45 – 0.9 (Figure 4.4 a), interpreted as representing the occurrence of a MIZ or more extended sea ice conditions (Müller et al., 2011). Secondly, and in direct contrast, P_BIP_{25} values were significantly lower (ca. 0.1 – 0.25) for the region mainly south of the MSIE and east of ca. 12° E, indicative of irregular or reduced sea ice cover, and inferred from the IP_{25} distributions here. In contrast to the IP_{25} data alone, however, where variable abundances were previously interpreted as possibly reflecting an inconsistent ice-edge position, the P_BIP_{25} data for locations in the eastern region (north of the MSIE) implied similar sea ice conditions to those of west and south Svalbard (*viz*. MIZ or extended sea ice cover). This difference in the IP_{25} and P_BIP_{25} records arises mainly due to the influence of the lower brassicasterol concentrations on the P_BIP_{25} index in the eastern region and provides a useful example of how the interpretation of individual biomarker records can sometimes be misleading and can be improved through combination with other biomarker data, at least in some cases. However some discrepancies between P_BIP_{25} values and sea ice concentrations (Figure 4.4 c) can be identified where, for the west side of Svalbard, P_BIP_{25} predicts permanent sea ice conditions whilst the satellite sea ice concentrations show less than 10% sea ice concentration. Thirdly, the P_BIP_{25} values for locations predominantly south of the MSIE either confirmed the ice-free conditions (P_BIP_{25} ca. 0) or, in the case of the south-west

region, where IP_{25} had also been detected, significant ice cover was implied (P_BIP_{25} = ca. 0.45 - 0.9).

In order to evaluate the P_BIP_{25} index further, the combined biomarker data was re-analysed in two further ways. In the first instance, the P_BIP_{25} values for the Barents Sea using a larger dataset of biomarker data were re-calculated, including IP_{25} and brassicasterol concentrations reported previously by Müller et al. (2011), for locations representing a wider spatial coverage within the northern North Atlantic. One consequential impact of this was a change to the c term used to balance differences in the abundances of IP_{25} and brassicasterol. In this instance, the analysis of a larger dataset resulted in an increase in the c term and a lowering of P_BIP_{25} values (Figure 4.4 b), although higher P_BIP_{25} values were still generally observed within the region bound by the MSIE compared to most of the locations beyond the maximum ice edge. For the Barents Sea and the larger datasets, some qualitative comparisons with the known mean spring sea ice concentrations (Figure 4.4 b) for the interval 1983-2002 were also made and these showed that, although there was some reasonable consistency between higher P_BIP_{25} values and increased sea ice concentrations for some locations to the east of Svalbard, there was relatively poor agreement for the regions west and south of Svalbard, with lower satellite-derived sea ice concentrations than those predicted by the P_BIP_{25} data.

PIP_{25} data were also calculated using 24-methylenecholesterol and dinosterol (Table A.2 in Appendix). The spatial distribution of the $P_{24M}IP_{25}$ index (Figure 4.4 c), predicted overestimated sea ice conditions for areas on the West margin of Svalbard and the Eastern Barents Sea (0.6 - 0.9) similar to outcomes for the P_BIP_{25} index. The $P_{24M}IP_{25}$ data also predicted much higher sea ice conditions for the Bear Island Trough when compared to satellite sea ice concentrations.

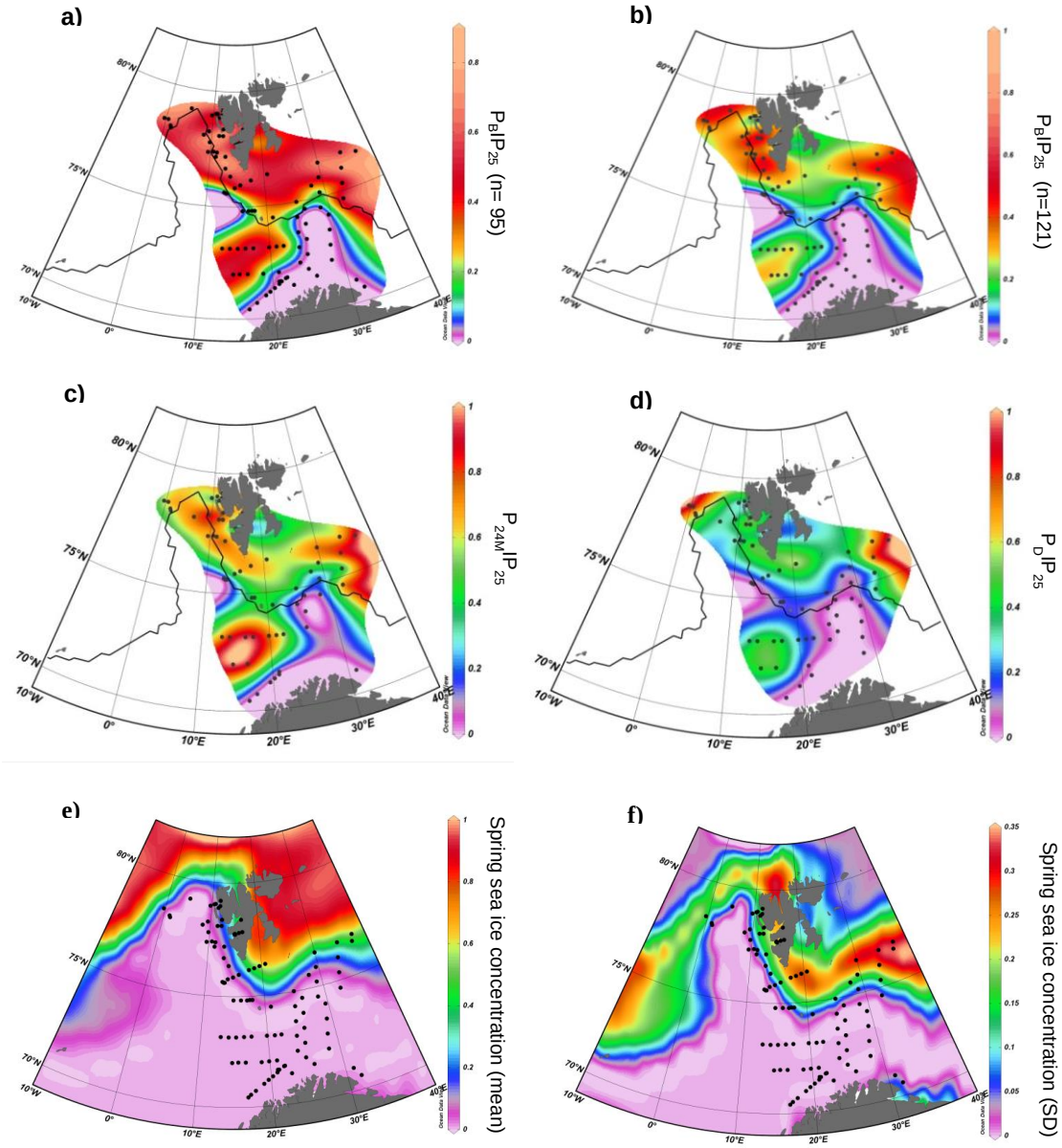

Figure.4.4. Combined biomarker indices (PIP_{25}) calculated using IP_{25} and different sterols concentrations and sea ice concentration data: (a) P_BIP_{25} values calculated using brassicasterol biomarker data presented in the current study (Table 1; n=95); (b) P_BIP_{25} values calculated using brassicasterol biomarker data presented here and additional values reported by Müller et al. (2011) (n=121); (c) $P_{24M}IP_{25}$ values calculated using 24-methylenecholesterol; (d) P_DIP_{25} values calculated using dinosterol (e) Satellite-derived (UK Met Office Hadley Centre database (HadISST) (Rayner et al., 2003)) mean spring sea ice concentration data (±5%) for the interval 1983-2002; (f) Standard deviations in sea ice concentrations. The maximum sea ice extent (MSIE) for 1983-2002 is represented by the continuous black line (calculated from NSIDC records). Maps are generated with Ocean Data View (ODV) software (v.4.5) using he Diva Gridding Algorithm.

P_DIP_{25}, reflects similar sea ice conditions for all the MSIE area (Svalbard vicinity, ca. 0.4 - 0.5) (Figure 4.4 d) which could be interpreted as marginal ice zone conditions to both east and west of Svalbard and also describes two regions of abundant sea ice on the eastern and northern west Barents Sea. When satellite records were compared to the P_DIP_{25} predictions, discrepancies were observed, although this approach provided better estimations of sea ice conditions than the other PIP_{25} indices (Figure 4.4 a, c), which in all cases predict severe sea ice conditions from 75° N northwards.

In conclusion, combining brassicasterol or 24-methylenecholesterol with IP_{25} did not improve the PIP_{25} index predictions of sea ice concentrations for the study area, while for dinosterol, better prediction was observed but still with some overestimated results.

4.4.4.1 PIP_{25} correlation to sea ice concentration

An attempt to make the comparisons more quantitative was carried out by comparing the IP_{25} and (re-calculated) PIP_{25} data with the corresponding mean spring sea ice concentrations using the method of Müller et al. (2011), although some of the data (e.g. 4 of the 87 P_BIP_{25} values from the current study) needed to be excluded from this analysis due to the lack of satellite sea ice concentration data. In terms of the linear relationship between the enhanced IP_{25} dataset (n=121; 83 from the current study; 38 from Müller et al., 2011) and sea ice concentrations (Figure 4.5 b), the regression coefficients were very similar to those reported by (Müller et al., 2011) and the same was true of the coefficient of determination (R^2 = 0.67 in both cases). In contrast, although the corresponding linear relationship between the larger P_BIP_{25} dataset and sea ice concentrations (Figure 4.5 a) yielded similar regression coefficients to those reported by Müller et al. (2011) using a smaller dataset (n=38), the variability was much greater. Thus, the R^2 for the larger P_BIP_{25} dataset (0.57) was significantly lower than found by

Müller et al. (2011) (R^2 = 0.74) and, additionally, was also less than for the relationship using the IP_{25} concentrations alone (R^2 = 0.67).

These quantitative comparisons could be carried out further, in order to test differences within the North Atlantic, by dividing the study area into two regions of different sea ice conditions (i.e. Barents Sea (seasonal) and East Greenland (multi-year)) and comparisons of P_BIP_{25} and IP_{25} values against sea ice concentrations were made for these two regions. The linear correlations between IP_{25} (R^2= 0.06) and P_BIP_{25} (R^2= 0.19) with sea ice concentrations (Figure 4.5 c, d) for the Barents Sea (seasonal sea ice) were much lower than for East Greenland (more permanent multi-year sea ice) (Figure 4.5 e, f), possibly showing differences in the different ecosystem structures.

The corresponding P_DIP_{25} and $P_{24M}IP_{25}$ correlations to sea ice concentrations were carried out, but for the Barents Sea only, due to data availability (e.g. 24-methyelenecholesterol data were not obtained by (Müller et al., 2011). Linear correlations between P_DIP_{25} and $P_{24M}IP_{25}$ and sea ice concentration were also very poor (R^2= 0.068; 0.26, Figure 4.5 g, h) suggesting that the PIP_{25} approach would not appear to work well for the Barents Sea even when employing different phytoplankton biomarkers.

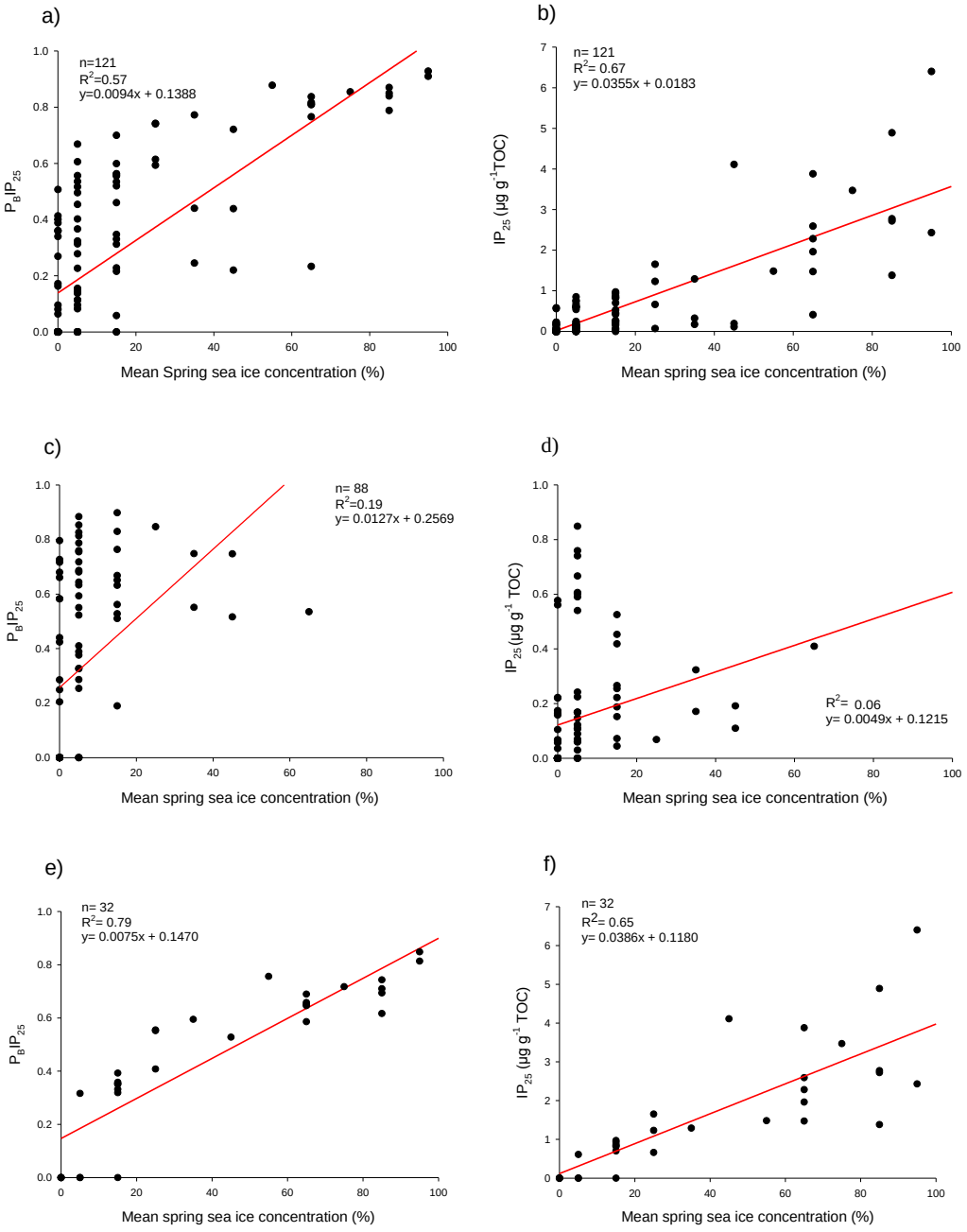

Figure 4.5 Linear relationship between P_BIP_{25} and IP_{25} values with mean spring sea ice concentrations (Hadley; HadISST) in the North Atlantic area (a ,b) Barents Sea (c, d) and East Greenland (e, f). a) The P_BIP_{25} data correspond to the combined biomarker concentrations reported here and by Müller et al. (2011) (n=121). b) Linear relationship between the, IP_{25} biomarker data and mean spring sea ice concentrations were also evaluated here for the same group of samples (n=121). c) P_BIP_{25} data for the Barents Sea only with the additional Müller samples overlapping on the west side of Svalbard for which the satellite sea ice data was available (n=88). d) IP_{25} for the same dataset (n=88). e) P_BIP_{25} for the East Greenland area Müller et al., 2011, (n=32). f) IP_{25} for the same dataset (n=32) *(continued on the next page).*

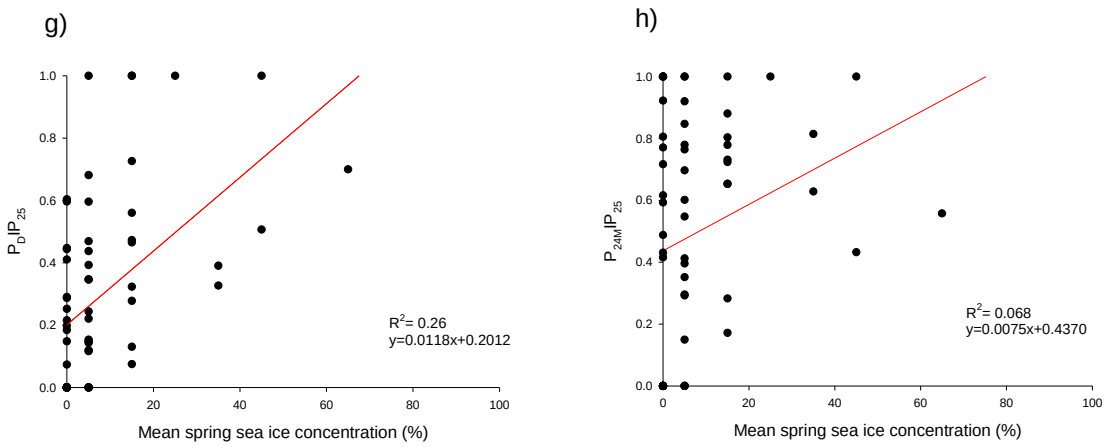

Figure 4.5 g) P_DIP_{25} calculated with dinosterol for the Barents Sea; h) $P_{24M}IP_{25}$ calculated with 24-methylenecholesterol for the Barents Sea.

Since the relationship to sea ice concentrations of one of the components of the PIP_{25} index (IP_{25}) has been studied, the same was carried out for the phytoplankton contributor to the index. Considering here the different nature of the sea ice conditions to biomarker production, further investigations on the relationships between general phytoplankton biomarker to sea ice concentrations were investigated for the same areas of the North Atlantic and the CAA.

Interestingly, all correlations for the phytoplankton biomarkers to sea ice concentrations for the Barents Sea showed positive linear regressions (Figure 4.6). It might have been expected to find negative relationships since both parameters are proposed to be inversely related (e.g. the more sea ice concentrations the less concentration of the open water biomarker) which was observed for brassicasterol and dinosterol in the Canadian Arctic Archipelago (CAA) (Stoynova et al., 2013) and Fram Strait-Greenland Sea (Müller, 2011). Nevertheless, caution doing interpretations must be taken, since recently Belt and co-workers (2013b) detected sterols in sea ice samples and noted that their contributions to the sedimentary budget may be significant.

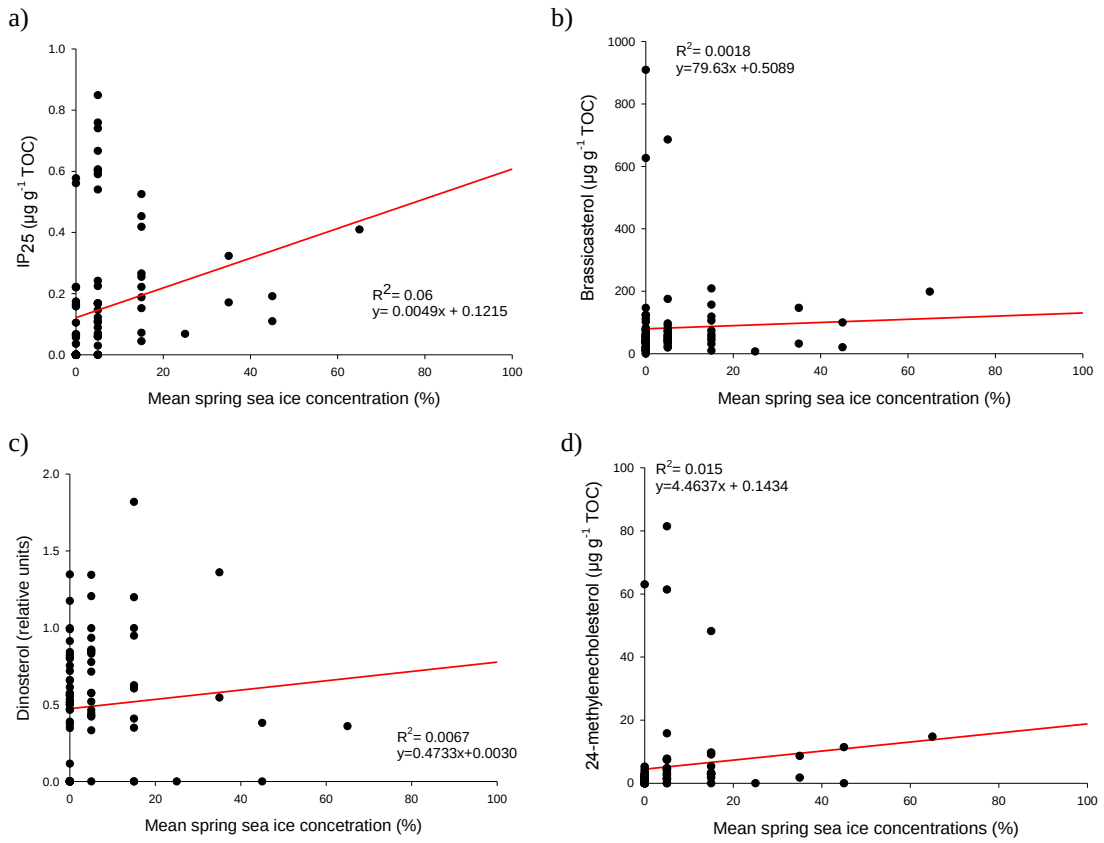

Figure 4.6 Biomarker linear correlation to mean spring sea ice concentrations Satellite-derived (UK Met Office Hadley Centre database (HadISST) (Rayner et al., 2003)) for the Barents Sea region (current study); a) IP_{25}; b) brassicasterol c) dinosterol; d) 24-methylenecholesterol

However, the phytoplankton correlations to sea ice concentrations could give information of the ecosystem biomarker signature, for example, the degree of correlation between phytoplankton abundances and sea ice concentrations could indicate to what extent phytoplankton biomarkers are also produced in sea ice (when this is permanent), an outcome that can be complicated for areas with seasonal conditions, where phytoplankton production occurs in sea ice free areas in summer that were previously sea ice covered in spring. The different correlations are most likely to be due to the different sea ice types in different areas of the Arctic, which demonstrates in last instance the differences between ecosystems.

Although the exact reasons for the poorer relationship between the combined PIP_{25} data and the satellite-derived sea ice concentrations in these two regions (East Greenland and Barents Sea) are not fully understood at this stage, some contributing factors may include: (i) a bias in the sampling frequency (it is noted that the majority of the points here fall within the low (<25%) sea ice concentration range); (ii) uncertainties of the time intervals that the surface sediments represent; (iii) errors associated with the sea ice concentrations derived from satellite records; (iv) variations in analytical methods for biomarker concentration determinations; (v) variability in environmental controls over the production and fate of IP_{25} and other biomarkers. (vi) lateral transport of sediment occurring in different areas of the Barents Sea.

To begin with, sedimentation rates may potentially be quite variable across the region, which makes it difficult to reliably predict the period for which the satellite sea ice data should be considered and, even if sedimentation rates are known (or can be reasonably estimated), the surface material will also reflect different time intervals depending on when sampling took place. In this respect, it is noted that samples analysed by Müller et al. (2011) were obtained from 1994 to 2003, while the samples in the current study were mainly collected from 2001 to 2004 and a few in 2011. This further complicates the correlational analysis between biomarker and satellite-derived concentration data since the latter are especially susceptible to short term changes. In terms of the analytical datasets, a recent study of inter-laboratory comparison of methods for the identification of IP_{25} was carried out in (Belt et al., 2014). This study showed generally good agreement within laboratories but greater variation between them. Since data from (Müller et al., 2011) has been compiled here, the combination of data obtained from different laboratories, potentially will be something to consider which could affect results and interpretations.

Recent analysis of surface sediments from different Arctic and sub-Arctic regions (Müller et al., 2011; Stoynova et al., 2013; Xiao et al., 2013) and this study here, demonstrates that concentrations of IP_{25} and phytoplankton biomarkers can be highly variable between locations. Some examples of potentially important factors that may control biomarker abundances have been considered in detail in Belt and Müller. (2013) such as nutrient availability, water depth or sea ice types /concentrations. The factors controlling the success (or otherwise) of biomarker-sea ice concentration correlations are likely to be most clearly identified through analysis of larger datasets representing different regions of the Arctic. For example, Stoynova et al. (2013) demonstrated clear differences between biomarker-sea ice concentration correlations for Arctic and sub-Arctic regions of the Atlantic and Pacific. Further, it was suggested that such differences may be attributed (in part) to variations in primary production or the nature of the sea ice between regions. Similarly, Xiao et al. (2013) attributed the poor biomarker-sea ice concentration correlations to different sea ice types and different environmental conditions of the Laptev and Kara seas i.e. important freshwater discharge into the marine ecosystem.

Further, any (linear or other) biomarker – sea ice concentration relationships that do exist, may be negatively impacted by any differential degradation or removal processes, and these also may be variable between locations (Belt and Müller, 2013). Such processes may include, but are not limited to, selective biodegradation of individual biomarkers in oxic surface sediments or physical redistribution of surface sediments as discussed later. One way to potentially reduce the impact of such degradation processes is to ratio biomarker concentrations using lipids of related origin or structure/reactivity. Such an approach is used routinely for the reconstruction of SSTs using alkenones

(Brassell et al., 1986) and glycerol dialkyl glycerol tetraethers (GDGTs) (Schouten et al., 2002; Kim et al., 2008) which are used to derive the $U^{K'}_{37}$ and TEX_{86} indices, respectively. This approach is, to some extent, applied through calculation of the PIP_{25} index, although the potential for differential degradation of IP_{25} versus the phytoplankton biomarkers such as brassicasterol remains a key issue. Such a limitation may be resolved to a large part by measuring the ratios of IP_{25} to a further lipid with similar chemical or physical characteristics and a potential candidate for this is the structural homologue of IP_{25}, namely the di-unsaturated C_{25} HBI lipid, also believed to be produced by Arctic sea ice diatoms. Indeed, recent studies by Fahl and Stein (2012), Cabedo-Sanz et al. (2013) and Xiao et al. (2013) have shown the potential for the ratio between this di-unsaturated HBI and IP_{25} (the so-called DIP_{25} index) to provide further information regarding Arctic sea ice conditions.

The impact of the balance factor, c, which is central to the determination of the PIP_{25} index was another point to consider and was commented on. Since this term corresponds to the ratio of the mean IP_{25} and phytoplankton biomarker concentrations under study, this means that PIP_{25} values are not fixed for a given location or sediment extract, but are also dependent on the number and nature of sample locations within a given investigation. As a consequence, for example, the P_BIP_{25} values reported previously by Müller et al. (2011) for 38 samples from the northern North Atlantic were subject to some modification when the corresponding biomarker datasets were combined with those from the current study from the Barents Sea, due to a change in the c term. Likewise, this c term and the corresponding P_BIP_{25} values were also modified when the P_BIP_{25} – sea ice concentration relationship for the East Greenland locations alone was considered. Apart from the requirement, therefore, to have to re-calculate this term and the corresponding PIP_{25} values when either adding or removing biomarker

data from individual locations, an additional consequence is that potentially all data may be negatively influenced by a relatively small number of anomalous biomarker concentrations or outliers and this impact may be especially apparent for correlations with sea ice concentrations. In contrast, greater consistency in mean IP_{25}/phytoplankton biomarker ratios may exist for a given sampling location, where the array of potential influences on each of the two biomarkers may be somewhat more constrained and determined more by the nature of the immediate oceanographic conditions such as the sea ice cover. In support of this, a number of studies have shown that the PIP_{25} index can provide meaningful down core analyses of past sea ice conditions, especially when evaluated against other proxy data (e.g. Fahl and Stein, 2012; Müller et al., 2012; Stein et al., 2012; Cabedo-Sanz et al., 2013).

Finally, another reason for the poor correlations between the sea ice biomarker and sea ice concentrations could be the lateral transport redistribution of sediment particles. The fate of the particles deposited on the sea bed can be diverse and could affect the distribution of biomarkers for further interpretations. The Barents Sea is a region in which physical processes of sediment redistribution have been studied (Quadfasel et al., 1988) since this process is driven by the formation of dense bottom water masses which occur in sea ice covered regions. This process will be explained in more detail in section 5.4.5.

5.4.5 Lateral transport of sediment particles- allochthonous input

Thus far, the data presented here combines biomarker proxy data that align reasonably well with known sea ice conditions for different regions of the Barents Sea, especially, in terms of presence or absence of the sea ice biomarker IP_{25} (Figure 4.1 b). Despite these agreements, however, a small number of sediments from locations beyond the

MSIE also contained low concentrations of IP_{25} and this apparent anomaly was made even clearer in all the PIP_{25} data and the spatial representations of both IP_{25} and PIP_{25} datasets (Figure 4.4; Figure 4.5). The occurrence of IP_{25} in some locations south of ca. 74° N, likely indicates further processes that are responsible for the deposition of IP_{25} in sediments rather than vertical transport following sea ice melt. Although it is possible that the temporal sampling interval associated with the surface sediments (0-1 cm) extends beyond the period covered by satellite records, this possibility could be excluded for the southern samples on the basis of some known sedimentation rates for the study area (e.g. Zaborska et al., 2008; Maiti et al., 2010) which indicate that surface sediments (0-1 cm) reflect a maximum age of ca. 20 years, yet even longer-term observational accounts of sea ice suggest that this region has been ice-free for at least the last 50 years or so (Vinje, 2001; Divine and Dick, 2006).

An alternative hypothesis is that the occurrence of the IP_{25} biomarker in the south-Barents Sea represents allochthonous input, probably as a result of lateral transport of sediments and particulate material from the shelves. This process is likely to occur in other areas with steep slopes and irregular bathymetry although the outcome may not necessarily be as clear as the one described in this particular region.

A number of studies carried out in the Southern Ocean (e.g. Sicre et al., 2005; Mollenhauer et al., 2006) as well as in the Nordic Sea (Sarnthein et al., 2003) have demonstrated that, in addition to the vertical flux of particles, sediments can be susceptible to re-deposition following lateral advection, especially in deep basins and troughs (Fohrmann et al., 2001). Evidence for this (marine) advection was observed in two near-bottom sediment traps moored at the Barents Sea continental margin through a combined study of biomarker analysis, quantitative microscopy and bulk parameters

(Thomsen et al., 2001) which demonstrated that differences between these parameters could not be explained by the vertical flux of particles alone.

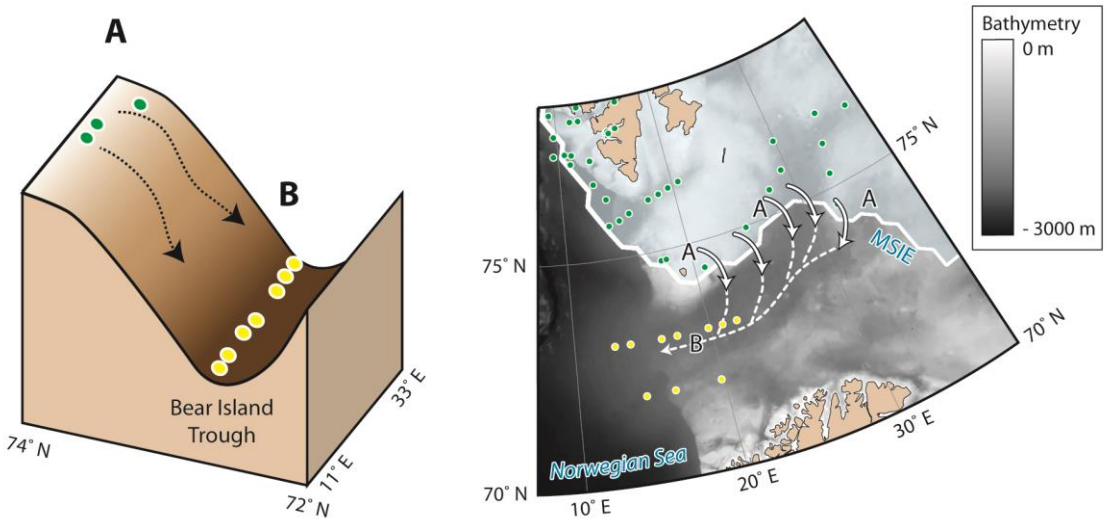

Figure 4.7 (a) schematic representation showing the proposed mechanism for advection of IP_{25} from within the MSIE to the Bear Island Trough (the solid arrows correspond to the potential source areas of advected IP_{25}; the dashed arrows represent the proposed direction of sediment transport); (b) Bathymetric map showing the sampling locations where IP_{25} was detected within the MSIE (green circles) and as a result of allochthonous input (yellow circles).

The presence of IP_{25} in sediments along the Bear Island Trough below 74° N (Figure 4.7) could likely be a result of dense water formation eventually reaching the bottom ocean. These dense bottom water masses are influenced by the bathymetry of the Barents Sea (Fohrmann et al., 2001), likely flowing cross-slope from the shelf edges and down banks such as Spitsbergen Bank and Stor Bank into the Bear Island Trough, which represents the maximum depth of the Barents Sea (Jakobsson et al., 2004) (Figure 4.7). These bottom water masses are denser, colder, more saline and CO_2 enriched which also were suggested to cause dissolution of the calcium carbonate foraminifera shells found in the Bear Island Trough (Steinsund and Hald, 1994) which therefore supports their presence in the Trough. These bottom water masses facilitate the transport and erosion of particles from the Barents Sea shelf, which subsequently

cascade down slopes into deep troughs. This process of sediment transportation and redistribution by lateral advection has previously been described in detail for parts of the Barents Sea (e.g. Fohrmann et al., 2001; Thomsen et al., 2001; Sarnthein et al., 2003). The same transport mechanism likely also influences the rest of the sterol biomarker abundances, but this is more difficult to decipher given the ubiquity of these biomarkers in all locations.

To further support this hypothesis of physical redistribution of sediment material (and associated biomarkers for the Bear Island Trough), Solignac et al. (2009) previously reported the presence of the Arctic dinoflagellate *I. minutum*, albeit in low abundances, in the Bear Island Trough. This could be interpreted as resulting from lateral advection from the neighbouring Spitsbergen Bank into the Bear Island Trough, since the otherwise dominant dinocyst species in this location was *Operculodinium Centrocarpum*, which is strongly related to Atlantic waters (de Vernal et al., 2005; Grøsfjeld et al., 2009; Solignac et al., 2009), consistent with the sampling location. A similar cascading of particulate material has been suggested to explain the occurrence of certain other microfossil remains in related troughs within the Barents Sea (Thomsen et al., 2001).

Similarly, this lateral transport process could be used to explain high (anomalous) IP_{25} concentrations found for the west shelf of Spitsbergen where satellite data describes sea ice concentration as less than 10%. This occurrence of higher IP_{25} in a very infrequent sea ice area could be due to allochthonous input from near Storfjorden where the sea ice concentrations reach up to 80%. Higher concentrations of sea ice in Storfjorden triggers an important amount of dense water masses formation, a process which has been reported and studied by (Quadfasel et al., 1988). Wobus et al. (2013) further developed and modelled the fate that the dense bottom water masses formed in Storfjorden would

follow and surprisingly, the path of the plume is described according to the highest concentrations of IP_{25}. Instead if we look at the biomarker brassicasterol, in most of the cases the concentrations are greater than 100 µg g^{-1} TOC, but in two cases lower than that value.

Clearly, the allochthonous input of IP_{25} into sediments within the Bear Island Trough and the west side of Svalbard will also influence the P_BIP_{25} index for these regions, and the consequence of non-zero PIP_{25} data for locations with no sea ice cover will also impact on the linear relationship between the PIP_{25} index and mean sea ice concentrations. This may explain, in part, the poorer agreement between these two parameters compared to the previous study by Müller et al. (2011). The lateral advection of biomarkers and other sedimentary proxies and the impacts that this can have in terms of influencing other palaeo-environmental proxy reconstructions has been presented previously (e.g. Benthien and Müller, 2000; Mollenhauer et al., 2006) but this is the first study that has provided clear evidence for the potential significance of such processes when conducting IP_{25}-based sea ice reconstructions.

4.4.6 Extended biomarker studies of Barents Sea surface sediments

4.4.6.1 Searching for new phytoplankton contribution to the PIP_{25} index

Following the previous IP_{25} and sterol biomarker analysis carried out in the Barents Sea, a suite of additional diatom derived HBI lipid biomarkers were analysed in order to determine if these could provide more information about the modern climatic conditions in the Barents Sea and identify under which environmental conditions each were produced.

Specifically, two HBI trienes, previously shown to be derived from certain phytoplankton diatoms (Belt et al., 2000; Belt et al., 2001; Massé et al., 2011; Collins et

al., 2013) were measured and their distributions considered in a manner analogous to those described previously for sterols. Therefore here, the suitability of alternative HBI lipids is evaluated in the PIP_{25} index in the search for better predictions of sea ice conditions.

4.4.6.2 Individual biomarker distribution (point location)

Within this slightly modified dataset (n=58), IP_{25} was analysed alongside the other HBI lipid biomarkers (Figure 4.8 a) and showed the same general distribution pattern to that found previously for a larger dataset (Figure 4.1 a, Table A.3 in Appendix). Specifically, IP_{25} was identified in 28 of the 58 samples and the same close association to sea ice was confirmed.

Diene II was found in 29 out of 58 samples (Figure 4.8 b). All the samples where diene II was present were located inside the maximum sea ice extent (MSIE) to the north Barents Sea with concentrations between 0.35 and 3.59 µg g^{-1} TOC, except for 5 samples located south of the MSIE. Of these 5, 4 of them were located in the Bear Island Trough and had relatively low concentrations (0.02-0.04 µg g^{-1} TOC). A further sample containing diene II was from the north coast of Norway (sample 690) also with a relatively low concentration (0.22 µg g^{-1} TOC). The distribution of diene II was very similar to that of IP_{25} (Figure 4.1 b and Figure 4.8 a).

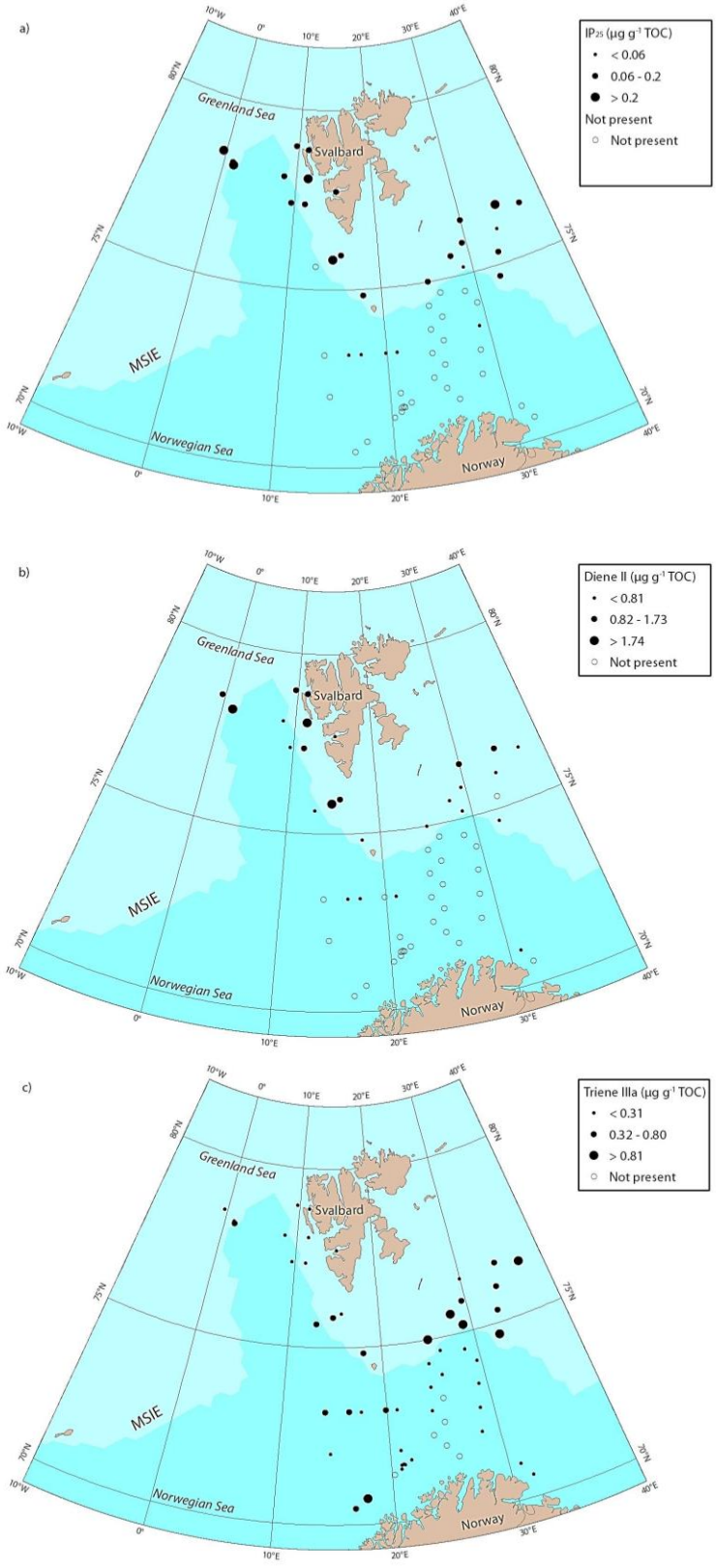

Figure 4.8 Maps of the region of the Barents Sea described in the current study: (a) occurrences and concentration ranges of IP_{25}; (b) occurrences and concentration ranges of diene II; (c) occurrences and concentration ranges of triene IIIa all in µg g^{-1} TOC. Maximum sea ice extent (MSIE) for the period 1983-2002 is also indicated (*continued on the next page)*.

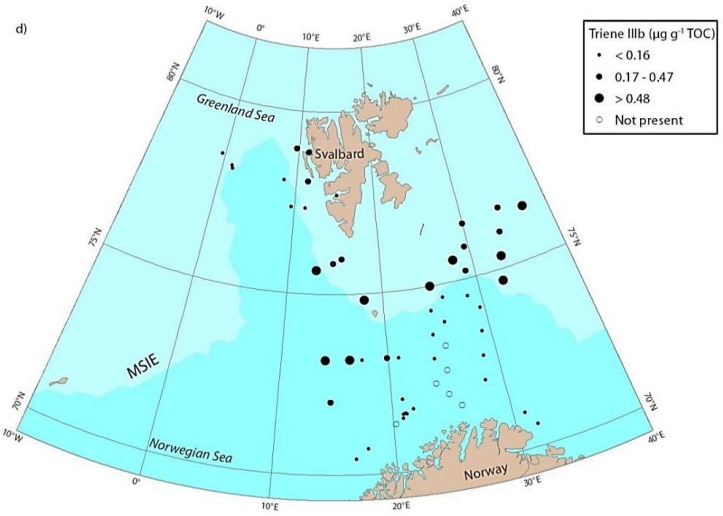

Figure 4.8 Individual biomarker representations in the Barents Sea study area, (for detailed description of currents see d) triene IIIb; in µg g^{-1} TOC. MSIE for the period 1983-2002 is also indicated.

The co-occurrence of diene II and IP_{25} has been observed previously (Belt et al., 2007; Massé et al., 2008; Vare et al., 2009) and more recently in surface sediments (Xiao et al., 2013) in the Arctic region.

In contrast to IP_{25} and diene II distribution, trienes IIIa and IIIb were present in the majority of the samples, including those beyond the MSIE (Figure 4.8 c, d). Distribution of triene IIIa and its isomer IIIb were very similar, being present or absent in the same samples. Both trienes were found in 53 out of 58 samples and the 5 samples where they were absent were situated in the mid Barents Sea between the MSIE and the north coast of Norway (Figure 4.8). In general, triene IIIa (0.29 µg g^{-1} TOC), was slightly more abundant in the Barents Sea than triene IIIb (0.21 mean values µg g^{-1} TOC) respectively where the major difference was found for the North eastern Barents Sea. Concentrations ranged from (0.02 - 1.49 µg g^{-1} TOC triene IIIa)-(0.02 - 0.81 µg g^{-1} TOC triene IIIb). Trienes IIIa and IIIb were present in all the 7 samples distributed along the Bear Island Trough with a concentration range (0.02 - 0.75 µg g^{-1} TOC).

4.4.6.3 Biomarker spatial representation

Extrapolation of individual lipid values into a spatial representation (Figure 4.9) facilitated further interpretations of the data. Distribution of diene II defined the marginal ice zone in agreement with distribution of IP_{25}, supporting its close association to a sea ice produced HBI. Diene II is absent for the southern Barents Sea which is in line with the relatively warmer Atlantic water entering the Barents Sea between Bear Island and the north coast of Norway which determines sea ice free conditions. Diene II was, in most cases, more abundant than IP_{25}, as is routinely observed in other studies in surface and down core sediments in the Arctic region, (Massé et al., 2011; Fahl and Stein 2012; Cabedo-Sanz et al., 2013; Xiao et al., 2013). An exception to this was in the Bear Island Trough, where concentrations were more comparable between these HBIs, even when they were very low.

The spatial distribution of triene IIIa and IIIb was remarkably similar (Figure 4.9 c, d). Both lipids were more abundant along the MSIE until the vicinity of southern Svalbard consistent with the marginal ice zone being a biologically productive area (Carmack and Wassmann, 2006). A distinctive area is revealed on the central southern Barents Sea with very low abundances / absence of both lipids. This result could indicate a low diatom population in this area, however diatoms are usually dominant as primary producers in the Barents Sea (Wassmann et al., 1999) where primary productivity is important (Carmack and Wassmann, 2006; Wassmann et al., 2006).

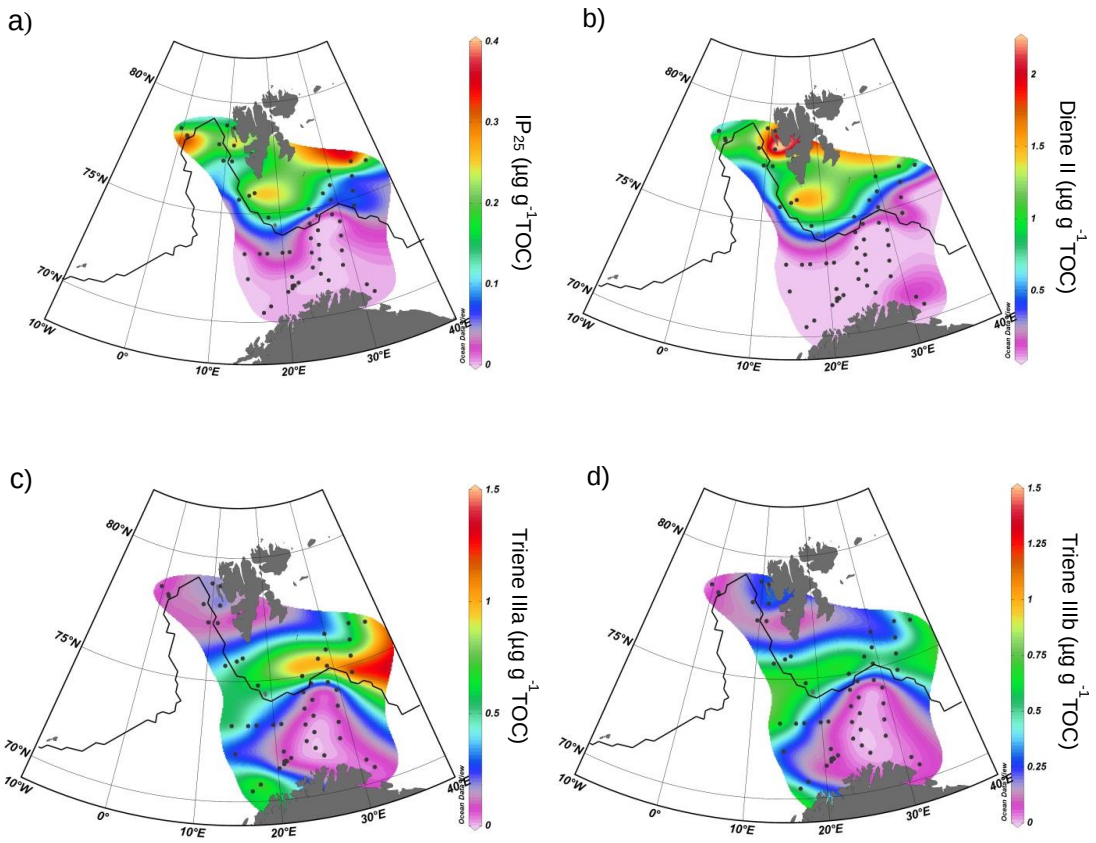

Figure 4.9 Spatial distributions of individual biomarker concentrations with ODV: a) IP_{25} (re-calculated values); b) diene II; c) triene IIIa; d) triene IIIb. Black line indicates the MSIE maximum sea ice extent.

A possible explanation for such low abundances of IIIa and IIIb could be that for the southern Barents Sea, which is sea ice free and characterised by relatively warmer Atlantic waters, the blooms are developed slowly and mainly by solar radiation (Wassmann et al., 1999). This causes a delay in the peak bloom (Wassmann et al., 2006) and provides an opportunity for zooplankton and fauna to graze the phytoplankton biomass (Sakshaug, 1997; Wexels Riser et al., 2008). Important zooplankton communities in the southern Barents sea are advected from the Norwegian Sea with the NAC (Wassmann, 2001) which can reduce or regulate the depletion of the phytoplankton biomass, thereby reducing the abundance of biomarkers in underlying sediments. Interestingly, the south eastern Barents Sea contains one of the world largest

fish stocks including the *Atlantic herring*, a boreal species which feeds on phytoplankton and migrates to follow food supplies. The same situation on the lipid distribution on the Barents Sea was observed for the sterols (e.g. brassicasterol and dinosterol) which showed absence or very low concentrations for the immediate south of the Barents Sea.

4.4.6.4 Assessment of PIP_{25} using HBI trienes

Previously, the use of ubiquitous phytoplankton sterol biomarkers in combination with IP_{25} did not satisfactorily reproduce sea ice conditions for the study area. Here, the opportunity to assess lipids within greater source specificity (diatoms) was investigated by calculating PIP_{25} indices using trienes IIIa and IIIb (Table 4.2).

Table 4.2 PIP_{25} indices and *c* terms. (P) phytoplankton biomarker origin, (SI) sea ice biomarker origin. Biomarkers corresponding to the dataset n=58.

P LIPID	SI	*C* term	INDEX
Triene IIIa	**IP_{25}**	0.279	$P_{IIIa}IP_{25}$
Triene IIIb	**IP_{25}**	0.388	$P_{IIIb}IP_{25}$

Respective spatial representations were very similar (Figures 4.10 a, b) and in both cases, was observed a boundary region similar to the one described by the MSIE. $P_{IIIa}IP_{25}$ and $P_{IIIb}IP_{25}$ values were 0.3 - 0.6 for the marginal ice zone and 0.6 - 0.8 for the area northwards 76° N the MSIE, representing more abundant sea ice. In both cases, the PIP_{25} based reconstructions of sea ice conditions did not align well with known satellite sea ice concentrations for the Bear Island Trough and for the West margin of Spitsbergen. These results have been observed previously for the PIP_{25} with the sterols (section 4.4.1). Both linear correlations between PIP_{25} and sea ice concentrations were

poor R^2= 0.17 and 0.16 (Figure 4.11) similar to those previously found for the PIP_{25} index with the sterols.

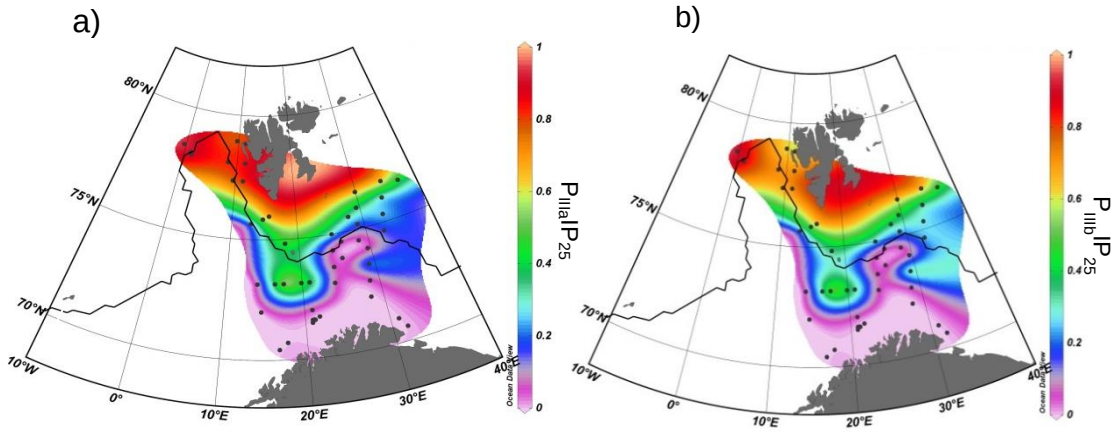

Figure 4.10. Combined biomarker indices (PIP_{25}) calculated using IP_{25} and triene IIIa $P_{IIIa}IP_{25}$ (a); IP_{25} and triene IIIb $P_{IIIb}IP_{25}$ (b). Black line indicates MSIE, maximum sea ice extent.

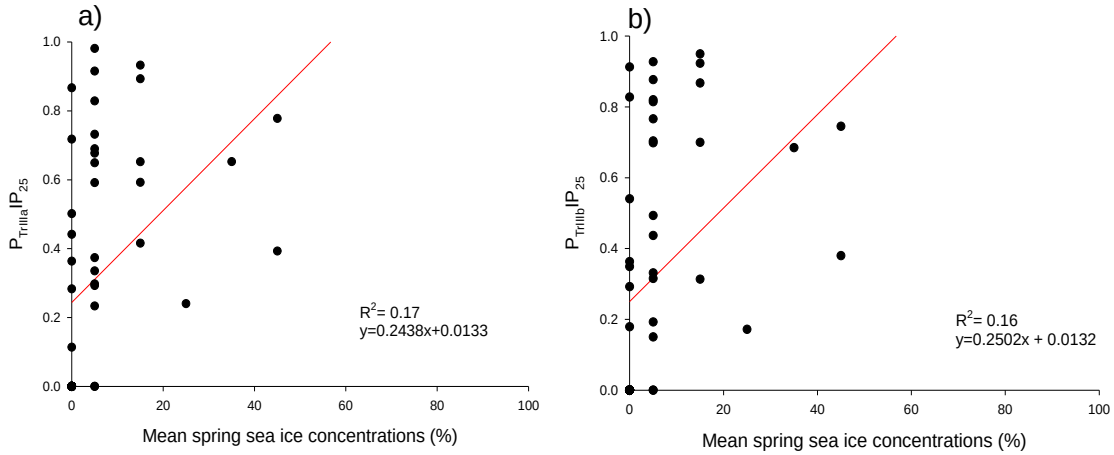

Figure 4.11 Linear relationship between (a) $P_{IIIa}P_{25}$; (b) $P_{IIIb}IP_{25}$ values and mean spring sea ice concentrations (Hadley; HadISST).Dataset of the study n=58.

In summary, none of the phytoplankton biomarkers i.e. sterol or HBI combined in the PIP_{25} index produced representative sea ice conditions for modern times in the Barents Sea. Following the same approach conducted in section 4.4.4, the relationship of the lipid biomarkers to sea ice concentrations was investigated. Once more, all lipids (sea

ice and phytoplankton origin) exhibited positive correlations (Figure 4.12), similarly to that observed for the phytoplankton steroidal lipids.

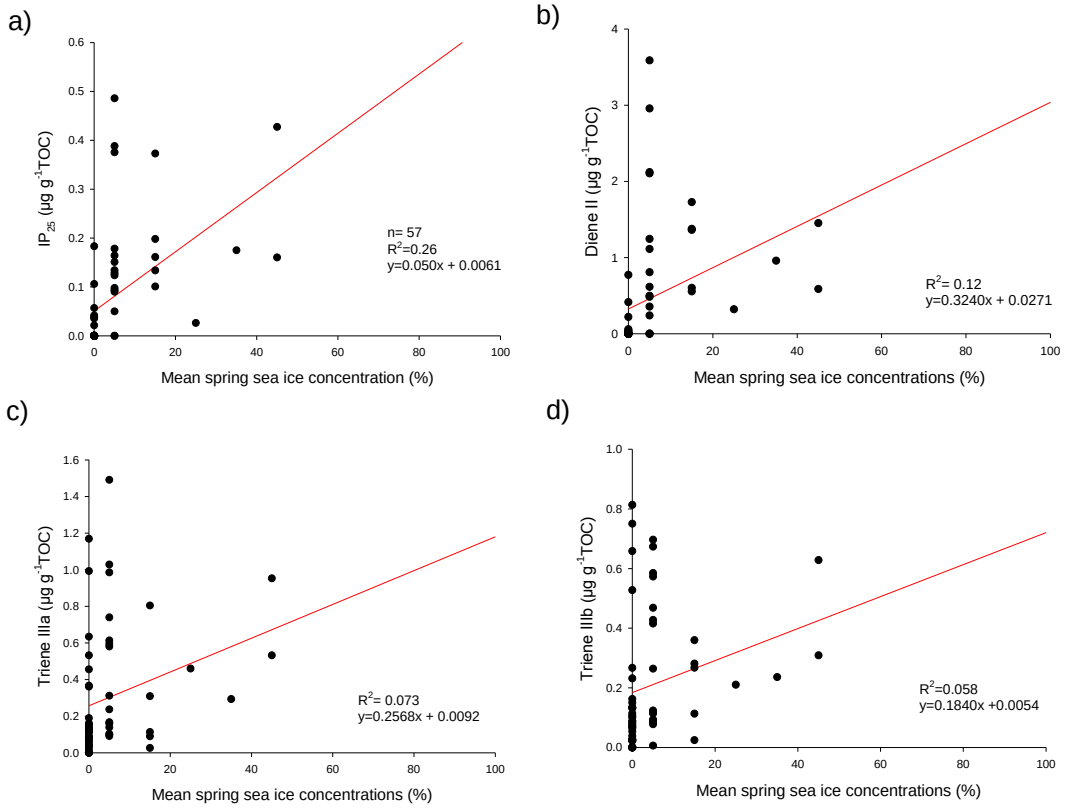

Figure 4.12 Linear relationships between (a) IP_{25}, (b) Diene II, (c) Triene IIIa, and (d) Triene IIIb. and mean spring sea ice concentrations (Hadley; HadISST). Dataset for the current study in the Barents Sea n=58.

4.4.6.6 Searching for better climatic reconstruction tools in the Barents Sea (relationship between individual biomarkers)

Although the use of HBIs and sterols within the PIP_{25} index did not yield helpful estimates of sea ice concentrations, it was believed that the proportion of HBI concentrations in sediments may be associated to ecological regimes in different areas. The calculation of the ratios between the biomarkers and its interpretation might help to identify specific productive areas by looking at the proportion of HBIs in sediment material, as a spatial fingerprint mechanism.

4.4.6.7 Relationship between HBI individual biomarkers

Prompted by the spatial similarity between IP_{25} and diene II, and trienes IIIa and IIIb observed in this study, the relationship between the studied biomarkers was investigated. Similarity between biomarker distributions was expected to be found given previous work. For instance Cabedo-Sanz et al. (2013) used the combination of the sea ice biomarker (IP_{25}) and the lipid (diene II) mostly produced under sea ice conditions for the description of the stability of the marginal ice zone. This was called the DIP_{25} ratio, and was successfully used to identify sea ice variations during the Younger Dryas which was in agreement with SST reconstructed from $\delta^{18}O$ values from foraminifera assemblages (Ebbesen and Hald, 2004) showing SST variations up to ca. 8° C according to the highest flickering on the DIP_{25} ratio for the same sub-periods of the Younger Dryas. Previously, this ratio was determined in other down core sediments studies from the Icelandic shelf, Barrow Strait and Dease Strait and compiled in Cabedo-Sanz et al. (2013). Correlations were R^2= 0.93 - 0.98. DIP_{25} ratios were also tested in a down core North Norway for different time periods of the Younger Dryas, (Cabedo-Sanz et al., 2013) revealing sub-periods interpreted as stable sea ice conditions, when the correlations was R^2= 0.94 and very unstable with correlations of R^2= 0.58 between diene II and IP_{25}. The DIP_{25} ratio has been also tested in surface sediments from the Kara and Laptev seas (Xiao et al., 2013) obtaining poorer correlations R^2= 0.57. Further, (Xiao et al., 2013) also studied any relationship existing between the combination of sea ice –phytoplankton HBI biomarkers which did not yield successful results. Nevertheless that attempt was also considered and studied here in surface sediments by comparing IP_{25} within trienes IIIa and IIIb for the Barents Sea.

In comparison to the well documented cases of DIP_{25} ratio, the relationship between the trienes IIIa and IIIb has not been studied in detail. Therefore, the opportunity of carrying

out analogous investigations to the DIP_{25} was presented here. Since the DIP_{25} has only been used to describe stability of sea ice, there is a lack of data for warmer geological periods such as the Holocene or warmer areas (sea ice free) for recent times. Thus, similar to the $DIP_{25,}$ the combination of two open water phytoplankton lipids e.g. trienes, could potentially be used to decipher variations in oceanographic conditions of the seasonally open waters or permanent open water areas, and this approach will be investigated here. A list of all the studied ratios is given in Table 4.3.

Table 4.3 Combination of lipid biomarkers (diatom source). Respective ratios are indicated.

BIOMARKER 1	BIOMARKER 2	RATIO
Diene II	IP_{25}	DIP_{25}
Triene IIIa	Triene IIIb	IIIb / (IIIa +IIIb)
Triene IIIa	IP_{25}	$Tr_{IIIa}IP_{25}$
Triene IIIb	IP_{25}	$Tr_{IIIb}IP_{25}$

4.4.6.7.1 Linear correlations between biomarkers

A very good linear relationship in the abundances of diene II and IP_{25} (R^2= 0.90) (Figure 4.13 a) was obtained. In the case presented here for surface sediments, high variability on the distribution could potentially have been materialized, as the analysis covers an extensive area influenced by different water masses, sea ice conditions and physical processes (Loeng, 1991; Sakshaug, 1997; Falk-Petersen et al., 2000; Wassmann et al., 2006). However the correlation in this study could have been also improved if we consider that physical processes such as lateral transport of particles, hypothesized to occur in the Bear Island Trough (Figure 4.7) might have modified the distribution of the HBIs in sediments. A physical process of such characteristics in nature is very unlikely to be homogeneous and reproducible, distributing equally sediment material across the seabed.

Similar to the relationship of the two sea ice indicators, a linear correlation between triene IIIa and IIIb was also good (R^2= 0.82, Figure 4.13 b), suggesting a common source and production under similar environmental conditions across the area.

However, when combining individual trienes with IP_{25} abundances results showed a much greater variability, likely due to the differences in the environmental conditions and sources that are responsible for their production. For the $Tr_{IIIa}IP_{25}$ ratio the coefficient of determination was R^2= 0.49, similarly to $Tr_{IIIb}IP_{25}$ R^2= 0.51 (Figure 4.13 c, d).

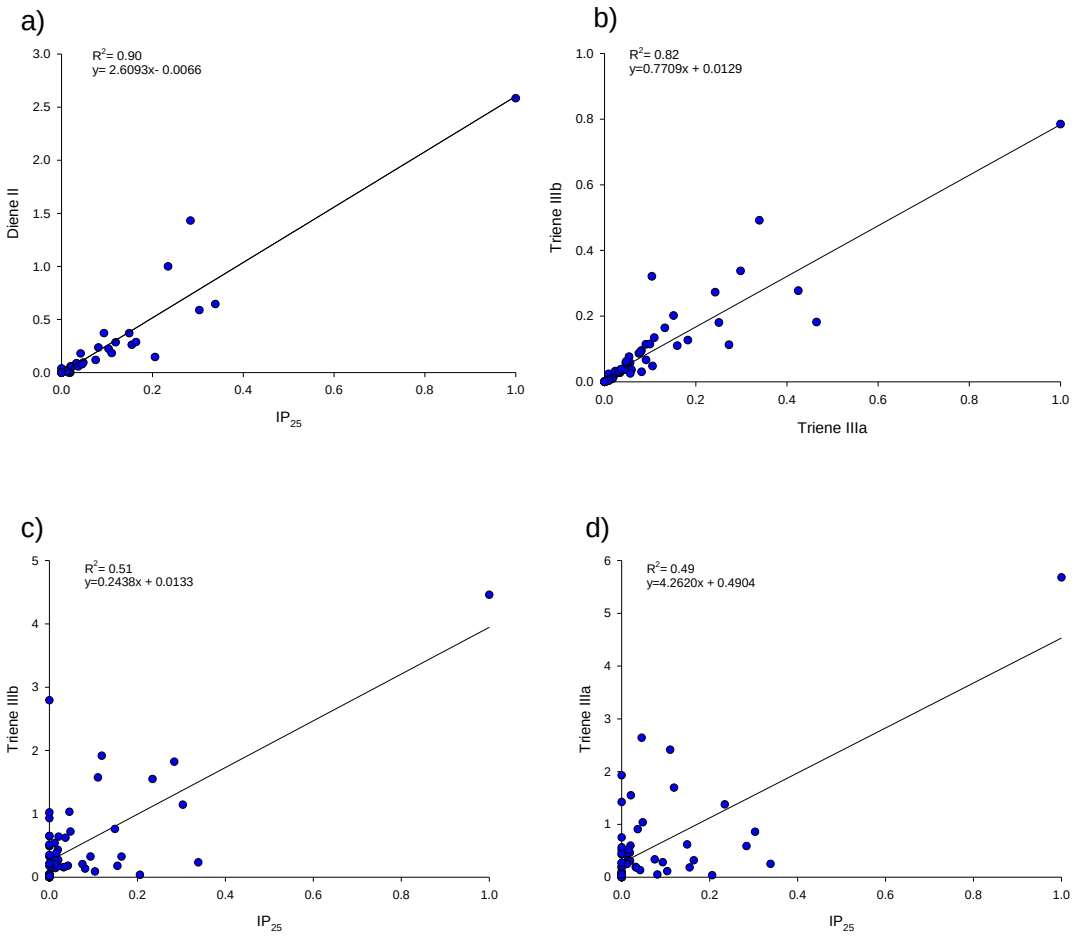

Figure 4.13 Linear relationship between normalized peak areas for; (a) IP_{25} and diene II, (b) Triene IIIa and IIIb, (c) Triene IIIa and IP_{25}, (d) Triene IIIb and IP_{25}.

4.6.7.2 Spatial representation and interpretation of the ratios

Previously it was proposed that when the DIP_{25} ratio is fairly constant it represents a more stable sea ice area, while variable ratios would represent drastic climatic changes resulting in unequal production of these two HBIs. Thus the spatial representation of the DIP_{25} ratios (Figure 4.14 a) in the Barents Sea made possible the distinction of 3 areas. The highest ratios, (high variability = high ratio) were located in the West margin of Spitsbergen close to shore, with values from 4-5 units. This area is influenced by Arctic water coming from the East Spitsbergen current moving along the shelf of Svalbard which in spring could lead to IP_{25} production and at the same time mixed up with Atlantic waters coming from the West Spitsbergen current which in summer could lead to phytoplankton lipid production. For the west margin of Spitsbergen we have two different scenarios occurring almost simultaneously. On one hand this area is part of the MIZ, so consequently it will experience the spring blooms when the marginal ice that is present here starts to retreat. On the other hand, Atlantic waters move along the shelf of Svalbard carrying warmer and more saline nutrient and phytoplankton enriched waters. Varying annually, strong WSC will cause short spring blooms which will lead to longer early summer phytoplankton blooms in this area. This situation corresponds to high sea ice variability and productivity which could be interpreted as very variable environment with relatively high DIP_{25} ratios. The other distinctive area is defined along the MSIE with values going from (2-3). The ratio in this area had smaller values, which suggests that the difference between the two biomarkers is less significant, possibly related to the fact that the sea ice conditions are more consistent in the immediate South Spitsbergen and East Barents Sea, suggesting relatively more abundant sea ice. Lastly it was identified another distinctive area in the Bear Island Trough where ratios were (0-1) units with different ratios to the rest of the areas, probably as a result of lateral transport.

A spatial comparison of the ratios between the trienes (IIIb / (IIIa +IIIb)) was also considered (Figure 4.14 b). The ratio avoids misinterpretations of total abundances which could be due simply to localised effects, e.g. areas richer in nutrients, different ecosystem or food webs. Instead, the ratio reflects the relative abundance of triene IIIb with respect to the total triene lipid abundance, independent of regional factors.

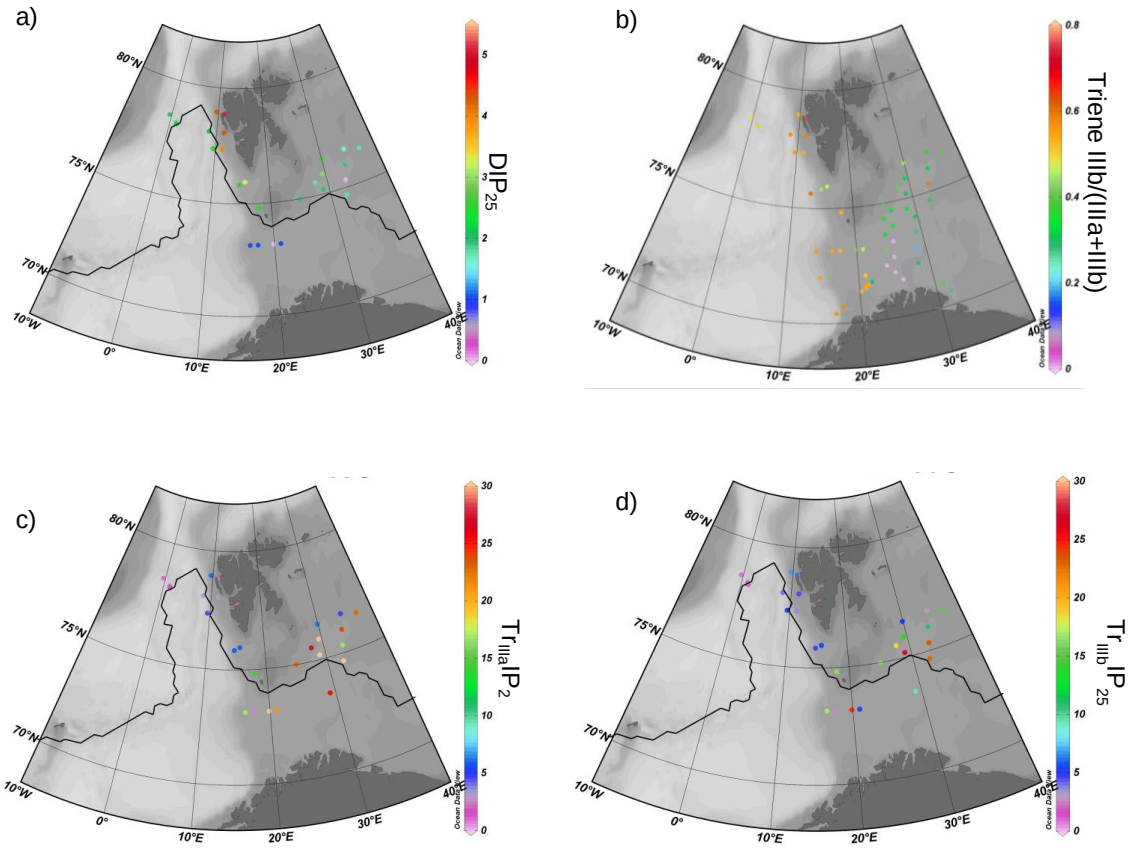

Figure 4.14 Spatial representations of the ratios in ODV: (a) for the DIP_{25} ratio, (b) ratio between trienes IIIa and IIIb, plotted as single point locations with the bathymetry of the study area.

From the spatial distribution was possible to differentiate areas according to the distribution of these two biomarkers. Ratio units of (0.5 - 0.9) identified abundances of the lipid triene IIIb with respect to the total triene production for the West Barents Sea, specifically from the West Norwegian coast, passing by the vicinity of Bear Island to the West margin of Spitsbergen, possibly reflecting the path of the Atlantic water

masses (NAC and WSC). Ratio units of (0.3 - 0.45) were identified at the eastern Barents Sea. This revealed a relative enhancement of triene IIIa, potentially reflecting the characteristic Arctic water masses which occur at this location entering the Barents Sea with the East Spitsbergen current from the north. However further studies are required before the significance of the changes in triene ratios can be fully understood.

Finally the ratio between the phytoplanktonic trienes and the sea ice (IP_{25}) lipids did not result in any clear identification of any association to any of the known oceanographic or sea ice modern conditions in the Barents Sea. Results showed a rather random distribution across the Barents Sea with high and low ratios simultaneously observed for all the study area.

4.5. Conclusions

To address objective 1, ca. 100 surface sediments from the Barents Sea were analysed for the presence and abundance of the sea ice diatom biomarker IP_{25} and sterols, indicators of open water phytoplankton. In summary, conclusions for the first objective were:

(1) The data shown in this study demonstrated a good relationship (presence /absence) between the occurrence of the sea ice proxy biomarker IP_{25} in surface sediments from the Barents Sea and known sea ice cover in recent decades derived from satellite records. As such, this study extended the application potential for the IP_{25} sea ice proxy to a climatically sensitive region of the Arctic and sub-Arctic regions.

(2) The number and spatial diversity of the surface sediments analysed here enabled to conduct a reasonable test of the P_BIP_{25} index, previously proposed by Müller et al. (2011) to provide more detailed descriptions of sea ice conditions in Arctic regions. The individual P_BIP_{25} values and spatial distributions were partially consistent with known

seasonal sea ice cover for the Barents Sea, providing overestimates of sea ice conditions especially for the western Barents Sea, where modern satellite records show less than 10% sea ice coverage. In addition, the agreement between the P_BIP_{25} data and known mean spring sea ice concentrations was quite variable and the extended dataset caused an overall decrease in the agreement of the P_BIP_{25} index to sea ice concentrations observed previously by Müller et al. (2011).

(3) Some other steroidal lipids (24-methylenecholesterol and dinosterol) were tested into the PIP_{25} index aiming to provide accurate sea ice conditions for the Barents Sea. The partial agreement of the new PIP_{25} indices to correlate well to known sea ice concentrations emphasized the idea of the Barents Sea being a complicated area to study. It was observed however, that dinosterol integrated index hold the best sea ice conditions for the region, providing reasonable marginal sea ice conditions at both side of the Svalbard Archipelago.

(4) The observation of IP_{25} in locations (Bear Island Trough) somewhat distal from the position of the maximum sea ice extent (1983 – 2002) provided the first example of the occurrence on this biomarker in surface sediments from regions of no recent sea ice cover. It was hypothesised that the occurrence of IP_{25} in such sediments may, potentially, be attributed to allochthonous input of this biomarker as a result of sediment transport.

Following objectives two, the additional HBI biomarkers were analysed and results were interpreted. Conclusions were:

(1) HBI data demonstrated in this study for surface sediment in the Barents Sea that the diene II is a good qualitative biomarker for sea ice occurrence. In contrast, trienes

showed to be more associated to phytoplankton origin. All biomarkers were compared to satellite records for recent decades.

(2) Marginal sea ice areas were identified to hold the highest abundances of all lipid biomarkers analysed in this study.

(3) Although the dataset was reduced due to sediment availability, analysis of the PIP_{25} index were still of a great value. The incorporation of both novel trienes into the PIP_{25} index gave similar outcomes predicting partially successfully the known sea ice conditions. However they both failed to predict sea ice conditions for the west margin of Svalbard similarly to that shown by all the PIP_{25} calculations. Therefore, PIP_{25} data should still be treated with caution and considering possible localised effects.

(4) In the attempt to find better sea ice reconstructions, DIP_{25} ratios were tested. It was confirmed that the relation between IP_{25} and diene II in the Barents Sea is strong.

(5) The observation of the apparent correlation of the lipid trienes to water masses characteristics provided new insights into these two novel geochemicals and their potential use to decipher oceanographic conditions. This regional observation however was novel in the Arctic region, therefore further investigation is required in order to confirm this suggested application of the ratio.

(6) The high variability in the ratios DIP_{25}, $Tr_{IIIa}IP_{25}$ and $Tr_{IIIb}IP_{25}$ observed in the Bear Island Trough helped to support the hypothesis formulated in section 4.4.5 of allochthonous input of sediment material from the near shelfs going down slope into the Trough.

CHAPTER FIVE

5. Palaeo-sea ice reconstructions in the western Barents Sea over the last ca. 3800 years

5.1 Introduction

The sea ice conditions in the Barents Sea are well known to be very variable in extension and concentration on an annual basis (Figure 5.1 a), mainly due to fact that the sea ice in this region is first year sea ice, which melts during the summer period (Petrich and Eicken, 2010). First year sea ice is normally 1.5-2 m thick (Polyak et al., 2010), which especially makes this relatively shallow sea ice cover sensitive to changes in temperature and salinity variation of the water masses, wind stress and air temperature. The western Barents Sea is an interesting and challenging location to study sea ice conditions due to the fact that different types of sea ice and water masses meet at this point, in comparison to the eastern Barents Sea, which is dominated by Arctic waters and first year sea ice (Figure 5.1 a, b). The western north Barents Sea (ca. 78-80° N) is connected to the Fram Strait, which is a very dynamic area in terms of sea ice, influenced by the amounts of multi-year drift ice entering from the Arctic Ocean on the Eastern Greenland, which records over the last ca. 150 years demonstrate (mainly sealer and ship logbooks) (Figure 5.2 b (April 1780-1796)) to reach great extensions into the western Barents Sea. Evidence of this high variability was described by (Divine and Dick, 2006), especially on the inflexion point of the margin sea ice at ca. 78° N which retreats over 150 km in over 150 years, while the sea ice edge along the Spitsbergen coast has remained approximately at the same location for April in the same period (Figure 5.2 b).

a) Averaged monthly sea ice edge position ca. last 20 yr.

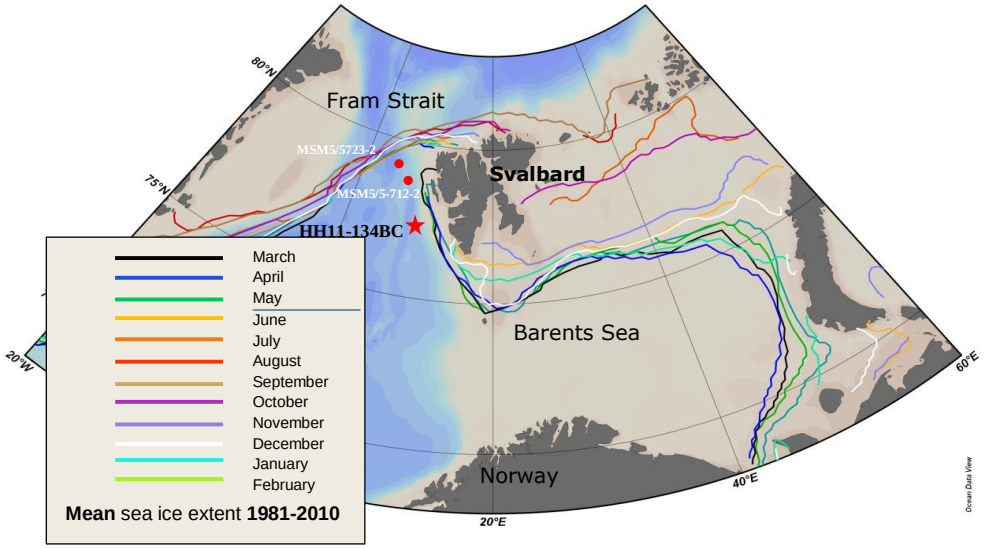

b) Oceanographic settings and core locations

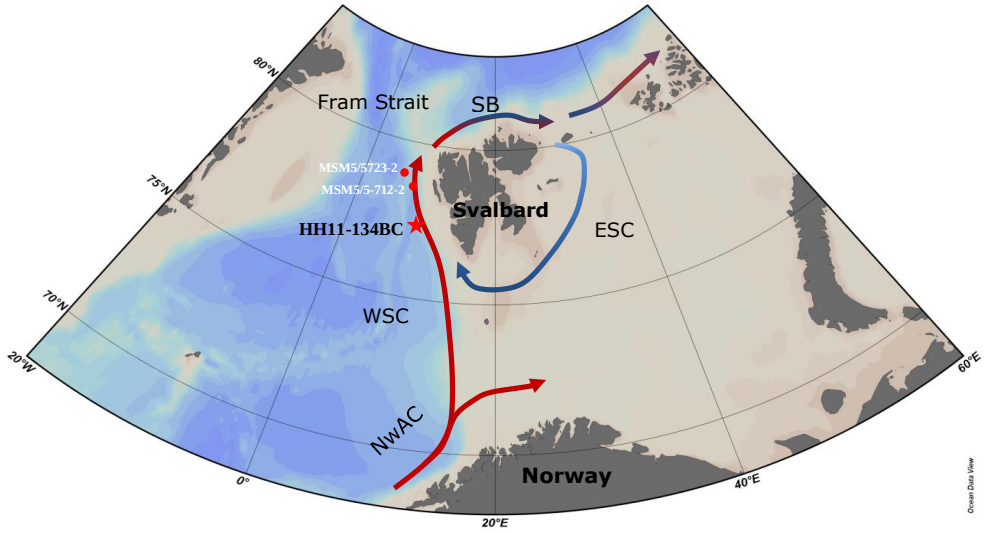

Atlantic water →	**Arctic water** →
NwAC – Norwegian Atlantic Current Current	**ESC**- East Spitsbergen
WSC- West Spitsbergen Current	**SB**- Svalbard Branch

Figure 5.1 a) Monthly mean sea ice extent for the period (1981-2010) National Snow and Ice Data Center (NSIDC), red dots indicating core locations, b) Oceanographic settings of the study area and location of the core study here (HH11-134-BC red star) and the cores which data was used for comparison MSM5/5-712-2, MSM5/5-723-2 (Müller, 2011).

a) Averaged sea ice edge position last ca.150 yrs

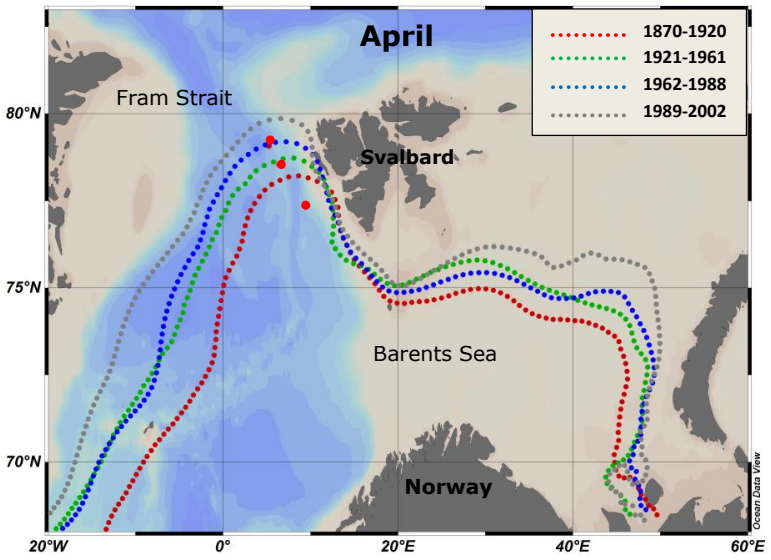

b) Particular "anomalies" in the sea ice edge positions

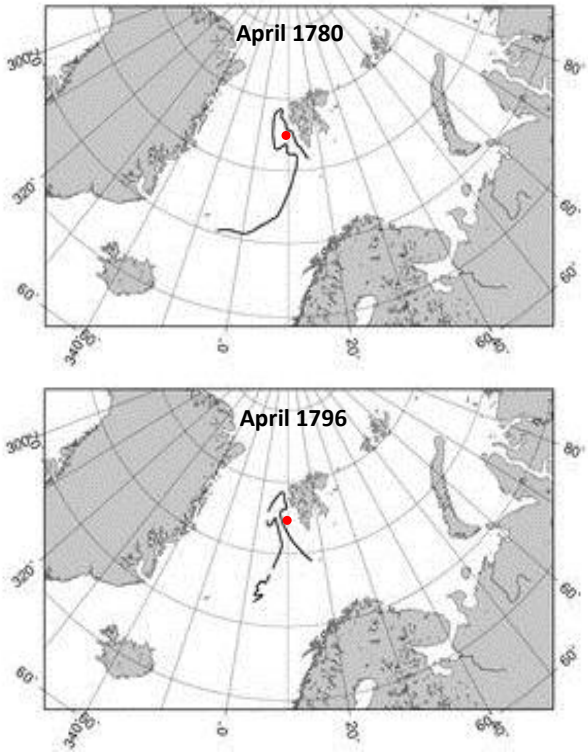

Figure 5.2 a) Multi-decadal sea ice position (mean) for April; (b) sea ice edge for April for particular years (NSIDC) (Divine and Dick, 2007). .Approximate location of HH11-134BC is indicated with a red dot.

Other anomalies in the sea ice extension and variability were observed in historical records, such as the formation a polynya type area (Figure 5.2 b (April 1796), Figure 5.3) which traps a space of open waters surrounded by sea ice, or the formation of isolated sea ice patches Figure 5.5.

Figure 5.3 Historical sea ice maps describing the Arctic sea ice for May 1924 collected by the Danish Meteorological Institute (DMI) in the (Nautisk Meteorologisk Aarbog). (www.pmle.noaa.gov/ accessed in March 2014)

Figure 5.4 Historical sea ice maps describing Arctic sea ice for May 1917 collected by the Danish Meteorological Institute (DMI) in the (Nautisk Meteorologisk Aarbog). (www.pmle.noaa.gov/ accessed in March 2014)

Figure 5.5 Historical sea ice maps description of Arctic sea ice for June 1913 collected from the Danish Meteorological Institute (DMI) in the (Nautisk Meteorologisk Aarbog) (www.pmle.noaa.gov/ accessed in March 2014)

Since the study area is relatively close (ca. 100 km) to the west coast of Svalbard, the main water masses converging in this region and freshwater input from melting of nearby glaciers and rivers result in very stratified waters which could have an important impact on the ecosystem if compared to truly marine areas. The most important mechanisms affecting the sea ice retreat and advance are the heat exchanges between the ocean and atmosphere and oscillations between the two which go some way to explaining the sea ice variability at least over the last centuries (Sorteberg and Kvingedal, 2006; Loeng and Drinkwater, 2007). The proximity of the sea ice extension to the Spitsbergen shelf is likely to be one of the reasons for the sea ice to be highly variable, extension of which could be easily triggered by winds and initiated by land fast ice. On the other hand, retreat is also likely to occur in very short time periods, since the main water mass circulating carries Atlantic waters, and the heat transported would be restricted by the Spitsbergen shelf which could lead to a rapid melt of the sea ice formed on the surface.

Another point to consider is to what extent the selection of the satellite records are important in order to understand the variability of the sea ice. Average concentrations of sea ice exclude the minima and maxima observed (anomalies), which are of a high importance to understand the high variability of the sea ice conditions for particular areas such as the western Barents Sea (Figure 5.6 a, b). Maximum sea ice concentrations would be the optimum satellite record to choose, in order to show the sea ice conditions to describe for IP_{25} distributions, since effective biological production could occur during "anomaly" sea ice conditions imprinting a sea ice signal where, otherwise mean sea ice concentrations would indicate sea ice free conditions.

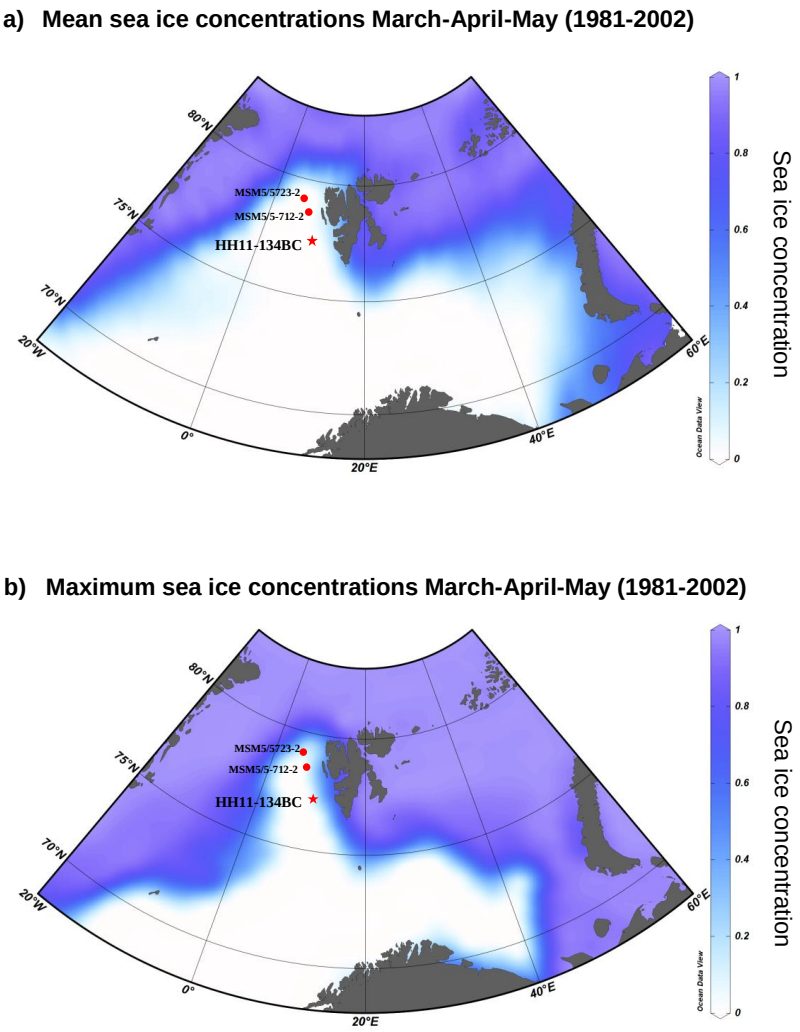

Figure 5.6 Satellite derived sea ice (UK Met Office Hadley Centre database (HadISST) (Rayner et al., 2003). a) mean and b) maximum spring sea ice concentrations for the interval (1983-2002) March-April-May. Red dots and star represent location of the cores.

Therefore, in order to gain more detailed information about the sea ice conditions in the western Barents Sea, a biomarker analysis was carried out where the main objectives were:

1. To analyse sea ice and phytoplankton biomarkers in a sediment core in a region where known sea ice conditions have been shown to be very variable.
2. To compare results with nearby core locations and contextualize the study area in terms of sea ice conditions.

3. To further investigate and compare IP_{25} derived sea ice reconstructions with other proxy derived sea ice reconstructions (dinocysts, and combination of biomarkers (P_BIP_{25})).
4. To propose sea ice settings based on biomarkers and make comparisons with historical records.

5.2 Regional settings

The oceanography of the Barents Sea is described in Chapter 4. Main water masses, bathymetry and location of the study cores are represented in Figure 5.1 b.

5.3 Material and methods

5.3.1 Chronology

A box core with the respective push core HH11-134BC was collected in July of 2011 by the *RV Helmer Hansen*, on the West Spitsbergen slope (77° 35' N 9° 53' E) with a length 41 cm at a water depth of 1383 m. Only the first 30.2 cm (corresponding to the oldest dated sample) were analysed in this study.

An age-depth model of HH11-34BC was constructed (Dylmer et al., 2013) based on three AMS (Accelerator Mass Spectrometry) ^{14}C dates which were calibrated using Calib. 6.1.1 (Stuiver and Reimer, 1993) and the Marine09 calibration curve (Reimer et al., 2009) (Table 5.1). Hence, the age-depth model ranges between 0 and 3774 cal. yr BP with a second order polynomial fit (Figure 5.7). Sedimentation rates of the studied push core ranged 8-18 cm kyr^{-1} which, according to the sampling resolution provided a temporal resolution record of 27-62.5 yr. This high resolution will enable to produce multi-decadal reconstructions of the sea ice conditions such as variability, retreat, advance and continuity of the sea ice cover for the western Svalbard shelf.

Table 5.1 Core, sample depth, dated material, ^{14}C AMS calibrated years BP, (Dylmer et al., 2013); * value excluded from the age model.

Core	Core depth (cm)	Dated material	^{14}C AMD age yr BP	Calibrated age (cal. yr BP)	Calibrated ages, 2σ range
HH11-134-BC	9.75	Bulk planktic foraminifera	826±23	462.5	420-505
HH11-134-BC	15.5	Bulk planktic foraminifera	2030±30	1602	1515-1688
HH11-134-BC	19.5*	Bulk planktic foraminifera	1995±28	1571*	1473-1669
HH11-134-BC	30.25	Bulk planktic foraminifera	3825±30	3774.5	3676-3873

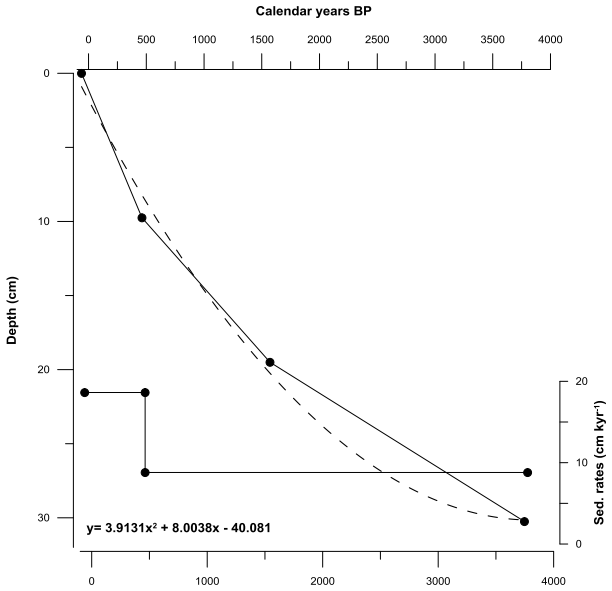

Figure 5.7 Calendar age-depth diagram and sedimentation rates of HH11-134-BC with second order polynomial fit (Dylmer et al., 2013).

5.3.2 Biomarker analysis

Biomarker analyses were conducted as described in Chapter 2 using SPE method, described in section 2.3.2 (Figure 2.14). IP_{25} and sterol biomarkers (brassicasterol and 24-methylenecholesterol) were analysed. Biomarker fluxes were calculated by combining biomarker concentrations with sediment densities and accumulation rates as described previously (Belt et al., 2012b). Additional P_BIP_{25} index was calculated following (Müller et al., 2011).

5.4 Results

Biomarker profiles for HH11-134-BC core (ca. 3.8 cal. kyr BP) showed increased fluctuation from around ca. 2 cal. kyr BP towards present day. Concentrations of the sea ice biomarker IP_{25} decreased in general towards present day with an optimum at ca. 1.5 cal. kyr BP (Figure 5.8) with concentrations of IP_{25} ranging from 0 to 7.70 ng g^{-1}, which was in accordance to IP_{25} concentrations of nearby locations (2.22-11.16 ng g^{-1}) (Müller et al., 2012) as well as concentrations found in surface sediments from the same area (Chapter 4 (Figure 4.1 b)). The phytoplankton biomarkers brassicasterol and 24-methylenecholesterol also showed higher concentrations at ca. 1.5 cal. kyr BP, however, a rapid increase over the last century was also observed. Similar trends to the concentration profile were identified in the biomarker flux for IP_{25}. However sterol fluxes did not clearly reflect the maximum in concentrations observed.

In addition to the biomarker data, the mean summer insolation curve (Laskar et al., 2004) describes a continuous cooling tendency to present days for the last 3800 years (Figure 5.8) at 78° N.

The profile of the sea ice biomarker IP_{25} for core HH11-134-BC describes a general decrease towards present days with a high signal fluctuation, in part due to the high resolution and in part reflecting the strong variation of the local sea ice conditions. The sea ice retreat has been more noticeable, but also more fluctuating during the last centuries (Jernas et al., 2013), especially when the minimum sea ice extension modelled over the last 60 years in the Barents Sea (Årthun et al., 2012) is occurring.

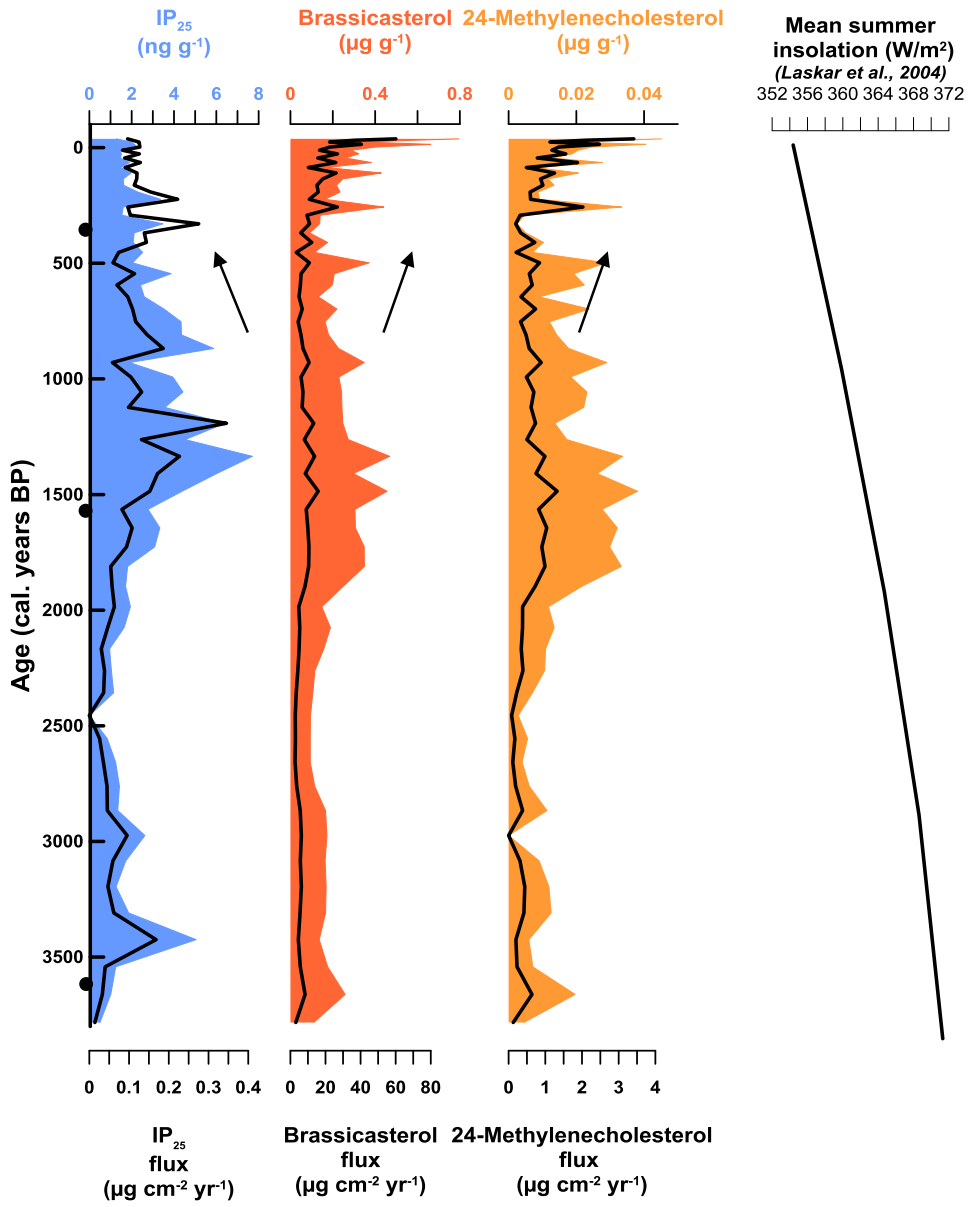

Figure 5.8 Concentration of biomarkers and fluxes at core site HH11-134BC for the last ca. 3.8 cal. kyr. BP. Age dates indicated with the black dots. Insolation curve (mean summer insolation is represented for 78° N latitude).

5.5 Discussion

The discussion is mainly focused on the most variable period (ca. last 2000 yr). For the period 3.8-2 kyr biomarker profiles did not show strong fluctuations or very interesting features, therefore could be associated to more stable sea ice conditions of a reduced marginal sea ice zone. Thus, the discussion of the last 2 kyr will be divided according to two concepts. The first one (4 sections) provides the application of IP_{25} sea ice based

reconstructions in three nearby locations which represent key dynamic features of the sea ice edge for the western Barents Sea. The nearby sediment cores to which IP_{25} data were compared to were, specifically, MSM/5 cores (Müller et al., 2012), which helped to further contextualize IP_{25} data from distinct margins of a highly variable sea ice edge. This information was very useful and potentially enabled tracking of sea ice changes with more accuracy. A time period division was then proposed according to similar features observed on the biomarker data for the three locations (e.g. in-phase, off-phase concentrations). Therefore, an interpretation of the sea ice conditions was described for four period divisions suggested over the last 2000 yr; 2-1.5 cal. kyr BP Period I, 1.5-0.9 Period II, 0.9-0.4 Period III, and last century, Period IV a) and b) last three decades.

The second concept of the discussion (section 5.5.5) contemplates the use of different proxies (IP_{25}, P_BIP_{25} and dinocyst) for a unique location (HH11-134-BC), and to what extent they agree in the reconstructions of sea ice.

Therefore, sea ice reconstructions proposed here for the western Barents Sea are derived mainly from interpretation of IP_{25} concentration trends and comparison to three nearby IP_{25} records and IRD data. These interpretations will be based on previous observations regarding sea ice and distributions of biological production in the Barents Sea for recent times (Chapter 4, e.g. higher productivity was observed to take place in the MIZ) which ultimately will provide sea ice scenarios.

Finally, the sea ice scenarios obtained are based on modern satellite records and historical observations (ca. last two centuries). These historical observations provide a valuable tool to use for comparison of IP_{25} data to previously observed sea ice conditions.

5.5.1 Sea ice conditions during Period I (2000-1500 cal. yr BP)

Biomarker data obtained from HH11-134-BC was compared to IP_{25} records of two northern nearby locations. In first instance, it was observed an out of phase tendency in the concentrations of IP_{25} between core MSM/5-712-2 (Figure 5.9) and the other two cores. IP_{25} concentrations for MSM/5-712-2 described one maximum in concentrations, while concentrations of the other two cores appear to be quite low increasing towards the end of this period. Marginal sea ice conditions have been observed to lead to highly productive areas (Chapter 4) producing effective algae blooms; therefore, maximum biomarker concentrations were expected to be observed under these conditions. The maximum concentrations for the records, were interpreted as marginal sea ice conditions, represented by the shaded areas (cut off point of the mean for each record). In particular, the concentrations of IP_{25} for surface (Chapter 4) or near surface sediments was ca. 2 ng g^{-1} for the last decades in which satellite records showed very infrequent sea ice cover. Therefore the assumption of higher frequency of sea ice cover when concentrations of IP_{25} increased to 4-6 ng g^{-1} down core HH11-134-BC has been reasonably based. The same assumption was extrapolated to the MSM/5 cores. Thus, the proposed scenario for the sea ice conditions for Period **I** (Figure 5.10 I) (Table 5.2) described marginal sea ice conditions for core MSM/5-712.

The sea ice proposed scenario (dotted black line) should be understood as an average estimation of the sea ice conditions, where by means of "anomaly years" there is a very inconsistent sea ice edge (producing weak spring blooms, "threshold concentrations" indicative of sea ice presence) over the other locations.

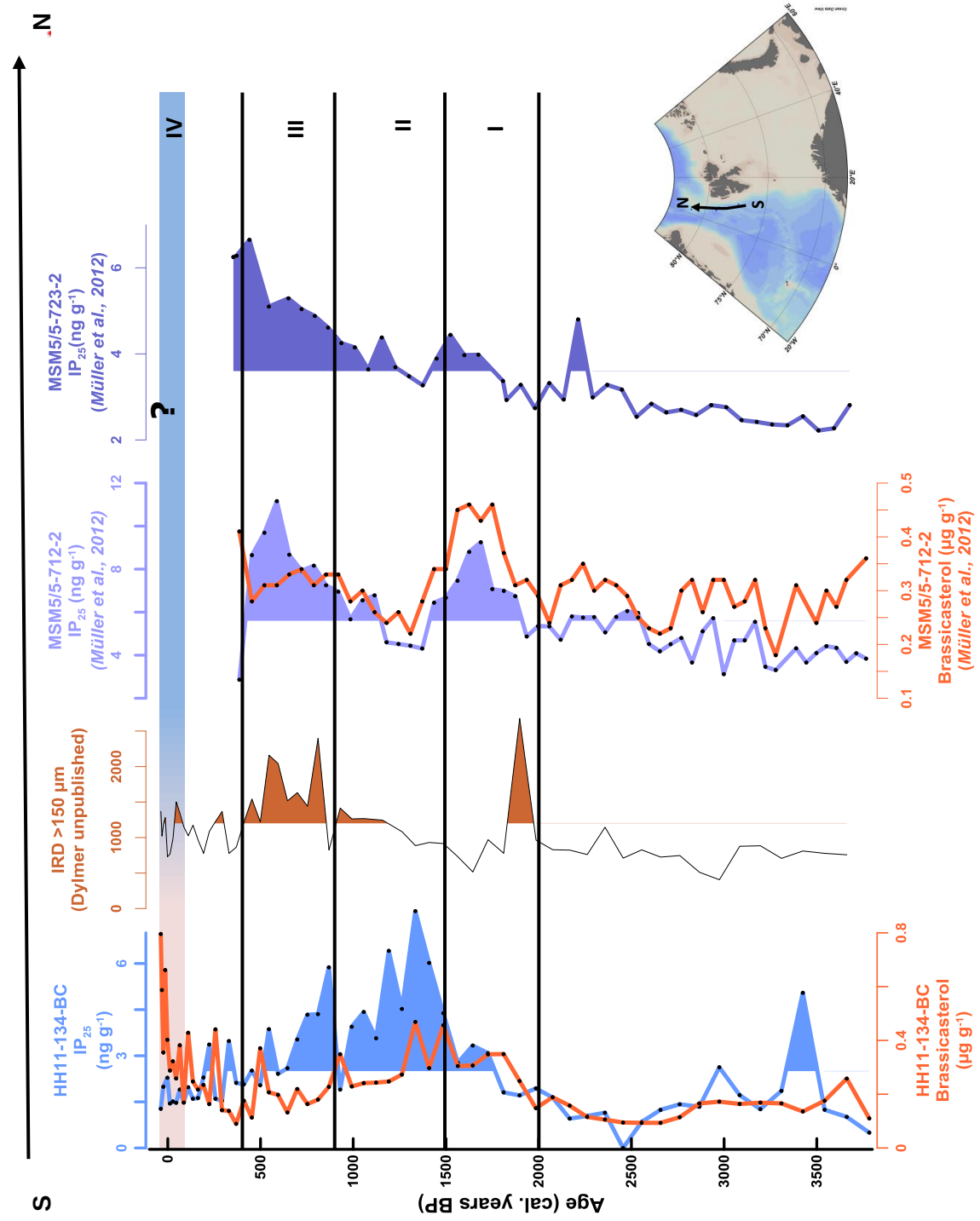

Figure 5.9 IP_{25} (blue line) and brassicasterol (orange line) concentrations for sediment cores organised along a south-north transect HH11-134 (77°N) MSM5/5-712-2 (78°N), MSM5/5723-2 (79°N) in the western Barents Sea. Shaded areas represent proposed marginal ice edge conditions for the respective locations and time periods. IRD data obtained from Dylmer (unpublished) for HH11-134-BC.

Table 5.2 Period division and interpreted sea ice conditions of the sediment records (organised according a north-south transect, first column) according to biomarker concentrations.

North-south Transect	3.8-2 Cal. yr BP	2-1.5 cal. kyr BP	1.5-0.9cal. kyr BP	0.9-0.4 cal. kyr BP	Last 100 cal. yr BP
MSM5273 79°09'N 5°2' E	Infrequent marginal sea ice cover	Boundary sea ice edge-open water)	Boundary sea ice edge-open water (more sporadic sea ice edge	Sea ice cover	-
MSM5712 78°54'N 6°77'E	Infrequent marginal sea ice cover	Marginal sea ice cover	Boundary sea ice edge-open water	Sea ice cover	-
HH11-134BC 77°36' N 9°53'E	Infrequent marginal sea ice cover	Boundary sea ice edge-open water	Marginal sea ice cover	Marginal sea ice cover	Boundary sea ice edge-open water (more sporadic sea ice edge)

5.5.2 Sea ice conditions during Period II (1500-900 cal. yr BP)

IP_{25} concentrations for HH11-134-BC during this period were identified to be out of-phase in comparison to the rest of the cores (Figure 5.9). While there was a maximum at the southern location, there was a minimum on the other two northern locations (MSM/5) (Table 5.2).

The proposed sea ice conditions (Figure 5.10 II) represent a northward retreat of the sea ice edge from the previous period leaving most of the time the northern locations sea ice free, and at the same time, the sea ice cover extended westwards, covering the location of HH134. Similarly to this situation has been observed in historical records e.g. (Figure 5.2) April 1780-1796 (Figure 5.3), where the sea ice extent advanced westwards possibly triggered by stronger atmospheric mechanisms and retreat northwards while the western front remains at the same location (Figure 5.2 a), forming a polynya type area (Figure 5.3).

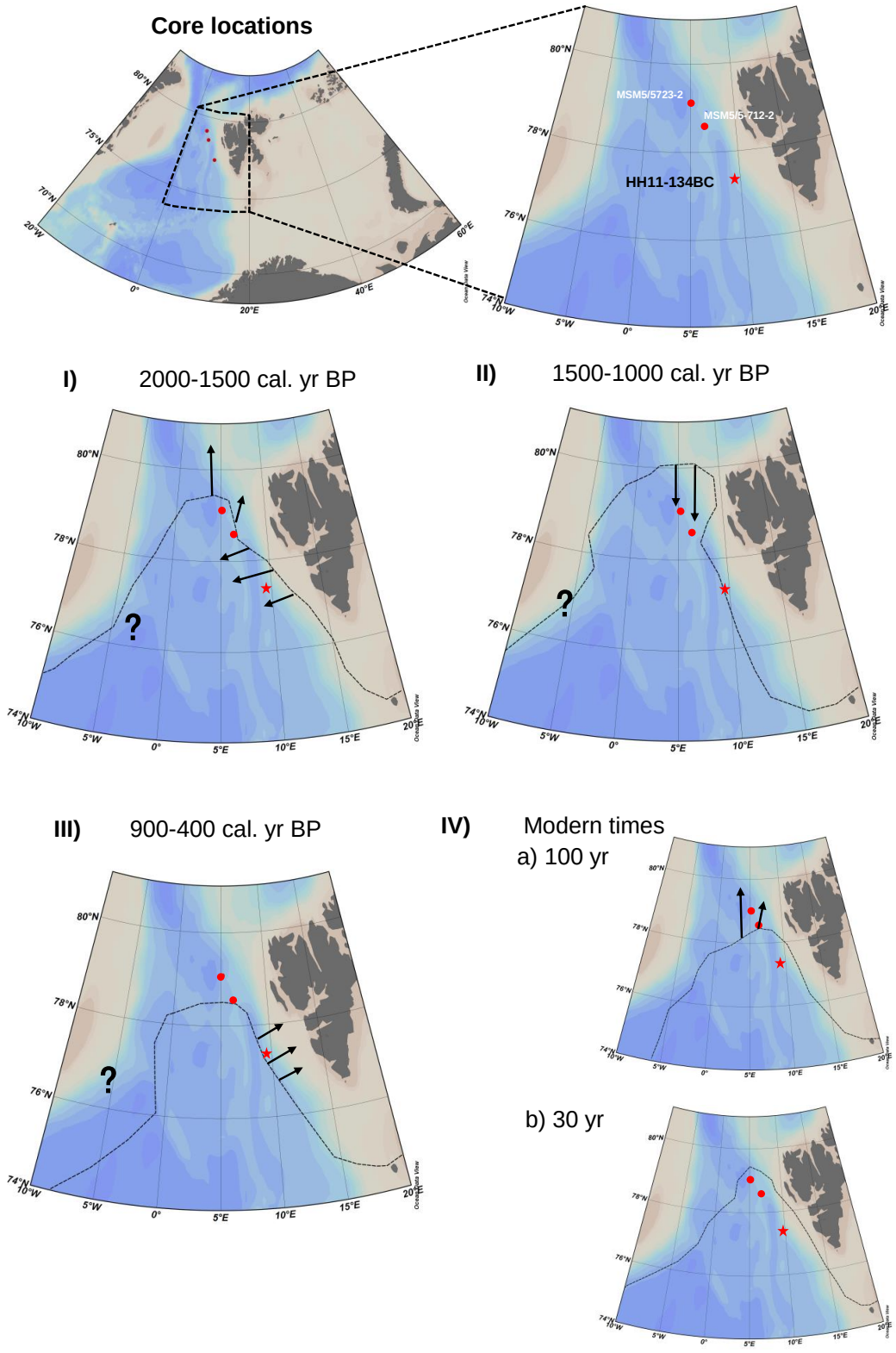

Figure 5.10 Location of the cores, and period divisions. Sea ice proposed variability for the western Barents Sea where dotted line represents the proposed spring marginal sea ice (most repeated scenario for the individual periods) while the black arrows represent the variation (transition) of the sea margin towards the next period. Arrows should be understood as the movement of the sea ice towards the next period. Question mark represents unknown sea ice cover/extent.

Polynya formations are oceanographic phenomena that have been observed before in the Barents Sea, especially on the west Kvitøya and Franz Joseph Land (Vinje and Kvambekk, 1991) which are known to be extremely dynamic, changing with intervals of hours and being displaced by wind.

5.5.3 Sea ice conditions during Period III (900-400 cal. yr BP)

It is only for this period, where the IP_{25} concentrations seemed to be in-phase for all the cores. This in-phase situation could reveal a general advance of the sea ice cover extending southwards from the previous period. Brassicasterol values describe very low concentrations for site HH11-134-BC which could support a heavier sea ice cover. This period also showed the highest IRD content, which could suggest more abundant sea ice cover. These results are in agreement with Muller et al. 2012 who proposed that more abundant shore/fast sea ice or more permanent sea ice was occurring at ca. 600 cal. yr BP at the West Spitsbergen margin, based on Forwick and Vorren, (2009). Recent studies in the provenance of IRD particles in the western Barents Sea area suggested that sea ice formed in Storfjorden could drift with the ESC eventually reaching the west margin of Spitsbergen (Müller and Knies, 2013) imprinting a characteristic mineralogical signature. This could suggest that drifted sea ice from Storfjorden could have covered the area of the West Spitsbergen margin, instead of, or in addition to drift or shore/fast ice of the immediate West Spitsbergen coast at this period, which reflects a cooling period. The proposed sea ice conditions for this period (Figure 5.10 III) revealed an extended sea ice cover which has been also observed in historical records, although in less extension than for this particular anomalous year of 1917 (Figure 5.4).

5.5.4 Sea ice conditions during Period IV (last 100 yr)

Biomarker concentrations reflect another very fluctuating period (Figure 5.9) for which was observed a rapid increase of brassicasterol and a continuous decrease (from the last ca. 1000 years) of IP_{25} which could be interpreted as indicative of warming conditions. In terms of sea ice conditions, this could be interpreted as a retreat of the marginal sea ice edge towards the Spitsbergen shore from the previous period to meet the sea ice scenario in Figure 5.10 IVa, probably as an increase in the heat transport of the Atlantic current followed a retreat northwards of the sea ice margin (Figure 5.10 IV b). Evidences for this sea ice dynamics was reported in historical records during the last 150 years (Figure 5.2 a), where the east marginal sea ice remained at the same location while the north edge retreated northwards.

5.5.5 Comparison with sea ice reconstructions from other proxies

Recent sea ice conditions have been proposed for the Nordic Seas obtained from dinocyst-based reconstruction (de Vernal et al., 2013). In particular, for the west margin of Svalbard, the estimated values of sea ice derived from satellite concentrations were 2-4 (/10) for the last 3000 years which was an overestimate when compared to modern sea ice conditions (highlighted by a big uncertainty 1.2 ± 1.2, note that sea ice concentrations are expressed in (0-10) annual scale). These conditions reflect the very variable sea ice distribution that occurs here (at least recorded over the last decades). Therefore centennial to millennial sea ice descriptions are required to understand the local variability of this region.

In order to investigate in more detail other sea ice proxy reconstructions for this area of the western Barents Sea, P_BIP_{25} index and dinocysts based sea ice reconstructions were compared to the sea ice interpretation derived from IP_{25} data for HH134 core.

In first instance, P_BIP_{25} index interpretation of the values (0-1) was established as 0.5 being marginal sea ice conditions (shaded areas), note that this interpretation holds some flexibility (Müller et al., 2011). In general terms, P_BIP_{25} values were 0.5-0.7 for Period II and III where interpretations for the same record derived from the IP_{25} data suggested marginal sea ice conditions (Figure 5.11).

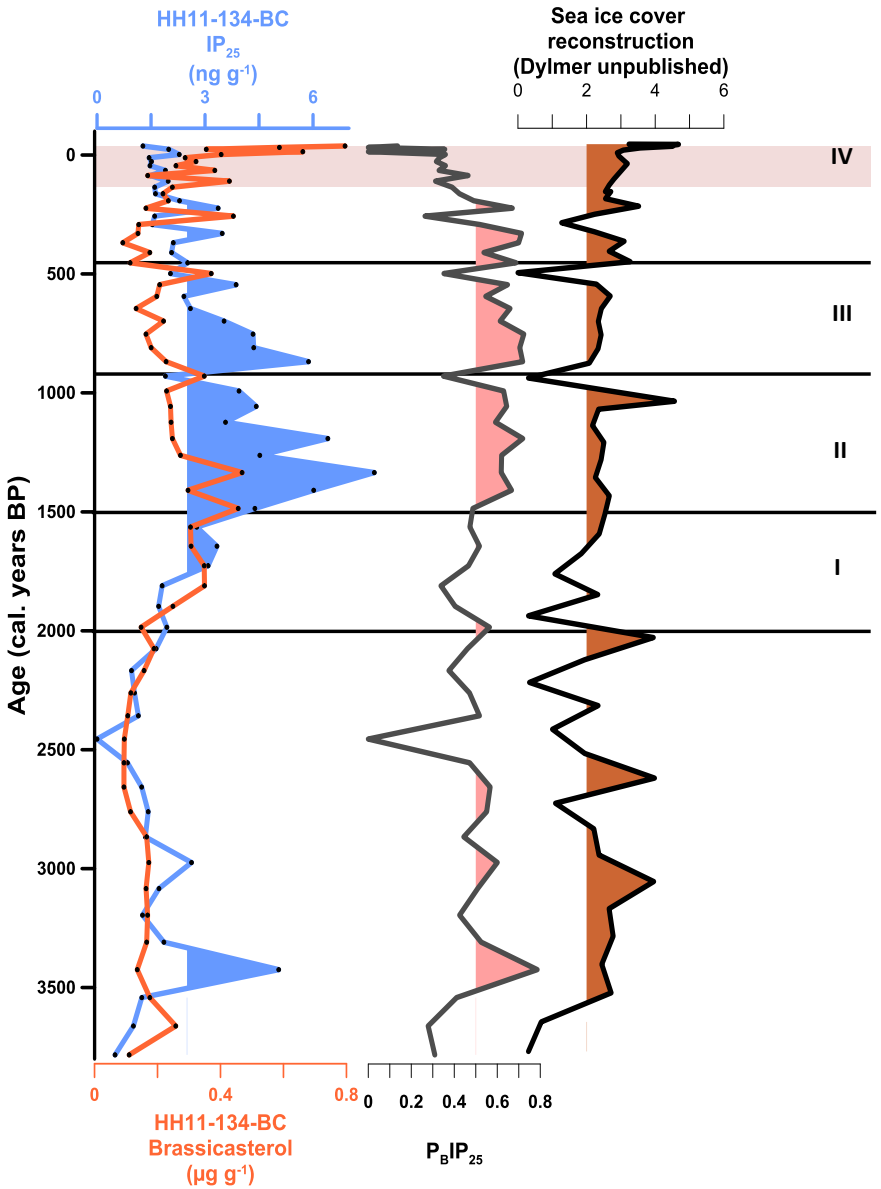

Figure 5.11 IP_{25} (blue lines) and brassicasterol (orange lines) concentrations for sediment cores organised along a south-north transect HH11-134 (77° N), Shaded areas represent proposed marginal ice edge conditions for the respective locations and time periods according to the mean of the record. Sea ice cover reconstructions from P_BIP_{25} index (grey line) and dinocysts black line, for core HH134.

Sea ice concentrations of 0.5-0.7 would imply rather consistent sea ice margin to be formed at the study site through the spring season, which in turn would be rather unlikely considering the high fluctuating sea ice conditions of the area. P_BIP_{25} index seems however to predict a drastic decrease in sea ice for the last century, mainly due to the fact that brassicasterol concentrations increase for this period. In this aspect, and in general trends, P_BIP_{25} index was identified to predict similar sea ice conditions to that for IP_{25} but it also appeared to give overestimated values for Period II and III, predicting quite strong sea ice conditions, the type of sea ice conditions observed for the Eastern Barents Sea for last decades (Figure 5.4). This overestimated values of the P_BIP_{25} are in accordance to the high predicted sea ice conditions obtained for the surface sediment study (Chapter 4; Figure 4.4 a), in which the averaged sea ice concentrations produced by the P_BIP_{25} index (ca. 0.8) proposed heavy sea ice conditions for the last decades.

Further comparison of the sea ice cover reconstructions based on dinocyst with previous P_BIP_{25} sea ice reconstructions was carried out. High similitudes were observed between the P_BIP_{25} and the dinocysts sea ice reconstructions (Dylmer unpublished) (Figure 5.11), where the major changes through the record were identified to mirror the P_BIP_{25} profile. However a difference was observed for the last 100 year Period IV, where in this case, increased sea ice concentrations were derived from the dinocyst reconstruction.

If both sea ice reconstructions (P_BIP_{25} and dinocyst based) are compared, there are contradictory results for the same parameter (sea ice predictions) for the last centuries. Similarly, multiproxy analysis in core MSM/5- 5712-2 provided multiple interpretations; an increase in Atlantic water temperature up to 4°C over the last 1000 years (Spielhagen et al., 2011); increased temperature and cooling of the mixed water layer (upper 50 m) (Rueda et al., 2013) and decrease in the SST for the last 300 years (Bonnet et al., 2010) at the same location (core JM06-WP04-MC). This however, is due to the high

stratification of the water masses in the western Barents Sea and to what extent the proxies are representative to which water masses.

5.6 Conclusions

IP_{25} records form the western Barents Sea helped to suggest more detailed sea ice conditions over the last ca. 3800 years concluding that the coldest period in terms of sea ice conditions was probably Period III, where the advance of the sea ice margin was suggested to occur in an uniform way (from the north and west) extending off shore covering at least the 150 km off land.

P_BIP_{25} index and dinocyst based sea ice reconstructions provided some similarity to that observed for the IP_{25} sea ice interpretation. However, the reliability of these data was questioned to what extent is a useful tool since has shown in other occasions that can be limited by regional effects.

CHAPTER SIX

6 Palaeo-sea ice reconstructions in the north eastern Barents Sea over the last 10.5 kyr

6.1 Introduction

The seasonal sea ice conditions occurring in the Barents Sea have been subjected to great variability during the last century, especially during summer months, where retreat of the sea ice margin on the eastern side reached about 250 km in few months (Divine and Dick, 2006). The study of the variability of the sea ice margin in the Barents Sea over longer time scales (e.g. Holocene) would provide more detailed climatic reconstructions for an area which appears to be very sensitive to global climate change. In order to produce detailed descriptions of sea ice conditions for the Holocene in the eastern Barents Sea, a previous study of lipid biomarkers in surface sediments (Chapter 4) will be used as a fingerprint to facilitate the comparison of biomarker distributions under known sea ice and oceanographic conditions in recent decades with those of the longer-term record.

Over the last decade, sediment cores from Svalbard Archipelago shelf region were analysed for plankton and benthic foraminifera, IRD and stable isotopes to reconstruct environmental conditions such as the distribution and behaviour of the main water masses for this area (Atlantic and Polar waters) since the last glacial period i.e. 20 kyr (Duplessy et al., 2001; Ślubowska et al., 2005; Rasmussen et al., 2007; Ślubowska-Woldengen et al., 2007; Ślubowska-Woldengen et al., 2008). In the present study, a multiproxy analysis (HBI and sterol biomarkers, stable isotopes data and plankton foraminifera) was used to gain more information and to produce detailed data for reconstructions of the sea ice conditions in the eastern Svalbard archipelago.

The main objectives of this study were:

1 To analyse a suite of sea ice and phytoplankton biomarkers in a sediment core.

2 To calculate the PIP_{25} index and other biomarker ratios and conduct a multiproxy (e.g. foraminifera and $\delta^{18}O$) analysis for sea ice reconstructions.

3 To further investigate and test biomarker ratios.

6.2 Regional settings

The oceanography of the Barents Sea is described in Chapter 4, since all the sediment material analysed in the project was collected in this region of the North Atlantic. Briefly, the oceanography of the Barents Sea is greatly influenced by the Svalbard Archipelago (northern Barents Sea (76°- 81° N)) and the Svalbard shelf which influence the path of the main water masses. The North Atlantic Current (NAC) carries warm saline Atlantic water along the coast of Norway. Some of this water enters the Barents Sea and surrounds the western side of the Svalbard Archipelago (West Spitsbergen Current (WSC)). This water mass continues north of Svalbard and enters the Nansen Basin (Svalbard Branch (SB)) (Figure 6.1). In the Nansen Basin, the Atlantic water (AW) masses mix with cooler and less saline Arctic waters (ArW) from the Arctic Ocean (Lind and Ingvaldsen, 2012) and, in part, enters the Barents Sea from the north (East Spitsbergen Current (ESC)) and also moves towards Franz Josef Land. The hydrography of the Barents Sea becomes a complex vertical mixing of water masses due to differences in salinity and temperature of the AW and ArW, the fresh water input from sea ice melting in summer, the dense bottom water masses formation from winter sea ice formation and wind stress (Lind and Ingvaldsen, 2012). The intensity of the NAC has changed through time, which is likely due to global ocean circulation in response to orbital forcing, possibly impacting greatly in the strength and mixing with Arctic waters in the Barents Sea (Ślubowska et al., 2005) and in the extent and

variability of the sea ice cover (Divine and Dick, 2006; Årthun et al., 2012; Lind and Ingvaldsen, 2012).

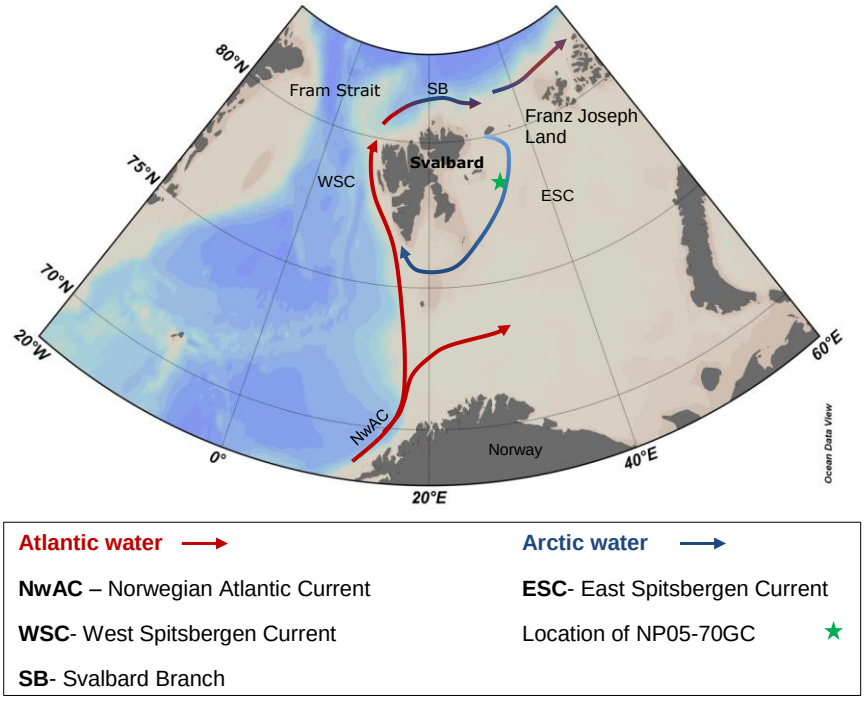

Figure 6.1 Bathymetry of the Nordic Seas with main water masses circulation. Location of the core represented with a green star.

Much of the Barents Sea is covered by sea ice during at least 10 months a year (Figure 6.2 a); however, the seasonal sea ice extent varies greatly, especially the abrupt retreat and advance that are generally observed from June -July and October –November respectively. During these two periods, important dense water formation due to brine rejection from sea ice formation and important release of fresh water with the sea ice melt are likely to influence the stratigraphy of the water column. The location of the core studied here is situated 78° N which, in any case, represents purely "Arctic" conditions at least for the last decades with a rather constant sea ice coverage (90 %) and open waters for 2-3 months a year (August-September) (Figure 6.2 b).

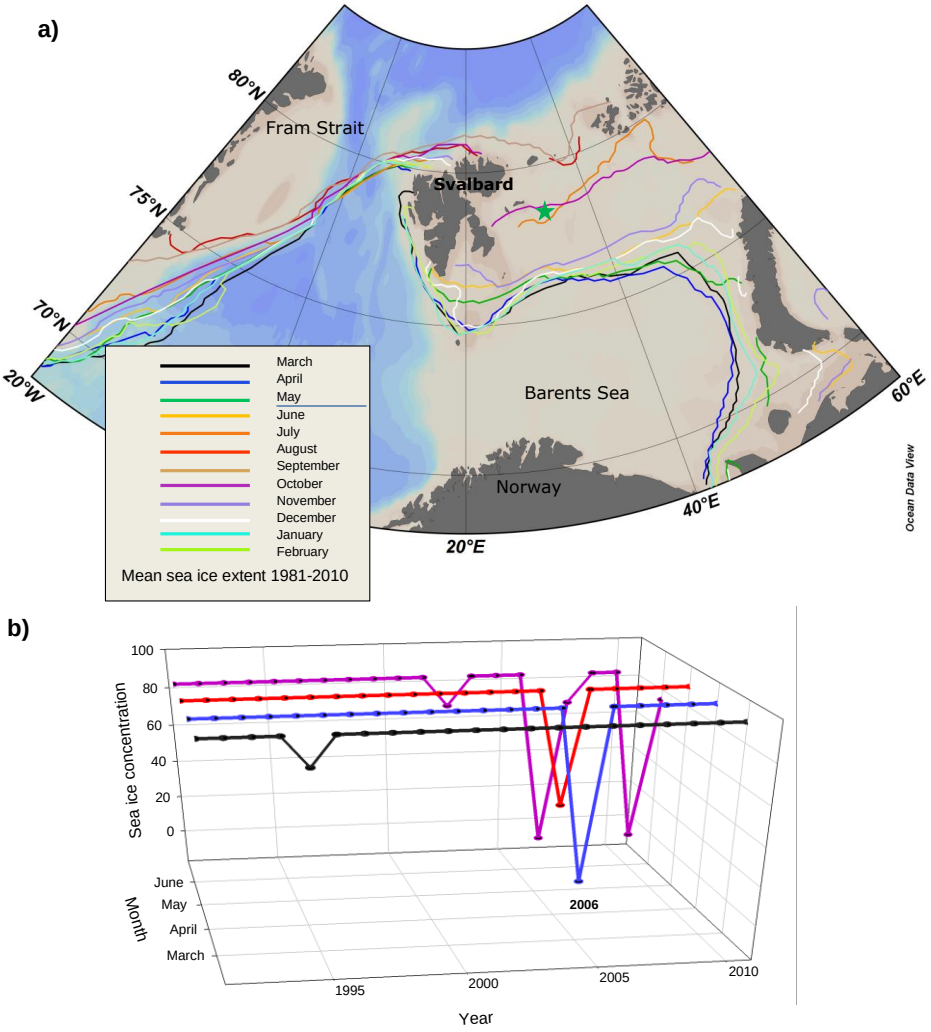

Figure 6.2 a) Monthly mean sea ice extent for the period (1981-2010) National Snow and Ice Data Center (NSIDC). b) Sea ice concentration data at the core location NP02-11-70GC for the period 1991-2011 obtained from the National Ice Center NOAA; *www.natice.noaa.gov/*; accessed October 2013).

6.3 Material and methods

A gravity core NP05-11-70GC was collected in August of 2005 by the *RV Lance*, on the Kong Karl Land 78° 40' N 32° 42' E northeast Barents Sea with a length 245 cm at a water depth of 293 m. Only the first 154 cm were analysed in this study due to the presence of a till from that depth to the core base.

6.3.2 Chronology

An age-depth model of NP05-11-70GC was constructed based on four AMS ^{14}C dates which were calibrated using Calib 6.1.1 (Stuiver and Reimer, 1993) and the Marine09 calibration curve (Reimer et al., 2009). A local reservoir age of cal. yr BP 105 ± 24 was indicated for the Svalbard area by Bondevik and Gulliksen in Mangerud et al. (2006) and subsequently used in the calibration here (Table 6.1 Figure 6.3). To constrain the age-depth model, a linear interpolation was applied between the 3 used calibrated AMS ^{14}C dated levels. It was assumed that the core top (10.0 cm) represents 0 cal. yr BP. For the latter part, the linear interpolation between 80.0 and 135.0 cm was used to extrapolate values towards 154.0 cm. This point was chosen to cut off the age-depth model as the lithology indicates the existence of a glacial till from this depth onwards (Aagaard-Sørensen et al., in prep). The AMS ^{14}C date at 232.0 cm was therefore not used in this age-depth model. Hence, the age-depth model ranges between 0 and 10 453 cal. yr BP and based on the 1.0 cm samples it shows sediment accumulation rates between 0.07 and 0.18 mm/yr resulting in a sub centennial temporal resolution (Figure 6.2).

Table 6.1: Age-depth model of NP05-11-70GC calibrated using Calib 6.1.1 (Stuiver and Reimer, 1993), the Marine09 calibration curve (Reimer et al., 2009) and a local reservoir of 105 ± 24 cal. yr BP after Bondevik and Gulliksen in Mangerud et al. (2006). Data in Berben et al., (in prep).

Lab ID	Core depth (cm)	Material	Uncorrected AMS ^{14}C age	1 σ	Calibrated age 2 σ range	Calibrated age used in age-depth model (cal yr BP)
Beta-331327	47 - 53	Benthic Foraminifera	2780	30	2281 - 2496	2389
Beta-346803	77 - 82	Benthic Foraminifera	6110	40	6298 - 6536	6417
Beta-331328	132 - 137	Benthic Foraminifera	8870	50	9307 - 9527	9417

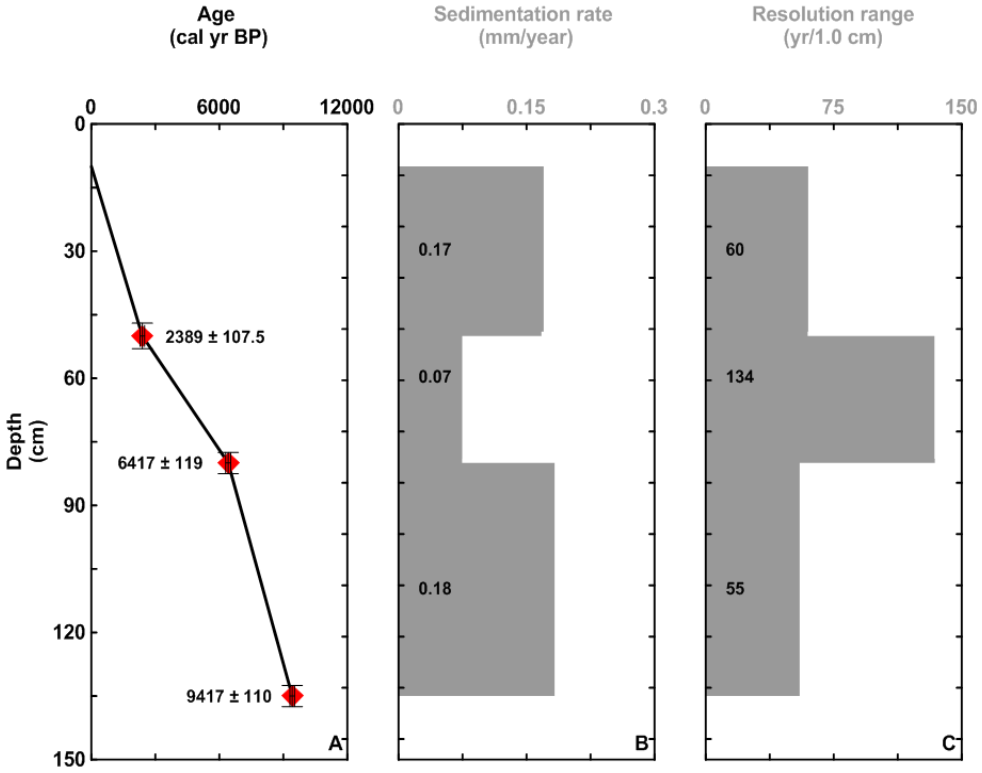

Figure 6.3 Age-depth chronology for the sediment core NP05-11-70GC. Individual linear fits for each data point, Berben et al., (in prep).

6.3.4 Biomarker analysis

Biomarker analysis was conducted as described in Chapter 2 including the removal of sulphur and further purification of extracts using silver ion solid phase extraction methods. HBIs (IP_{25}, diene II and trienes IIIa and IIIb) and sterol biomarkers (brassicasterol and 24-methylenecholesterol) were analysed. Biomarker fluxes were

calculated by combining biomarker concentrations with sediment densities and accumulation rates as described previously in Chapter 2 (Belt et al., 2012b).

6.4 Results

6.4.1 Biomarker analysis

Observation of the lipid biomarker profiles for the last ca. 10.5 kyr (Holocene) revealed interesting patterns in concentrations. Firstly, IP_{25} and diene II, the sea ice lipid indicators, presented very similar profiles. Both were present in all the horizons with the exemption of one sample at ca. 10 kyr, were IP_{25} was absent (Figure 6.4). Diene II was more abundant throughout the entire record (0.034 - 2.7 µg g^{-1} TOC) in comparison to IP_{25} (0 - 0.439 µg g^{-1} TOC) which was consistent with previous studies (Vare et al., 2010; Cabedo-Sanz et al., 2013;). Overall, a continuous increase in the concentrations of both sea ice biomarkers was observed from 10.5 cal. kyr BP towards present. However, characteristic trends indicative of variations in the sea ice conditions through the record could be distinguished. The higher fluctuation in concentrations was observed for the bottom of the core (ca.10 cal. kyr) and for the top of the core (ca. 1.9 kyr). Biomarker fluxes followed the biomarker concentrations from 10 cal. kyr to ca 6.1 cal. kyr BP at which point the sediment accumulation rates diminished to 0.07 mm yr^{-1} thus reducing the fluxes to more steady values. A continuously increasing trend from 5.9 - 2.2 cal. kyr BP until ca. present days was observed for the sea ice biomarkers Figure 6.4. Fluxes at ca. 2.7 cal. kyr BP where the sediment accumulation rates increased again (0.17 mm yr^{-1}) followed closely by the biomarker concentration profile.

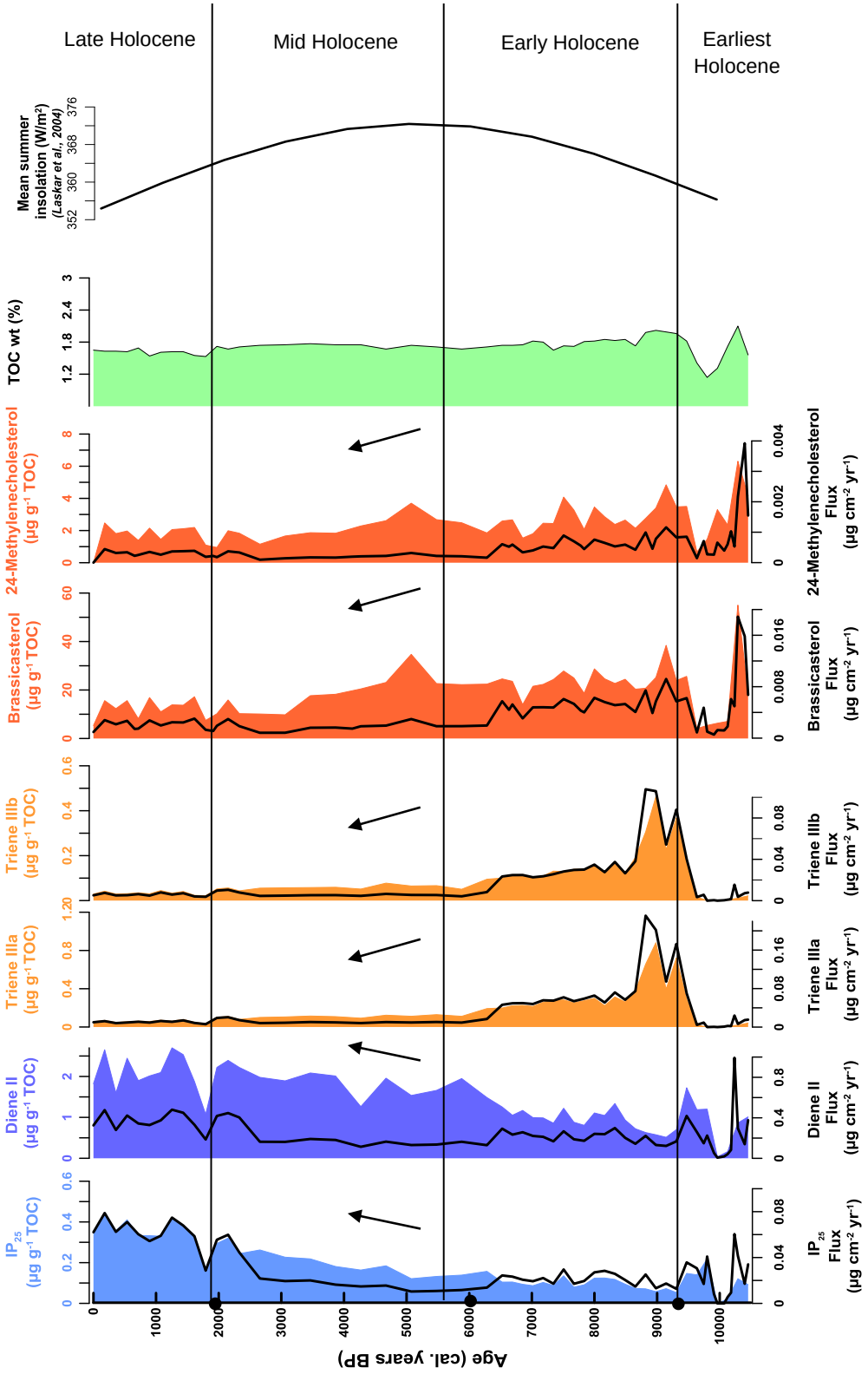

Figure 6.4 Biomarker concentrations, fluxes and TOC values divided according to the proposed period division. Black dots represent ^{14}C dates. Summer insolation data obtained from (Laskar et al., 2004)

The HBI trienes IIIa and IIIb exhibited remarkably similar profiles, being present in all the samples with the exception of two samples at ca. 9.7 - 9.9 cal. kyr BP (Figure 6.4) where both were absent. For both trienes, an opposite trend compared to the sea ice indicators was observed, however, with a continuous decrease in concentrations towards present days. Maximum concentrations (0.97; 0.51 µg g^{-1} TOC for triene IIIa and IIIb) with a clear abrupt peak were observed at around 9.5 - 8.5 cal. kyr BP. A continuous and smooth decrease for both lipids towards present was also observed (Figure 6.4) with a further small decrease at ca. 1.9 cal. kyr BP, similar to that found for the sea ice biomarkers. Fluxes of the two trienes followed the same profile for the entire record, with smaller values for the period where the sediment accumulation rates were lower.

The brassicasterol and 24-methylenecholesterol concentrations showed a similar general decreasing profile towards the present, although with more variability (Figure 6.4). The two steroidal lipids were present almost throughout the entire record with concentrations ranging from 4 - 55 µg g^{-1} TOC for brassicasterol and 0 - 6.3 µg g^{-1} TOC for 24-methylenecholesterol which was absent for the upper most sample point (0 cm). Higher concentrations for both sterols were observed for the deepest sample point of the record (154 cm). Minimum concentrations were observed for ca. 9.6 cal. kyr BP for both generic sterols (4; 0.06 µg g^{-1} TOC; brassicasterol and 24-methylenecholesterol). A slight decreased was also observed at 1.9 cal. kyr BP similarly to that seen by the other biomarkers. In both cases, there was a continuous decrease in fluxes towards present.

Total organic carbon (TOC) remained fairly constant through the record with a slight decrease towards the present day .Values ranged from 1.14 – 2.02 wt. (%) (Figure 6.4) with the highest fluctuation at about 9.6 kyr which was observed with a rapid and sudden decrease to 1.14 wt. (%) followed by a sudden increase to 2 wt. (%).

6.5 Discussion

6.5.1 Palaeo-climate reconstructions for the north-eastern Barents Sea

The biomarker and other proxy data for the NP05 study site revealed interesting changes throughout the record. Changes in biomarker concentrations were used for the identification of different periods throughout the Holocene corresponding to changes in climatic conditions (sea ice conditions). In addition, the mean summer insolation curve at 78° N (Laskar et al., 2004) for the last 10 kyr shows a steady continuous cooling towards present days (Figure 6.4) which was also apparent through the biomarker trends. For discussion purposes, the record was divided into four periods. The transition into the first main interval was defined according to the last ^{14}C date at 9.4 kyr BP (Table 6.1), although the entire record extends to 10.5 cal ky BP (earliest Holocene). The main intervals are thus defined as: the early Holocene period (9.4 - 5.9 cal. kyr BP), the mid Holocene period (5.9 - 2.2 cal. kyr BP) and late Holocene (to present) (2.2 - 0 kyr BP) (Figure 6.5). For individual periods, the mean concentrations for each biomarker/ratio were calculated (Table 6.2) in order to facilitate the discussion. The discussion of the biomarker data begins with the early Holocene interval and continues towards the present. The earliest Holocene, however is discussed last, largely due to uncertainties in the age model for this period.

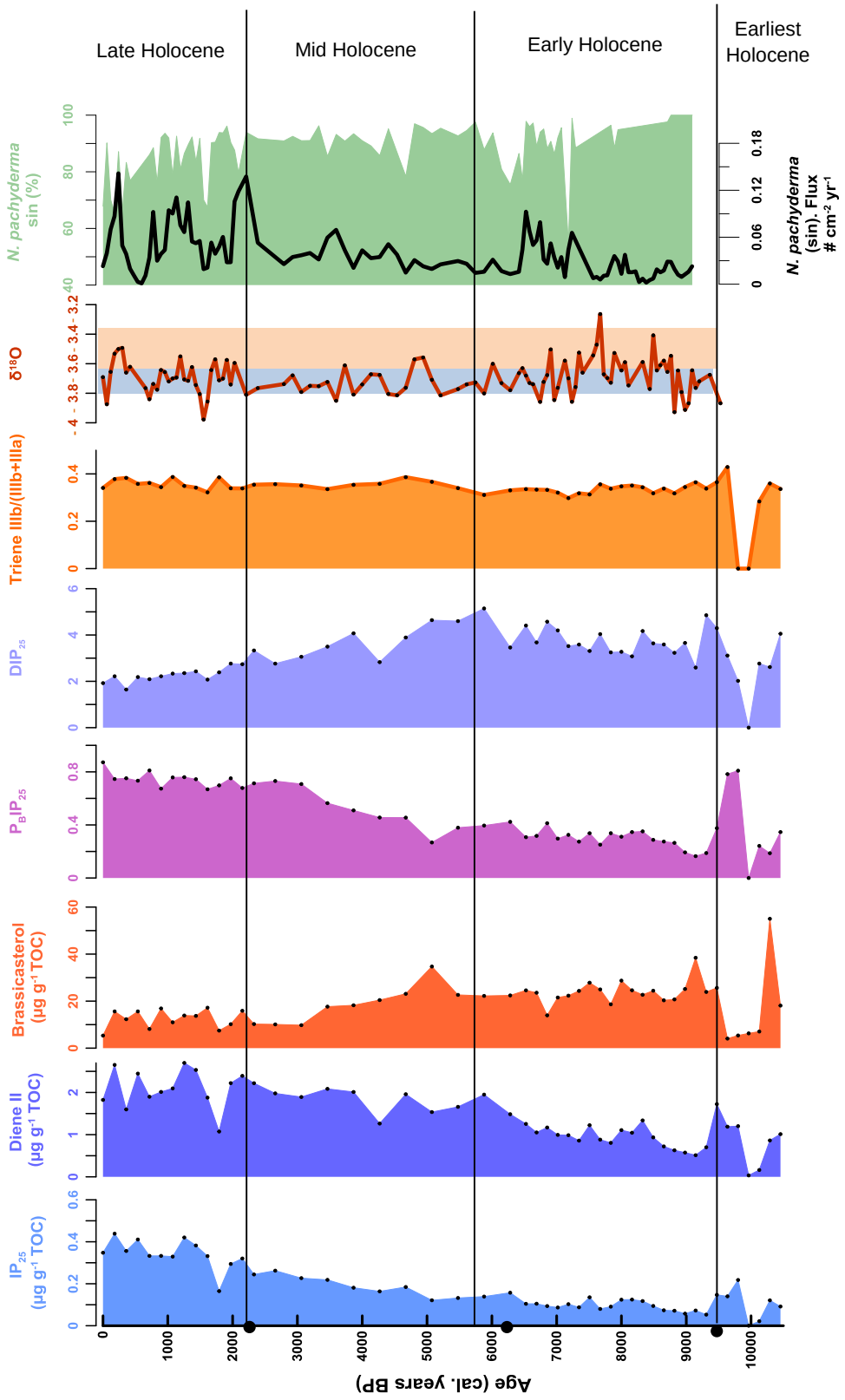

Figure 6.5 Biomarker concentrations, DIP_{25} ratio and P_BIP_{25} index and triene ratio (triene IIIb/ (IIIb+IIIa). $\delta^{18}O$ values and foraminifera (*N pachyderma* (sin)) abundances and fluxes were obtained from Berben et al., (in prep). Black dots indicating calibrated ^{14}C data points and black lines indicating the period division

6.5.2 Early Holocene (9.4 – 5.9 cal. kyr BP)

The biomarkers showed particularly interesting trends for this period. The sea ice indicators (Figure 6.4) were at their lowest within the 10.5 cal. kyr record (0.10, 1.04 µg g^{-1} TOC for IP_{25} and diene II, Table 6.2). Individual concentrations generally showed a continuous increase towards the end of the period with only slight fluctuations. In contrast, the individual phytoplankton-derived HBI trienes IIIa and IIIb showed a clear and abrupt peak within this interval with maximum concentrations with respect to the entire record (0.6; 0.3 µg g^{-1} TOC, Table 6.2, Figure 6.4) at ca. 9.5 - 8.5 cal. kyr BP followed by a continuous decrease until 5.9 cal. kyr BP. The sterol biomarkers were also at their highest values during this period (Figure 6.5) (24; 3 µg g^{-1} TOC; Table 6.2), although individual data points described a slight fluctuating profile towards ca. 5.9 cal. kyr BP. In addition, total organic carbon remained fairly stable (1.8 wt. (%)) with the maximum value for the record, possibly suggesting a period of high productivity.

Table 6.2 Mean concentration of all biomarkers in (µg g^{-1} TOC), P_BIP_{25} index and DIP_{25} ratio for the selected time periods during the Holocene 10.5 kyr. Present days represented by surface sediments (20-30 years).

Period (cal. kyr BP) / Biomarker (µg g^{-1} TOC)	Late Holocene (0-2.2)	Mid Holocene (2.2-5.9)	Early Holocene (5.9-9.4)	Earliest Holocene (9.4-10.5)	HTM (8.5-9.5)	Present days
IP_{25}	0.34	0.20	0.10	0.11	0.08	0.22
Diene II	2.10	1.90	1.04	0.88	0.83	0.58
Triene IIIa	0.07	0.11	0.33	0.05	0.51	0.008
Triene IIIb	0.04	0.06	0.17	0.03	0.26	0.005
Brassicasterol	12.56	18.64	23.86	17.36	25.52	21.07
24-Methylenecholesterol	1.66	2.19	2.80	3.11	3.25	2.84
P_BIP_{25}	0.76	0.56	0.32	0.36	0.26	-
DIP_{25}	2.26	3.69	3.82	3.34	3.67	-
RSD% DIP_{25}	12	22	16	33	18	-

The presence of the lipids IP_{25} and diene II confirms the existence of spring sea ice. However the data suggest less frequent or less severe sea ice conditions compared to the present day, where this is normally 90 % sea ice cover from March-June (Figure 6.2 b) if concentrations for the youngest part of the core (IP_{25} (0.35); diene II (1.84) µg g^{-1} TOC) are compared to the concentrations observed for the early Holocene (Table 6.2). This estimate assumes that the top of the core represents modern conditions and that the surface sediment layer was not lost during the collection of the core. Biomarker concentrations (sea ice and phytoplankton) were used to propose a schematic biomass production (Figure 6.6 d). The biomarker data for the Early Holocene are interpreted in terms of a relatively short spring season with low or no sea ice cover during May, possibly due to an early sea ice retreat, which would limit the production of the sea ice biomarkers (Table 6.2). Longer periods of a marginal ice edge and partially open waters could favour the phytoplankton blooms in the area where the environmental conditions evolve from a minimum sea ice algae spring bloom to a phytoplankton summer maximum (Figure 6.7 d). Maximum concentrations for the phytoplankton biomarkers suggest favourable conditions for biological production found near the marginal ice edge (see Chapter 4). During this interval, it is proposed that the maximum extent of the marginal sea ice edge (Figure 6.7 d) is consistently at, or near to, the location of the core (78° N) without an extensive change between seasons (spring-summer).

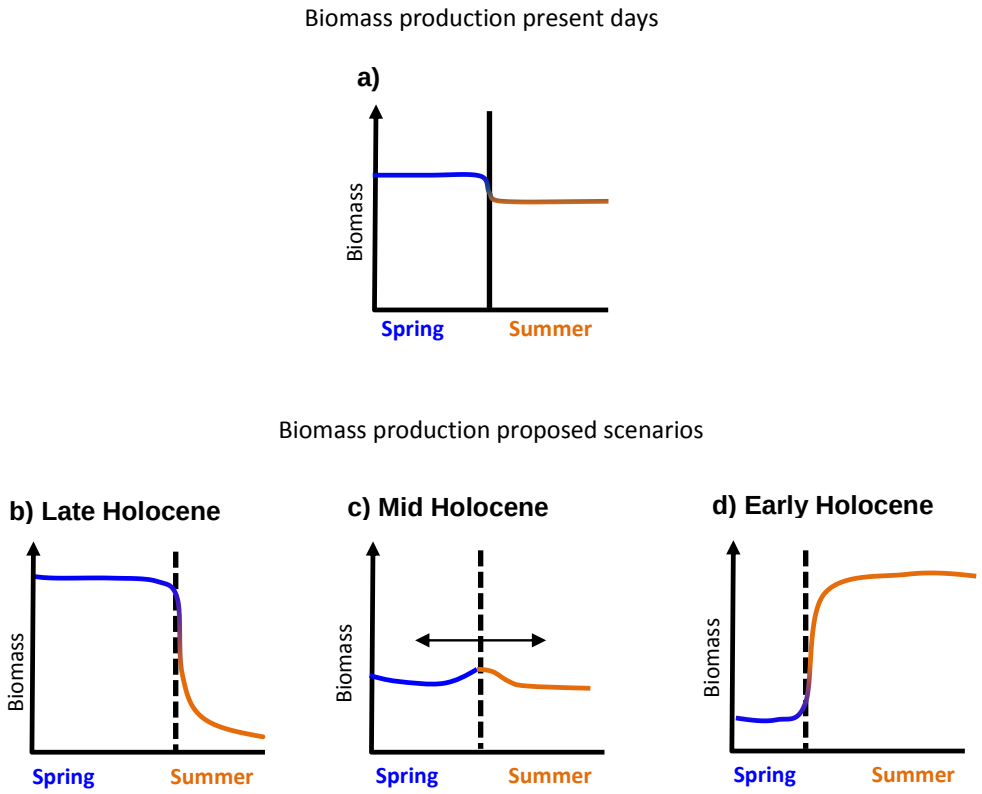

Figure 6.6 Scheme showing proposed biomass production at the NP05-70GC11 location based on sea ice and phytoplankton biomarker concentrations. a) for present days; b) Late Holocene; c) Mid Holocene; d) Early Holocene

In addition, the mean value of the P_BIP_{25} index for this period (0.3) suggests lower sea ice conditions according to Muller et al. (2011). In addition to the biomarker data, stable $\delta^{18}O$ isotopes values Berben et al., (in prep) extracted from *N. pachyderma* (sin) species (associated to Arctic conditions) indicated a warming event (Figure 6.5) during the Early Holocene. Values showed enrichment in ^{18}O which could be associated with a higher evaporation of surface waters as a consequence of warmer atmospheric conditions and increased solar radiation, producing an enrichment of heavier isotopes in the water column reflected in the carbonate shells of the foraminifera.

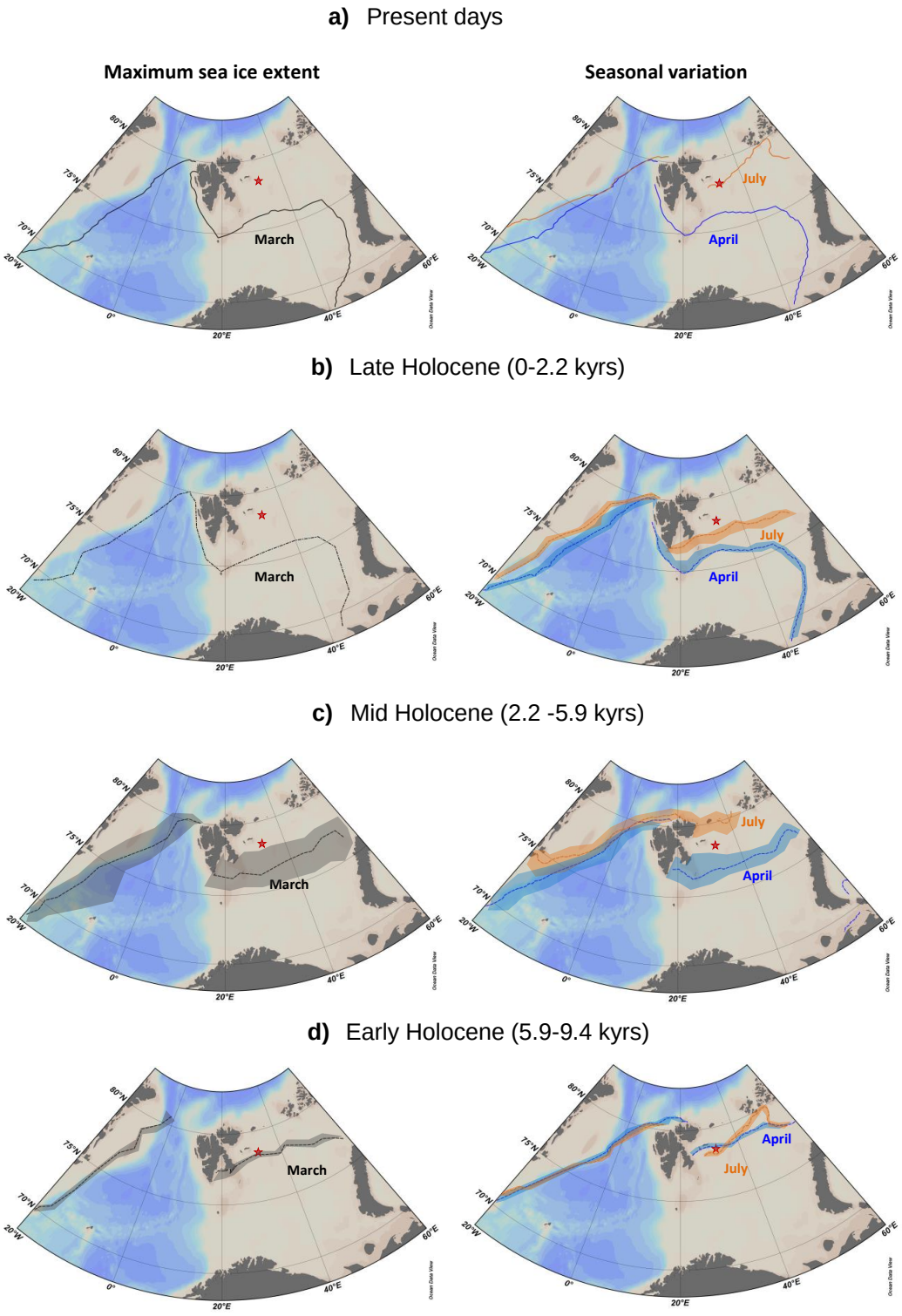

Figure 6.7 Sea ice conditions for the Barents Sea. Location of the core is represented with a red star. a) Present day sea ice conditions from satellite data (mean sea ice extent (1981-2010) NSIDC data for March (left figure), April and July (right figure). Proposed sea ice conditions for selected time windows during the Holocene. Column on the left represents maximum sea ice extent and column on the right represents seasonal variability of the marginal ice edge for b) Late Holocene; c) Mid Holocene; and d) Earliest Holocene. Shaded areas represent proposed variability of the marginal ice edge

Foraminifera assemblages were constantly dominated by the Arctic associated species *N. Pachyderma* (sin) during the whole record which emphasized the strong Arctic water influence. This time period frequently includes the Holocene Thermal Maximum (HTM) whose initiation and termination varies by location over the Arctic region (Kaufman et al., 2004). In the Barents Sea, the HTM represents generally high productivity associated to a strong Atlantic water input (Duplessy et al., 2001; Ślubowska et al., 2005). This strengthening in Atlantic waters, also observed for recent decades into the Barents Sea, has been termed "Atlantification" of the Barents Sea (Årthun et al., 2012) and as a consequence, warmer and more saline water masses and a retreat and reduction in concentration of the sea ice. This situation could be strengthened further by southern winds which can increase the inflow of Atlantic waters (Lind and Ingvaldsen, 2012) and expose the majority of the Barents Sea to open water conditions annually. This situation was proposed to have occurred during the Early Holocene (Figure 6.7 d).

6.5.3 Mid Holocene (5.9 – 2.2 cal. kyr BP)

The next proposed division covers the period from ca. 5.9 to 2.2 cal. kyr BP. A general cooling was revealed relative to the previous period (Early Holocene) as shown by a decrease in concentrations in the phytoplankton biomarkers and an increase in the concentrations of the sea ice biomarkers (Table 6.2, Figure 6.4). The most notable changes relative to the previous period occurred for the HBI biomarkers, with an almost two times increase in the concentrations of IP_{25} and diene II (0.20 and 1.90 µg g^{-1} TOC) and ca. three times reduction in the trienes IIIa and IIIb (0.11 and 0.06 µg g^{-1} TOC). There was also a slight decrease in the sterol concentrations (Table 6.2). The proposed biological production scheme for the period (Figure 6.6 c) suggested well divided

seasons where the duration of spring and summer could remain comparable with the consequent peak blooms. This scenario could, however, fluctuate between the two extremes (Early Holocene, and Late Holocene, explained in detail in next section) representing a transition period in terms of sea ice conditions. Thus, the proposed sea ice conditions with respect to the previous period would describe a further south extent of the maximum sea ice coverage (March) (Figure 6.7 c) with fluctuations between 76-77° N. However, the seasonal retreat of sea ice extent may have displayed a greater degree of variation (Figure 6.7 c) on decadal to centennial timeframes (Figure 6.7. b, d).

$\delta^{18}O$ data revealed a relatively stable period with small changes probably also due to the age model and the sedimentation rates, which decreased the age resolution (Figure 6.3). Foraminiferal distributions (Figure 6.5) revealed the dominance of the Arctic species N *pachyderma* possibly reinforcing that Arctic waters masses characterised the north core location. Increased values for the PIP_{25} index (0.56) probably also reflect more consistent sea ice conditions at the core location.

6.5.4 Late Holocene (2.2 – 0 cal. kyr BP)

Biomarker trends for this period suggest a further general cooling from the Mid Holocene to present day. The mean biomarker concentration distributions for this period suggested long spring seasons and short summers, according to relatively high concentrations for the sea ice lipids and low concentrations of the four phytoplankton biomarkers (Figure 6.6 b; Table 6.2). An extensive and consistent sea ice cover at the core location from April to early July is proposed (Figure 6.7 b) which likely would produce high abundances of sea ice biomarkers suggesting a very productive season (0.34 and 2.1 µg g^{-1} TOC for IP_{25} and diene II trend values (Table 6.2), along with a late

and short summer bloom limited by the extensive sea ice coverage which could diminish the phytoplankton production (0.07 and 0.04, µg g^{-1} TOC; trienes IIIa and IIIb and 12.6 and 1.7 µg g^{-1} TOC for sterols) (Table 6.2). When compared with data from a nearby surface sample (present conditions, Figure 6.7 a) obtained from a box core (78° 39' N; 32° 7' E), the current data indicate colder conditions or longer annual sea ice coverage compared to the present day. For example, IP_{25} concentrations was 0.22 µg g^{-1} TOC in the surface and 0.34 µg g^{-1} TOC on the top core if both are compared (Table 6.2). In general terms, the sea ice conditions interpreted for this period suggest a rather stable maximum sea ice margin (Figure 6.7 b) reaching latitudes observed for modern times in spring (75° N) (Figure 6.7 a) but with a late and slow receding of the sea ice edge in e.g. mid July. This slow recession of the sea ice coverage would be fairly stable (inter-annually), emphasising strong sea ice coverage. This interpretation agrees with the lower values observed for $\delta^{18}O$ which probably represent a cooling phase (Figure 6.5). In addition, the P_BIP_{25} index had a mean value of 0.8, which was the highest value recorded, and which is indicative of more permanent sea ice conditions (Table 6.2).

Interestingly, in this period, fluctuation in the sea ice biomarkers was observed with an abrupt decrease in concentrations at ca. 1.8 cal. kyr (Figure 6.4) This change was also observed for all biomarkers. This observation could be supported by the lowest recorded values of $\delta^{18}O$ at around ca 1.7 cal. kyr (Figure 6.5; -3.98 ‰) which were indicative of colder temperatures. The time interval (1.8 - 1.7 cal. yr BP) that reflects the minimum of the proxies might be due to the different water masses that each proxy represent and the time that is needed to reflect that signal into the proxy data. Sensitivity of the proxy could also amplify or reduce the impact that the climatic change imprints in the proxy.

6.5.5 Earliest Holocene 10.5-9.4 kyr BP

To conclude the discussion, an interpretation of the climatic conditions during the Earliest Holocene is also given here. The most unstable conditions for all biomarkers were characteristic of the short period of the Earliest Holocene, in which high fluctuations in concentrations were observed (Figure 6.4). Generally, HBI concentrations for individual data points were either relatively low or below the analytical limits of detection of IP_{25}. IP_{25} and diene concentrations (Table 6.2) were the lowest for the 10.5 cal. kyr BP record. On their own, these data could produce an ambiguous interpretation, since the absence of IP_{25} could be associated to open water conditions (no sea ice presence) or heavy sea ice cover limiting bio-production (there is no phytoplankton/ sea ice bio-production). To resolve this ambiguity, a comparison with phytoplankton biomarkers was considered essential for the interpretation. In addition, concentrations of the phytoplankton indicators (HBI trienes) demonstrated the lowest individual data point concentrations (absence for trienes) with the lowest concentration trend for the record (0.06 and 0.03 µg g^{-1} TOC) for triene IIIa and IIIb. The sterols fluctuated in concentration with both highest and lowest concentrations of brassicasterol and 24-methylenecholesterol being observed (55 and 4; 6 and 0.6 µg g^{-1} TOC).

Although the variation of TOC is minimal through the record, the lowest concentrations of all biomarkers (sea ice and phytoplankton) could be reflected by the lowest values for TOC (1,6 wt. (%)) (Table 6.2) which could suggest strong sea ice conditions. Total absence of foraminiferal data (Figure 6.5) for this particular period reinforced the idea of strong sea ice conditions. However, P_BIP_{25} data (0.5) suggests more sea ice marginal conditions (Müller et al., 2012).

The high fluctuation of concentrations could however be influenced by the age model. The last reliable ^{14}C data point was obtained for ca. 9.4 cal. kyr BP (132-137 cm depth)

as it was impossible to obtain any data further down the core due to the absence of foraminifera. The presence of a till at 154 cm downwards suggested that sediment mixing disruption was taking place. Since the Earliest Holocene period comprises the bottom of the core with the boundary of the till, this could have an effect on biomarker concentrations for that period (10.5 - 9.4 cal. kyr BP) and could explain the high fluctuation of all biomarkers.

6.5.6 Biomarker correlations

This study presented the opportunity to investigate the abundance relationship between both HBI lipid sea ice indicators (IP_{25} and diene II) for a northern location of the Barents Sea throughout the Holocene. The relation between both lipids was visually observed by the biomarker trends and verified numerically (R^2= 0.77) (Figure 6.8). This result reinforces the previous good relationship observed for these two biomarkers for other down core locations of the northern hemisphere (Cabedo-Sanz et al., 2013) as well as for surface sediments in the Barents Sea (Chapter 4) and the Laptev and Kara seas (Xiao et al., 2013).

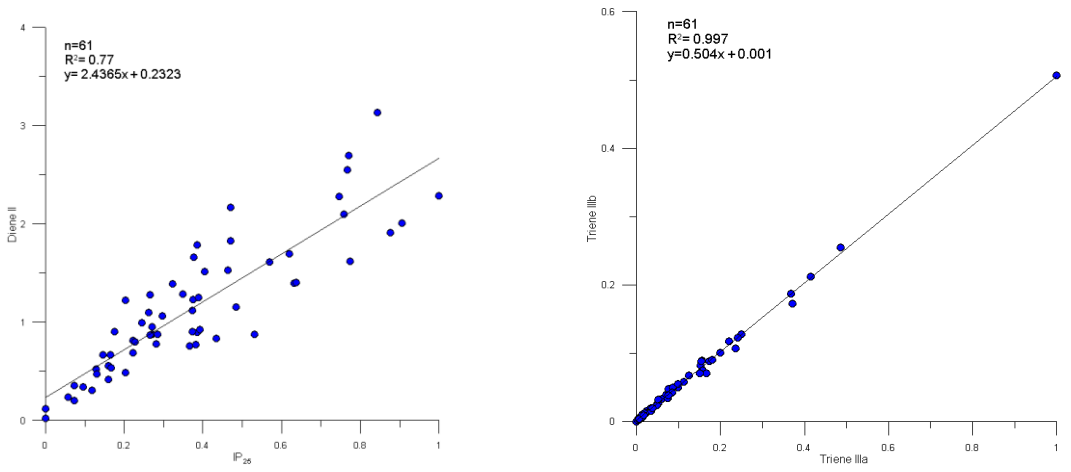

Figure 6.8 Biomarker correlation (area peaks) of: a) diene II and IP_{25}; b) triene IIIa and IIIb for core NP05-11-70GC.

Certain variability in the DIP_{25} ratio was observed through the record towards the present day (3.3; 3.8; 3.7 and 2.3 (Figure 6.5 Table 6.2)). Further RSD % values were calculated for each period (Table 7.2) to identify the variability through the periods. The highest values and variability for the DIP_{25} ratio were identified for the Earliest, Early and Mid-Holocene (3.3-3.8) (16-33 RSD %). The sea ice position was suggested to reach maximum latitudes ca. 78° N which in other terms indicate marginal sea ice conditions. The marginal sea ice edge, was suggested to gradually extend south arriving to the conditions proposed for the Late Holocene, reaching maximum extents similar to modern times (75° N) and providing more stable and continuously sea ice cover during spring at the core location. DIP_{25} for the Late Holocene value was reduced to 2.3, but more interestingly, the RSD also diminished to 12 %, probably indicating that under e.g. 90 % sea ice coverage (similar to modern times) the production of both biomarkers occur in a more consistent ratio. On the other hand, under marginal ice conditions (more dynamic ecosystems) the production of both biomarkers holds greater variability.

An exceptionally good correlation between the two HBI trienes was observed (R^2=0.997) (Figure 6.8). The triene ratio was investigated at this location after the observation that was made in Chapter 4 for the surface study, where the distribution of the trienes resembled the distribution of the Arctic and Atlantic waters masses (Figure 4.14 b). This observation would indicate that triene IIIb is somehow favoured under Atlantic waters and triene IIIa favoured under Arctic waters. Values for the trienes ratio down core are consistently around ca. 0.4, which is similar to the values observed for the surface study for nearby location (Figure 4.14 b). This observation could suggest that the core site has been continuously influenced by Arctic waters, a hypothesis supported by the foraminiferal data (Figure 6.6) which identified the Arctic species as the dominant species throughout the Holocene. It is known that the Atlantic water

masses at the core location extends under the fresher Arctic water masses (Lind and Ingvaldsen, 2012) which occupy the upper 20-100 meters. Assuming that the diatoms responsible for the triene formation live in the upper water column, this aligns with the observation of higher triene IIIb values for present day which relate to Arctic waters.

6.6 Conclusions

The work presented here aimed to reconstruct the sea ice and climatic conditions of the north eastern Barents Sea during the Holocene. Generally, a clear cooling trend towards present days through the last 10.5 cal. kyr BP record was identified.

Maximum sea ice extent and seasonal variability was proposed for such period. Starting from the Early Holocene (ca. 9.4 kyr BP), the maximum sea ice cover was suggested to reach ca 78° N and gradually advanced further south to ca. 76° N during the Mid Holocene, and ca. 75° N for the late Holocene (similar to the present day). The seasonal variability was proposed for spring-summer based on the relative sea ice and phytoplankton biomarker concentrations. Seasonal sea ice variability was suggested to be consistently placed over the maximum sea ice extent during the Early Holocene with the increase in variability probably a reflection of multi-decadal fluctuating water masses. The seasonality proposed for the Late Holocene would represent a slower retreat of the marginal ice edge (ca. 3 months to reach the minimum sea ice extent) when compared with the last 30 years, where the minimum is reached within a month or two.

CHAPTER SEVEN

7. Reproducibility of biomarker analysis within box core sediments

7.1 Introduction

Multicores and box cores are devices designed to collect undisturbed near-surface sediment material from the ocean floor with little or no perturbation. In contrast, piston or gravity cores, which are designed to collect longer sediment records, operate via more aggressive retrieval mechanisms and, as such, surface material is often lost.

A further issue that arises with sediment sampling is the extent to which an individual sediment core is representative of the study region. Potentially, this can be addressed by the analysis of replicate cores from the region, although this is rarely carried out (if ever), in practice. For box core sampling, a further question relates to the possible inconsistency that may exist within the box core itself, although it is likely assumed that such differences are relatively minor. However, given the time constrains associated with most proxy determinations, this assumption has not really been tested. Since biomarker analysis is relatively rapid, compared to most proxy methods (e.g. foraminifera, or dinocysts counts and identification), it was decided to investigate the representative nature of box core sediment material using a biomarker-based method.

The aims of this study were, therefore, to examine the lipid biomarker content of individual push cores obtained from a single box core to assess for consistency (or otherwise) between them. The specific objectives were:

1. To measure the concentrations of selected HBI and sterol biomarkers in 6 push cores obtained from a box core collected from Rijpfjorden, Svalbard.

2. To make comparisons between down core profiles of each biomarker and biomarker ratios (using a combination of visual inspection and statistical methods).
3. To propose explanations for any variability identified, on the basis of a number of sampling, lipid origin and environmental and human factors.

7.2 Regional setting

Rijpfjorden is located on the North coast of Nordaustlandet, within the Svalbard archipelago (Figure 7.1). The fjord opens towards the Arctic Ocean so the oceanographic conditions are dominated by cold Arctic waters (Ambrose et al., 2006). As a consequence, Rijpfjorden is covered in sea ice for up to 9 months a year. Sea ice break-up normally occurrs in mid- July (Ambrose et al., 2006; Wang et al., 2013) leading to a very short period of open waters and drift ice (Nygård et al., 2012).

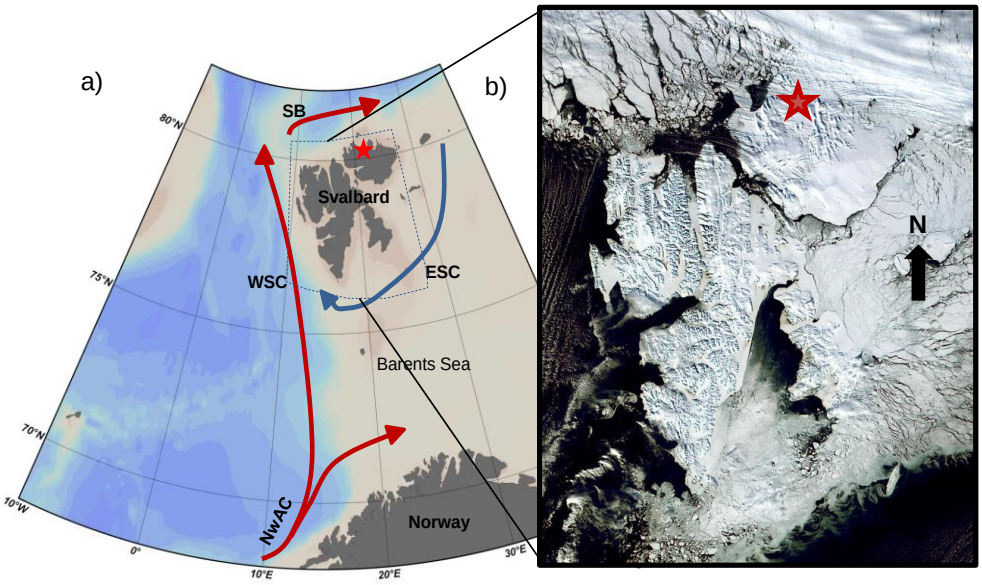

Figure 7.1 a) Map of the region of the Barents Sea. Bathymetry, main oceanic currents and location of the box core (red star) are indicated. Red arrows represent Atlantic water and blue arrows Arctic water. Abbreviations for the main currents are: NwAC:- Norwegian Atlantic Current, WSC- West Spitsbergen Current, SB- Svalbard Branch, ESC- East Spitsbergen Current, b) Satellite image of Svalbard on 20 of April 2000 taken by Modis/Modisland.

From a biological perspective, primary production is normally abundant and divided into two distinct algal blooms, a sea ice algal bloom in late April followed by a second phytoplankton bloom in early July following ice melt (Søreide et al., 2010). Even during one of the warmest years of the last decades (2006) (NSIDC) the zooplankton communities and cyst assemblages in Rijpfjorden were predominantly of an Arctic origin (Howe et al., 2010; Nygård et al., 2012).

7.3 Material and Methods

7.3.1Sediment Material

A box core was taken from Rijpfjorden (80° 19' N, 22° 14' E) during the Polar Night Cruise (January-2012) by colleagues on-board the RV "Helmer Hanssen" (Brown et al., 2013). 6 push cores were obtained by driving plastic tubes by hand into the sediment within the box core. Each push core was sliced into 0.5 cm sections for the top 2 cm; cm slices from 2-5 cm and every 2 cm from 5-10 cm depth. Sediment material was placed in plastic bags and stored in dark and low temperature (-20 °C) for lipid analysis.

7.3.2 Biomarker analysis

For the current study, the biomarkers analysed were selected HBIs and sterols (Table 7.1). All samples were freeze-dried (-45° C; 0.2 mbar; 24 h) prior to analysis. Biomarker analysis was carried out as described in Chapter 2.

For the majority of lipids, peak area integration (GC-MS) was relatively straightforward due to the occurrence of well-defined peak shapes with little or no interference from co-eluting biomarkers (Figure 7.2 a, c). However in the case of diene II, the integration was difficult due to the occurrence of shoulders and rather inconsistent peaks varying between cores (Figure 7.2 b, d). In order to minimize the effect that the integration

could have to absolute abundances, it was suggested to consistently integrate in several ways (main peak, main peak and one shoulder, and three peaks together (Figure 7.3 a, b, c)) for each chromatogram. Since the correlations between diene II and IP_{25} have been determined to be quite strong in previous studies, the integration approach providing a better relationship between biomarkers was adopted (Figure 7.3 a1, b1, c1). Results provided better correlations for approach b (R^2= 0.76) and c (R^2= 0.74), with little variation between them. In this case, integration of the 3 peaks (c) was chosen due to it was the most common scenario and differed little to the Figure 7.3 b1.

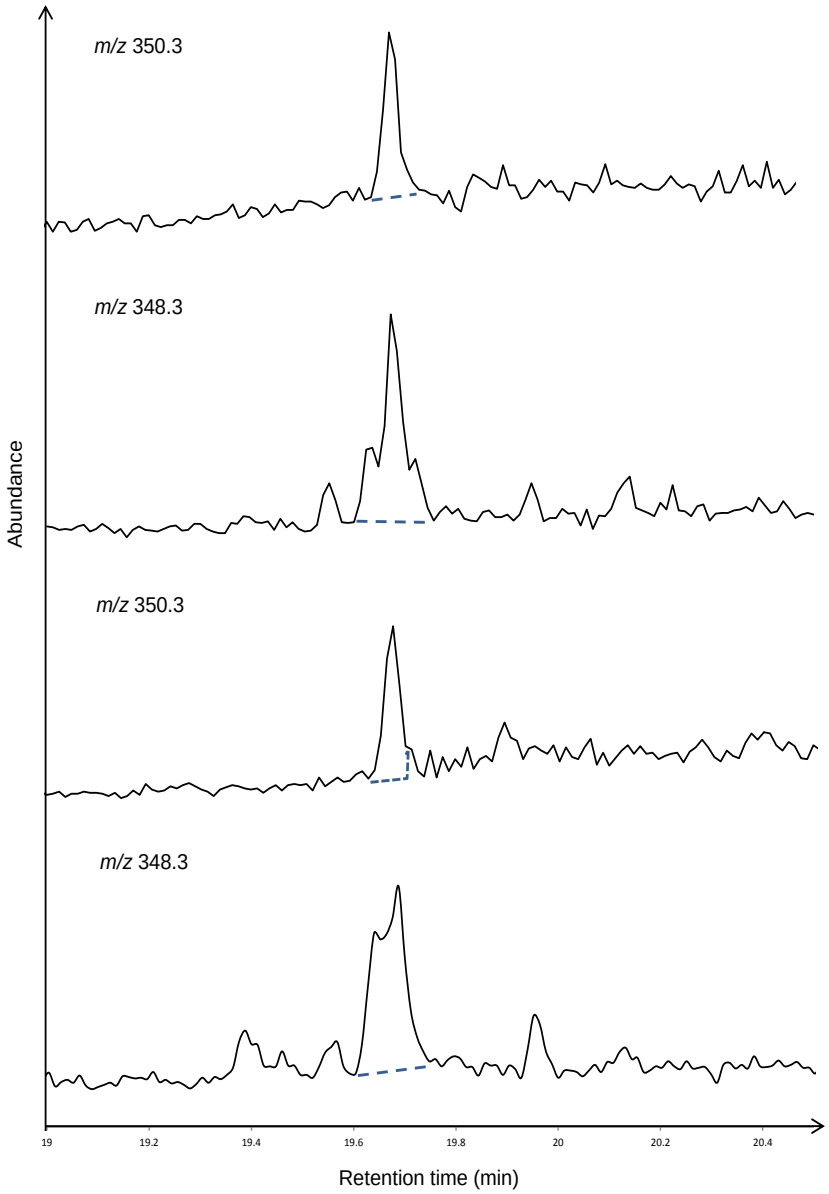

Figure 7.2 Partial SIM chromatograms of sediment from Rijpfjorden (selected ions *m/z* 350.3 and 348.3). Abundances and retention times are shown in the Y and X axis respectively. Peak appearing at ca 19.7 min. corresponds to IP_{25} (*m/z* 350.3) and diene II (*m/z* 348.3) which shoulders are isomer forms. Integration of the peak area was preceded delimited by the dotted blue line.

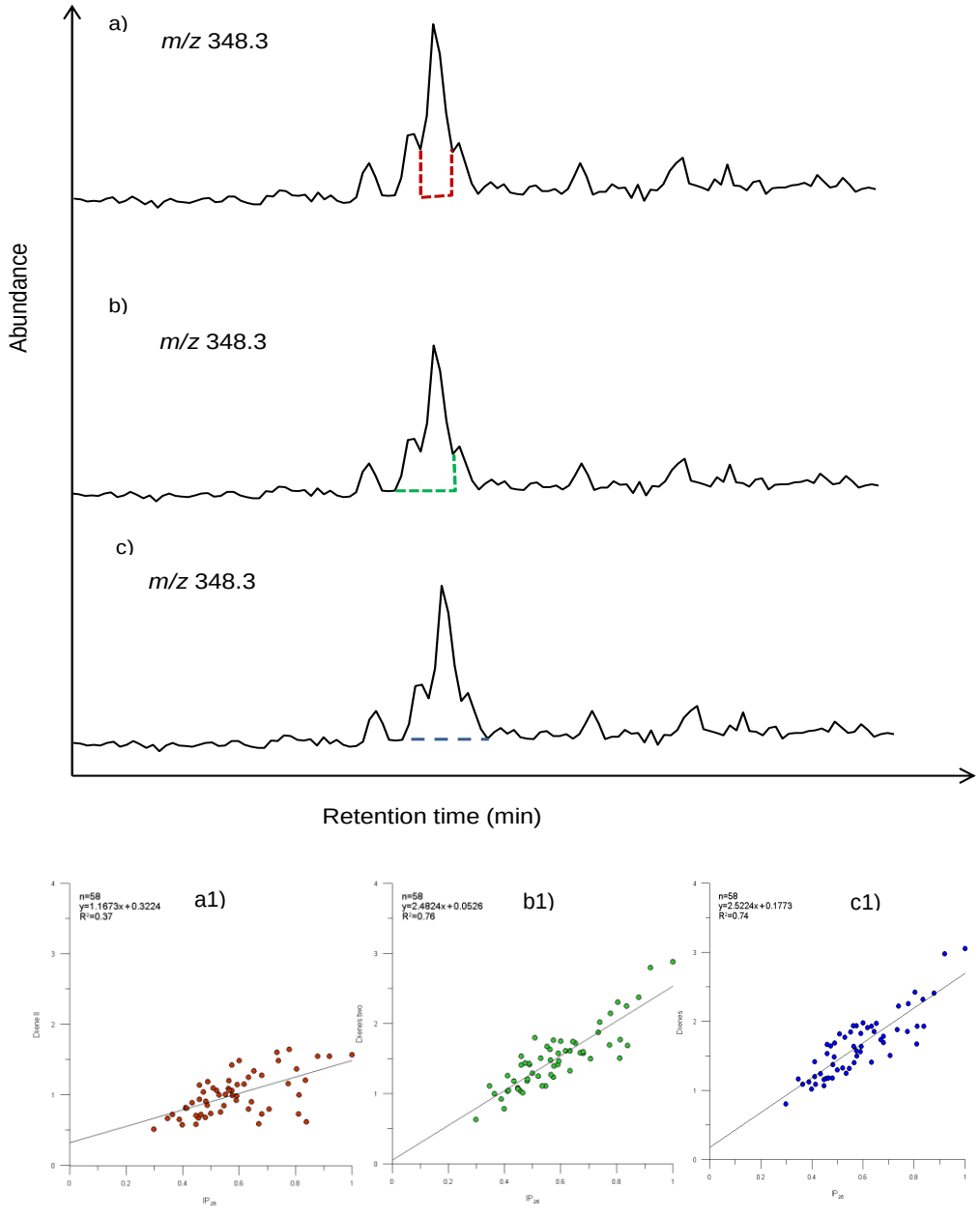

Figure 7.3 Partial SIM chromatograms of sediment from Rijpfjorden (selected ion *m/z* 348.3) for the same sample, integration conducted in different ways a); b); c). Correlations for the respective different integrations of one peak (a1), two peaks (b1) and three peaks (c1).

Reference sediment from the Canadian Arctic, was also analysed to establish the reproducibility of the analytical method for each lipid. Thus, for this study, 5 sub-samples of homogenised reference sediment material were analysed to determine the %

RSD values from which comparisons with the data from the box core analysis could be made.

Analysis of lipid data was carried out using standard methods (mean, standard deviation, relative standard deviation (% RSD) and t-test using Minitab® 16.1.1).

7.4 Results

7.4.1 Individual description and interpretation for biomarkers

IP_{25} and HBI diene II were detected in all sediment samples throughout the 10 cm short cores (Figure 7.4 a, b). Diene concentrations were higher than IP_{25}, (126 - 826 ng g^{-1}; 21 - 139 ng g^{-1}) which was in agreement with previous findings (Massé et al., 2008; Vare et al., 2009; Cabedo-Sanz et al., 2013; Xiao et al., 2013). The presence of IP_{25} and diene II in Rijpfjorden sediments was also in agreement with known sea ice occurrence for the region (Howe et al., 2010; Wang et al., 2013) and HBI biomarker concentrations observed in Brown et al. (2013). Concentration profiles for HBI biomarkers showed great similitudes with high consistency found for the upper 1.5 cm, followed by a sudden increase in the concentrations of all biomarkers from 1.5 to 2 cm (Figure 7.4 a, b). Concentrations from this horizon to the botom of the short core slightly decreased in all cases. The variability (% RSD) in the IP_{25} (33) and diene II (30) concentrations for the six cores (Table 7.1) was higher than that of the reference sediment (IP_{25}: 15, diene II: 20) (Table 7.2).

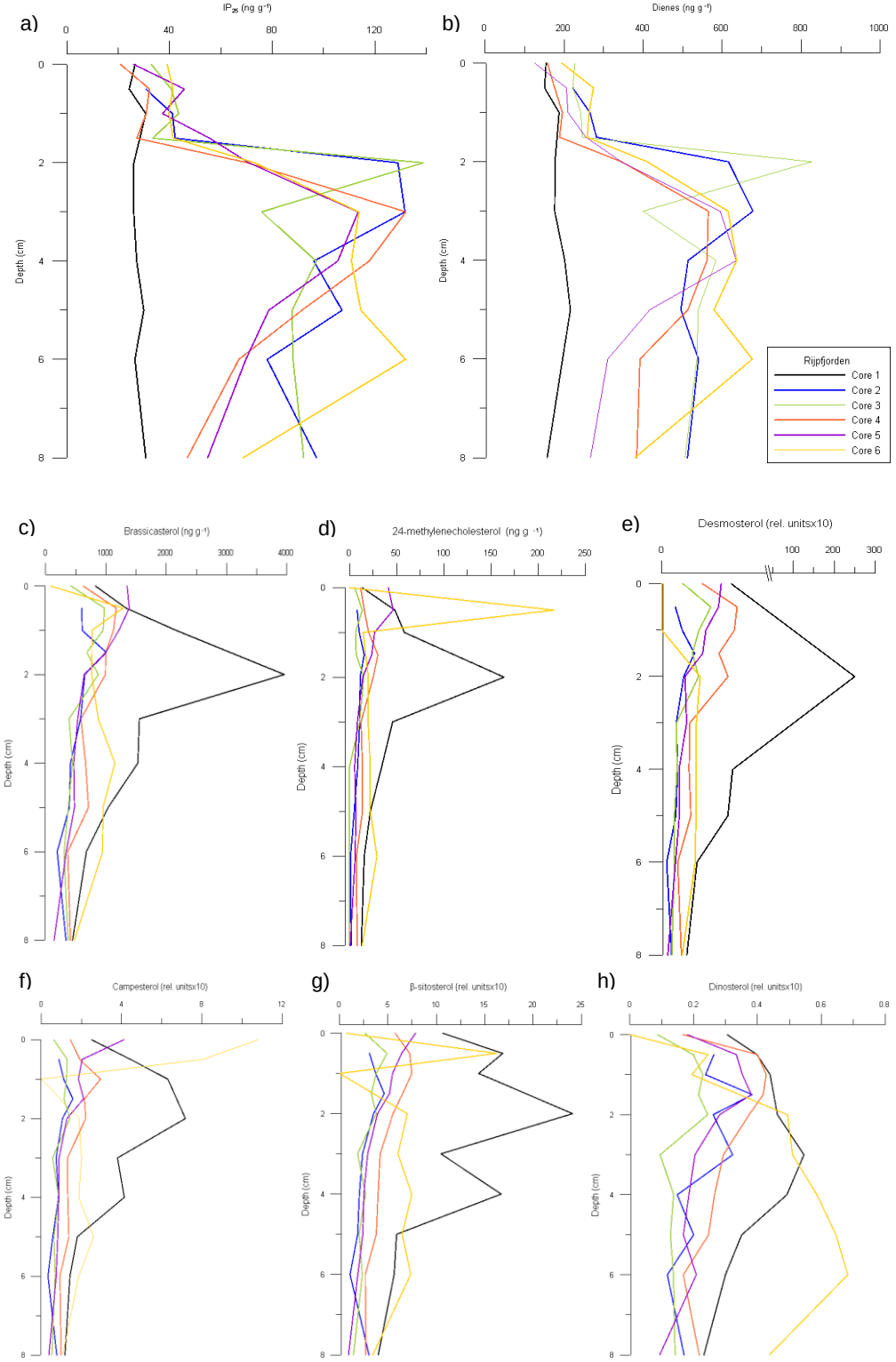

Figure 7.4 Biomarker profiles for the six push cores taken within a box core in Rijpfjorden, depth and concentration (ng g^{-1}) (or relative units x 10) are represented in Y and X axis respectively. a) IP_{25}; b) diene II; c) brassicasterol ;d) 24-methylenecholesterol; e) desmosterol; f) campesterol; g) β-sitosterol; h) dinosterol

Table 7.1 n= 6 (6 cores). Values correspond to the mean ± SD (% RSD). Concentrations are given in (ng g^{-1}) for the HBIs and (ng g^{-1}) for the sterols S1 and S2 and relative units x10 for S4, 5 and 6. Sterol biomarkers are: S1, brassicasterol; S2, 24-methylenecholesterol; S3, desmosterol; S4, campesterol; S5, β-sitosterol; and S6, dinosterol. Data is expressed to 1 decimal place (>0.1) or 1 significant value when (<0.1).

Depth (cm)	IP_{25}	Diene	S1	S2	S3	S4	S5	S6
0	29±7 (24)	172±39 (23)	659±474 (72)	14±16 (111)	2±1 (45)	4±4 (104)	6±4 (72)	0.1±0.1 (77)
0.5	36±8 (22)	209±43 (20)	1124±295 (26)	58±80 (137)	5±4 (90)	3±3 (88)	9±6 (35)	0.3±0.08 (27)
1	37±5 (14)	227±34 (15)	1437±549 (48)	23±19 (83)	4±3 (95)	3±2 (80)	7±4 (63)	0.3±0.1 (34)
1.5	40±11 (27)	246±35 (14)	919±158 (17)	19±10 (52)	2±0.6 (30)	2±0.5 (28)	5±1 (27)	0.3±0.09 (26)
2	85±42 (50)	454±231 (51)	1312±1304 (99)	41±60 (145)	43±101 (235)	3±2 (93)	8±8 (100)	0.4±0.1 (30)
3	99±41 (42)	505±186 (37)	751±424 (56)	18±14 (79)	2±2 (108)	2±1 (79)	5±3 (69)	0.3±0.2 (53)
4	92±33 (36)	522±164 (31)	776±460 (59)	14±12 (89)	2±2 (105)	2±1 (77)	6±6 (96)	0.3±0.2 (63)
5	85±30 (35)	460±131 (29)	657±288 (44)	12±9 (79)	1±1 (70)	1±0.8 (62)	4±2 (54)	0.3±0.2 (66)
6	77±34 (44)	442±175 (40)	470±283 (60)	10±11 (111)	0.9±0.6 (64)	1±0.6 (56)	4±2 (70)	0.3±0.2 (79)
8	65±26 (40)	368±138 (37)	363±121 (33)	6±6 (101)	0.7±0.4 (50)	0.8±0.3 (39)	3±1 (46)	0.2±0.1 (56)
Mean %RSD	-±- (33)±11	-±- (30) ±12	-±- (52) ±24	-±- (99) ±28	-±- (89) ±58	-±- (71) ±24	-±- (66)±22	-±- (55) ±24

Table 7.2 Reference sediment values for n=5 samples. S1, brassicasterol; S2, 24-methylenecholesterol; S3, desmosterol; S4, campesterol; S5, β-sitosterol and S6 dinosterol.

	IP_{25}	Diene	S1	S2	S3	S4	S5	S6
Ref. sed. % RSD n= 5	15	20	8	15	17	7	9	11

Sterol concentrations were even more variable and, in some samples, these biomarkers were absent or below the limit of detection. Generally, abundances of sterols decreased towards the bottom of the core (Figure 7.4 c-h). The greater variability in sterol concentrations compared to the HBIs could most readily be observed by examination of the % RSD data. For example, the horizon at 2 cm presented the highest % RSD for the majority of the biomarkers (Table 7.3). In any case, mean % RSD values (down core) for sterols were always higher to that for the reference sediment (Table 7.2) and the variability (% RSD) of the sterols for the 5 replicates of the reference sediment was, in all cases, similar to that found for IP_{25} and diene II (Table 7.2).

In general, the lipid concentration profiles in a group of five cores were similar (visual inspection), while one of the cores appears to be consistently different (Figure 7.4 a-g black line).

Having identified this likely outlier via visual inspection, the data were re-presented as means (+SD) using the entire dataset and with the apparent outlier removed from the mean (five cores) (Figure 7.5 b, c). The progression from Figure 7.5 b to c visually showed a decrease in variation when the anomalous core was removed. This approach was then applied to the rest of biomarkers (Figure 7.6). By excluding the anomalous core (black line), the mean % RSD of the down core diminished considerably for biomarkers e.g. IP_{25} (22); diene II (20) but still remained high for sterol biomarkers e.g. S1 (41); S3 (61) (Table 7.3), in comparison to the HBI biomarkers and the reference sediment % RSD for individual compounds (Table 7.2). A decrease in the % RSD values for sterols from specific horizons e.g. 2 cm (S2: 145; S3: 235 for n=6 to S2: 32; S3: 48 for n= 5) was also evident. These results suggest that the variability in the biomarker abundances within a box core (even when the outlier core was removed from the rest) was still relatively high and it could be consequence of a series of environmental processes and or human causes (collection, sectioning). These will be described in more detail in section 7.5.

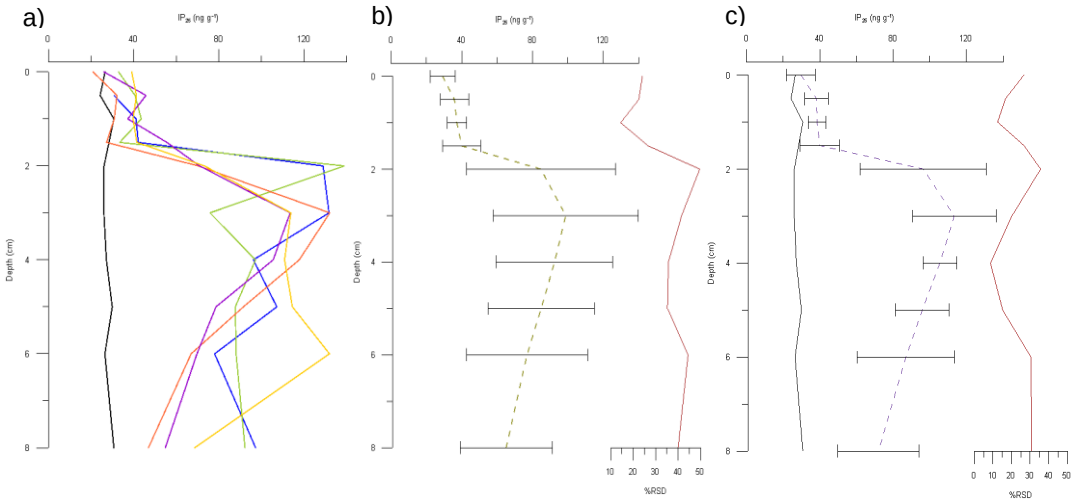

Figure 7.5 IP_{25} profiles for the six push cores taken within a box core in Rijpfjorden, depth and concentration are represented in Y and X axis respectively. a) individual 6 cores; b) average of 6 cores with standard deviation and % RSD values aside; c) Core 1, average of 5 cores with standard deviation and % RSD values aside.

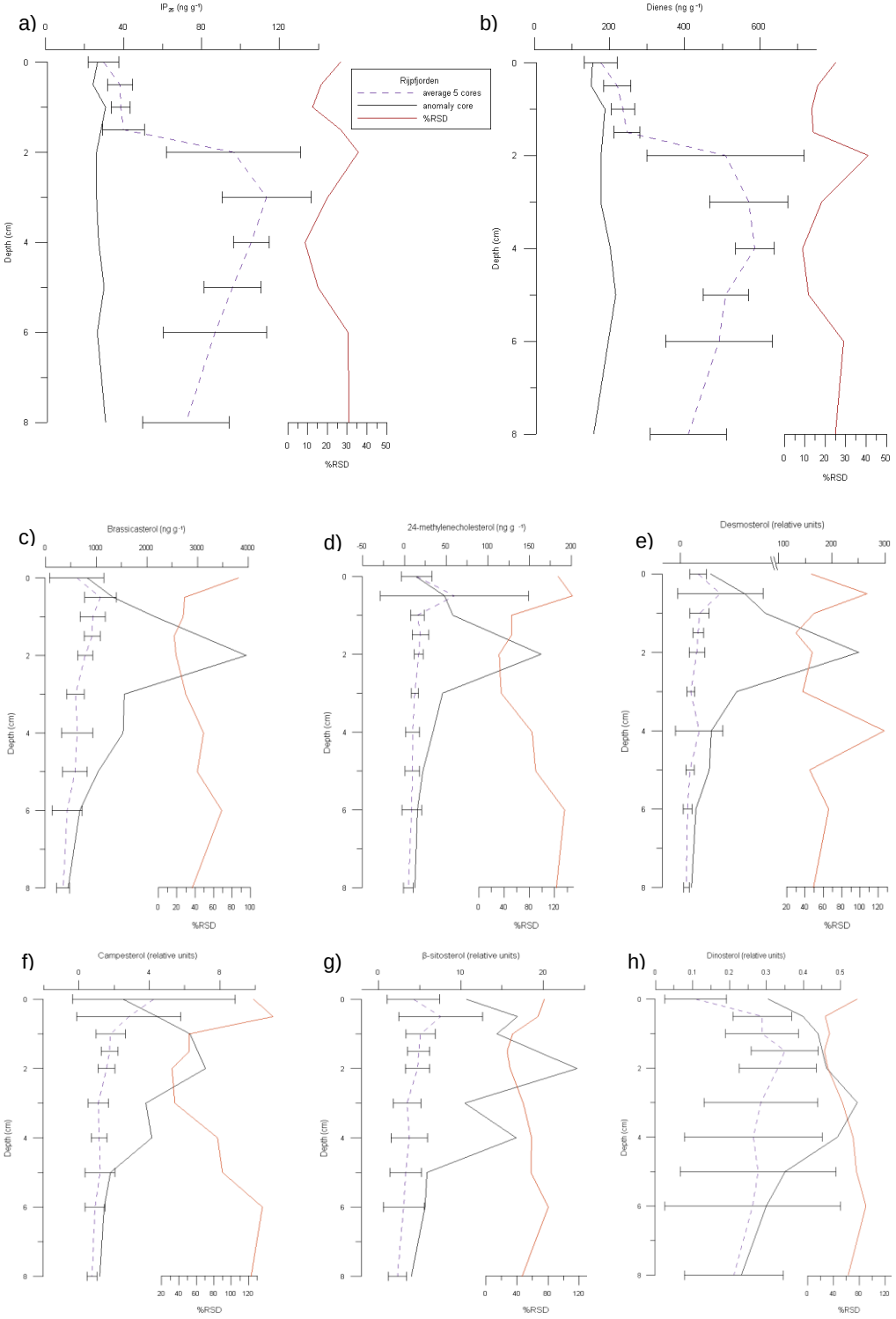

Figure 7.6 Biomarker profiles for the six push cores taken within a box core in Rijpfjorden, depth and concentration (or relative units) are represented in Y and X axis respectively. SD is represented with the error bars and % RSD indicated with the red line. a) IP_{25}; b) and diene; c) 24-methylenecholesterol; d) brassicasterol; e) β-sitosterol; f) campesterol; g) desmosterol; h) dinosterol.

Table 7.3 n= 5 (5 cores) (excluding core number 1). Values correspond to the mean ± SD (% RSD). Concentrations are given in (ng g^{-1}) for the HBIs and (µg g^{-1}) for the sterols S1 and S2 and relative units x10 for S4, 5 and 6. Sterol biomarkers are: S1 brassicasterol, S2 24-methylenecholesterol, S3 desmosterol S4 campesterol, S5 β-sitosterol and S6 dinosterol. Data is expressed to 1 decimal place (>0.1) or 1 significant value when (<0.1).

Depth (cm)	IP_{25}	Diene	S1	S2	S3	S4	S5	S6
0	30±8 (27)	176±44 (25)	617±536 (87)	15±18 (126)	2±0.9 (47)	4±5 (109)	4±3 (75)	0.1±0.08 (77)
0.5	38±6 (17)	220±36 (16)	1082±310 (29)	60±89 (148)	4±5 (108)	3±3 (104)	8±5 (67)	0.3±0.08 (27)
1	39±5 (13)	235±31 (13)	932±251 (27)	16±8 (52)	2±1 (50)	2± 0.8 (47)	5±2 (34)	0.3±0.1 (34)
1.5	40±11 (27)	246±35 (14)	919±158 (17)	19±10 (52)	2±0.6 (30)	2±0.5 (28)	5±1 (27)	0.3±0.09 (26)
2	96±34 (36)	509±209 (41)	782±151 (19)	17±5 (32)	2±0.9 (48)	2±0.5 (30)	5±1 (31)	0.3±0.1 (31)
3	113±23 (20)	571±104 (18)	590±176 (30)	12±4 (35)	1±0.4 (38)	1±0.6 (53)	3±2 (48)	0.3±0.2 (54)
4	105±9 (9)	587±52 (9)	626±308 (49)	10±8 (84)	2±3 (127)	1±0.4 (38)	4±2 (59)	0.3±0.2 (71)
5	96±15 (15)	509±60 (12)	581±246 (42)	9±9 (90)	1±0.5 (45)	1±0.8 (71)	3±2 (58)	0.3±0.2 (76)
6	87±26 (30)	491±142 (29)	429±295 (69)	9±12 (136)	0.8±0.5 (66)	0.9±0.6 (63)	3±2 (80)	0.3±0.2 (91)
8	72±22 (31)	410±102 (25)	346±127 (37)	5±6 (123)	0.6±0.3 (49)	0.7±0.3 (40)	2±1 (48)	0.2±0.1 (63)
Mean % RSD	-±- (22)±9	-±- (20) ±10	-±- (41) ±22	-±- (88) ±44	-±- (61) ±31	-±- (58) ±29	-±-(51)±18	-±- (51) ±20

7.4.1.1 Statistical analysis

In order to examine the variability in the biomarker data in more detail a statistical study was then conducted to identify significant differences between the presumed anomalous core (black line) and the average of the remaining 5. One sample t-test analysis was conducted for every horizon (10) for all individual biomarkers in order to determine if the average of the 5 cores was statistically different to the anomalous core. Calculated p-values for the t-test (Table 7.4) show that in the majority of the cases there was a significant difference between the group of 5 cores and the anomalous core for all biomarkers ($p < 0.05$ corresponding to 95 % confidence interval). IP_{25} and diene II responded to the t-test in a similar way where significant differences were observed for all depths except for the 0-0.5 cm top section. Amongst the sterols, more diverse results were observed. Higher dispersion in the results was identified for the sterols (e.g. no significantly differences ($p> 0.05$) for the first two horizons for sterols S1-S4 while significant differences for S5 and S6 were observed). No significant differences were observed for the last four horizons for S6. Only horizon 6 cm showed no differences for S5. This greater diversity in the response of the lipid sterols to the t-test could suggest

that these suit of biomarkers are subjected to a greater variability in comparison to the HBIs. This will be discussing in section 7.5.

Table 7.4 Significant p- values (one sample t-test) differences between the mean (5 cores) to the anomalous core for individual horizons. Samples that are not significantly different with a 95% confidence interval are represented with (N) P>0.05 and (Y) when they are P<0.05. P< 0.05 are not indicated (there is significant difference (Y) from the target (anomaly core) and the mean of the 5 cores. Sterols are; S1 brassicasterol, S2 24-methylenecholesterol, S3 desmosterol S4 campesterol, S5 β-sitosterol and S6 dinosterol.

Depth (cm)	IP_{25}	Diene	S1	S2	S3	S4	S5	S6
0	0.484(N)	0.384(N)	0.495(N)	0.872(N)	0.054(N)	0.504(N)	< 0.05(Y)	< 0.05(Y)
0.5	< 0.05(Y)	< 0.05(Y)	0.143(N)	0.777(N)	0.272(N)	0.291(N)	< 0.05(Y)	< 0.05(Y)
1	< 0.05(Y)	< 0.05(Y)	< 0.05(Y)	< 0.05(Y)	< 0.05(Y)	< 0.05(Y)	< 0.05(Y)	< 0.05(Y)
1.5	< 0.05(Y)	< 0.05(Y)	< 0.05(Y)	< 0.05(Y)	< 0.05(Y)	< 0.05(Y)	< 0.05(Y)	< 0.05(Y)
2	< 0.05(Y)	< 0.05(Y)	< 0.05(Y)	< 0.05(Y)	< 0.05(Y)	< 0.05(Y)	< 0.05(Y)	< 0.05(Y)
3	< 0.05(Y)	< 0.05(Y)	< 0.05(Y)	< 0.05(Y)	< 0.05(Y)	< 0.05(Y)	< 0.05(Y)	< 0.05(Y)
4	< 0.05(Y)	< 0.05(Y)	< 0.05(Y)	< 0.05(Y)	0.316(N)	< 0.05(Y)	< 0.05(Y)	0.054(N)
5	< 0.05(Y)	< 0.05(Y)	< 0.05(Y)	< 0.05(Y)	< 0.05(Y)	0.179(N)	< 0.05(Y)	0.483(N)
6	< 0.05(Y)	< 0.05(Y)	0.136(N)	0.238(N)	< 0.05(Y)	0.113(N)	0.080(N)	0.741(N)
8	< 0.05(Y)	< 0.05(Y)	0.154(N)	< 0.05(Y)	< 0.05(Y)	< 0.05(Y)	< 0.05(Y)	0.776(N)

7.4.2 Biomarker ratios

7.4.2.1 P_BIP_{25}

In order to make sea ice reconstructions more quantitative and descriptive and moving from the individual biomarker reconstructions to the combination of them to achieve this objective, the PIP_{25} ratio was developed (Müller et al., 2011). In principle, the combination of two biomarkers capable to describe two different environmental conditions i.e. sea ice (IP_{25}), and phytoplankton (open water like conditions, brassicasterol) was successfully applied to various Arctic regions and timescales e.g. recent times in the Greenland sea (Müller et al., 2011) and Canadian Arctic (Stoynova et al., 2013) and northern Norway for the Younger Dryas interval (Cabedo-Sanz et al., 2013). The main common parameter between this 3 areas, i.e. including the YD, is that sea ice conditions are mostly permanent. However when the PIP_{25} index is applied to seasonal sea ice areas, e.g. Barents Sea (Cabedo-Sanz, 2014) Kara and Laptev Seas

(Xiao et al., 2013) or Chapter 4, results were not representative of the sea ice conditions. More information and studies are necessary in order to evaluate whether this discrepancy is prompted by localised/ regional effects or might be related to the robustness of the own ratio amongst other causes. Thus, PIP_{25} ratios were calculated here and results were compared between the six nearby push cores to evaluate variability. Variability down core, mean % RSD values, for n= 6 was high (22), and similar values were obtained for n=5 cores (18). Interestingly, high variability on the PIP_{25} ratios was observed for specific horizons (0; 0.5 cm) (57-34) (% RSD), which remained high after removing the anomalous core (horizon 0; 68 %RSD). This high variability may be related to the completely different nature and possible reactivity of the two biomarkers combined for the calculation of the P_BIP_{25} index for example, it was noted that some horizons had very high concentrations of brassicasterol, which will considerably change the *c* factor for the individual six nearby cores, and consequently the final P_BIP_{25} values.

Table 7.5 DIP_{25} values calculated with abundances of IP_{25} and diene II normalized to the maximum value for IP_{25}. PIP_{25} values calculated with concentrations of IP_{25} and brassicasterol (Müller et al., 2011). Values correspond to the mean ± SD (% RSD).

Depth (cm)	DIP_{25} (6cores)	DIP_{25} (5cores)	PIP_{25} (6 cores)	PIP_{25}(5 cores)
0	3.0±0.5 (18)	3.0±0.6 (20)	0.46±0.27 (57)	0.42±0.29 (68)
0.5	3.0±0.5 (17)	2.9±0.6 (19)	0.29±0.10 (34)	0.25±0.01 (5)
1	3.0±0.2 (6)	3.0±0.2 (7)	0.31±0.07 (23)	0.29±0.04 (15)
1.5	3.0±0.5 (15)	3.0±0.5 (15)	0.28±0.08 (28)	0.28±0.08 (28)
2	2.7±0.4 (13)	2.6±.0.2 (8)	0.48±.0.11 (24)	0.53±.0.05 (9)
3	2.6±0.3 (12)	2.5±0.2 (10)	0.62±0.09 (15)	0.64±0.07 (11)
4	2.9±0.4 (15)	2.8±.0.3 (10)	0.60±.0.09 (15)	0.63±.0.08 (13)
5	2.8±0.4 (14)	2.6±0.2 (9)	0.62±0.04 (6)	0.62±0.04 (6)
6	2.9±0.5 (16)	2.8±0.4 (15)	0.68±0.04 (7)	0.68±0.05 (7)
8	2.7±0.2 (9)	2.7±0.2 (9)	0.68±0.1 (15)	0.66±0.09 (14)
Mean %RSD	-±- (13)	-±- (12)	-±- (22)	-±- (18)

7.4.2.2 DIP_{25}

Prompted by the study conducted by Belt and co-workers (2013) where it was demonstrated that the inter-laboratory variability was much higher for individual biomarkers than for the DIP_{25} ratio since the production of both biomarkers involved in the ratio are well known to be highly associated to the same environmental conditions, the DIP_{25} ratio was also calculated here. The objective was to follow the example of this previous study and determine whether the use of this ratio might provide more consistent data instead of individual biomarker concentrations could prevent from reproducibility issues between cores within the same box core device. Thus, further analysis of the correlation between IP_{25} and diene II to determine the DIP_{25} ratio was carried out. Results revealed a good agreement between biomarkers, R^2= 0.74; n= 6 cores (Figure 7.7 a) similar to that found for the north Atlantic area in other studies (Cabedo-Sanz et al., 2013) and little improvement was observed when the anomaly core was removed from the dataset R^2= 0.77; n= 5 cores (Figure 7.7 b). The variability (% RSD) observed for the ratio for the six push cores (DIP_{25}; 13) was lower than that found for the individual biomarkers themselves IP_{25} (22), diene II (20). Interestingly, little difference was observed when the anomalous core was removed DIP_{25} (12). This result suggests that whichever were the causes of the high variability observed for the individual biomarkers, these seem to affect both IP_{25} and diene II equally and by measuring the ratio between them, such factors are reduced. % RSD values were even lower (% RSD <15) in the majority of cases of individual horizons than that established by the reference sediments for any of the biomarkers.

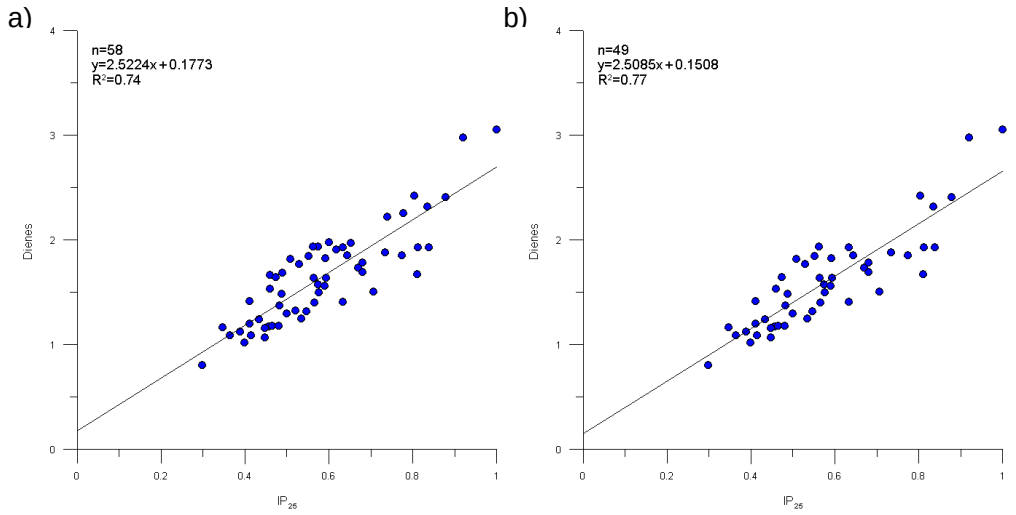

Figure 7.7 Abundances of diene and IP_{25} for the Rijpfjorden 6 push cores (58 sediment samples). a) Abundances were normalized to the maximum IP_{25} value observed for the dataset. b) Abundances of diene and IP_{25} for the Rijpfjorden 5 short cores (49 sediment samples, excluding core 1). Abundances were normalized to the maximum IP_{25} value observed for the dataset.

7.5 Discussion and significance of study

A biomarker reproducibility study was conducted by analysing and comparing concentrations of a series of biomarkers between six individual push cores retrieved from a box core. The suite of biomarkers contained specific sea ice indicators (IP_{25} and diene II) together with more generic biomarker (sterols) from terrestrial to marine sources.

Firstly, the biomarker results allowed the visual identification of a possible outlier core which was further investigated by the analysis of the data (e.g. means, ± SD and % RSD) and the application of statistical tools (t-test). Generally, a decrease in the variability (% RSD) was observed for all biomarkers when the anomalous core was removed (33-7 % improvement) and two interesting results emerged from the biomarker analysis at this point. Firstly, % RSD values for the HBI (IP_{25} and diene II for n= 5 cores) were still slightly higher for some horizons (e.g. 2, 6 and 8 cm; 36, 30, 31) (e.g. 41, 29, 25) respectively, than that for the reference sediment. Secondly, % RSD values for sterols were still very high for n= 5 cores (being also higher than that for the reference

sediment and for the HBIs; e.g. horizons 0 cm (111 - 72; S1 - S6); 4 cm (49 - 105; S1 - S6)) and high inconsistency was reflected between cores for individual lipid sterols. Possible factors influencing the biomarker distribution will be discussed in next section.

7.5.1 Biomarker variability between cores

7.5.1.1 HBIs

The variability in concentrations for the HBIs (IP_{25} and diene II) observed between cores, could substantially be explained in first instance by considering sediment re-distribution in the natural environment and its effect on sedimentation rates. Examples of highly variable environments are illustrated for a collection of box cores (Figure 7.8) which showed different characteristics such as: stone intrusion, irregular surface topography, variable water content box cores and sediment re-distribution by benthic activity (bioturbation) (Figure 7.8 a, b, c, d); the last two images corresponding to the Rijpfjorden box core. Other process such as lateral transport of sediment particles are well documented, which could modify the sedimentation rates of individual push cores within a box core. In addition to the natural contribution of sediment mixing, human impact (regarding physical collection and sectioning of sediment cores) could also contribute to potential changes in sedimentation rates. For example, the sectioning of the core is a delicate process in which the integrity of producing replicable horizons (within the box core) could be affected. Depending on the resolution, 0.3 - 0.5 cm sectioning, and the properties of the sediment core (clay, coarse, water content) the accuracy of the sectioning could also be affected.

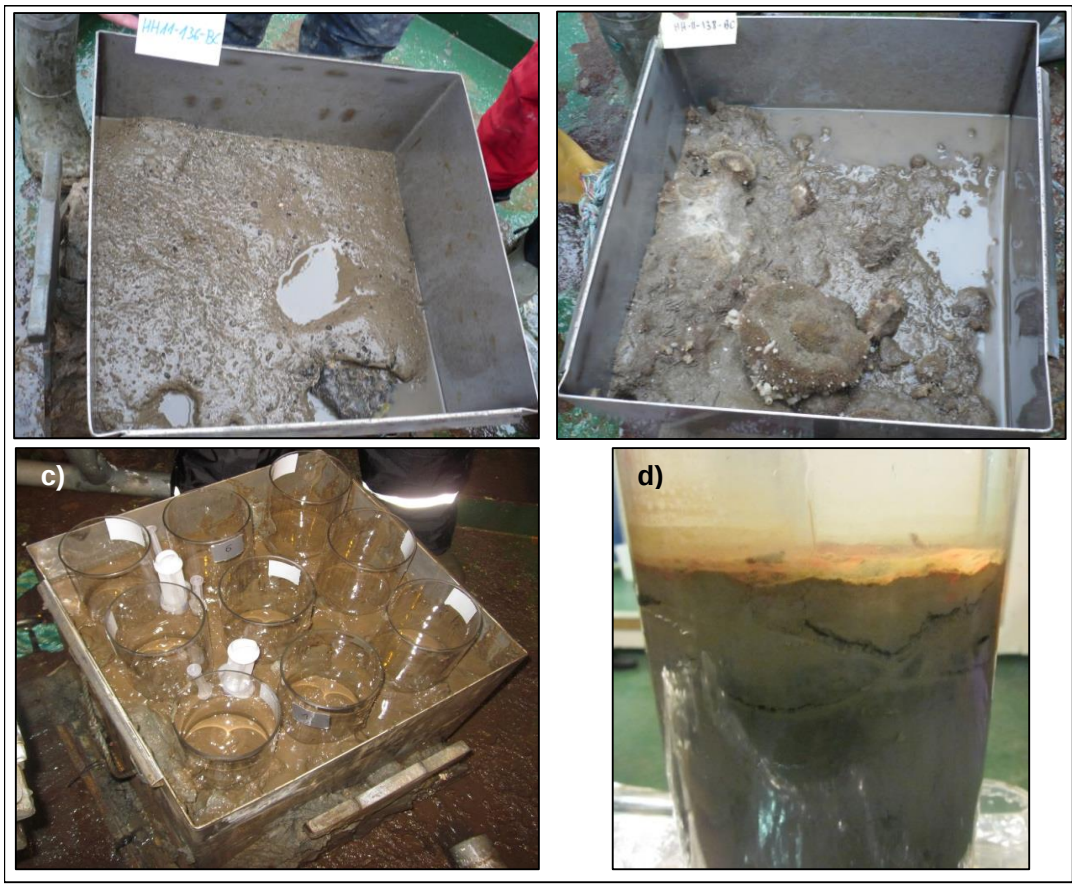

Figure 7.8 Box core sediments taken from West margin of Svalbard a) 78°N 0.46' W b) 78°N 1.35' E during July 2011 by the RV "Helmer Hanssen", c) box core and push cores from Rijpfjorden d) individual push core with worm bioturbation activity in the upper part.

An example of inconsistencies between sedimentation rates in multicores collected from the same site (cores within a multicore device) was observed in two studies conducted by Bonnet et al. (2010) and Zamelczyk et al. (2013). Although additional radiocarbon measurements (^{210}Pb, ^{137}Cs) were conducted to investigate possible variation in the interpretation of sedimentation rates by Bonnet et al. (2010), various acceptable hypothesis were derived producing discrepancy in sedimentation rates.

Regarding the biological activity, these HBIs are believed to be source specific to a few sea ice algal species, therefore important variability related to biological contribution e.g. irregular depletion and burial of zooplankton or benthic fauna contributing to the lipid signal was not expected, it would be more probably indicative of an Arctic diet

signal (Brown and Belt, 2012) and therefore a signal moved to a higher trophic level. This could be supported by the HBI relative consistency in concentration observed between the n= 5 cores. In addition, preservation of these lipids in the environment has been proved to be enough to be able to detect them in sediment records over thousands of years (Stein and Fahl, 2013). This nevertheless would not exclude that degradation of this lipids occur at some extent.

7.5.1.2 Sterols

The mentioned contributions to the variability of the HBI concentrations so far could affect in fact to any biomarker since they only account for physical re-distribution and mixing of sediment material.

However more selective biological causes could also cause variability in the biomarker distributions. High variability in the lipid sterol concentrations was observed between cores (% RSD Table 7.4). Since these biomarkers are produced by a large number of sources from terrigenous to marine input, the biological contribution, which could substantially modify concentrations in sediments, is important. For example, presence of benthic fauna trapped in sediment horizons e.g. worms or irregular depletion and burial of zooplankton (e.g. amphipods can be very rich in certain sterols e.g. desmosterol (Nelson et al., 2001), could greatly impact the variability in certain biomarker concentrations of individual horizons.

The preservation of biomarkers in relation to particular environmental conditions could be in addition a potential cause for variability, e.g. certain biomarkers could be more resistant to degradation under differences in temperature, oxic/anoxic conditions, biodegradation, photooxidation, aoutooxidation (Rontani et al., 2012).

7.6 Conclusions

The presence of IP_{25} and diene II in Rijpfjorden and their qualitative interpretation to identify spring sea ice conditions in the area was supported by satellite records. This result is consistent with the specificity of the HBI lipid biomarkers related to sea ice production and their successful use for sea ice reconstructions.

Variability between the six push cores was observed through the inspection of biomarker concentrations.

Sterol data showed much higher variability in comparison to HBI lipids between push cores. This could reflect a higher source origin or alternatively higher reactivity of the sterol lipids in environmental conditions. This result shows that sterol concentrations can be greatly and easily affected by external processes which make them less robust either individually or integrated in other proxies for palaeo-climate reconstructions.

DIP_{25} ratio provided more reliable values in comparison to the individual biomarkers used for its calculation, IP_{25} and diene II, and the P_BIP_{25} index for the six different push cores. Finally, these outcomes should be considered carefully when making biomarker interpretations.

CHAPTER EIGHT

8. Conclusions

This chapter summarises the main outcomes obtained in this study. In particular, this study provided recommendations for the analytical laboratory procedures for IP_{25} measurements, new interpretations of palaeo-sea ice conditions in the Barents Sea, and awareness of the reproducibility issues regarding sediment sampling.

Firstly, IP_{25} was successfully isolated and purified from marine sediment material and shown to have the same NMR and mass spectra as IP_{25} synthesised in the laboratory. Thus the structural confirmation of IP_{25} in Arctic sediments has been achieved.

Secondly, the use of an instrumental response factor (Chapter 3) has been demonstrated to be essential for producing reliable/quantitative data and should be adopted by any laboratory intending to conduct IP_{25} measurements (Belt et al., 2014), especially when comparing IP_{25} data produced by different laboratories. It was shown that the instrumental response factor varies with time. Therefore regular instrumental calibrations with a reference standard of IP_{25} are highly recommended. The same recommendation applies to other biomarkers of interest.

Thirdly, once the laboratory and instrumental procedures were established, the application of IP_{25} for sea ice reconstructions in sediments coming from the Barents Sea was conducted. The sediment material studied here contains a suite of surface sediments, two down cores, and a set of multicores.

Specifically, the data reported for the surface sediment study provided the foundation for further sea ice interpretations in the down core studies. The main outcomes are summarised in 8.1-8.3.

8.1 Surface study (Chapter 4)

The conclusions derived from the spatial study of surface sediments demonstrated that IP_{25} reports an excellent qualitative sea ice indicator in the Barents Sea, describing successfully the position of the modern sea ice margin (30 years) (Figure 8.1). However there was poor correlation between sea ice cover (%) and IP_{25} concentrations (Chapter 4), which limited its applications in a quantitative aspect.

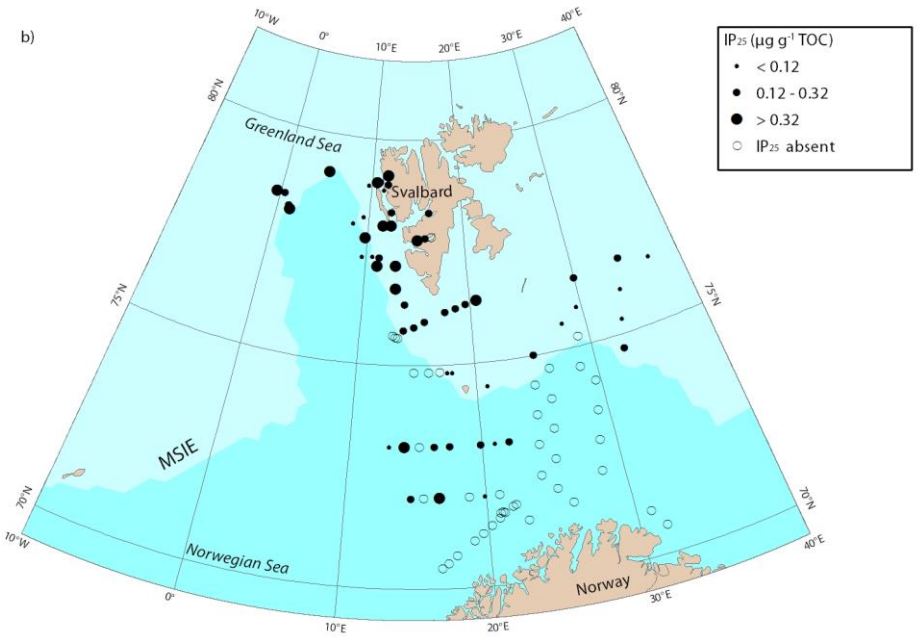

Figure 8.1 Map of the region of the Barents Sea described in the current study. Occurrence and concentration ranges of IP_{25}. The maximum sea ice extent (MSIE) for the period 1983-2002 is also indicated.

A series of environmental characteristics were observed for the Barents Sea through the analysis of the geochemical proxies (HBIs and sterols). The marginal ice zone seemed to hold the highest concentrations of all biomarkers studied, supporting the notion of high productivity of this particularly dynamic ecosystem. Such observations were subsequently used for long term reconstructions of sea ice conditions (Chapter 5-6). Lateral transport of sediment particles was hypothesized to take place in Bear Island Trough, displacing sediment from the Spitsbergen Bank, relatively abundant in IP_{25}

(under marginal sea ice conditions) being deposited in free sea ice areas, according the satellite records for at least the last century (Divine and Dick, 2006). The lateral transport of particles has been observed to be a common phenomenon in the Barents Sea (Quadfasel et al., 1988; Thomsen et al., 2001; Sarnthein et al., 2003) due to the formation of dense bottom water masses as a result of brine rejection from the formation of sea ice. Thus, this hypothesis is likely to explain the presence of IP_{25} for this sea ice free area.

Following further investigation, the spatial correlation of the recent DIP_{25} ratio (Cabedo-Sanz et al., 2013) was tested for the Barents Sea. The correlation was R= 0.98 which suggests a strong relationship between components (IP_{25} and diene II), likely related to a common source (sea ice diatoms). This would support the relation to sea ice observed by a heavier isotopic ^{13}C signature for both biomarkers (Belt et al., 2008).

Further observation on the spatial biomarker distribution relates to the HBI trienes and the relationship to the main water mass distribution (Atlantic waters, Arctic waters) of the region. Triene IIIa was observed to be relatively more abundant in the north eastern region which is dominated by Arctic water and triene IIIb was observed to be more abundant in the area characterised by Atlantic water. Alternatively, changes in the geochemical distributions may reflect changes in temperature, salinity or any other characteristic parameter associated to the water masses.

Finally, a further test of the P_BIP_{25} index (Müller et al., 2011) in surface sediments was carried out in order to provide a wider database and evaluate the capacity of the index to provide more quantitative sea ice reconstructions than those obtained by IP_{25} alone. The P_BIP_{25} index values for the Barents Sea samples generally provided overestimates of sea ice concentration, especially for the West Spitsbergen area (0.8) suggesting heavy sea ice conditions, when satellite records show averaged sea ice concentrations of less than

10%. For the other regions of the Barents Sea, the P_BIP_{25} index seemed to define the main sea ice margin remarkably well according to satellite records. These results suggest that the reliability of the P_BIP_{25} index is likely be locally dependent, possibly due to uncertainties regarding the specific (and variable) sources of brassicasterol, which is proposed as an indicator of open water conditions.

8.2 Down core studies (Chapter 5-6)

Analysis of the push core (HH11-134-BC; Chapter 5) located at the western Barents Sea margin provided biomarker based evidence (last 3000 yr) of a highly fluctuating sea ice margin (patchy sea ice, isolated sea ice formation, polynya formation), for this area in comparison to, for example, the eastern Barents Sea, which is better characterised by the seasonal advance of stable ice margin. High variability in the sea ice margin in the western Barents Sea has been recorded (based on historical and satellite observations) which reflects strong inter-annual variation. Biomarker data here was compared to two nearby IP_{25} records (Müller et al., 2011) which facilitated the interpretation of the sea ice conditions. The coldest period likely took place ca. 900 - 400 cal. yr BP. The determination was based upon in-phase maximum IP_{25} abundances in all the cores considered in the study and high IRD content, which suggested that the strong sea ice coverage for this period remained quite extended in comparison of the rest of the record. This would suggest a further extension of a more stable marginal sea ice condition, which could lead to longer time period of sea ice cover over the site locations before retreating due to melting.

Moving on to the core location on the eastern margin of Svalbard (NP05-70-GC; Chapter 6), the sea ice reconstructions derived from biomarker data (IP_{25}, HBIs and

sterols) suggested a general advance of the sea ice marginal position over the ca. 9.5 cal. kyr BP differentiating characteristic periods and sea ice dynamism. In the earliest Holocene (ca. 9.5 - 6.9 cal. kyr BP) the sea ice conditions suggested, located the position of the marginal sea ice likely minimally oscillating at ca 78° N (core location), progressively advancing (ca. 76° N) during the Mid Holocene (5.9 - 2.1 cal. kyr BP) until the maximum sea ice extent (75° - 74° N) for the Late Holocene (to present days). All the sea ice proposed scenarios were based on the biomarker data, taking as a reference the surface study (Chapter 5; e.g. marginal sea ice zone was proposed when concentrations of the biomarkers down core resembled the general concentrations of the marginal sea ice observed for modern days).

Good correlations were observed between diene II and IP_{25} and between triene IIIa and IIIb supporting the idea of a common sources for each pair of biomarkers.

8.3 Reproducibility study (Chapter 8)

The study derived from the six multicores retrieved from Rijpfjorden (north Svalbard) provided information regarding the robustness of a series of individual biomarker datasets and the combination of them.

Firstly, an "outlier" core was statistically identified through the analysis of a suite of geochemicals in six nearby push cores (ca. 1 m^2).

Sterols showed much more variability through the inspection of the 6 push cores and, more importantly, an arbitrary distribution for each individual one. In comparison, IP_{25} and diene, showed great correlation through the six push cores, even when one was identify to be statistically different.

Finally, DIP_{25} ratio showed to provide a more robust dataset for the six push cores than the ratio of other biomarkers (PIP_{25}) reducing the % RSD. This result could indicate that

by combining compounds of similar geochemical properties and more specific sources (e.g. IP_{25} and diene II), the factors that potentially could affect their distribution would more likely be compensated.

8.4 Areas of potential future work

Since triene lipid distribution was observed to hold certain potential uses for oceanographic reconstructions, more studies assessing the application of this biomarkers, and studies in the investigation of the source origin and degradation in sediments, regarding its use especially for palaeoclimate reconstructions could be an important area of further work. These HBI lipids (trienes IIIa and IIIb) could be more susceptible (compared to IP_{25}) to degrade in natural conditions since their structure contains three double bounds.

Further studies to better identify the sources of brassicasterol could help to clarify anomalies in localised areas (especially using the PIP_{25} index) in which has been commonly interpreted as a phytoplankton biomarker.

Similarly, a better understanding of the factors that regulate IP_{25} production with respect to sea ice (concentrations, conditions) could be conducted especially in the anomaly areas already identified in the Arctic region where concentrations of IP_{25} were discordant to observed sea ice cover e.g. Chapter 4 Western Barents Sea, by the depletion of mooring traps and or sea ice sample collection for these areas.

References

Aagaard-Sørensen, S., K. Husum, M. Forwick, M. Hald, K. Andreassen, and N. Koç (in prep.), Paleoceanographic reconstruction in the Olga Basin, northern Barents Sea during the Holocene

Ambrose, W.G., Carroll, M.L., Greenacre, M., Thorrold, S.R., McMahon, K.W., 2006. Variation in Serripes groenlandicus (Bivalvia) growth in a Norwegian high-Arctic fjord: evidence for local- and large-scale climatic forcing. Global Change Biology 12, 1595-1607.

Andrews, J.T., Belt, S.T., Olafsdottir, S., Massé, G., Vare, L.L., 2009. Sea ice and marine climate variability for NW Iceland/Denmark Strait over the last 2000 cal. yr BP. The Holocene 19.5, 775-784.

Andrews, J.T., Eberl, D.D., 2012. Determination of sediment provenance by unmixing the mineralogy of source-area sediments: The "SedUnMix" program. Marine Geology 291–294, 24-33.

Archer, D., Maier-Reimer, E., 1994. Effect of deep-sea sedimentary calcite preservation on atmospheric CO_2 concentration. Nature 367, 260-263.

Årthun, M., Eldevik, T., Smedsrud, L.H., Skagseth, Ø., Ingvaldsen, R.B., 2012. Quantifying the Influence of Atlantic heat on Barents Sea ice variability and retreat. Journal of Climate 25, 4736-4743.

Barbara, L., Crosta, X., Massé, G., Ther, O., 2010. Deglacial environments in eastern Prydz Bay, East Antarctica. Quaternary Science Reviews 29, 2731-2740.

Belt, S.T., Allard, W.G., Massé, G., Robert, J.-M., Rowland, S.J., 2000. Highly branched isoprenoids (HBIs): identification of the most common and abundant sedimentary isomers. Geochimica et Cosmochimica Acta 64, 3839-3851.

Belt, S.T., Brown, T.A., Ampel, L., Cabedo-Sanz, P., Fahl, K., Kocis, J.J., Massé, G., Navarro-Rodriguez, A., Ruan, J., Xu, Y., 2014. An inter-laboratory investigation of the Arctic sea ice biomarker proxy IP_{25} in marine sediments: key outcomes and recommendations. Climate of the Past 10, 155-166.

Belt, S.T., Brown T.A., Cabedo Sanz, P. and Navarro Rodriguez, A., 2012a Structural confirmation of the sea ice biomarker IP_{25} found in Arctic marine sediments. Environmental Chemistry Letters 10**,** 189-192

Belt, S.T., Brown, T.A., Navarro-Rodriguez, A., Cabedo-Sanz, P., Tonkin, A., Ingle, R., 2012b. A reproducible method for the extraction, identification and quantification of the Arctic sea ice proxy IP_{25} from marine sediments. Analytical Methods 4, 705-713

Belt, S.T., Brown, T.A., Ringrose, A.E., Cabedo-Sanz, P., Mundy, C.J., Gosselin, M., Poulin, M., 2013b. Quantitative measurement of the sea ice diatom biomarker IP_{25} and sterols in Arctic sea ice and underlying sediments: Further considerations for palaeo sea ice reconstruction. Organic Geochemistry 62, 33-45.

Belt, S.T., Cooke, D.A., Hird, S.J., Rowland, S., 1994. Structural determination of a highly branched C_{25} sedimentary isoprenoid biomarker by NMR spectroscopy and mass spectrometry. Journal of the Chemical Society, Chemical Communications 0, 2077-2078.

Belt, S.T., Cooke, D.A., Robert, J.-M., Rowland, S., 1996. Structural characterisation of widespread polyunsaturated isoprenoid biomarkers: A C_{25} triene, tetraene and pentaene from the diatom Haslea ostrearia simonsen. Tetrahedron Letters 37, 4755-4758.

Belt, S.T., Massé, G., Allard, W.G., Robert, J.-M., Rowland, S.J., 2001. C_{25} highly branched isoprenoid alkenes in planktonic diatoms of the Pleurosigma genus. Organic Geochemistry 32, 1271-1275.

Belt, S.T., Massé, G., Allard, W.G., Robert, J.-M., Rowland, S.J., 2002. Effects of auxosporulation on distributions of C_{25} and C_{30} isoprenoid alkenes in Rhizosolenia setigera. Phytochemistry 59, 141-148.

Belt, S.T., Massé, G., Rowland, S.J., Poulin, M., Michel, C., LeBlanc, B., 2007. A novel chemical fossil of palaeo sea ice: IP_{25}. Organic Geochemistry 38, 16-27.

Belt, S.T., Massé, G., Vare, L.L., Rowland, S.J., Poulin, M., Sicre, M.-A., Sampei, M., Fortier, L., 2008. Distinctive ^{13}C isotopic signature distinguishes a novel sea ice biomarker in Arctic sediments and sediment traps. Marine Chemistry 112, 158-167.

Belt, S.T., Müller, J., 2013. The Arctic sea ice biomarker IP_{25}: a review of current understanding, recommendations for future research and applications in palaeo sea ice reconstructions. Quaternary Science Reviews 79, 9-25.

Belt, S.T., Vare, L.L., Massé, G., Manners, H.R., Price, J.C., MacLachlan, S.E., Andrews, J.T., Schmidt, S., 2010. Striking similarities in temporal changes to spring sea ice occurrence across the central Canadian Arctic Archipelago over the last 7000 years. Quaternary Science Reviews 29, 3489-3504.

Benthien, A., Müller, P.J., 2000. Anomalously low alkenone temperatures caused by lateral particle and sediment transport in the Malvinas Current region, western Argentine Basin. Deep Sea Research Part I: Oceanographic Research Papers 47, 2369-2393.

Berben, S.M.P., Husum, K., Navarro-Rodriguez, A., Belt, S.T., Aagaard-Sørensen. S., (in prep.), Atlantic water inflow and sea ice distribution in the northern Barents Sea: A Holocene paleoceanographic evolution.

Boitsov, S., Jensen, H.K.B., Klungsøyr, J., 2009. Geographical variations in hydrocarbon levels in sediments from the Western Barents Sea. Norwegian Journal of Geology 89, 91-100.

Bondevik, S., and S. Gulliksen., 2006. Alternative discussion and recommendations by Bondevik and Gulliksen, in Marine ^{14}C reservoir ages for 19th century whales and molluscs from the North Atlantic, edited by Mangerud J., S. Bondevik, S. Gulliksen, A. K. Hufthammer, and T. Høisæter, Quaternary Science Review 25, 3228-3245.

Bonnet, S., de Vernal, A., Hillaire-Marcel, C., Radi, T., Husum, K., 2010. Variability of sea-surface temperature and sea-ice cover in the Fram Strait over the last two millennia. Marine Micropaleontology 74, 59-74.

Brassell, S.C., Eglinton, G., Marlowe, I.T., Pflaumann, U., Sarnthein, M., 1986. Molecular stratigraphy: a new tool for climatic assessment. Nature 320, 129-133.

Brown, T., Belt, S., Philippe, B., Mundy, C., Massé, G., Poulin, M., Gosselin, M., 2011. Temporal and vertical variations of lipid biomarkers during a bottom ice diatom bloom in the Canadian Beaufort Sea: further evidence for the use of the IP_{25} biomarker as a proxy for spring Arctic sea ice. Polar Biology 34, 1857-1868.

Brown, T.A., 2011. Production and preservation of the arctic sea ice diatom biomarker IP_{25}, *PhD Thesis*. University of Plymouth.

Brown, T.A., Belt, S.T., 2012. Identification of the sea ice diatom biomarker IP_{25} in Arctic benthic macrofauna: direct evidence for a sea ice diatom diet in Arctic heterotrophs. Polar Biology 35, 131-137.

Brown, T.A., Hegseth, E.N., Belt, S.T., 2013. A biomarker-based investigation of the mid-winter ecosystem in Rijpfjorden, Svalbard. Polar Biology, 1-14.

Cabedo-Sanz, P., 2013. Identification of variability in Sub-Arctic sea ice conditions during the Younger Dryas and Holocene, *PhD Thesis*. Plymouth University.

Cabedo-Sanz, P., Belt, S.T., Knies, J., Husum, K., 2013. Identification of contrasting seasonal sea ice conditions during the Younger Dryas. Quaternary Science Reviews 79, 74-86.

Carmack, E., Wassmann, P., 2006. Food webs and physical–biological coupling on pan-Arctic shelves: Unifying concepts and comprehensive perspectives. Progress In Oceanography 71, 446-477.

Collins, L.G., Allen, C.S., Pike, J., Hodgson, D.A., Weckström, K., Massé, G., 2013. Evaluating highly branched isoprenoid (HBI) biomarkers as a novel Antarctic sea-ice proxy in deep ocean glacial age sediments. Quaternary Science Reviews 79, 87-98.

Comiso, J.C., Cavalieri, D.J., Parkinson, C.L., Gloersen, P., 1997. Passive microwave algorithms for sea ice concentration: A comparison of two techniques. Remote Sensing of Environment 60, 357-384.

Crosta, X., Koç, N., 2007. Diatoms: From micropaleontology to isotope geochemistry. In: Hillaire-Marcel, C., and De Vernal, A., (eds.), Proxies in Late Cenozoic Paleoceanography. Oxford: Elsevier, pp 327-369.

de Vernal, A., Eynaud, F., Henry, M., Hillaire-Marcel, C., Londeix, L., Mangin, S., Matthiessen, J., Marret, F., Radi, T., Rochon, A., Solignac, S., Turon, J.L., 2005. Reconstruction of sea-surface conditions at middle to high latitudes of the Northern Hemisphere during the Last Glacial Maximum (LGM) based on dinoflagellate cyst assemblages. Quaternary Science Reviews 24, 897-924.

de Vernal, A., Gersonde, R., Goosse, H., Seidenkrantz, M.-S., Wolff, E.W., 2013. Sea ice in the paleoclimate system: the challenge of reconstructing sea ice from proxies – an introduction. Quaternary Science Reviews 79, 1-8.

de Vernal, A., Hillaire-Marcel, C., Rochon, A., Fréchette, B., Henry, M., Solignac, S., Bonnet, S., 2013. Dinocyst-based reconstructions of sea ice cover concentration during the Holocene in the Arctic Ocean, the northern North Atlantic Ocean and its adjacent seas. Quaternary Science Reviews 79, 111-121.

de Vernal, A., and Rochon, A., 2011. Dinocysts as tracers of sea-surface conditions and sea-ice cover in polar and subpolar environments. IOP Conference Series: Earth and Environmental Science 14. doi:10.1088/1755-1315/14/1/012007.

Denis, D., Crosta, X., Barbara, L., Massé, G., Renssen, H., Ther, O., Giraudeau, J., 2010. Sea ice and wind variability during the Holocene in East Antarctica: insight on middle–high latitude coupling. Quaternary Science Reviews 29, 3709-3719.

Divine, D.V., and Dick, C., 2006. Historical variability of sea ice edge position in the Nordic Seas. Journal of Geophysical Research 111 C01001. doi:10.1029/2004JC002851.

Divine, D.V., and Dick, C., 2007. March through August ice edge position in the Nordic Seas, 1750-2002. [ACSYS Historical Ice Chart Archive (ACSYS, 2003)]; [SSM/I passive microwave data (Cavalieri et al., 1990)]. Boulder, Colorado USA: National Snow adn Sea Ice Data Center. http://dx.doi.org/10.7265/N59884X1.

Duplessy, J.-C., Ivanova, E., Murdmaa, I., Paterne, M., Labeyrie, L., 2001. Holocene paleoceanography of the northern Barents Sea and variations of the northward heat transport by the Atlantic Ocean. Boreas 30, 2-16.

Dylmer, C.V., Giraudeau, J., Eynaud, F., Husum, K., de Vernal, A., 2013. Northward advection of Atlantic water in the eastern Nordic Seas over the last 3000 yr. Climate of the Past 9, 1505-1518.

Ebbesen, H., Hald, M., 2004. Unstable Younger Dryas climate in the northeast North Atlantic. Geology 32, 673-676.

Eynaud, F., 2011. Planktonic foraminifera in the Arctic: potentials and issues regarding modern and quaternary populations. IOP Conference Series: Earth and Environmental Science 14. doi:10.1088/1755-1315/14/1/012005.

Fahl, K., and Stein, R., 2012. Modern seasonal variability and deglacial/Holocene change of central Arctic Ocean sea-ice cover: New insights from biomarker proxy records. Earth and Planetary Science Letters 351–352, 123-133.

Falk-Petersen, S., Hop, H., Budgell, W.P., Hegseth, E.N., Korsnes, R., Løyning, T.B., Børre Ørbæk, J., Kawamura, T., Shirasawa, K., 2000. Physical and ecological processes in the marginal ice zone of the northern Barents Sea during the summer melt period. Journal of Marine Systems 27, 131-159.

Fetterer, F., Knowles, K., Meier, W., Savoie, M., 2002. Updated 2009 Sea ice index. National Snow and Ice Data Center, Boulder CO.

Fietz, S., Huguet, C., Rueda, G., Hambach, B., Rosell-Melé, A., 2013. Hydroxylated isoprenoidal GDGTs in the Nordic Seas. Marine Chemistry 152, 1-10.

Fohrmann, H., Backhaus, J.O., Blaume, F., Haupt, B.J., Kämpf, J., Michels, K., Mienert, J., Posewang, J., Ritzrau, W., Rumohr, J., Weber, M., Woodgate, R., 2001. Modern Ocean Current-Controlled Sediment Transport in the Greenland-Iceland-Norwegian (GIS) Seas, In: Schäfer, P.R., W. Schulter, M. Thiede, J. (eds.), The Northern North Atlantic: A Changing Environment Springer, Berlin, pp. 135-154.

Forwick, M., Vorren, T.O., 2009. Late Weichselian and Holocene sedimentary environments and ice rafting in Isfjorden, Spitsbergen. Palaeogeography, Palaeoclimatology, Palaeoecology 280, 258-274.

Grøsfjeld, K., Harland, R., Howe, J., 2009. Dinoflagellate cyst assemblages inshore and offshore Svalbard reflecting their modern hydrography and climate. Norwegian Journal of Geology 89, 121-134.

Grossi, V., Beker, B., Geenevasen, J.A.J., Schouten, S., Raphel, D., Fontaine, M.-F., Sinninghe Damsté, J.S., 2004. C_{25} highly branched isoprenoid alkenes from the marine benthic diatom Pleurosigma strigosum. Phytochemistry 65, 3049-3055.

Ho, S.L., Mollenhauer, G., Fietz, S., Martínez-Garcia, A., Lamy, F., Rueda, G., Schipper, K., Méheust, M., Rosell-Melé, A., Stein, R., Tiedemann, R., 2014. Appraisal of TEX_{86} and thermometries in subpolar and polar regions. Geochimica et Cosmochimica Acta 131, 213-226.

IPCC, 2007. Intergovernamental Panel on Climate Change (IPCC) (2007) Climate Change 2007: the Scientific Basis. In: Contribution of Working Group I to the Third Assessment Report of the Intergovernamental Panel on Climate Change. Cambridge University Press, Cambridge.

Howe, J.A., Harland, R., Cottier, F.R., Brand, T., Willis, K.J., Berge, J.R., Grøsfjeld, K., Eriksson, A., 2010. Dinoflagellate cysts as proxies for palaeoceanographic conditions in Arctic fjords. Geological Society 344, 61-74.

Jakobsson, M., Grantz, A., Kristoffersen, Y., Macnab, R., 2004. Physiography and bathymetry of the Arctic Ocean, In: Stein, R., Macdonald, R.W. (eds.), The Organic Carbon Cycle in the Arctic Ocean. Springer, New York, pp. 1-5.

Jensen, S., Renberg, L., Reuterqärdh, L., 1977. Residue analysis of sediment and sewage sludge for organochlorines in the presence of elemental sulfur. Analytical chemistry 49, 316-318.

Jernas, P., Klitgaard Kristensen, D., Husum, K., Wilson, L., Koç, N., 2013. Palaeoenvironmental changes of the last two millennia on the western and northern Svalbard shelf. Boreas 42, 236-255.

Johns, L., Wraige, E.J., Belt, S.T., Lewis, C.A., Massé, G., Robert, J.M., Rowland, S.J., 1999. Identification of a C_{25} highly branched isoprenoid (HBI) diene in Antarctic sediments, Antarctic sea-ice diatoms and cultured diatoms. Organic Geochemistry 30, 1471-1475.

Kim, J.-H., Schouten, S., Hopmans, E.C., Donner, B., Sinninghe Damsté, J.S., 2008. Global sediment core-top calibration of the TEX_{86} paleothermometer in the ocean. Geochimica et Cosmochimica Acta 72, 1154-1173.

Kim, J.H., van der Meer, J., Schouten, S., Helmke, P., Willmott, V., Sangiorgi, F., 2010. New indices and calibrations derived from the distribution of crenarchaeal isoprenoid tetraether lipids: implications for past sea surface temperature reconstructions. Geochimica et Cosmochimica Acta 74, 4639–4654.

Kinnard, C., Zdanowicz, C.M., Fisher, D.A., Isaksson, E., de Vernal, A., Thompson, L.G., 2011. Reconstructed changes in Arctic sea ice over the past 1,450 years. Nature 479, 509-512.

Knies, J., 2005. Climate-induced changes in sedimentary regimes for organic matter supply on the continental shelf of northern Norway. Geochimica et Cosmochimica Acta 69, 4631-4647.

Knies, J., 2009. MAREANO thematic issue: Sediment charachteristics and environmental implications in the Lofoten-Barents Sea region. Norwegian Journal of Geology Editorial, 1-2.

Knies, J., Martinez, P., 2009. Organic matter sedimentation in the western Barents Sea region: Terrestrial and marine contribution based on isotopic composition and organic nitrogen content. Norwegian Journal of Geology 89, 79-89.

Laskar, J., Robutel, P., Joutel, F., Gastineau, M., Correia, A.C.M., Levrard, B., 2004. A long-term numerical solution for the insolation quantities of the Earth. Astronomy and Astrophysics 428, 261-285.

Lind, S., Ingvaldsen, R.B., 2012. Variability and impacts of Atlantic Water entering the Barents Sea from the north. Deep Sea Research Part I: Oceanographic Research Papers 62, 70-88.

Loeng, H., 1991. Features of the physical oceanographic conditions of the Barents Sea. Polar Research 10.

Loeng, H., Drinkwater, K., 2007. An overview of the ecosystems of the Barents and Norwegian Seas and their response to climate variability. Deep Sea Research Part II: Topical Studies in Oceanography 54, 2478-2500.

Maiti, K., Carroll, J., Benitez-Nelson, C.R., 2010. Sedimentation and particle dynamics in the seasonal ice zone of the Barents Sea. Journal of Marine Systems 79, 185-198.

Massé, G., 2003. Highly branched isoprenoids alkenes from diatoms: a biosynthetic and life cycle investigation: *PhD Thesis.* University of Plymouth.

Massé, G., Belt, S.T., Crosta, X., Schmidt, S., Snape, I., Thomas, D.N., Rowland, S.J., 2011. Highly branched isoprenoids as proxies for variable sea ice conditions in the Southern Ocean. Antarctic Science 23, 487-498.

Massé, G., Rowland, S.J., Sicre, M.-A., Jacob, J., Jansen, E., Belt, S.T., 2008. Abrupt climate changes for Iceland during the last millennium: Evidence from high resolution sea ice reconstructions. Earth and Planetary Science Letters 269, 565-569.

Matthiessen, J., Baumann, K.-H., Schröder-Ritzrau, A., Hass, H.C., Andruleit, H., Baumann, A., Jensen, S., Kohly, A., Pflaumann, U., Samtleben, C., Schäfer, P., Thiede, J., 2001. Distribution of calcareous, siliceous and organic-walled planktic microfossils in surface sediments of the Nordic Seas and their relation to surface-water masses In: Schäfer, P.R., W. Schulter, M. Thiede, J. (eds.), The Northern North Atlantic: A Changing Environment. Springer, Berlin, pp. 105-127.

Mollenhauer, G., McManus, J.F., Benthien, A., Müller, P.J., Eglinton, T.I., 2006. Rapid lateral particle transport in the Argentine Basin: Molecular ^{14}C and $^{230}Th_{xs}$ evidence. Deep Sea Research Part I: Oceanographic Research Papers 53, 1224-1243.

Müller, J., 2011. Last Gacial to Holocene variability in the sea ice distribution in Fram Strait / Arctic Gateway- A novel biomarker approach-, *PhD Thesis*. Bremen University.

Müller, A., Knies, J., 2013. Trace elements and cathodoluminescence of detrital quartz in Arctic marine sediments – a new ice-rafted debris provenance proxy. Climate of the Past 9- 2615-2630.

Müller, J., Massé, G., Stein, R., Belt, S.T., 2009. Variability of sea-ice conditions in the Fram Strait over the past 30,000 years. Nature Geoscience 2, 772-776.

Müller, J., Wagner, A., Fahl, K., Stein, R., Prange, M., Lohmann, G., 2011. Towards quantitative sea ice reconstructions in the northern North Atlantic: A combined biomarker and numerical modelling approach. Earth and Planetary Science Letters 306, 137-148.

Müller, J., Werner, K., Stein, R., Fahl, K., Moros, M., Jansen, E., 2012. Holocene cooling culminates in sea ice oscillations in Fram Strait. Quaternary Science Reviews 47, 1-14.

Nelson, M.M., Mooney, B.D., Nichols, P.D., Phleger, C.F., 2001. Lipids of Antarctic Ocean amphipods: food chain interactions and the occurrence of novel biomarkers. Marine Chemistry 73, 53-64.

Nichols, P.D., Palmisano, A.C., Volkman, J.K., Smith, G.A., White, D.C., 1988. Occurrence of an isoprenoid C_{25} diunsaturataed alkane and high neutral lipid content in Antarctic sea-ice diatom communities. Journal of Phycology 24, 90-96.

Nygård, H., Berge, J., Søreide, J.E., Vihtakari, M., Falk-Petersen, S., 2012. The amphipod scavenging guild in two Arctic fjords: seasonal variations, abundance and trophic interactions. Aquatic Biology 14, 247-264.

Parkinson, C.L., 2008. Satellite Passive-Microwave Measurements of Sea Ice, In: Editors-in-Chief: John, H.S., Karl, K.T., Steve, A.T. (eds.), Encyclopedia of Ocean Sciences (Second Edition). Academic Press, Oxford, pp. 80-90.

Petrich, C., Eicken, H., 2010. Growth, Structure and Properties of Sea Ice, Sea Ice. Wiley-Blackwell, pp. 23-77.

Polyak, L., Alley, R.B., Andrews, J.T., Brigham-Grette, J., Cronin, T.M., Darby, D.A., Dyke, A.S., Fitzpatrick, J.J., Funder, S., Holland, M., Jennings, A.E., Miller, G.H., O'Regan, M., Savelle, J., Serreze, M., St. John, K., White, J.W.C., Wolff, E., 2010. History of sea ice in the Arctic. Quaternary Science Reviews 29, 1757-1778.

Quadfasel, D., Rudels, B., Kurz, K., 1988. Outflow of dense water from a Svalbard fjord into the Fram Strait. Deep Sea Research Part A. Oceanographic Research Papers 35, 1143-1150.

Rayner, N.A., Parker, D.E., Horton, E.B., Folland, C.K., Alexander, L.V., Rowell, D.P., Kent, E.C., Kaplan, A., 2003. Global analyses of sea ice surface temperature, sea ice and night marine air temperature since the laste nineteenth century. Journal of Geophysical Research 108 (D14), 4407.

Rasmussen, T.L., Thomsen, E., Ślubowska, M.A., Jessen, S., Solheim, A., Koç, N., 2007. Paleoceanographic evolution of the SW Svalbard margin (76°N) since 20,000 ^{14}C yr BP. Quaternary Research 67, 100-114.

Reigstad, M., Wexels Riser, C., Wassmann, P., Ratkova, T., 2008. Vertical export of particulate organic carbon: Attenuation, composition and loss rates in the northern Barents Sea. Deep Sea Research Part II: Topical Studies in Oceanography 55, 2308-2319.

Reimer, P.J., Baillie, M.G.L., Bard, E., Bayliss, A., Beck, J.W., Blackwell, P.G., Bronk Ramsey, C., Buck, C.E., Burr, G.S., Edwards, R.L., Friedrich, M., Grootes, P.M., Guilderson, T.P., Hajdas, I., Heaton, T.J., Hogg, A.G., Hughen, K.A., Kaiser, K.F., Kromer, B., McCormac, F.G., Manning, S.W., Reimer, R.W., Richards, D.A., Southon, J.R., Talamo, S., Turney, C.S.M., van der Plitch, J., Weyhenmeyer, C.E., 2009. IntCal09 and Marine09 radiocarbon age calibration curves, 0 - 50,000 years cal BP. Radiocarbon. Radiocarbon 15, 1111-1150.

Rochon, A., de Vernal, A., Turon, J.L., Matthiessen, J., Head, M., 1999. Distribution of dinoflagellate cyst assemblages in surface sediments from the North Atlantic Ocean and adjacent basins and quantitative reconstructions of sea-surface parameters. American Association of Stratigraphic Palynologist Foundation, Contribution Series Number 35.

Rontani, J.F., Charriere, B., Petit, M., Vaultier, F., Heipieper, H.J., Link, H., Chaillou, G., Sempéré, R., 2012. Degradation state of organic matter in surface sediments from the Southern Beaufort Sea: a lipid approach. Biogeosciences 9, 3513-3530.

Rowland, S.J., Robson, J.N., 1990. The widespread ocurrence of highly branched acyclic C_{20}, C_{25} and C_{30} hydrocarbons in recent sediments and biota - A review. Marine Environmental Research 30, 191-216.

Rudels, B., 2009. Arctic Ocean Circulation, In: Editors-in-Chief: John, H.S., Karl, K.T., Steve, A.T. (Eds.), Encyclopedia of Ocean Sciences (Second Edition). Academic Press, Oxford, pp. 211-225.

Rueda, G., Fietz, S., Rosell-Melé, A., 2013. Coupling of air and sea surface temperatures in the eastern Fram Strait during the last 2000 years. The Holocene 23, 692-698.

Sakshaug, E., 1997. Biomass and productivity distributions and their variability in the Barents Sea. ICES Journal of Marine Science: Journal du Conseil 54, 341-350.

Sarnthein, M., kreveld, S.V., Erlenkeuser, H., Grootes, P.M., Kucera, M., Pflaumann, U., Schulz, M., 2003. Centennial-to-millennial-scale periodicities of Holocene climate and sediment injections off the western Barents shelf, 75°N. Boreas 32, 447-461.

Schlitzer, R., 2012. Ocean Data View. http://odv.awi.de.

Schouten, S., Hopmans, E.C., Schefusz, E., Sinninghe Damste, J.S., 2002. Distributional variations in marine crenarchaeotal membrane lipids: a new tool for reconstructing ancient sea water temperatures? Earth and Planetary Science Letters 204, 265-274.

Sicre, M.A., Labeyrie, L., Ezat, U., Duprat, J., Turon, J.L., Schmidt, S., Michel, E., Mazaud, A., 2005. Mid-latitude Southern Indian Ocean response to Northern Hemisphere Heinrich events. Earth and Planetary Science Letters 240, 724-731.

Ślubowska-Woldengen, M., Koç, N., Rasmussen, T.L., Klitgaard-Kristensen, D., Hald, M., Jennings, A.E., 2008. Time-slice reconstructions of ocean circulation changes on the continental shelf in the Nordic and Barents Seas during the last 16,000 cal. yr B.P. Quaternary Science Reviews 27, 1476-1492.

Ślubowska-Woldengen, M., Rasmussen, T.L., Koç, N., Klitgaard-Kristensen, D., Nilsen, F., Solheim, A., 2007. Advection of Atlantic Water to the western and northern Svalbard shelf since 17,500 cal. yr BP. Quaternary Science Reviews 26, 463-478.

Ślubowska, M.A., Koç, N., Rasmussen, T.L., Klitgaard-Kristensen, D., 2005. Changes in the flow of Atlantic water into the Arctic Ocean since the last deglaciation: Evidence from the northern Svalbard continental margin, 80 °N. Paleoceanography 20, PA4014 doi:10.1029/2005PA001141

Solignac, S., de Vernal, A., Giraudeau, J., 2008. Comparison of coccolith and dinocyst assemblages in the northern North Atlantic: How well do they relate with surface hydrography? Marine Micropaleontology 68, 115-135.

Solignac, S., Grøsfjeld, K., Giraudeau, J., Vernal, A.d., 2009. Distribution of recent dinocyst assemblages in the western Barents Sea. Norwegian Journal of Geology 89, 109-119.

Søreide, J.E., Leu, E., Berge, J., Graeve, M., Falk-Petersen, S., 2010. Timing of blooms, algal food quality and Calanus glacialis reproduction and growth in a changing Arctic. Global Change Biology 16, 3154-3163.

Sorteberg, A., Kvingedal, B., 2006. Atmospheric forcing on the Barents Sea winter ice extent. Journal of Climate 19, 4772-4784.

Spielhagen, R.F., Werner, K., Sørensen, S.A., Zamelczyk, K., Kandiano, E., Budeus, G., Husum, K., Marchitto, T.M., Hald, M., 2011. Enhanced modern heat transfer to the Arctic by warm Atlantic water. Science 331, 450-453.

Stein, R., Fahl, K., 2013. Biomarker proxy shows potential for studying the entire Quaternary Arctic sea ice history. Organic Geochemistry 55, 98-102.

Stein, R., Fahl, K., Müller, J., 2012. Proxy reconstruction of Arctic Ocean sea ice history: from IRD to IP_{25}. Polarforschung 82, 37-71.

Steinsund, P.I., Hald, M., 1994. Recent calcium carbonate dissolution in the Barents Sea: Paleoceanographic applications. Marine Geology 117, 303-316.

Stoynova, V., Shanahan, T.M., Hughen, K.A., de Vernal, A., 2013. Insights into Circum-Arctic sea ice variability from molecular geochemistry. Quaternary Science Reviews 79, 63-73.

Stuiver, M., Reimer, P.M., 1993. Extended ^{14}C database and revised CALIB radiocarbon calibration program. Radiocarbon 35, 215-230.

Thomas, D.N., 2012. Sea ice, In: Bell, M.E. (ed.), Life in extremes: environments, organisms and strategies for survival, Oxford, UK.

Thomsen, C., Blaume, F., Fohrmann, H., Peeken, I., Zeller, U., 2001. Particle transport processes at slope environments — event driven flux across the Barents Sea continental margin. Marine Geology 175, 237-250.

Thorsnes, T., 2009. MAREANO - an introduction. Norwegian Journal of Geology 89, 3.

Vare, L.L., Massé, G., Belt, S.T., 2010. A biomarker-based reconstruction of sea ice conditions for the Barents Sea in recent centuries. The Holocene 20, 637.

Vare, L.L., Massé, G., Gregory, T.R., Smart, C.W., Belt, S.T., 2009. Sea ice variations in the central Canadian Arctic Archipelago during the Holocene. Quaternary Science Reviews 28, 1354-1366.

Vinje, T., 2001. Anomalies and trends of sea-ice extent and atmospheric circulation in the Nordic seas during the period 1864-1998. Journal of Climate 14, 255-267.

Vinje, T., Kvambekk, Å.S., 1991. Barents Sea drift ice characteristics. Polar Research 10, 59-68.

Vogt, C., Knies, J., 2009. Sediment pathways in the western Barents Sea inferred from clay mineral assemblages in surface sediments. Norwegian Journal of Geology 89, 41-55.

Volkman, J.K., 1986. A review of sterols markers for marine and terrigenous organic matter Organic Geochemistry 9, 83-99.

Volkman, J.K., Barrett, S.M., Blackburn, S.I., Mansour, M.P., Sikes, E.L., Gelin, F., 1998. Microalgal biomarkers: A review of recent research developments. Organic Geochemistry 29, 1163-1179.

Volkman, J.K., Barrett, S.M., Dunstan, G.A., 1994. C_{25} and C_{30} highly branched isoprenoid alkenes in laboratory cultures of two marine diatoms. Organic Geochemistry 21, 407-414.

Wang, C., Shi, L., Gerland, S., Granskog, M.A., Renner, A.H.H., Li, Z., Hansen, E., Martma, T., 2013. Spring sea-ice evolution in Rijpfjorden (80° N), Svalbard, from in situ measurements and ice mass-balance buoy (IMB) data. Annals of Glaciology 54, 253-260.

Wassmann, P., 2001. Vernal export and retention of biogenic matter in the north-eastern North Atlantic and adjacent Arctic Ocean: The role of the Norwegian Atlantic Current and topography (review). Memoirs of National Institute of Polar Research. Special issue 54, 377-392.

Wassmann, P., Duarte, C.M., Agusti, S., Sejr, M.K., 2011. Footprints of climate change in the Arctic marine ecosystem. Global Change Biology 17, 1235-1249.

Wassmann, P., Ratkova, T., Andreassen, I., Vernet, M., Pedersen, G., Rey, F., 1999. Spring Bloom Development in the Marginal Ice Zone and the Central Barents Sea. Marine Ecology 20, 321-346.

Wassmann, P., Reigstad, M., Haug, T., Rudels, B., Carroll, M.L., Hop, H., Gabrielsen, G.W., Falk-Petersen, S., Denisenko, S.G., Arashkevich, E., Slagstad, D., Pavlova, O., 2006. Food webs and carbon flux in the Barents Sea. Progress In Oceanography 71, 232-287.

Weckström, K., Massé, G., Collins, L.G., Hanhijärvi, S., Bouloubassi, I., Sicre, M.-A., Seidenkrantz, M.-S., Schmidt, S., Andersen, T.J., Andersen, M.L., Hill, B., Kuijpers, A., 2013. Evaluation of the sea ice proxy IP_{25} against observational and diatom proxy data in the SW Labrador Sea. Quaternary Science Reviews 79, 53-72.

Wexels Riser, C., Wassmann, P., Reigstad, M., Seuthe, L., 2008. Vertical flux regulation by zooplankton in the northern Barents Sea during Arctic spring. Deep Sea Research Part II: Topical Studies in Oceanography 55, 2320-2329.

Wobus, F., Shapiro, G.I., Huthnance, J.M., Maqueda, M.A.M., 2013. The piercing of the Atlantic Layer by an Arctic shelf water cascade in an idealised study inspired by the Storfjorden overflow in Svalbard. Ocean Modelling 51, 54-65.

Xiao, X., Fahl, K., Stein, R., 2013. Biomarker distributions in surface sediments from the Kara and Laptev seas (Arctic Ocean): indicators for organic-carbon sources and sea-ice coverage. Quaternary Science Reviews 79, 40-52.

Zaborska, A., Carroll, J., Papucci, C., Torricelli, L., Carroll, M.L., Walkusz-Miotk, J., Pempkowiak, J., 2008. Recent sediment accumulation rates for the Western margin of the Barents Sea. Deep Sea Research Part II: Topical Studies in Oceanography 55, 2352-2360.

Zamelczyk, K., Rasmussen, T.L., Husum, K., Hald, M., 2013. Marine calcium carbonate preservation vs. climate change over the last two millennia in the Fram Strait: Implications for planktic foraminiferal paleostudies. Marine Micropaleontology 98, 14-27.

Appendix

Table A1. Summary of station numbers, water depths, locations, biomarker data and satellite-derived sea ice concentrations (Hadley; HadISST) for the surface sediment material described in the current study. Sterol 1 corresponds to brassicasterol, Sterol 2 to 24-methylenecholesterol, expressed in µg g^{-1} TOC and sterol 3 to dinosterol expressed in relative units. Data are organised in decreasing latitude. TOC and MOC data were taken from Knies et al. (2009) or determined as part of the current study. Where TOC and MOC data were not available, estimates were made on the basis of nearest locations (*). For a few locations, there was insufficient sediment material to complete the biomarker analysis (-). Where data was not available, was indicated with (//).

Sample	Water depth (m)	Lat.	Long.	TOC wt.%	MOC (%)	IP_{25} µg g^{-1} TOC	IP_{25} µg g^{-1} MOC	Sterol 1	Sterol 2	Sterol 3	Satellite sea ice conc.(%)
1287	364	79.19	11.77	0.97	0.68	0.53	0.75	156.92	9.1	1.2	15
PS57/166-2	527	79.13	4.89	1.29	0.65*	0.67	1.32	100.45	//	//	5
1289	319	79.03	10.84	2.23	1.36	0.27	0.44	73.75	2.96	0.62	15
PS57/127-1	307	79.03	10.51	1.87	0.79*	0.76	1.80	234.22	//	//	5
1288	308	78.98	11.82	1.38	0.88	0.22	0.35	118.73	5.35	0.95	15
1290	250	78.95	9.62	0.95	0.58	0.07	0.11	96.80	7.53	0.85	5
1286	159	78.87	11.33	1.13	0.79	0.04	0.06	105.60	9.72	0.6	15
HH11-135GC	2242	78.47	-0.46	0.89	0.65*	0.15	0.21	9.60	0	0	15
HH11-136BC	2240	78.47	-0.46	0.36	0.65*	0.42	0.23	208.77	48.22	0	15
1265	87	78.37	16.37	1.88	0.26	0.25	1.78	61.32	3.69	0.71	nd
1269	169	78.37	12.30	2.00	0.76	0.25	0.67	43.94	3.28	0.41	15
1273	600	78.25	9.32	0.85	0.30	0.06	0.17	51.70	0	0.43	5
HH11-140BC	1258	78.22	1.18	0.70	0.65*	0.15	0.16	55.97	4.4	0.46	5
HH11-137BC	1709	78.14	1.36	0.30	0.65*	0.74	0.34	686.14	81.45	0	5
HH11-138GC	1707	78.14	1.36	1.00	0.65*	0.11	0.17	19.36	1.53	0.42	5
1270	259	78.08	12.30	2.41	1.30	0.45	0.84	51.92	2.79	0.35	15
HH11-133GC	271	78.08	11.47	2.59	1.30*	0.61	1.21	44.28	7.79	0.84	5
WP08 337	1733	78.08	8.30	1.27	0.65*	0.10	0.20	41.78	1.88	0.53	0
1254	76	77.83	16.59	2.03	0.43	0	0	10.65	12.95	0.33	nd
PS57/136-2	589	77.81	15.89	1.68	0.29*	0.28	1.62	93.35	//	//	nd
PS57/130-1	388	77.78	9.68	0.86	0.40*	0.85	1.83	108.52	//	//	5
PS57/137-2	1442	77.77	15.06	2.11	0.38*	0.41	2.26	100.42	//	//	nd
1251	115	77.75	14.92	1.84	0.48	0.03	0.10	57.42	4.35	0.35	nd
1255	83	77.72	15.19	1.74	0.38	0.06	0.29	60.89	4.58	0.31	nd
1261	1291	77.39	10.60	0.89	0.40	0.06	0.13	42.60	1.59	0.47	0
1262	603	77.36	11.27	0.82	0.24	0.17	0.57	42.71	1.37	0.44	5
HH11-134BC	1381	77.36	9.53	1.50	0.40*	0.12	0.46	31.93	4.58	0.78	5
1263	196	77.20	12.93	1.96	0.86	0.60	1.37	57.67	2.38	0.58	5
PS57/131-2	320	77.17	11.10	0.83	0.40*	0.59	1.23	129.33	//	//	5
PS57/138-1	1013	76.68	12.99	0.87	0.78*	0.54	0.60	63.38	//	//	5
679	193	76.62	34.45	1.82	0.78	0.19	0.45	99.88	11.42	0.38	45
643	291	76.49	29.91	2.24	1.26	0.17	0.30	32.03	1.77	0.55	35
681	249	76.43	37.17	1.23	0.78*	0.11	0	20.60	0	0	45
St32	228	76.38	20.58	2.40	1.32	0.41	0.74	198.46	14.75	0.36	65
PS57/145-1	1502	76.33	13.93	1.19	0.78*	0.17	0.26	85.54	//	//	5
St31	258	76.31	19.57	2.66	1.49	0.26	0.46	-	-	-	55
St30	257	76.22	18.58	2.24	1.32	0.29	0.50	-	-	-	45
St29	309	76.16	17.62	2.31	1.25	0.32	0.60	146.69	8.66	1.36	35
677	276	75.97	33.73	1.91	0.77	0.07	0.17	6.87	0	0	25
St27	369	75.95	15.72	2.17	1.24	0.19	0.33	60.85	3.13	1	15
645	296	75.86	29.46	2.20	0.62	0.07	0.26	31.31	1.73	1.82	15
St26	370	75.83	14.77	1.66	0.85	0.24	0.47	78.04	4.77	0.93	5
St25	807	75.75	13.84	0.82	0.36	0.17	0.38	-	-	-	5
St24	1500	75.64	12.92	1.11	0.67	0	0	123.67	2.82	1.35	0
WP08 348	1264	75.60	13.17	0.82*	0.36*	0	0	32.80	1.86	0.56	0
WP08 349	1046	75.59	13.38	0.82*	0.36*	0	0	22.91	1.15	0.33	5
639	263	75.57	27.90	2.74	1.62	0.09	0.15	71.49	7.46	1.34	5
675	209	75.33	33.07	2.11	0.77*	0.06	0	70.34	15.78	0.71	5
647	343	75.20	29.01	2.20*	0.62	0	0	60.54	2.87	0.83	5

Sample	Water depth (m)	Lat.	Long.	TOC wt.%	MOC (%)	IP_{25} µg g^{-1} TOC	IP_{25} µg g^{-1} MOC	Sterol 1	Sterol 2	Sterol 3	Satellite sea ice conc.(%)
635	182	75.00	24.94	2.45	1.32	0.17	0.31	76.65	5.24	0.84	0
1241	297	74.82	17.58	2.14	1.35	0.06	0.10	89.67	4.16	1.21	5
St20	296	74.82	18.02	1.97	1.22	0.11	0.17	175.21	7.4	0	5
St21	280	74.82	17.00	0.90	0.52	0	0	53.26	0	0	0
St22	356	74.82	16.03	0.73	0.33	0	0	33.57	0	1	0
St23	1507	74.82	14.79	0.95	0.62	0	0	-	-	-	5
673	165	74.67	32.49	1.28	0.61	0.22	0.47	40.61	0	0.52	5
651	317	74.64	26.08	2.08	1.19*	0	0	48.33	3.18	0.86	5
649	394	74.54	28.58	2.08*	1.19*	0	0	38.61	61.41	0.57	5
1239	178	74.46	20.83	1.70	0.97	0.03	0.05	33.81	1.88	0.35	0
633	373	74.34	24.69	1.26	0.54	0	0	56.29	2.38	0.57	0
671	366	74.15	29.55	1.37*	0.82*	0	0	29.38	0	0.81	0
653	441	73.97	25.81	1.73	0.97	0	0	21.17	1.04	0.5	0
631	451	73.67	24.47	1.26*	0.54*	0	0	52.19	0	0.51	0
669	414	73.50	29.15	1.37	0.82	0	0	37.38	0	0.39	0
655	412	73.31	25.54	1.53	0.84	0	0	41.53	1.75	0.66	0
St11	1499	73.17	12.94	0.74	0.54	0.07	0.09	146.68	3.22	0.61	0
St12	1030	73.17	14.09	0.42	0.29	0.56	0.81	123.80	0	0.75	0
St13	485	73.17	15.23	0.33	0.19	0	0	19.15	0	0	0
St14	475	73.17	16.38	0.79	0.50	0.22	0.35	58.30	0.85	0.56	0
St15	460	73.17	17.54	0.88	0.54	0.22	0.36	62.96	0	0.56	0
St17	441	73.17	19.86	1.15	0.62	0.16	0.29	111.83	2.12	1.17	0
St18	463	73.17	20.95	1.41	0.83	0.04	0.06	59.70	2.13	0.91	0
St19	444	73.17	22.01	1.40	0.85	0.16	0.27	65.78	1.8	1	0
629	404	73.01	24.25	1.39	0.75	0	0	38.85	0	0.37	0
667	305	72.84	28.76	0.78*	0.48*	0	0	43.44	0	0.47	0
657	268	72.64	25.27	1.53*	0.84*	0	0	12.01	0	0	0
627	264	72.32	24.06	0.62	0.39	0	0	19.49	0	0	0
665	289	72.17	28.41	0.78	0.48	0	0	909.24	0	0.82	0
St03	324	72.03	19.85	1.01	0.74	0.05	0.07	-	-	-	0
St02	371	72.02	20.92	0.92	0.63	0	0	51.65	0	0.66	0
St06	362	72.02	16.62	0.37	0.26	0.58	0.82	82.60	0	0	0
St04	315	72.02	18.77	0.97	0.72	0	0	76.16	0	0.8	0
St07	767	72.02	15.52	0.29	0.12	0	0	8.43	0	0	0
St09	1317	72.01	14.62	0.67	0.52	0.17	0.22	36.46	0	0.51	0
659	256	71.98	25.06	0.71*	0.47*	0	0	15.20	0	0	0
St34	356	71.75	22.00	0.76	0.54	0	0	36.06	0	0	0
625	360	71.72	21.76	0.62*	0.39*	0	0	20.27	0	0	0
St35	319	71.62	21.07	0.60	0.42	0	0	40.82	0	0	0
663	291	71.61	25.99	0.71*	0.47*	0	0	12.19	0	0	0
St37	335	71.60	21.19	0.58	0.42	0	0	36.36	0	0	0
St36	320	71.60	20.86	0.80	0.62	0	0	54.91	0.76	0.12	0
St38	310	71.49	20.82	0.75*	0.61*	0	0	54.29	0.75	0	0
661	408	71.37	22.76	0.71	0.47	0	0	13.68	0	0	0
St39	234	71.34	20.19	0.75	0.61	0	0	101.87	4.17	0	0
St40	225	71.18	19.56	0.83	0.69	0	0	74.36	2.13	0.72	0
St41	199	71.03	18.95	0.37	0.29	0	0	41.81	0	0	0
690	283	71.02	30.96	0.39	0.15	0	0	9.70	1.39	0	0
St43	273	70.72	17.75	0.20*	0.17*	0	0	626.66	63.05	0.99	0
692	252	70.62	31.72	0.39*	0.15*	0	0	7.41	0	0	0
St44	706	70.55	17.14	0.20	0.17	0	0	0	0	0	0
St45	1500	70.44	16.75	0.20*	0.17*	0	0	44.48	1.06	0	0

Table A.2. Summary of station numbers and locations. The P_BIP_{25} index was calculated using the balance factor 'c' derived from the mean IP_{25} and brassicasterol data presented here and 8 additional samples (PS cores) from Müller et al. (2011). For a few locations, there was insufficient sediment material to complete the biomarker analysis (-). Cases where calculation of the P_BIP_{25} index was not possible since both biomarkers were absent (/).Where data was not available, was indicated with (//).

Sample	Lat.	Long.	IP_{25} µg g^{-1} TOC	Sterol 1	Sterol 2	Sterol 3	$P_{24M}IP_{25}$	P_DIP_{25}	P_BIP_{25}	Satellite sea ice conc.(%)
1287	79.19	11.77	0.53	156.92	9.1	1.2	0.72	0.47	0.65	15
PS57/166-2	79.13	4.89	0.67	100.45	//	//	//	//	0.79	5
1289	79.03	10.84	0.27	73.75	2.96	0.62	0.8	0.47	0.67	15
PS57/127-1	79.03	10.51	0.76	234.22	//	//	//	//	0.64	5
1288	78.98	11.82	0.22	118.73	5.35	0.95	0.65	0.32	0.51	15
1290	78.95	9.62	0.07	96.80	7.53	0.85	0.3	0.14	0.29	5
1286	78.87	11.33	0.04	105.60	9.72	0.6	0.17	0.13	0.19	15
HH11-135GC	78.47	-0.46	0.15	9.60	0	0	1	1	0.9	15
HH11-136BC	78.47	-0.46	0.42	208.77	48.22	0	0.28	1	0.53	15
1265	78.37	16.37	0.25	61.32	3.69	0.71	0.75	0.42	0.69	nd
1269	78.37	12.30	0.25	43.94	3.28	0.41	0.78	0.56	0.76	15
1273	78.25	9.32	0.06	51.70	0	0.43	1	0.22	0.39	5
HH11-140BC	78.22	1.18	0.15	55.97	4.4	0.46	0.6	0.39	0.59	5
HH11-137BC	78.14	1.36	0.74	686.14	81.45	0	0.29	1	0.37	5
HH11-138GC	78.14	1.36	0.11	19.36	1.53	0.42	0.76	0.35	0.76	5
1270	78.08	12.30	0.45	51.92	2.79	0.35	0.88	0.73	0.83	15
HH11-133GC	78.08	11.47	0.61	44.28	7.79	0.84	0.78	0.6	0.88	5
WP08 337	78.08	8.30	0.10	41.78	1.88	0.53	0.72	0.29	0.58	0
1254	77.83	16.59	0	10.65	12.95	0.33	0	0	0	nd
PS57/136-2	77.81	15.89	0.28	93.35	//	//	//	//	0.62	nd
PS57/130-1	77.78	9.68	0.85	108.52	//	//	//	//	0.81	5
PS57/137-2	77.77	15.06	0.41	100.42	//	//	//	//	0.69	nd
1251	77.75	14.92	0.03	57.42	4.35	0.35	0.22	0.14	0.21	nd
1255	77.72	15.19	0.06	60.89	4.58	0.31	0.39	0.3	0.37	nd
1261	77.39	10.60	0.06	42.60	1.59	0.47	0.62	0.2	0.42	0
1262	77.36	11.27	0.17	42.71	1.37	0.44	0.85	0.44	0.69	5
HH11-134BC	77.36	9.53	0.12	31.93	4.58	0.78	0.55	0.24	0.68	5
1263	77.20	12.93	0.60	57.67	2.38	0.58	0.92	0.68	0.85	5
PS57/131-2	77.17	11.10	0.59	129.33	//	//	//	//	0.72	5
PS57/138-1	76.68	12.99	0.54	63.38	//	//	//	//	0.83	5
679	76.62	34.45	0.19	99.88	11.42	0.38	0.43	0.51	0.52	45
643	76.49	29.91	0.17	32.03	1.77	0.55	0.81	0.39	0.75	35
681	76.43	37.17	0.11	20.60	0	0	1	1	0.75	45
St32	76.38	20.58	0.41	198.46	14.75	0.36	0.56	0.7	0.53	65
PS57/145-1	76.33	13.93	0.17	85.54	//	//	//	//	0.52	5
St31	76.31	19.57	0.26	-	-	-	-	-	-	55
St30	76.22	18.58	0.29	-	-	-	-	-	-	45
St29	76.16	17.62	0.32	146.69	8.66	1.36	0.63	0.33	0.55	35
677	75.97	33.73	0.07	6.87	0	0	1	1	0.85	25
St27	75.95	15.72	0.19	60.85	3.13	1	0.73	0.28	0.63	15
645	75.86	29.46	0.07	31.31	1.73	1.82	0.65	0.07	0.56	15
St26	75.83	14.77	0.24	78.04	4.77	0.93	0.7	0.35	0.63	5
St25	75.75	13.84	0.17	-	-	-	-	-	-	5
St24	75.64	12.92	0	123.67	2.82	1.35	0	0	0	0
WP08 348	75.60	13.17	0	32.80	1.86	0.56	0	0	0	0
WP08 349	75.59	13.38	0	22.91	1.15	0.33	0	0	0	5
639	75.57	27.90	0.09	71.49	7.46	1.34	0.35	0.12	0.41	5
675	75.33	33.07	0.06	70.34	15.78	0.71	0.15	0.15	0.33	5
647	75.20	29.01	0	60.54	2.87	0.83	0	0	0	5
635	75.00	24.94	0.17	76.65	5.24	0.84	0.59	0.29	0.55	0
1241	74.82	17.58	0.06	89.67	4.16	1.21	0.41	0.12	0.28	5
St20	74.82	18.02	0.11	175.21	7.4	0	0.4	0.15	0.25	5
St21	74.82	17.00	0	53.26	0	0	/	/	0	0
St22	74.82	16.03	0	33.57	0	1	/	/	0	0
St23	74.82	14.79	0	-	-	-	-	-	-	5

Sample	Lat.	Long.	IP_{25} µg g^{-1} TOC	Sterol 1	Sterol 2	Sterol 3	$P_{24M}IP_{25}$	P_DIP_{25}	P_BIP_{25}	Satellite sea ice conc.(%)
673	74.67	32.49	0.22	40.61	0	0.52	1	0.47	0.75	5
651	74.64	26.08	0	48.33	3.18	0.86	0	0	0	5
649	74.54	28.58	0	38.61	61.41	0.57	0	0	0	5
1239	74.46	20.83	0.03	33.81	1.88	0.35	0.42	0.15	0.33	0
633	74.34	24.69	0	56.29	2.38	0.57	0	0	0	0
671	74.15	29.55	0	29.38	0	0.81	/	0	0	0
653	73.97	25.81	0	21.17	1.04	0.5	0	0	0	0
631	73.67	24.47	0	52.19	0	0.51	/	0	0	0
669	73.50	29.15	0	37.38	0	0.39	/	0	0	0
655	73.31	25.54	0	41.53	1.75	0.66	0	0	0	0
St11	73.17	12.94	0.07	146.68	3.22	0.61	0.49	0.18	0.2	0
St12	73.17	14.09	0.56	123.80	0	0.75	1	0.6	0.72	0
St13	73.17	15.23	0	19.15	0	0	/	/	0	0
St14	73.17	16.38	0.22	58.30	0.85	0.56	0.92	0.45	0.68	0
St15	73.17	17.54	0.22	62.96	0	0.56	1	0.44	0.66	0
St17	73.17	19.86	0.16	111.83	2.12	1.17	0.77	0.22	0.44	0
St18	73.17	20.95	0.04	59.70	2.13	0.91	0.43	0.07	0.25	0
St19	73.17	22.01	0.16	65.78	1.8	1	0.81	0.25	0.58	0
629	73.01	24.25	0	38.85	0	0.37	/	0	0	0
667	72.84	28.76	0	43.44	0	0.47	/	0	0	0
657	72.64	25.27	0	12.01	0	0	/	/	0	0
627	72.32	24.06	0	19.49	0	0	/	/	0	0
665	72.17	28.41	0	909.24	0	0.82	/	0	0	0
St03	72.03	19.85	0.05	-	-	-	-	-	-	0
St02	72.02	20.92	0	51.65	0	0.66	/	0	0	0
St06	72.02	16.62	0.58	82.60	0	0	1	0.6	0.8	0
St04	72.02	18.77	0	76.16	0	0.8	/	/	0	0
St07	72.02	15.52	0	8.43	0	0	/	/	0	0
St09	72.01	14.62	0.17	36.46	0	0.51	1	0.41	0.73	0
659	71.98	25.06	0	15.20	0	0	/	/	0	0
St34	71.75	22.00	0	36.06	0	0	/	/	0	0
625	71.72	21.76	0	20.27	0	0	/	/	0	0
St35	71.62	21.07	0	40.82	0	0	/	/	0	0
663	71.61	25.99	0	12.19	0	0	/	/	0	0
St37	71.60	21.19	0	36.36	0	0	/	0	0	0
St36	71.60	20.86	0	54.91	0.76	0.12	0		0	0
St38	71.49	20.82	0	54.29	0.75	0	0	/	0	0
661	71.37	22.76	0	13.68	0	0	/	/	0	0
St39	71.34	20.19	0	101.87	4.17	0	0	/	0	0
St40	71.18	19.56	0	74.36	2.13	0.72	0	0	0	0
St41	71.03	18.95	0	41.81	0	0	/	/	0	0
690	71.02	30.96	0	9.70	1.39	0	0	/	0	0
St43	70.72	17.75	0	626.66	63.05	0.99	0	0	0	0
692	70.62	31.72	0	7.41	0	0	/	/	0	0
St44	70.55	17.14	0	0	0	0	/	/	/	0
St45	70.44	16.75	0	44.48	1.06	0	0	/	0	0

Table A.3. Summary of station numbers and locations, biomarker data and satellite derived sea ice concentrations (Hadley; HadISST) for surface sediment material from the Barents Sea. HBI1 corresponds to Diene II, HBI2 to triene IIIa and HBI3 to triene IIIb. Data are organized in decreased latitude, all expressed in µg g^{-1}TOC. Respective PIP_{25} indices and ratios were also calculated.

Sample	Lat.	IP_{25} µg g^{-1}TOC	HBI1	HBI2	HBI3	$P_{trIIIa}IP_{25}$ C= 0.279	$P_{trIIIb}IP_{25}$ C=0.388	DIP_{25}	$TrIP_{25}$ Z	$TrIP_{25}E$	Sea ice concentration (%)
1290	78.95	0.15	1.24	0.24	0.26	0.70	0.59	4.26	5.88	6.61	5
1286	78.87	0.16	1.73	0.09	0.28	0.87	0.59	5.05	2.07	6.42	15
HH11-135GC	78.47	0.13	0.55	0.03	0.02	0.95	0.93	1.91	0.74	0.69	15
HH11-136BC	78.47	0.37	1.38	0.11	0.11	0.92	0.89	1.69	1.17	1.15	15
HH11-140BC	78.22	0.18	0.61	0.09	0.09	0.88	0.83	1.75	1.94	1.98	5
HH11-137BC	78.14	0.49	2.10	0.14	0.11	0.93	0.92	2.16	1.08	0.87	5
HH11-138GC	78.14	0.12	2.96	0.01	0.01	0.44	0.98	0.71	0.17	0.18	5
HH11-133GC	78.08	0.38	3.59	0.31	0.43	0.81	0.69	4.28	3.14	4.28	5
WP08 337	78.08	0.11	0.41	0.08	0.11	0.83	0.72	1.94	2.84	3.77	0
1255	77.72	0.09	0.60	0.02	0.04	0.96	0.85	2.90	0.60	1.65	nd
1262	77.36	0.13	1.11	0.10	0.12	0.82	0.73	3.97	3.02	3.48	0
HH11-134BC	77.36	0.09	0.50	0.10	0.12	0.77	0.65	2.49	4.16	5.11	5
679	76.62	0.43	1.45	0.53	0.31	0.75	0.78	1.58	4.47	2.73	45
643	76.49	0.17	0.96	0.29	0.24	0.68	0.65	2.56	6.06	4.90	35
681	76.43	0.16	0.59	0.95	0.63	0.38	0.39	1.72	22.63	14.76	45
677	75.97	0.03	0.32	0.46	0.21	0.17	0.24	1.88	23.60	10.52	25
St27	75.95	0.20	1.36	0.31	0.27	0.70	0.65	3.19	5.8	5.1	15
645	75.86	0.10	0.60	0.80	0.36	0.31	0.42	2.95	29.79	13.46	15
St26	75.83	0.39	2.12	0.59	0.47	0.70	0.68	2.58	5.68	4.46	5
St24	75.64	0	0.06	0.36	0.53	0.00	0.00				0
639	75.57	0.13	0.48	0.99	0.67	0.33	0.34	1.71	26.98	18.53	5
675	75.33	0.09	0.00	0.74	0.57	0.32	0.29	0.00	16.43	23.27	5
647	75.2	0.05	0.24	1.03	0.42	0.15	0.23	1.91	65.37	26.90	5
635	75.00	0.18	0.77	1.17	0.81	0.36	0.36	1.89	22.90	15.87	0
St20	74.82	0.16	0.81	0.61	0.70	0.49	0.37	2.40	14.23	16.10	5
673	74.67	0.10	0.35	1.49	0.59	0.19	0.30	1.73	58.05	22.67	5
651	74.64	0	0	0.16	0.08	0.00	0.00				5
649	74.54	0	0	0.17	0.08	0.00	0.00				5
633	74.34	0	0	0.15	0.09	0.00	0.00				0
671	74.15	0	0	0.06	0.02	0.00	0.00				0
653	73.97	0	0	0.14	0.07	0.00	0.00				0
631	73.67	0	0	0.16	0.07	0.00	0.00				0
669	73.5	0.02	0	0.14	0.05	0.35	0.50		24.9	9.2	0
655	73.31	0	0	0	0						0
St12	73.17	0	0	0.53	0.66	0.00	0.00				0
St14	73.17	0.04	0.04	0.63	0.75	0.18	0.11	1.00	16.69	16.69	0
St15	73.17	0.06	0.03	0.02	0.02	0.91	0.87	1.00	0.58	0.58	0
St17	73.17	0.04	0.00	0.37	0.27	0.29	0.28	0	33.34	24.21	0
St18	73.17	0.04	0.02	0.11	0.11	0.54	0.44	1.00	21.11	5.16	0
629	73.01	0	0	0.04	0.03	0.00	0.00				0
667	72.84	0	0	0.04	0.03	0.00	0.00				0
657	72.64	0	0	0	0						0
627	72.32	0	0	0	0						0
665	72.17	0	0	0.06	0.02	0.00	0.00				0
St02	72.02	0	0	0.13	0.13	0.00	0.00				0
St09	72.01	0	0	0.19	0.23	0.00	0.00				0
659	71.98	0	0	0	0						0
625	71.72	0	0	0.64	0.08	0.00	0.00				0
St35	71.62	0	0	0.09	0.10	0.00	0.00				0
663	71.61	0	0	0	0						0
St37	71.6	0	0	0.12	0.13	0.00	0.00				0
St36	71.6	0	0	0.13	0.16	0.00	0.00				0
St38	71.49	0	0	0.12	0.13	0.00	0.00				0
St39	71.34	0	0	0.04	0.04						0
690	71.02	0	0.22	0.06	0.04	0.00	0.00				0
St43	70.72	0	0	0.99	0.13	0.00	0.00				0
692	70.62	0	0	0.03	0.05	0.00	0.00				0
St45	70.44	0	0	0.46	0.59	0.00	0.00				0

Publications

Quaternary Science Reviews 79 (2013) 26–39

Contents lists available at SciVerse ScienceDirect

Quaternary Science Reviews

journal homepage: www.elsevier.com/locate/quascirev

Mapping recent sea ice conditions in the Barents Sea using the proxy biomarker IP_{25}: implications for palaeo sea ice reconstructions

Alba Navarro-Rodriguez [a], Simon T. Belt [a,*], Jochen Knies [b], Thomas A. Brown [a]

[a] Biogeochemistry Research Centre, School of Geography, Earth and Environmental Sciences, University of Plymouth, Drake Circus, Plymouth, Devon PL4 8AA, UK
[b] Geological Survey of Norway, 7491 Trondheim, Norway

ARTICLE INFO

Article history:
Received 23 June 2012
Received in revised form
23 November 2012
Accepted 30 November 2012
Available online 1 January 2013

Keywords:
IP_{25}
Barents Sea
Sea ice
Proxy
Advection
Sediment

ABSTRACT

An analysis of the sea ice proxy IP_{25} and the open water phytoplankton indicator brassicasterol has been carried out for 93 surface sediments collected from the Barents Sea and some additional data from previous studies have been included to augment the analysis further. Consistent with a specific and selective sea ice diatom origin for IP_{25}, this biomarker was identified in virtually all sediments from seasonally ice-covered locations, but was absent from the majority of sites beyond the maximum sea ice extent (MSIE) for the period 1983–2002. In contrast, brassicasterol was detected in virtually all sediments from the region and concentrations were not at all associated with the MSIE. Instead, more localised regions of brassicasterol concentrations were identified and these likely reflect different influences on production and deposition. When the IP_{25} and brassicasterol concentrations were combined together in the form of the previously proposed P_BIP_{25} index, the aforementioned association between IP_{25} occurrence and the MSIE was clarified further and, in addition, provided more detailed descriptions of sea ice cover. In particular, P_BIP_{25} data indicated seasonal sea ice or marginal ice zone conditions for the region of the Barents Sea within the MSIE according to previously defined P_BIP_{25} ranges. We also amalgamated the biomarker data from the current study with those derived previously by Müller et al. (2011) and compared these larger datasets with satellite-derived mean spring sea ice concentrations. Significantly, although the correlation between the combined IP_{25} concentration dataset with the satellite data was very similar to that reported previously by Müller et al. (2011), the corresponding correlation using the P_BIP_{25} values was poorer with the larger dataset and some possible reasons for this are discussed. Finally, in a small number of cases, IP_{25} was identified in sediments somewhat distal from the MSIE, and it is hypothesised that the occurrence of IP_{25} in these sediments results from allochthonous input following sediment advection between shelf and trough environments. This is the first reported example that provides evidence for the allochthonous input of IP_{25} into marine sediments and it is recommended that this should be considered carefully when carrying out palaeo sea ice reconstructions based on the occurrence of this biomarker in the future.

1. Introduction

Arctic sea ice plays an important role in climate regulation on Earth since it influences global heat and moisture exchange between the oceans and the atmosphere, provides a mechanism for the transportation of cold water masses into the Atlantic and also influences water column stratification and the thermohaline circulation in the Atlantic (Thomas, 2012). As seasonal Arctic sea ice fluctuates southwards each year during autumn and winter, the boundary between areas covered by sea ice and those with open water is ecologically important (Falk-Petersen et al., 2000). This boundary provides a unique and dynamic habitat, which influences not only the ice edge flora and fauna, but also the underlying water column and sediments (e.g. Wassmann et al., 2011). This biologically productive region is often referred to as the marginal ice zone (MIZ).

In recent decades, the characteristics and variability of sea ice cover have been determined in detail via satellite passive microwave measurements since the launch of Nimbus-5 in 1972 (e.g. Comiso et al., 1997; Parkinson, 2008). In contrast, longer-term sea ice reconstructions prior to historical observations (ca 1750 AD; Divine and Dick, 2006) have been based mainly on micropalaeontological studies, including assemblages of dinoflagellate cysts (de Vernal et al., 2005; Bonnet et al., 2010) and the species

* Corresponding author. Tel.: +44 (0)1752 584799; fax: +44 (0)1752 584709.
E-mail address: sbelt@plymouth.ac.uk (S.T. Belt).

0277-3791/$ – see front matter © 2012 Elsevier Ltd. All rights reserved.
http://dx.doi.org/10.1016/j.quascirev.2012.11.025

composition of foraminifera (e.g. Aagaard-Sørensen et al., 2010; Werner et al., 2011), mineralogical and sedimentological data (e.g. Stein et al., 1994; Vogt et al., 2001; Spielhagen et al., 2004; Andrews, 2009) and various other geochemical proxies (e.g. Knies, 2005).

A novel organic geochemical biomarker (IP_{25}) has also been proposed as a proxy for sea ice in recent years and its presence in marine sediments has provided the basis for several palaeo sea ice reconstructions across the Arctic (e.g. Massé et al., 2008; Andrews et al., 2009; Müller et al., 2009, 2012; Belt et al., 2010; Vare et al., 2010; see Belt and Müller, 2013 for a comprehensive review). A key attribute of the IP_{25} biomarker is that it is most likely biosynthesized selectively by a limited number of sea ice diatoms during the spring bloom (Brown et al., 2011) and is thus considered to be highly specific as a sea ice proxy (Belt et al., 2007). IP_{25} has also been shown to be present in marine sediments up to at least 30 ka BP (Müller et al., 2009) making it particularly suitable for palaeo sea ice reconstructions. However, the continued utility of IP_{25} to palaeo-environmental marine studies relies, to some extent, on a wider spatial examination of its presence in Arctic sediments, together with a demonstration that sedimentary signatures of IP_{25} correlate well with known sea ice conditions (e.g. from satellite records) and respond rapidly, and with sufficient sensitivity, to changes in contemporary sea ice conditions. In addition, it will be important to establish through these studies, whether the occurrence of IP_{25} not only provides a valuable qualitative indicator of past sea ice, but also if abundance data can be used to provide more quantitative reconstructions (e.g. Müller et al., 2011).

In contrast to IP_{25}, brassicasterol is a steroidal lipid considered to be a more general biomarker indicator of phytoplankton since it is derived from numerous algal groups (e.g. Volkman, 1986; Volkman et al., 1998), dinoflagellates and coccolithophores. Despite this lower specificity in terms of origin, the use of brassicasterol (and other phytoplankton sterols) alongside IP_{25} provides a potential means of improving the interpretation of IP_{25} in marine sediments through the calculation of the so-called PIP_{25} index (Müller et al., 2011). In particular, since the absence of IP_{25} in Arctic sediments has previously been interpreted in terms of representing either ice-free or permanent sea ice conditions (Belt et al., 2007; Müller et al., 2009), the relative abundance of brassicasterol provides a potential means of distinguishing between these two extreme case scenarios. For more intermediate cases, the relative concentrations of IP_{25} and phytoplanktic biomarkers such as brassicasterol have also been used to provide more detailed descriptions of sea ice conditions (e.g. Müller et al., 2011). To date, however, the development of the PIP_{25} index has been carried out following the analyses of a relatively small number of surface sediments from the northern North Atlantic and the further testing of this proxy would clearly benefit from the analysis of a greater number of sediments covering different regions of the Arctic.

One important region for carrying out sea ice reconstruction studies is the Barents Sea since it is particularly sensitive to reductions in sea ice cover during polar amplification of global warming (IPCC, 2007). Further, the Barents Sea has attracted a considerable number of previous investigations studying the relationships between Arctic food webs and sea ice cover (e.g. Falk-Petersen et al., 2000; Reigstad et al., 2008; Wexel Riser et al., 2008), not least since this is one of the most productive regions of the Arctic (Wassmann et al., 2006). Previously, the Marine AREal Database for NOrwegian Waters (MAREANO) programme (2005–2010) was undertaken to provide a comprehensive map of the physical, chemical and biological characteristics of the sea bed for the Western Barents Sea (Knies, 2009; Thorsnes, 2009) and a range of biological proxy data (e.g. dinocyst assemblages; Grøsfjeld et al., 2009; Solignac et al., 2009), organic matter composition (Knies and Martinez, 2009), hydrocarbon distributions (Boitsov et al., 2009) and mineralogical data (Vogt and Knies, 2009) were compiled. The availability of a comprehensive suite of samples with an array of complementary background data, therefore, presented an excellent opportunity to contribute to this programme further and, in particular, compile specific biomarker data that could be used to perform sea ice reconstructions and compare these outcomes with known sea ice characteristics (recent decades), with the overall aim of improving our understanding of the calibration aspects of current biomarker-based sea ice proxies. In modern times, approximately 60% of the Barents Sea is covered with sea ice during peak coverage in March–April (Loeng and Drinkwater, 2007) and this figure provides a useful foundation upon which to examine the ability for specific biomarkers (and combinations of these) to accurately represent known sea ice conditions so that quantitative palaeo sea ice reconstructions might be made with greater confidence.

As such, the objectives of the current study were to: (1) establish the spatial distribution of the sea ice diatom biomarker IP_{25} in a large number (ca 100) of contemporary surface sediments from the Barents Sea; (2) compare these IP_{25} biomarker data with the known position of the maximum sea ice extent in recent decades derived from satellite data; (3) determine the corresponding brassicasterol concentrations in surface sediments and use these alongside the IP_{25} contents to estimate sea ice concentrations using the recently established P_BIP_{25} index and to further validate the use of this combinatory approach to provide more detailed and quantitative sea ice conditions.

2. Regional setting

The Barents Sea is one of the most productive of the Arctic Seas (Wassmann et al., 2006) and is located between the north Norwegian coast and the Svalbard archipelago. The Barents Sea is a relatively shallow continental shelf with an average depth of 230 m although the bathymetry is rather variable. Shallow banks of less than 50 m are found in Spitsbergenbanken (Spitsbergen Bank) and in the south-eastern region, while deeper troughs such as the Bear Island Trough are also found with depths up to 500 m (Loeng, 1991).

A detailed description of the oceanic circulation of the region can be found in Loeng (1991). The North Atlantic Drift carries warm and saline Atlantic water (AW) northwards. One of its main branches is the West Spitsbergen Current (WSC) (Fig. 1a), which is defined by temperatures >2 °C and salinities >34.9 psu. Separated by the polar front, colder ($T < 0$ °C; $S < 34.4$) and ice-covered Arctic waters (ArW) cross the northern Barents Sea and join the East Spitsbergen Current (ESC) (Fig. 1a). The ESC flows southward along the SE coast of Spitsbergen and transports cold water from the Arctic Ocean, which mixes with ambient water, including fresh water outflow from fjords, before continuing northward along the continental shelf off Spitsbergen. The density barrier separates the warm, saline AW from the relatively cold, fresh ArW on the shelf. The frontal region prevents intrusions of warm AW into the shelf and fjord region during winter. During winter (January–March), the ice edge in the Barents Sea achieves its maximum southward extent and corresponds to the MIZ, where the ice edge is located most frequently during spring. Because the MIZ is topographically trapped, its location during maximum extent is fairly constant, being located near the 250 m isobaths north of the Bjørnøya and Hopen troughs (Loeng, 1991) (Fig. 1a). During the winter months of the sampling year 2004, the south and west coasts of Spitsbergen were regularly covered by drift ice. Sea ice coverage is susceptible to global climate changes on Earth, however, and this is reflected by high inter-annual variability of sea ice extent of hundreds of

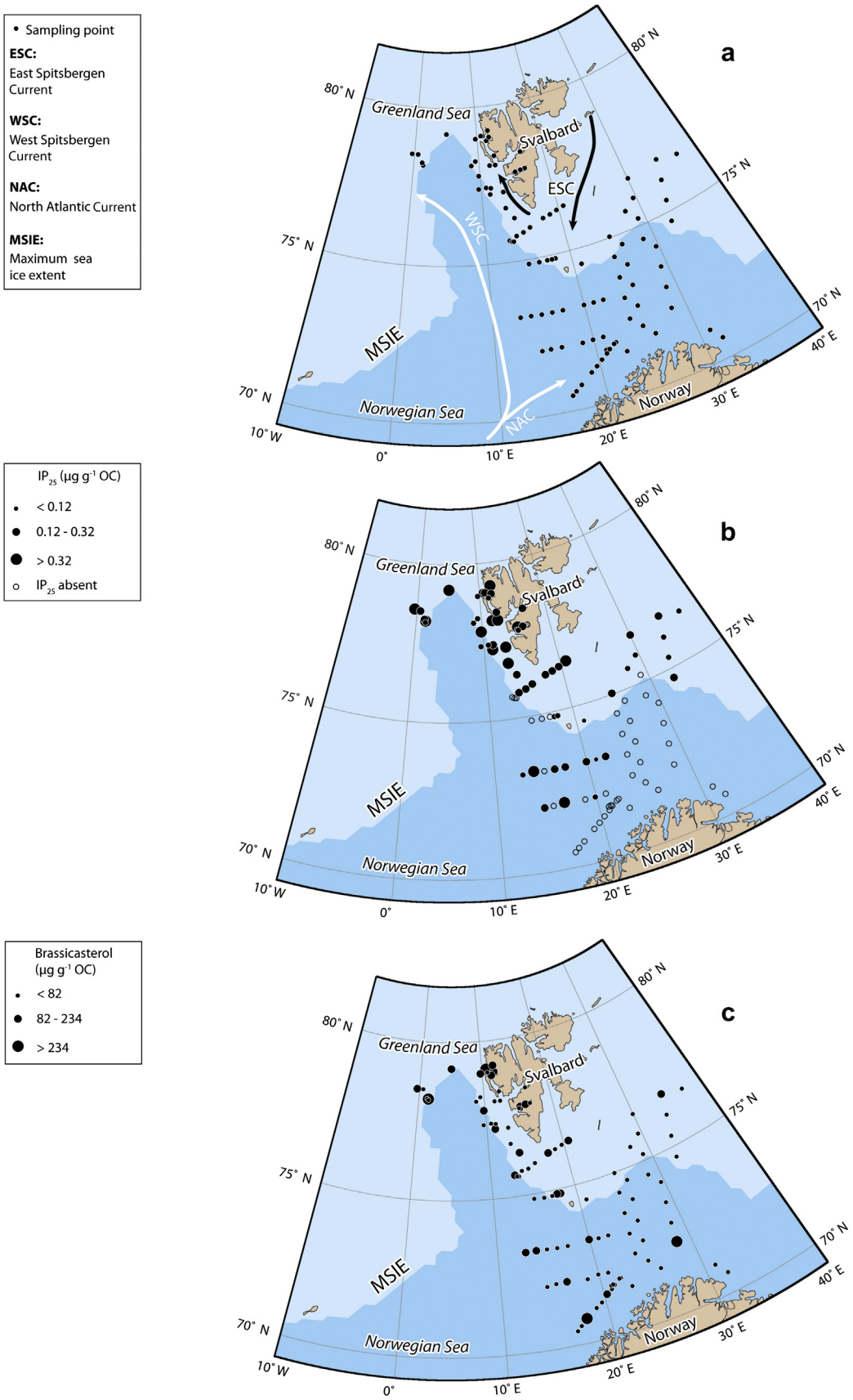

Fig. 1. Maps of the region of the Barents Sea described in the current study: (a) key oceanographic currents and sampling locations; (b) occurrences and concentration ranges of IP_{25}; (c) occurrences and concentration ranges of brassicasterol. The maximum sea ice extent (MSIE) for the period 1983–2002 is also indicated.

kilometres (Vinje, 2001; Divine and Dick, 2006). The reduction in sea ice within the Barents Sea in recent decades has been attributed to increased heat transport as a result of the strengthening and warming of Atlantic waters and this, in turn, controls the position of the ice edge in the western region (Årthun et al., 2012).

3. Material and methods

3.1. Sediment material

In total, 93 surface sediment samples were collected and analysed from a broad range of locations within the Barents Sea (Fig. 1a) using box cores and multicores in all cases. The majority (86) of the surface sediment samples (0–1 cm) were collected from 2001 to 2004 (Boitsov et al., 2009; Knies and Martinez, 2009) and later included as part of the MAREANO program (2005–2010) (Thorsnes, 2009) which provided fundamental physical, chemical and biological characteristics of the sea bed of the Western Barents Sea (Knies, 2009). Additional multicores and gravity cores (×7) were obtained in 2011 aboard the RV *Helmer Hanssen* as part of the Changing Arctic and Sub-Arctic Environment International Training Network research project, from which further surface material was obtained and these were stored frozen (−20 °C) prior to being freeze-dried for extraction and analysis. Finally, some data reported previously by Müller et al. (2011) obtained from sediment samples from the northern North Atlantic were also considered, especially when making comparisons between PIP_{25} data and mean sea ice concentrations.

3.2. Biomarker analysis

Analysis of the sea ice biomarker IP_{25} was carried out following the method described previously by Belt et al. (2012) and the procedure was slightly adapted to also permit the analysis of brassicasterol. Briefly, aliquots of freeze-dried surface sediment material (ca 1 g) were extracted with dichloromethane/methanol (2:1 v/v; ultrasonication; 15 min; 30 °C). 7-hexylnonadecane (7-HND), 9-octylheptadec-8-ene (9-OHD) and 5α–androstan-3β-ol (all 10 μL; 0.01 mg mL^{-1}) were added prior to extraction to facilitate quantification of IP_{25} and brassicasterol, respectively. Following extraction, samples were centrifuged (2500 rpm; 1 min), filtered (SiO_2/hexane) and the solvent evaporated under a slow stream of N_2 (25 °C). Dried total organic extracts (TOE) were re-suspended in hexane (ca 0.5 mL), ultrasonicated (5 min) and the resulting TOEs separated by column chromatography into two fractions containing IP_{25} (hexane; 6 mL) and brassicasterol (hexane/methylacetate; 6 mL; 80:20 v/v) (Müller et al., 2011). In a few cases, the IP_{25} and brassicasterol analyses were carried out on separate sub-samples from the same surface sediment material but the same extraction and fractionation procedures to those described above were employed. Fractions containing brassicasterol were dried under nitrogen and silylated with BSTFA (50 μL; 70 °C; 1 h) prior to analysis by gas chromatography–mass spectrometry (GC–MS). All partially purified extracts were analysed by GC–MS using an Agilent 7890A GC coupled to a 5975 series mass selective detector (MSD) fitted with an Agilent HP-5ms column (30 m × 0.25 mm × 0.25 μm). The GC oven temperature program (40–300 °C; 10 °C min^{-1}) was followed by an isothermal interval (300 °C; 10 min). Helium was the carrier gas with a constant flow rate (1 mL min^{-1}).

Identification of biomarkers was achieved by comparison of GC–MS retention indices and mass spectra of individual analytes with those of reference compounds. Quantification of IP_{25} was carried out in selected ion monitoring (SIM) mode using the intensities of the (*m/z* 350.3) ion for this biomarker and the corresponding responses from the internal standard (9-OHD) and adjusting for the instrumental response factor (Belt et al., 2012). Brassicasterol was quantified as its trimethylsilyl ether using the intensity of its molecular ion (*m/z* 470) compared to that of a diagnostic ion from the internal standard (5α–androstan-3β-ol; *m/z* 333.3). Given the limit of detection of IP_{25} by GC–MS determined previously (Belt et al., 2012), the corresponding value for sediments is 5×10^{-4} μg g^{-1}. In all cases, biomarker concentrations were normalised to the mass of sediment extracted and to the corresponding total organic carbon (TOC) content. Normalisation of biomarker concentrations using TOC data was carried out to compensate for different sediment accumulation rates and burial processes (e.g. Simon et al., 1994; Wassmann et al., 2006; Carroll et al., 2008; Maiti et al., 2010; Zonneveld et al., 2010). TOC data were determined previously for the MAREANO samples (Knies and Martinez, 2009) or following the procedure described by Vare et al. (2009) for surface samples obtained in 2011. In addition, since the relative contributions to the TOC from OM of marine versus terrigenous origin had previously been shown to be quite variable (Knies and Martinez, 2009), biomarker concentrations were also normalised to marine organic carbon (MOC) which was estimated using the method described by Knies and Martinez (2009) and is based on simple mixing of end member values for parameters such as $\delta^{13}C_{org}$, organic nitrogen (N_{org}) and terrigenous organic matter (TOM). In cases where MOC data were not available, values from nearest available locations were used. Calculation of P_BIP_{25} values was performed according to the method of Müller et al. (2011) using Equation (1), where IP_{25} and B represent the concentrations of IP_{25} and brassicasterol, respectively. The c term is included to compensate for the significantly higher concentrations of brassicasterol compared to IP_{25} and corresponds to the ratio of the mean concentrations of the two biomarkers across all sediments under study. For the Barents Sea sediments analysed here (Table 1) and the larger dataset that includes all of the samples analysed by Müller et al. (2011), the c terms were 0.0018 and 0.0068, respectively.

$$PIP_{25} = IP_{25}/(IP_{25} + (B \times c)) \quad (1)$$

3.3. Representations of biomarker data – point sources and spatial distributions

IP_{25} and brassicasterol concentrations were presented and interpreted as point location and regionalised representations using ArcGIS (ArcGIS 10 service pack 3; Fig. 1) and Ocean Data View (ODV; Version 4.5; Schlitzer, 2012) (Figs. 2 and 3) software, respectively. The latter approach, which uses the same primary data as used for the ArcGIS representations, extrapolates individual biomarker concentrations to provide potentially useful estimates of data for areas where samples were not measured and results in a continuous estimation of concentrations and gradients for the region under study. It is useful, therefore, as a conceptual model that predicts spatial variations in concentrations and this can be useful when the study region has independently defined regions, as is the case here with a sea ice margin, but has the potential limitation of oversimplifying trends or concealing more localised phenomena.

3.4. Sea ice data

Satellite records for Arctic sea ice extent derived from Nimbus-7 SSMR and DMSP SSM/I passive microwave data (Fetterer et al., 2002) were taken from the National Snow and Ice Data Center (NSIDC). In order to decide on an appropriate time interval from

Table 1
Summary of station numbers, water depths, locations, biomarker data and satellite-derived sea ice concentrations (Hadley; HadISST) for the surface sediment material described in the current study. Data are organised in decreasing latitude. TOC and MOC data were taken from Knies (2009) or determined as part of the current study. The P_BIP_{25} index was calculated using the balance factor 'c' derived from the mean IP_{25} and brassicasterol data presented here and 8 additional samples (PS cores) from Müller et al. (2011). Where TOC and MOC data were not available, estimates were made on the basis of nearest locations (*). For a few locations, there was insufficient sediment material to complete the biomarker analysis (–). In one case, calculation of the P_BIP_{25} index was not possible since both biomarkers were absent (/).

Sample	Water depth (m)	Lat.	Long.	TOC wt.%	MOC (%)	IP_{25} μg g^{-1} TOC	IP_{25} μg g^{-1} MOC	Brassicasterol μg g^{-1} TOC	P_BIP_{25}	Satellite sea ice conc. (%)
1287	364	79.19	11.77	0.97	0.68	0.53	0.75	156.92	0.65	15
PS57/166-2	527	79.13	4.89	1.29	0.65*	0.67	1.32	100.45	0.79	5
1289	319	79.03	10.84	2.23	1.36	0.27	0.44	73.75	0.67	15
PS57/127-1	307	79.03	10.51	1.87	0.79*	0.76	1.80	234.22	0.64	5
1288	308	78.98	11.82	1.38	0.88	0.22	0.35	118.73	0.51	15
1290	250	78.95	9.62	0.95	0.58	0.07	0.11	96.80	0.29	5
1286	159	78.87	11.33	1.13	0.79	0.04	0.06	105.60	0.19	15
HH11-135GC	2242	78.47	−0.46	0.89	0.65*	0.15	0.21	9.60	0.90	15
HH11-136BC	2240	78.47	−0.46	0.36	0.65*	0.42	0.23	208.77	0.53	15
1265	87	78.37	16.37	1.88	0.26	0.25	1.78	61.32	0.69	nd
1269	169	78.37	12.30	2.00	0.76	0.25	0.67	43.94	0.76	15
1273	600	78.25	9.32	0.85	0.30	0.06	0.17	51.70	0.39	5
HH11-140BC	1258	78.22	1.18	0.70	0.65*	0.15	0.16	55.97	0.59	5
HH11-137BC	1709	78.14	1.36	0.30	0.65*	0.74	0.34	686.14	0.37	5
HH11-138GC	1707	78.14	1.36	1.00	0.65*	0.11	0.17	19.36	0.76	5
1270	259	78.08	12.30	2.41	1.30	0.45	0.84	51.92	0.83	15
HH11-133GC	271	78.08	11.47	2.59	1.30*	0.61	1.21	44.28	0.88	5
WP08 337	1733	78.08	8.30	1.27	0.65*	0.10	0.20	41.78	0.58	0
1254	76	77.83	16.59	2.03	0.43	0	0	10.65	0.00	nd
PS57/136-2	589	77.81	15.89	1.68	0.29*	0.28	1.62	93.35	0.62	nd
PS57/130-1	388	77.78	9.68	0.86	0.40*	0.85	1.83	108.52	0.81	5
PS57/137-2	1442	77.77	15.06	2.11	0.38*	0.41	2.26	100.42	0.69	nd
1251	115	77.75	14.92	1.84	0.48	0.03	0.10	57.42	0.21	nd
1255	83	77.72	15.19	1.74	0.38	0.06	0.29	60.89	0.37	nd
1261	1291	77.39	10.60	0.89	0.40	0.06	0.13	42.60	0.42	0
1262	603	77.36	11.27	0.82	0.24	0.17	0.57	42.71	0.69	5
HH11-134BC	1381	77.36	9.53	1.50	0.40*	0.12	0.46	31.93	0.68	5
1263	196	77.20	12.93	1.96	0.86	0.60	1.37	57.67	0.85	5
PS57/131-2	320	77.17	11.10	0.83	0.40*	0.59	1.23	129.33	0.72	5
PS57/138-1	1013	76.68	12.99	0.87	0.78*	0.54	0.60	63.38	0.83	5
679	193	76.62	34.45	1.82	0.78	0.19	0.45	99.88	0.52	45
643	291	76.49	29.91	2.24	1.26	0.17	0.30	32.03	0.75	35
681	249	76.43	37.17	1.23	0.78*	0.11	0	20.60	0.75	45
St32	228	76.38	20.58	2.40	1.32	0.41	0.74	198.46	0.53	65
PS57/145-1	1502	76.33	13.93	1.19	0.78*	0.17	0.26	85.54	0.52	5
St31	258	76.31	19.57	2.66	1.49	0.26	0.46	–	–	55
St30	257	76.22	18.58	2.24	1.32	0.29	0.50	–	–	45
St29	309	76.16	17.62	2.31	1.25	0.32	0.60	146.69	0.55	35
677	276	75.97	33.73	1.91	0.77	0.07	0.17	6.87	0.85	25
St27	369	75.95	15.72	2.17	1.24	0.19	0.33	60.85	0.63	15
645	296	75.86	29.46	2.20	0.62	0.07	0.26	31.31	0.56	15
St26	370	75.83	14.77	1.66	0.85	0.24	0.47	78.04	0.63	5
St25	807	75.75	13.84	0.82	0.36	0.17	0.38	–	–	5
St24	1500	75.64	12.92	1.11	0.67	0	0	123.67	0	0
WP08 348	1264	75.60	13.17	0.82*	0.36*	0	0	32.80	0.00	0
WP08 349	1046	75.59	13.38	0.82*	0.36*	0	0	22.91	0.00	5
639	263	75.57	27.90	2.74	1.62	0.09	0.15	71.49	0.41	5
675	209	75.33	33.07	2.11	0.77*	0.06	0	70.34	0.33	5
647	343	75.20	29.01	2.20*	0.62	0	0	60.54	0	5
635	182	75.00	24.94	2.45	1.32	0.17	0.31	76.65	0.55	0
1241	297	74.82	17.58	2.14	1.35	0.06	0.10	89.67	0.28	5
St20	296	74.82	18.02	1.97	1.22	0.11	0.17	175.21	0.25	5
St21	280	74.82	17.00	0.90	0.52	0	0	53.26	0	0
St22	356	74.82	16.03	0.73	0.33	0	0	33.57	0	0
St23	1507	74.82	14.79	0.95	0.62	0	0	–	–	5
673	165	74.67	32.49	1.28	0.61	0.22	0.47	40.61	0.75	5
651	317	74.64	26.08	2.08	1.19*	0	0	48.33	0	5
649	394	74.54	28.58	2.08*	1.19*	0	0	38.61	0	5
1239	178	74.46	20.83	1.70	0.97	0.03	0.05	33.81	0.33	0
633	373	74.34	24.69	1.26	0.54	0	0	56.29	0	0
671	366	74.15	29.55	1.37*	0.82*	0	0	29.38	0	0
653	441	73.97	25.81	1.73	0.97	0	0	21.17	0	0
631	451	73.67	24.47	1.26*	0.54*	0	0	52.19	0	0
669	414	73.50	29.15	1.37	0.82	0	0	37.38	0	0
655	412	73.31	25.54	1.53	0.84	0	0	41.53	0	0
St11	1499	73.17	12.94	0.74	0.54	0.07	0.09	146.68	0.20	0
St12	1030	73.17	14.09	0.42	0.29	0.56	0.81	123.80	0.72	0
St13	485	73.17	15.23	0.33	0.19	0	0	19.15	0	0
St14	475	73.17	16.38	0.79	0.50	0.22	0.35	58.30	0.68	0

Table 1 (*continued*)

Sample	Water depth (m)	Lat.	Long.	TOC wt.%	MOC (%)	IP_{25} μg g^{-1} TOC	IP_{25} μg g^{-1} MOC	Brassicasterol μg g^{-1} TOC	P_BIP_{25}	Satellite sea ice conc. (%)
St15	460	73.17	17.54	0.88	0.54	0.22	0.36	62.96	0.66	0
St17	441	73.17	19.86	1.15	0.62	0.16	0.29	111.83	0.44	0
St18	463	73.17	20.95	1.41	0.83	0.04	0.06	59.70	0.25	0
St19	444	73.17	22.01	1.40	0.85	0.16	0.27	65.78	0.58	0
629	404	73.01	24.25	1.39	0.75	0	0	38.85	0	0
667	305	72.84	28.76	0.78*	0.48*	0	0	43.44	0	0
657	268	72.64	25.27	1.53*	0.84*	0	0	12.01	0	0
627	264	72.32	24.06	0.62	0.39	0	0	19.49	0	0
665	289	72.17	28.41	0.78	0.48	0	0	909.24	0	0
St03	324	72.03	19.85	1.01	0.74	0.05	0.07	–	–	0
St02	371	72.02	20.92	0.92	0.63	0	0	51.65	0	0
St06	362	72.02	16.62	0.37	0.26	0.58	0.82	82.60	0.80	0
St04	315	72.02	18.77	0.97	0.72	0	0	76.16	0	0
St07	767	72.02	15.52	0.29	0.12	0	0	8.43	0	0
St09	1317	72.01	14.62	0.67	0.52	0.17	0.22	36.46	0.73	0
659	256	71.98	25.06	0.71*	0.47*	0	0	15.20	0	0
St34	356	71.75	22.00	0.76	0.54	0	0	36.06	0	0
625	360	71.72	21.76	0.62*	0.39*	0	0	20.27	0	0
St35	319	71.62	21.07	0.60	0.42	0	0	40.82	0	0
663	291	71.61	25.99	0.71*	0.47*	0	0	12.19	0	0
St37	335	71.60	21.19	0.58	0.42	0	0	36.36	0	0
St36	320	71.60	20.86	0.80	0.62	0	0	54.91	0	0
St38	310	71.49	20.82	0.75*	0.61*	0	0	54.29	0	0
661	408	71.37	22.76	0.71	0.47	0	0	13.68	0	0
St39	234	71.34	20.19	0.75	0.61	0	0	101.87	0	0
St40	225	71.18	19.56	0.83	0.69	0	0	74.36	0	0
St41	199	71.03	18.95	0.37	0.29	0	0	41.81	0	0
690	283	71.02	30.96	0.39	0.15	0	0	9.70	0	0
St43	273	70.72	17.75	0.20*	0.17*	0	0	626.66	0	0
692	252	70.62	31.72	0.39*	0.15*	0	0	7.41	0	0
St44	706	70.55	17.14	0.20	0.17	0	0	0	/	0
St45	1500	70.44	16.75	0.20*	0.17*	0	0	44.48	0	0

which to compile the sea ice records, some assessment of sedimentation rates for the Barents Sea was carried out and these were assumed to be fairly representative for the entire region. Since sedimentation rates are typically in the region (0.7–1.1) ± 0.4 mm yr^{-1} for the Barents Sea (e.g. Zaborska et al., 2008; Maiti et al., 2010), but can be both lower and higher than this range (e.g. 1.16 ± 0.11 mm yr^{-1}; Vare et al., 2010), it was decided to use a 20-year time interval for the sea ice compilations. In practice, however, the outcomes from 10 and 15 year analyses showed little variation from the 20-year dataset. Polyline shapefiles of sea ice extent for the 20-year period 1983–2002 (NSIDC) were used to generate a maximum sea ice extent (hereafter referred to as the MSIE; Fig. 1) for this interval. Additional estimates of mean spring (March–May) sea ice concentrations (±5%) for the region within the MSIE boundary were obtained for the interval 1983–2002 from the UK Met Office Hadley Centre database (HadISST) (Rayner et al., 2003). This method was also used to re-calculate the estimates of sea ice concentrations for locations described previously by Müller et al. (2011) who used data from the NSIDC. In practice, however, only 8 out of the 38 values reported by Müller et al. (2011) were different between the two methods and these differences were never more than 10%.

4. Results and discussion

4.1. Individual biomarker data – distributions of IP_{25} and brassicasterol

Of the 93 surface sediments analysed in the current study, the sea ice biomarker IP_{25} was detected in 51 samples and was absent or, at least, below the limit of detection in the remaining 42. When present, the concentrations of IP_{25} ranged from 0.03 to 0.74 μg g^{-1} TOC (0.05–1.78 μg g^{-1} MOC; Table 1) consistent with values found in samples analysed by Müller et al. (2011) from some nearby locations (west Svalbard). In general, there was an approximate north–south division between samples containing IP_{25} compared to those where it was absent, although there was a much more consistent classification according to the position of each sampling location relative to the MSIE (Fig. 1b). Thus, of the 59 samples containing IP_{25} (51 from the current work and 8 in the study by Müller et al. (2011), 47 were from locations within the MSIE for the period 1983–2002 (Fig. 1b) and a further two samples were within close proximity of this boundary (76°–78°N; 5°–10°E). Finally, IP_{25} was also detected in 10 samples that were somewhat remote from the MSIE and were located at ca 72°–73°N; 13°–22°E (Fig. 1b).

In contrast to the IP_{25} distributions, the more general phytoplanktic biomarker brassicasterol was detected in sediments from across the entire study area (with the exception of a single sample point located near to the Norwegian coast) (Fig. 1c) and was present with a much greater range of concentrations (ca 6.87–909.24 μg g^{-1} TOC; 13.15–1477.52 μg g^{-1} MOC) compared to IP_{25}.

4.2. Influence of organic carbon on biomarker distributions

At the beginning of the biomarker data interpretation, we considered the possible influences of variable primary production, sediment accumulation and burial rates by normalising biomarker concentrations to organic carbon content, especially as TOC is known to be somewhat variable in the Barents Sea. This is, in part, because of the strong productivity association with the MIZ (Knies, 2009), which provides a suitable habitat for a wide range of microorganisms (Thomas, 2012), but also because vertical particulate organic carbon (POC) export is thought to be relatively weak in the Atlantic region of the Barents Sea compared to regions of the

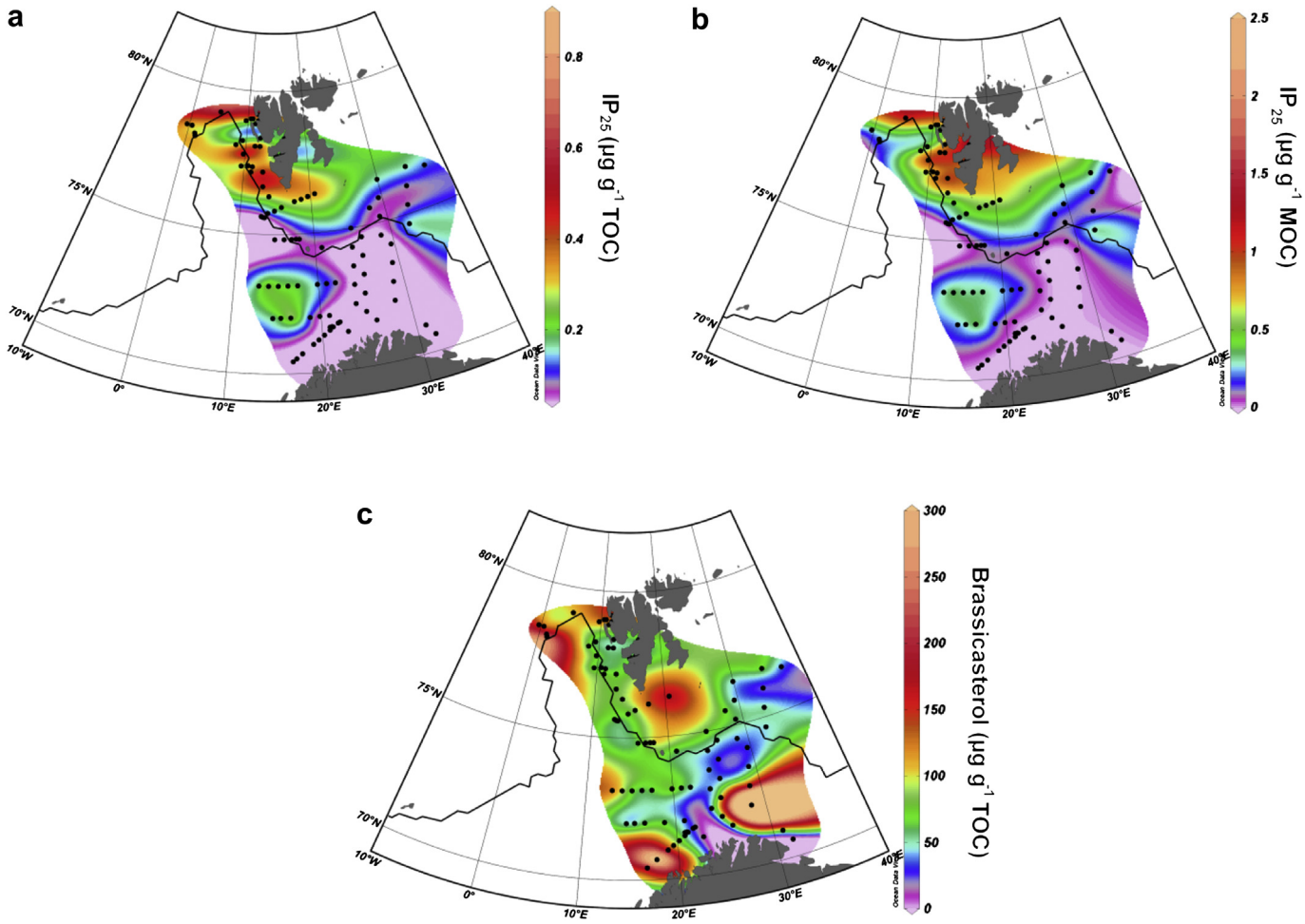

Fig. 2. Distributions of individual biomarker concentrations and other organic geochemical parameters derived from analysis of 101 surface sediments (93 from the current study and 8 from Müller et al. (2011)) from the Barents Sea and nearby regions: (a) IP_{25} (normalised to TOC); (b) IP_{25} (normalised to MOC); (c) brassicasterol (normalised to TOC).

MIZ where pelagic–benthic coupling is stronger (Wassmann et al., 2006; Maiti et al., 2010). Further, we considered the potential influence of alternative methods of normalising sedimentary concentrations using total versus marine organic matter. Significant differences between the two approaches could potentially have materialised, especially since the contribution of MOC to TOC has also been shown to be variable in Barents Sea sediments (Knies and Martinez, 2009), likely as a result of differential productivity and input of terrigenous material.

In practice, although the ranges of TOC- versus MOC-normalised concentrations were slightly different (necessarily), the distributions in concentrations across the study area were largely unaffected by the method of choice (Fig. 2a, b). As such, since we had a larger dataset of TOC values and previous TOC-normalised data were also available for comparison purposes, we based the biomarker interpretations on TOC-normalised concentration data.

4.3. Distributions of IP_{25} and brassicasterol

4.3.1. Point locations

When comparing the concentrations and distributions of the sea ice biomarker IP_{25} with the MSIE for the 20-year period 1983–2002 (NSIDC), a clear relationship between the two was identified (Fig. 1b), providing further evidence of the potential for IP_{25} to be used as a reliable sea ice proxy in the Arctic. Thus, of the 59 sample locations where IP_{25} was detected (or had been reported previously; Müller et al., 2011), 47 were within the MSIE and two further locations were within close proximity to this boundary. In contrast, IP_{25} was absent in 42 samples that represented locations for which no sea ice has been observed in the same 20-year interval (NSIDC). Exceptionally, IP_{25} was absent in only two samples from sites that have had at least partial sea ice cover (647; north east Barents Sea and St21; western Barents Sea) and these represented locations that are extremely close to the MSIE and may, therefore, have only experienced infrequent sea ice occurrence. A further sample with no IP_{25} and a very low brassicasterol concentration (10.65 µg g^{-1} TOC) (1254; Table 1) was collected from the innermost part of van Mijenfjorden in Svalbard, a location for which extremely low numbers of dinocysts had been reported previously (Grøsfjeld et al., 2009), possibly reflecting low nutrient levels. This, in turn, may have resulted from severe sea ice conditions during the spring, followed by a rapid melt in the summer, leading to very low productivity in sea ice and the pelagic environment.

These occurrences of IP_{25} in virtually all sediments from locations within the boundary of the MSIE is consistent with the outcomes of previous analyses of dinocyst assemblages from a subset of the same sample locations, namely the identification of (variable) seasonal sea ice cover (Solignac et al., 2009). Specifically, Solignac et al. (2009) observed the dominance of *Islandinium minutum*, which is related to Arctic waters, in two transects south of Svalbard (74°–76° N) and within the MSIE where IP_{25} was also detected. Further, *I. minutum* was generally identified as the

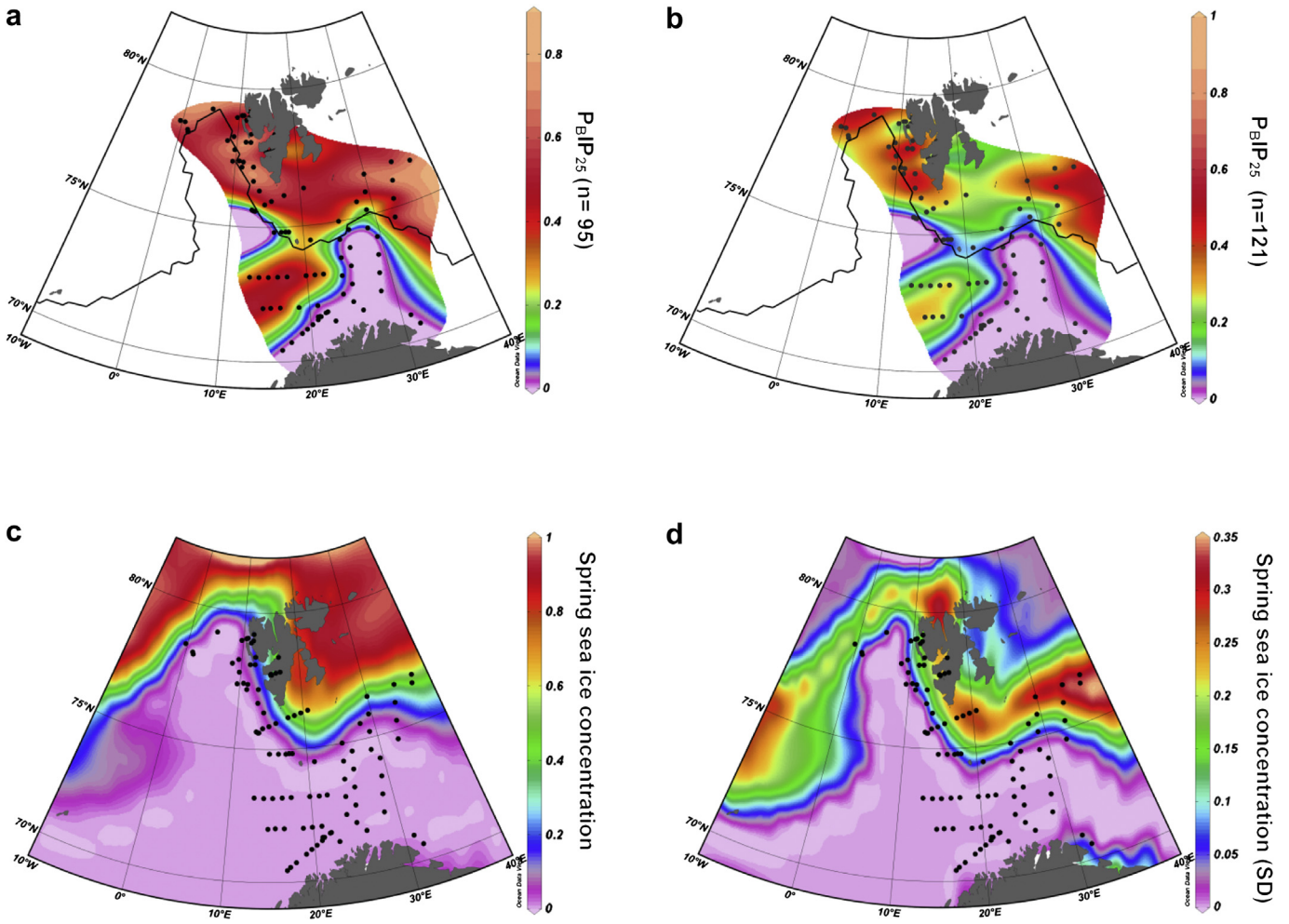

Fig. 3. Combined biomarker indices (P_BIP_{25}) calculated using IP_{25} and brassicasterol concentrations and sea ice concentration data: (a) P_BIP_{25} values using biomarker data presented in the current study (Table 1; $n = 95$); (b) P_BIP_{25} values calculated using biomarker data presented here and additional values reported by Müller et al. (2011) ($n = 121$); (c) Satellite-derived (UK Met Office Hadley Centre database (HadISST) (Rayner et al., 2003)) mean spring sea ice concentration data (±5%) for the interval 1983–2002; (d) Standard deviations in sea ice concentrations. The maximum sea ice extent (MSIE) for 1983–2002 is represented by the continuous black line (calculated from NSIDC records). Maps are generated with Ocean Data View (ODV) software (v.4.5) using the Diva Gridding Algorithm.

major dinocyst species west of Spitsbergen (Grøsfjeld et al., 2009), coincident with the highest concentrations of IP_{25} observed here (77°–79° N; 10°–16° E). As such, both sets of proxy data indicate the strong influence of Arctic waters and the occurrence of spring sea ice in this region.

Of the 47 sample locations within (or near to) the MSIE where IP_{25} was detected, two regions could be identified broadly according to IP_{25} concentrations (Fig. 1b), possibly suggesting different sea ice conditions between two seasonal ice-edge regimes. Currently, the factors that control IP_{25} production and transfer to sediments are not fully understood which prevents detailed quantitative assessments from being carried out on the basis of IP_{25} concentrations alone. It is noted, however, that for sample locations on the eastern side of Svalbard, IP_{25} concentrations were relatively low (ca 0.06–0.22 μg g^{-1} TOC; mean 0.13 μg g^{-1} TOC; $n = 9$) or, at least, lower than for sites to the immediate south and west of Svalbard. Spring sea ice extent is more variable on an annual basis for the eastern Barents Sea compared to the western and southern regions of Svalbard (NSIDC) reflecting the different relative influences of the inflowing Atlantic and Arctic waters in different regions (Årthun et al., 2012). This increased variability in the position of the maximum ice edge potentially results in a smaller number of months per year of sea ice cover over a fixed (e.g. 20-yr) interval. As such, it is possible that less frequent spring sea ice occurrences may contribute to the observation of lower IP_{25} concentrations in the eastern region, although uncertainties in the sedimentation rates prevents this suggestion being tested more quantitatively. Higher concentrations of IP_{25} (0.03–0.74 μg g^{-1} TOC; mean 0.23 μg g^{-1} TOC; $n = 30$) were found to the west and immediate south of Svalbard (Fig. 1b) where winter/spring sea ice extent is slightly more consistent on an annual basis, possibly resulting in a higher frequency of spring algal blooms during which IP_{25} is produced (Brown et al., 2011). In contrast, three sample locations further south of Svalbard and in close proximity to the MSIE (St 20, 1239, 1241; Table 1) had very low IP_{25} concentrations (0.03–0.11 μg g^{-1} TOC), potentially as a result of the greater variability of the ice edge in this region.

Alternatively, variations in IP_{25} concentrations within the boundary of the MSIE may better reflect post-production influences, with relative depletions resulting from removal processes such as degradation (water column and the sediment interface), scavenging of OM by heterotrophs or weaker pelagic–benthic coupling, in general. As such, this study reinforces the notion that while the occurrence of IP_{25} provides an excellent qualitative proxy for past sea ice, quantitative interpretations need to be treated with caution and should be considered alongside other proxy data.

In contrast to the relatively localised occurrence of IP_{25}, brassicasterol was present in virtually all sediments and the distribution of concentrations (Fig. 1c) showed little, if any, relationship to either sea ice cover or the position of the MSIE. Instead, this biomarker, which is generally considered to be representative of open water phytoplankton (Müller et al., 2011), was distributed in sediments representing both seasonally ice-covered and ice-free conditions over the entire study area, with the exception of one location off the north coast of Norway. Within the region covered by the MSIE boundary, brassicasterol concentrations were within the range 9.60–686.14 μg g^{-1} TOC (mean 86.20 μg g^{-1} TOC), while equivalent values for more temperate locations (i.e. in permanently open water conditions), were between 0 and 909.24 μg g^{-1} TOC (mean 77.34 μg g^{-1} TOC). These data suggest that brassicasterol can be considered as a non-specific indicator for either of these two regional divisions (i.e. seasonally sea ice covered or open water conditions) in the Barents Sea and it follows that the production of brassicasterol by phytoplankton during the summer bloom (all sampling locations are ice-free in the summer) is not substantially negatively impacted by winter sea ice, at least on a relatively broad spatial scale. Alternatively, these data may imply that there is a significant contribution to sedimentary brassicasterol from ice algae. We are not aware of specific investigations into this possibility and it would appear to be an important area of future research.

4.3.2. Spatial distributions

When the (point location) IP_{25} and brassicasterol concentrations were re-examined as broader spatial representations (ODV; Fig. 2a, c), the trends identified from the point location analyses were confirmed and more detailed distribution patterns were also identified. For example, the regions of highest concentrations of IP_{25} were shown to be within the boundary defined by the MSIE and to the west and south of Svalbard (ca 0.32–0.85 μg g^{-1} TOC; Fig. 2a), while the lowest concentrations (0.03–0.06 μg g^{-1} TOC; Fig. 2a) were found for locations near to the MSIE in the south and for the sites within the boundary of the MSIE in the east. Further, the majority of locations south of the MSIE had IP_{25} concentrations less than 0.042 μg g^{-1} TOC, which corresponds to the analytical limit of detection, and is consistent with the failure to detect IP_{25} in the majority of sediment extracts from this area. Exceptionally, a region of relatively low-mid range concentrations of IP_{25} was also identified within the south-west of the study area (72°–73°N and 13°–22°E), consistent with the detection of IP_{25} in 10 samples from this region (a more detailed discussion of this will be given in Section 4.5).

In direct contrast to these IP_{25} concentration data, the distributions of brassicasterol (Fig. 2c) were not at all closely defined by the MSIE and, indeed, ranges and mean concentrations of brassicasterol from locations within the MSIE were not significantly different from those representing ice-free locations. Instead, brassicasterol distributions were found to be influenced more by other regional influences on primary production, which is consistent with the biosynthesis of this biomarker by a wide range of algal sources (e.g. Volkman, 1986; Volkman et al., 1998). The more general production of brassicasterol likely also explains its significantly higher abundance in sediments compared to IP_{25} which, in contrast, is thought to be produced selectively by a small number of diatom species living in sea ice (Belt et al., 2007; Brown et al., 2011). Within the spatial heterogeneity of the brassicasterol distributions, however, two relatively high concentration regions could be identified that can be attributed to distinct events; the first of which was on the north Norwegian coast where phytoplanktic blooms have been detected in summer months (MODIS-Aqua 8-2011) and a second, to the south of Svalbard, where high biological productivity occurs within the MIZ (Knies, 2009). In contrast, the reduced brassicasterol concentrations for some parts of the north coast of Norway presumably reflect influences other than sea ice on the production of this biomarker and such factors may also impact on the outcomes of combined biomarker indices such as the PIP_{25} index (discussed later).

4.4. Quantitative assessment of sea ice coverage – application of the PIP_{25} index

In order to extend the qualitative aspects of the biomarker distributions further and, with the specific aim of identifying whether the outcomes could be made more quantitative, we adopted a method proposed recently by Müller et al. (2011) who introduced the potential benefits of combining the individual sea ice diatom (IP_{25}) and phytoplankton (brassicasterol) biomarkers together into a single index (P_BIP_{25}), resulting in more detailed descriptions of past sea ice conditions. Although the outcomes of this initial study were reasonably convincing, Müller et al. (2011) also recommended that a more extensive set of samples covering a wider spatial range would be needed in order to assess the full potential of this novel approach. Nevertheless, the principles behind the P_BIP_{25} index are reasonably clear and, on the basis of their initial findings, Müller et al. (2011) suggested that individual P_BIP_{25} values had the potential to identify discrete oceanographic or sea ice scenarios. Thus, high (0.75–1.0) P_BIP_{25} values were suggested as representing extensive sea ice conditions (IP_{25} is favoured relative to phytoplankton biomarkers), mid-range values (0.50–0.75) indicated MIZ or seasonal ice cover (conditions favour both types of biomarker), while P_BIP_{25} values less than ca 0.5 represent infrequent or ice-free conditions (IP_{25} is low or absent). It was also accepted, however, that the boundaries between these classifications should also be considered with some flexibility.

The biomarker datasets collected as part of the current study, therefore, provided the opportunity to test the applicability of the P_BIP_{25} index further and, in particular, propose more detailed descriptions of the sea ice conditions within the region defined by the MSIE within the Barents Sea. Thus, we combined the individual IP_{25} and brassicasterol data measured in the current study, together with those reported by Müller et al. (2011) for the same region (8 sample locations), to obtain P_BIP_{25} data for the Barents Sea. In doing so, we note that the ranges in concentration of IP_{25} and brassicasterol measured as part of the current study (0–0.60 μg g^{-1} TOC and ca 10–157 μg g^{-1} TOC, respectively) were consistent with those from Müller et al. (2011) (0.17–0.85 μg g^{-1} TOC and 63–234 μg g^{-1} TOC, respectively) where there was overlap between sampling regions (i.e. west Svalbard). It is also noted that, since there was no significant difference in the mean brassicasterol concentrations either side of the MSIE, it was unlikely that P_BIP_{25} data would be substantially misrepresented by exceptionally high/low brassicasterol values in these two regions and that the magnitude of the P_BIP_{25} index would better reflect the nature of, and changes to, the sea ice conditions as a result of variations in the IP_{25} data. Further, although 93 sediments were analysed for IP_{25} in the current study, there was insufficient material from five locations to also analyse for brassicasterol and, for one sample location, both IP_{25} and brassicasterol were below the limit of detection. As such, P_BIP_{25} indices could only be calculated for 87 samples.

The outcomes of the spatial representation of the P_BIP_{25} data are in reasonable agreement with those derived from the IP_{25} data alone and, in addition, provide potentially more detailed insights into the sea ice conditions. Firstly, for locations which experienced sea ice cover during (at least part of) the 1983–2002 sampling period (i.e. those generally north of the MSIE), P_BIP_{25} values were

consistently in the range ca 0.45–0.9 (Fig. 3a), interpreted as representing the occurrence of a MIZ or more extended sea ice conditions (Müller et al., 2011). Secondly, and in direct contrast, P_BIP_{25} values were significantly lower (ca 0.1–0.25) for the region mainly south of the MSIE and east of ca 12° E, indicative of irregular or reduced sea ice cover, and inferred from the IP_{25} distributions here. In contrast to the IP_{25} data alone, however, where variable abundances were previously interpreted as possibly reflecting an inconsistent ice-edge position, the P_BIP_{25} data for locations in the eastern region (north of the MSIE) implied similar sea ice conditions to those of west and south Svalbard (*viz.* MIZ or extended sea ice cover). This difference in the IP_{25} and P_BIP_{25} records arises mainly due to the influence of the lower brassicasterol concentrations on the P_BIP_{25} index in the eastern region and provides a useful example of how the interpretation of individual biomarker records can sometimes be misleading and can be improved through combination with other biomarker data, at least in some cases. Thirdly, the P_BIP_{25} values for locations predominantly south of the MSIE either confirmed the ice-free conditions (P_BIP_{25} ca 0) or, in the case of the south-west region, where IP_{25} had also been detected, significant ice cover was implied (P_BIP_{25} = ca 0.45–0.9).

In order to evaluate the P_BIP_{25} index further, we re-analysed the combined biomarker data in two further ways. In the first instance, we re-calculated the P_BIP_{25} values for the Barents Sea using a larger biomarker dataset, including IP_{25} and brassicasterol concentrations reported previously by Müller et al. (2011), for locations representing a wider spatial coverage within the northern North Atlantic. One consequential impact of this was a change to the c term used to balance differences in the abundances of IP_{25} and brassicasterol. In this instance, the analysis of a larger dataset resulted in an increase in the c term and a lowering of P_BIP_{25} values (Fig. 3b), although higher P_BIP_{25} values were still generally observed within the region bound by the MSIE compared to most of the locations beyond the maximum ice edge. For the Barents Sea and the larger datasets, some qualitative comparisons with the known mean spring sea ice concentrations (Fig. 3c) for the interval 1983–2002 were also made and these showed that, although there was some reasonable consistency between higher P_BIP_{25} values and increased sea ice concentrations for some locations to the east of Svalbard, there was relatively poor agreement for the regions west and south of Svalbard, with lower satellite-derived sea ice concentrations than those predicted by the P_BIP_{25} data.

Secondly, we attempted to make these comparisons more quantitative by comparing the IP_{25} and (re-calculated) P_BIP_{25} data with the corresponding mean spring sea ice concentrations using the method of Müller et al. (2011), although some of the data (e.g. 4 of the 87 P_BIP_{25} values from the current study) needed to be excluded from this analysis due to the lack of satellite sea ice concentration data. In terms of the linear relationship between the enhanced IP_{25} dataset (n = 121; 83 from the current study; 38 from Müller et al., 2011) and sea ice concentrations (Fig. 4a), the regression coefficients were very similar to those reported by Müller et al. (2011) and the same was true of the coefficient of determination (R^2 = 0.67 in both cases). In contrast, although the corresponding linear relationship between the larger P_BIP_{25} dataset and sea ice concentrations (Fig. 4b) yielded similar regression coefficients to those reported by Müller et al. (2011) using a smaller dataset (n = 38), the variability was much greater. Thus, the R^2 for the larger P_BIP_{25} dataset (0.57) was significantly lower than that found by Müller et al. (2011) (R^2 = 0.74) and, additionally, was also less than for the relationship using the IP_{25} concentrations alone (R^2 = 0.67). Although the exact reasons for the poorer relationship between the combined P_BIP_{25} data and the satellite-derived sea ice concentrations are not fully understood at this stage, some contributing factors may include: (i) a bias in the sampling frequency (it is noted that the majority of the points here fall within the low (<25%) sea ice concentration range); (ii) uncertainties of the time intervals that the surface sediments represent; (iii) errors associated with the sea ice concentrations derived from satellite records; (iv) variations in analytical methods for biomarker concentration determinations; (v) variability in environmental controls over the production and fate of IP_{25} and other biomarkers.

To begin with, sedimentation rates may potentially be quite variable across the region, which makes it difficult to reliably predict the period for which the satellite sea ice data should be considered and, even if sedimentation rates are known (or can be reasonably estimated), the surface material will also reflect different time intervals depending on when sampling took place. In this respect, it is noted that samples analysed by Müller et al. (2011) were obtained from 1994 to 2003, while the samples in the current study were mainly collected from 2001 to 2004 and a few in 2011. This further complicates the correlational analysis between biomarker and satellite-derived concentration data since the latter are especially susceptible to short-term changes, as has been noted in recent decades and seen in the current study through the (variable) standard deviations in sea ice concentrations for the Barents Sea (Fig. 3d). Further, variability in sea ice concentration data may depend on the origin of the source data and the methods

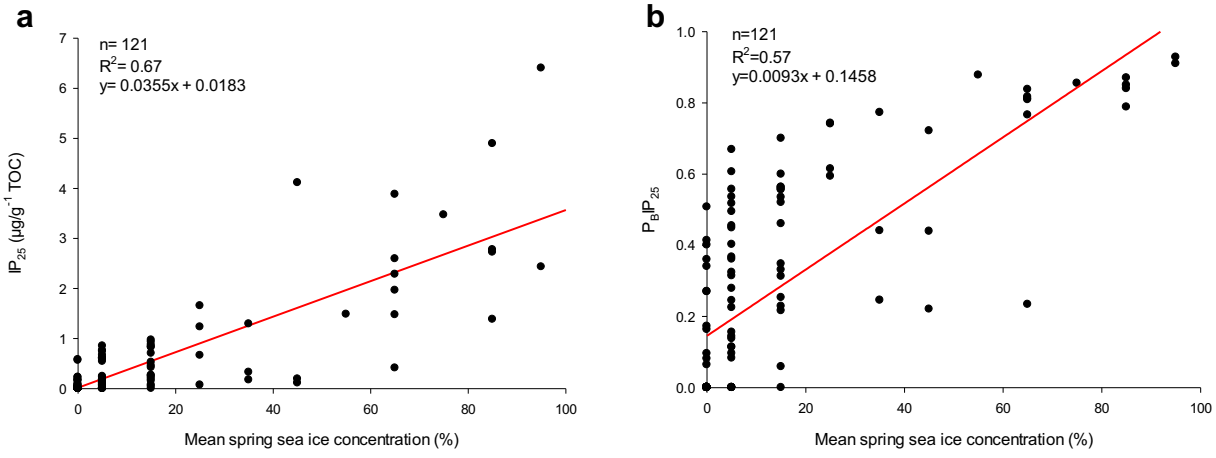

Fig. 4. Linear relationship between (a) IP_{25} and (b) P_BIP_{25} values and mean spring sea ice concentrations (Hadley; HadISST). The IP_{25} and P_BIP_{25} data are compilations of the values determined here (n = 83) and by Müller et al. (2011; n = 38).

used to interpret these, although we have not found this to be a major factor, as described earlier.

In terms of the analytical datasets, a number of alternative approaches have been used to determine concentrations of individual biomarkers in previous studies and this too could potentially lead to discrepancies, especially when datasets are combined from separate studies, as has been the case here. For example, Müller et al. (2011) determined IP_{25} concentrations in sediments from the northern North Atlantic using a GC–MS-based approach whereby mass spectral responses of IP_{25} and the internal standard were assumed to be the same, whereas the concentration data presented here have been determined using an authentic standard of IP_{25} isolated from Arctic sediments, so calibrations against the internal standards could be verified experimentally. Whether the adoption of alternative approaches of this type results in significant differences in biomarker concentrations probably requires further investigation, but the implementation of an inter-laboratory comparison of methods as suggested by Belt and Müller (2013) or adoption of a Standard Operating Procedure (e.g. Belt et al., 2012) would seem to be a sensible way forward, especially if quantitative biomarker-based studies are to develop further.

A more fundamental factor that may limit the applicability of the use of IP_{25} or PIP_{25} data more quantitatively for sea ice concentration reconstructions is the extent to which environmental controls have a consistent (or otherwise) influence over the production of IP_{25} and other biomarkers, since it may be that parameters such as nutrient availability, water depth, light intensity, etc., may have a greater or more significant control over biomarker abundances than sea ice concentration(s) alone. Some further examples of potentially important factors that may control biomarker abundances have been considered in greater detail by Belt and Müller (2013); however, regardless of these potential cause(s), it is clear from previous studies (e.g. Vare et al., 2009, 2010; Belt et al., 2010) and from a more recent analysis of surface sediments from different Arctic and sub-Arctic regions (Stoynova et al., 2013) that concentrations of IP_{25} and phytoplanktic biomarkers can be highly variable between locations with similar sea ice cover. We also note from the current study that concentrations of brassicasterol exhibited a high degree of variability, even within the open water regions (Fig. 2c), suggesting that the significance of environmental influences on primary production and associated biomarker signatures, both on local and pan-Arctic scales, should not be underestimated. Such factors, and their influence on the success (or otherwise) of biomarker-sea ice concentration correlations are likely to be most clearly identified through analysis of larger datasets representing different regions of the Arctic. For example, Stoynova et al. (2013) demonstrated clear differences between biomarker-sea ice concentration correlations for Arctic and sub-Arctic regions of the Atlantic and Pacific and also with those reported previously for Fram Strait (Müller et al., 2011). Further, it was suggested that such differences may be attributed (in part) to variations in primary production or the nature of the sea ice between regions (Stoynova et al., 2013). Returning to the current study, we note that the linear correlations between biomarker data and sea ice concentrations for the Barents Sea and West Svalbard locations alone are poorer ($R^2 = 0.06$ and 0.19 for the IP_{25} and P_BIP_{25} – sea ice correlations, respectively; Suppl. Fig. A1) compared to the findings of Müller et al. (2011) or the combined datasets presented here (Fig. 4). In contrast, the most consistent linear biomarker-sea ice concentration correlations can be observed for locations from the continental margin of East Greenland ($R^2 = 0.65$ and 0.79; for the IP_{25} and P_BIP_{25} – sea ice correlations, respectively; data from Müller et al. (2011); Suppl. Fig. A2). The reason for the differences between the two regions (Barents Sea/West Svalbard versus East Greenland) may potentially be related to the different sea ice types in the two regions (*viz.* first year ice versus a combination of first year and multi-year drift ice, respectively) and these observations provide the basis for future investigation.

Further, any (linear or other) biomarker – sea ice concentration relationships that do exist, may be negatively impacted by any differential degradation or removal processes, and these also may be variable between locations (see Belt and Müller, 2013, for a review of this topic). Such processes may include, but are not limited to, selective biodegradation of individual biomarkers in oxic surface sediments or physical redistribution of surface sediments as discussed later. One way to potentially reduce the impact of such degradation processes is to ratio biomarker concentrations using lipids of related origin or structure/reactivity. Such an approach is used routinely for the reconstruction of SSTs using alkenones (Brassell et al., 1986) and glycerol dialkyl glycerol tetraethers (GDGTs) (Schouten et al., 2002; Kim et al., 2008) which are used to derive the $U^{K'}_{37}$ and TEX_{86} indices, respectively. This approach is, to some extent, applied through calculation of the PIP_{25} index, although the potential for differential degradation of IP_{25} versus the phytoplanktic biomarkers such as brassicasterol remains a key issue. Such a limitation may be resolved to a large part by measuring the ratios of IP_{25} to a further lipid with similar chemical or physical characteristics and a potential candidate for this is the structural homologue of IP_{25}, namely the di-unsaturated C_{25} HBI lipid, also believed to be produced by Arctic sea ice diatoms. Indeed, recent studies by Fahl and Stein (2012), Cabedo-Sanz et al. (2013) and Xiao et al. (2013) have shown the potential for the ratio between this di-unsaturated HBI and IP_{25} (the so-called DIP_{25} index) to provide further information regarding Arctic sea ice conditions.

Finally, we comment on the impact of the balance factor, c, which is central to the determination of the PIP_{25} index. Since this term corresponds to the ratio of the mean IP_{25} and phytoplankton biomarker concentrations under study, this means that PIP_{25} values are not fixed for a given location or sediment extract, but are also dependent on the number and nature of sample locations within a given investigation. As a consequence, for example, the P_BIP_{25} values reported previously by Müller et al. (2011) for 38 samples from the northern North Atlantic were subject to some modification when the corresponding biomarker datasets were combined with those from the current study from the Barents Sea, due to a change in the c term. Likewise, this c term and the corresponding P_BIP_{25} values were also modified when we considered the P_BIP_{25} – sea ice concentration relationship for the East Greenland locations alone. Apart from the requirement, therefore, to have to re-calculate this term and the corresponding PIP_{25} values when either adding or removing biomarker data from individual locations, an additional consequence is that potentially all data may be negatively influenced by a relatively small number of anomalous biomarker concentrations or outliers and this impact may be especially apparent for correlations with sea ice concentrations. In contrast, greater consistency in mean IP_{25}/phytoplankton biomarker ratios may exist for a given sampling location, where the array of potential influences on each of the two biomarkers may be somewhat more constrained and determined more by the nature of the immediate oceanographic conditions such as the sea ice cover. In support of this, a number of studies have shown that the PIP_{25} index can provide meaningful downcore analyses of past sea ice conditions, especially when evaluated against other proxy data (e.g. Fahl and Stein, 2012; Müller et al., 2012; Stein et al., 2012; Cabedo-Sanz et al., 2013).

In summary, the outcomes of this part of the study suggest that, while there remains the potential to make sea ice concentration

data based on combined biomarker data more quantitative, a substantial amount of further work is still required before the potential of this method can be fully realised.

4.5. Allochthonous input – influences of sediment transport

Thus far, we have presented individual and combined biomarker proxy data that align reasonably well with known sea ice conditions for different regions of the Barents Sea, especially in terms of presence or absence of the sea ice biomarker IP_{25} (Fig. 1b). Despite these agreements, however, a small number of sediments from locations beyond the MSIE also contained low concentrations of IP_{25} and this apparent anomaly was made even clearer in the P_BIP_{25} data and the spatial representations of both IP_{25} and P_BIP_{25} datasets (Figs. 2a and 3a,b). The occurrence of IP_{25} in some locations south of ca 74° N likely indicates further processes that are responsible for the deposition of IP_{25} in sediments rather than vertical transport following sea ice melt. Although it is possible that the temporal sampling interval associated with the surface sediments (0–1 cm) extends beyond the period covered by satellite records, we can exclude this possibility on the basis of some known sedimentation rates for the study area (e.g. Zaborska et al., 2008; Maiti et al., 2010) which indicate that surface sediments (0–1 cm) reflect a maximum age of ca 20 years, yet even longer-term observational accounts of sea ice suggest that this region has been ice-free for at least the last 50 years or so (Vinje, 2001; Divine and Dick, 2006).

An alternative hypothesis is that the occurrence of the IP_{25} biomarker in the south-west Barents Sea sediments represents allochthonous input, probably as a result of lateral transport of sediments and particulate material from the shelves. A number of studies carried out in the Southern Ocean (e.g. Sicre et al., 2005; Mollenhauer et al., 2006) as well as in the Nordic Seas (Sarnthein et al., 2003) have demonstrated that, in addition to the vertical flux of particles, sediments can be susceptible to re-deposition following lateral advection, especially in deep basins and troughs (Fohrmann et al., 2001). Evidence for this (marine) advection was observed in two near-bottom sediment traps moored at the Barents Sea continental margin through a combined study of biomarker analysis, quantitative microscopy and bulk parameters (Thomsen et al., 2001) which demonstrated that differences between these parameters could not be explained by the vertical flux of particles alone.

The presence of IP_{25} in sediments along the Bear Island Trough below 74° N (Fig. 5) could likely be a result of dense water formation eventually reaching the bottom ocean. These dense bottom water masses are influenced by the bathymetry of the Barents Sea (Fohrmann et al., 2001), likely flowing cross-slope from the shelf edges and down banks such as Spitsbergen Bank and Stor Bank into the Bear Island Trough, which represents the maximum depth of the Barents Sea (Jakobsson et al., 2004) (Fig. 5). These dense water masses facilitate the transport and erosion of particles from the Barents Sea shelf, which subsequently cascade down slopes into deep troughs. This process of sediment transportation and redistribution by lateral advection has previously been described in detail for parts of the Barents Sea (e.g. Fohrmann et al., 2001; Thomsen et al., 2001; Sarnthein et al., 2003). The same transport mechanism likely also influences the brassicasterol abundances, but this is more difficult to decipher given the ubiquity of this biomarker in all locations.

To further support this hypothesis of physical redistribution of sediment material (and associated biomarkers), Solignac et al. (2009) previously reported the presence of the Arctic dinoflagellate *I. minutum*, albeit in low abundances, in the Bear Island Trough. This could be interpreted as resulting from lateral advection from the neighbouring Spitsbergen Bank into the Bear Island Trough, since the otherwise dominant dinocyst species in this location was *Operculodinium centrocarpum*, which is strongly related to Atlantic waters (de Vernal et al., 2005; Grøsfjeld et al., 2009; Solignac et al., 2009), consistent with the sampling location. A similar cascading of particulate material has been suggested to explain the occurrence of certain other microfossil remains in related troughs within the Barents Sea (Thomsen et al., 2001).

Clearly, the allochthonous input of IP_{25} into sediments within the Bear Island Trough will also influence the P_BIP_{25} index for this region, so we suggest the same explanation may be used to account for the apparent anomaly in the P_BIP_{25} data. The consequence of non-zero PIP_{25} data for locations with no sea ice cover will also impact on the linear relationship between the PIP_{25} index and mean sea ice concentrations (Fig. 4) and this may explain, in part, the poorer agreement between these two parameters compared to the previous study by Müller et al. (2011). The lateral advection of biomarkers and other sedimentary proxies and the impacts that this can have in terms of influencing other palaeoenvironmental proxy reconstructions has been presented previously (e.g. Benthien

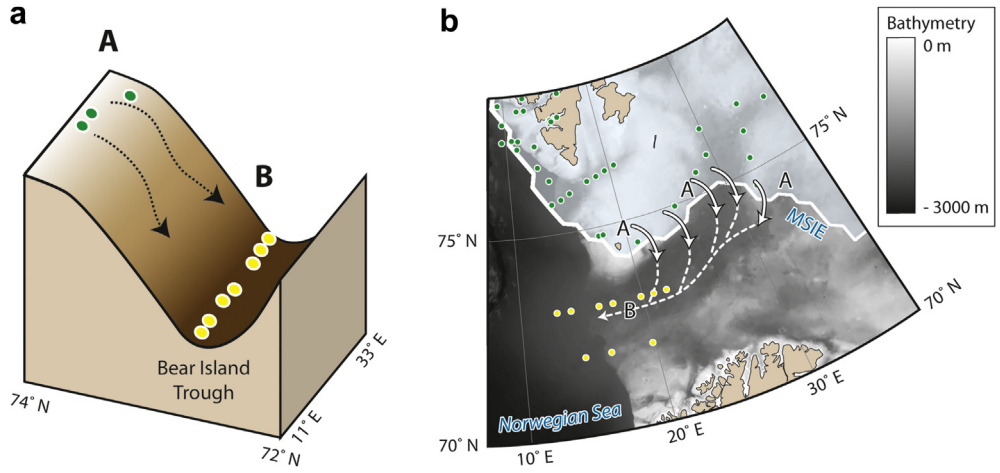

Fig. 5. (a) Schematic representation showing the proposed mechanism for advection of IP_{25} from within the MSIE to the Bear Island Trough (the solid arrows correspond to the potential source areas of advected IP_{25}; the dashed arrows represent the proposed direction of sediment transport); (b) Bathymetric map showing the sampling locations where IP_{25} was detected within the MSIE (green dots) and as a result of allochthonous input (yellow dots). (For interpretation of the references to colour in this figure legend, the reader is referred to the web version of this article.)

and Müller, 2000; Mollenhauer et al., 2006), but this is the first study that has provided clear evidence for the potential significance of such processes when conducting IP_{25}-based sea ice reconstructions. In the future, it may be possible to confirm the proposed sediment transport process and assess the impact that this might have on biomarker abundances using ^{230}Th tracer methods (Francois et al., 2004). In any case, we suggest that care should be taken when performing IP_{25}-based palaeo sea ice investigations in the future, ideally by cross-referencing outcomes with other proxy data. On the other hand, the specificity of IP_{25} to a sea ice origin potentially provides the opportunity to actively investigate such allochthonous processes for other Arctic or sub-Arctic regions, especially for those that are normally ice-free. In this respect, although somewhat different to the current physical processes, it is noted that the use of IP_{25} as a tracer of the transfer of sea ice-derived organic matter in Arctic food webs has also recently been achieved with some success (e.g. Brown and Belt, 2012).

5. Conclusions

In the current study, we have analysed ca 100 surface sediments from the Barents Sea for the presence and abundance of the sea ice diatom biomarker IP_{25} and brassicasterol, an indicator of open water phytoplankton. Three main outcomes can be identified.

(1) Our data demonstrate a good relationship between the occurrence of the sea ice proxy biomarker IP_{25} in surface sediments from the Barents Sea and known sea ice cover in recent decades derived from satellite records. As such, this study has extended the application potential for the IP_{25} sea ice proxy to a climatically sensitive region of the Arctic and sub-Arctic regions.

(2) The number and spatial diversity of the surface sediments analysed has enabled us to conduct a reasonable test of the P_BIP_{25} index, previously proposed by Müller et al. (2011) to provide more detailed descriptions of sea ice conditions in Arctic regions. The individual P_BIP_{25} values and spatial distributions are broadly consistent with known seasonal sea ice cover for the Barents Sea, although the agreement between the PIP_{25} data and known mean spring sea ice concentrations is quite variable and the overall agreement is poorer compared to that reported in a previous study (Müller et al., 2011). We suggest, therefore, that PIP_{25} data should still be treated with caution at this stage and that any interpretations are also made with reference to the individual biomarker data and other proxies, where available.

(3) The observation of IP_{25} in locations (Bear Island Trough) somewhat distal from the position of the maximum sea ice extent (1983–2002) provides the first example of the occurrence on this biomarker in surface sediments from regions of no recent sea ice cover. It is hypothesised that the occurrence of IP_{25} in such sediments may, potentially, be attributed to allochthonous input of this biomarker as a result of sediment transport. These observations highlight the importance of considering this possibility when reconstructing past sea ice conditions in other Arctic regions.

Acknowledgements

This work is a contribution to the CASE Initial Training Network funded by the European Community's 7th Framework Programme FP7 2007/2013, Marie-Curie Actions, under Grant Agreement No. 238111. This paper is also a product of the MAREANO programme (www.mareano.no) and all MAREANO partners and cruise participants are thanked for their contributions. We thank Michael Blaschek (VU, Amsterdam) for help in obtaining the satellite-derived sea ice data and to Shaun Lewin (Plymouth University) for assistance with the cartography. We are also grateful to two anonymous reviewers who made helpful suggestions to improve the manuscript and encouraged us to discuss the merits of the PIP_{25} index, in particular.

Appendix A. Supplementary data

Supplementary data related to this article can be found at http://dx.doi.org/10.1016/j.quascirev.2012.11.025.

References

Aagaard-Sørensen, S., Husum, K., Hald, M., Knies, J., 2010. Paleoceanographic development in the SW Barents Sea during the Late Weichselian–Early Holocene transition. Quaternary Science Reviews 29, 3442–3456.

Andrews, J.T., Belt, S.T., Ólafsdóttir, S., Massé, G., Vare, L.L., 2009. Sea ice and marine climate variability for NW Iceland/Denmark Strait over the last 2000 cal. yr BP. The Holocene 19, 775–784.

Andrews, J.T., 2009. Seeking a Holocene drift ice proxy: non-clay mineral variations from the SW to N-central Iceland shelf: trends, regime shifts, and periodicities. Journal of Quaternary Science 24, 664–676.

Årthun, M., Eldevik, T., Smedsrund, L.H., Skagseth, Ø., Ingvaldsen, R.B., 2012. Quantifying the influence of Atlantic heat on Barents Sea ice variability and retreat. Journal of Climate 25, 4736–4743.

Belt, S.T., Müller, J., 2013. The Arctic Sea ice biomarker IP_{25}: a review of current understanding, recommendations for future research and applications in palaeo sea ice reconstructions. Quaternary Science Reviews 79, 9–25.

Belt, S.T., Massé, G., Rowland, S.J., Poulin, M., Michel, C., LeBlanc, B., 2007. A novel chemical fossil of palaeo sea ice: IP_{25}. Organic Geochemistry 38, 16–27.

Belt, S.T., Vare, L.L., Massé, G., Manners, H.R., Price, J.C., MacLachlan, S.E., Andrews, J.T., Schmidt, S., 2010. Striking similarities in temporal changes to spring sea ice occurrence across the central Canadian Arctic Archipelago over the last 7000 years. Quaternary Science Reviews 29, 3489–3504.

Belt, S.T., Brown, T.A., Navarro-Rodriguez, A., Cabedo-Sanz, P., Tonkin, A., Ingle, R., 2012. A reproducible method for the extraction, identification and quantification of the Arctic sea ice proxy IP_{25} from marine sediments. Analytical Methods 4, 705–713.

Benthien, A., Müller, P.J., 2000. Anomalously low alkenone temperatures caused by lateral particle and sediment transport in the Malvinas Current region, western Argentine Basin. Deep Sea Research II 47, 2369–2393.

Boitsov, S., Jensen, H.K.B., Klungsøyr, J., 2009. Geographical variations in hydrocarbon levels in sediments from the Western Barents Sea. Norwegian Journal of Geology 89, 91–100.

Bonnet, S., de Vernal, A., Hillaire-Marcel, C., Radi, T., Husum, K., 2010. Variability of sea-surface temperature and sea-ice cover in the Fram Strait over the last two millennia. Marine Micropaleontology 74, 59–74.

Brassell, S.C., Eglinton, G., Marlowe, I.T., Sarntheim, M., Pflauman, U., 1986. Molecular stratigraphy: a new tool for climate assessment. Nature 320, 129–133.

Brown, T.A., Belt, S.T., Philippe, B., Mundy, C.J., Massé, G., Poulin, M., Gosselin, M., 2011. Temporal and vertical variations of lipid biomarkers during a bottom ice diatom bloom in the Canadian Beaufort Sea: further evidence for the use of the IP_{25} biomarker as a proxy for spring Arctic sea ice. Polar Biology 34, 1857–1868.

Brown, T.A., Belt, S.T., 2012. Identification of the sea ice diatom biomarker IP_{25} in Arctic benthic macrofauna: direct evidence for a sea ice diatom diet in Arctic heterotrophs. Polar Biology 35, 131–137.

Cabedo-Sanz, P., Belt, S.T., Knies, J.K., 2013. Identification of contrasting seasonal sea ice conditions during the Younger Dryas. Quaternary Science Reviews 79, 74–86.

Carroll, J., Zaborska, A., Papucci, C., Schirone, A., Carroll, M.L., Pempkowiak, J., 2008. Accumulation of organic carbon in western Barents Sea sediments. Deep Sea Research Part II: Topical Studies in Oceanography 55, 2361–2371.

Comiso, J.C., Cavalieri, D.J., Parkinson, C.L., Gloersen, P., 1997. Passive microwave algorithms for sea ice concentration: a comparison of two techniques. Remote Sensing of Environment 60, 357–384.

de Vernal, A., Eynaud, F., Henry, M., Hillaire-Marcel, C., Londeix, L., Mangin, S., Matthiessen, J., Marret, F., Radi, T., Rochon, A., Solignac, S., Turon, J.-L., 2005. Reconstruction of sea-surface conditions at middle to high latitudes of the Northern Hemisphere during the Last Glacial Maximum (LGM) based on dinoflagellate cyst assemblages. Quaternary Science Reviews 24, 897–924.

Divine, D.V., Dick, C., 2006. Historical variability of sea ice edge position in the Nordic Seas. Journal of Geophysical Research 111, C01001.

Fahl, K., Stein, R., 2012. Modern seasonal variability and deglacial/Holocene change of central Arctic Ocean sea-ice cover: new insights from biomarker proxy records. Earth and Planetary Science Letters 351–352, 123–133.

Falk-Petersen, S., Hop, H., Budgell, W.P., Hegseth, E.N., Korsnes, R., Løyning, T.B., Ørbæk, J.B., Kawamura, T., Shirasawa, K., 2000. Physical and ecological processes in the marginal ice zone of the northern Barents Sea during the summer melt period. Journal of Marine Systems 27, 131–159.

Fetterer, F., Knowles, K., Meier, W., Savoie, M., 2002. Updated 2009 Sea Ice Index. National Snow and Ice Data Center. Digital Media, Boulder, CO. Retrieved May, 2012.

Fohrmann, H., Backhaus, J.O., Blaume, F., Haupt, B.J., Kämpf, J., Michels, K., Mienert, J., Posewang, J., Tritzrau, W., Rumohr, J., Weber, M., Woodgate, R., 2001. Modern ocean current-controlled sediment transport in the Greenland-Iceland-Norwegian (GIN) seas. In: Schäfer, P., Ritzrau, W., Schulter, M., Thiede, J (Eds.), The Northern North Atlantic: a changing environment. Springer, Berlin, pp. 135–154.

Francois, R., Frank, M., Rutgers van der Loeff, M.M., Bacon, M.P., 2004. ^{230}Th normalization: an essential tool for interpreting sedimentary fluxes during the late Quaternary. Paleoceaongraphy 19, PA1018.

Grøsfjeld, K., Harland, R., Howe, J., 2009. Dinoflagellate cyst assemblages inshore and offshore Svalbard reflecting their modern hydrography and climate. Norwegian Journal of Geology 89, 121–134.

IPCC, 2007. Intergovernmental Panel on Climate Change (IPCC) (2007) Climate Change 2007: the Scientific Basis. In: Contribution of Working Group I to the Third Assessment Report of the Intergovernmental Panel on Climate Change. Cambridge University Press, Cambridge.

Jakobsson, M., Grantz, A., Kristoffersen, Y., Macnab, R., 2004. Physiography and bathymetry of the Arctic Ocean. In: Stein, R., Macdonald, R.W. (Eds.), The Organic Carbon Cycle in the Arctic Ocean. Springer, New York, pp. 1–5.

Kim, J.-H., Schouten, S., Hopmans, E.C., Donner, B., Sinninghe Damsté, J.S.S., 2008. Global sediment core-top calibration of the TEX_{86} paleothermometer in the ocean. Geochimica et Cosmochimica Acta 72, 1154–1173.

Knies, J., 2005. Climate-induced changes in sedimentary regimes for organic matter supply on the continental shelf of northern Norway. Geochimica et Cosmochimica Acta 69, 4631–4647.

Knies, J., 2009. MAREANO thematic issue: sediment characteristics and environmental implications in the Lofoten–Barents Sea region. Norwegian Journal of Geology Editorial, 1–2.

Knies, J., Martinez, P., 2009. Organic matter sedimentation in the western Barents Sea region: terrestrial and marine contribution based on isotopic composition and organic nitrogen content. Norwegian Journal of Geology 89, 79–89.

Loeng, H., 1991. Features of the physical oceanographic conditions of the Barents Sea. Polar Research 10, 5–18.

Loeng, H., Drinkwater, K., 2007. An overview of the ecosystems of the Barents and Norwegian Seas and their response to climate variability. Deep Sea Research Part II: Topical Studies in Oceanography 54, 2478–2500.

Maiti, K., Carroll, J., Benitez-Nelson, C.R., 2010. Sedimentation and particle dynamics in the seasonal ice zone of the Barents Sea. Journal of Marine Systems 79, 185–198.

Massé, G., Rowland, S.J., Sicre, M.-A., Jacob, J., Jansen, E., Belt, S.T., 2008. Abrupt climate changes for Iceland during the last millennium: evidence from high resolution sea ice reconstructions. Earth and Planetary Science Letters 269, 565–569.

Mollenhauer, G., McManus, J.F., Benthien, A., Müller, P.J., Eglinton, T.I., 2006. Rapid lateral particle transport in the Argentine Basin: molecular ^{14}C and $^{230}Th_{xs}$ evidence. Deep Sea Research Part I: Oceanographic Research Papers 53, 1224–1243.

Müller, J., Massé, G., Stein, R., Belt, S.T., 2009. Variability of sea-ice conditions in the Fram Strait over the past 30,000 years. Nature Geoscience 2, 772–776.

Müller, J., Wagner, A., Fahl, K., Stein, R., Prange, M., Lohmann, G., 2011. Towards quantitative sea ice reconstructions in the northern North Atlantic: a combined biomarker and numerical modelling approach. Earth and Planetary Science Letters 306, 137–148.

Müller, J., Werner, K., Stein, R., Fahl, K., Moros, M., Jansen, E., 2012. Holocene cooling culminates in sea ice oscillations in Fram Strait. Quaternary Science Reviews 47, 1–14.

Parkinson, C.L., 2008. Satellite passive-microwave measurements of sea ice. In: Steele, H.J., Thorpe, A.S., Turekian, K.K. (Eds.), Encyclopedia of Ocean Sciences, second ed. Academic Press, Oxford, pp. 80–90.

Rayner, N.A., Parker, D.E., Horton, E.B., Folland, C.K., Alexander, L.V., Rowell, D.P., Kent, E.C., Kaplan, A., 2003. Global analyses of sea surface temperature, sea ice and night marine air temperature since the late nineteenth century. Journal of Geophysical Research 108 (D14), 4407.

Reigstad, M., Wexels Riser, C., Wassmann, P., Ratkova, T., 2008. Vertical export of particulate organic carbon: attenuation, composition and loss rates in the northern Barents Sea. Deep Sea Research Part II: Topical Studies in Oceanography 55, 2308–2319.

Sarnthein, M., Kreveld, S.V., Erlenkeuser, H., Grootes, P.M., Kucera, M., Pflaumann, U., Schultz, M., 2003. Centennial-to-millennial-scale periodicities of Holocene climate and sediment injections off the western Barents shelf, 75°N. Boreas 32, 447–461.

Schlitzer, R., 2012. Ocean Data View. http://odv.awi.de.

Schouten, S., Hopmans, E.C., Schefuss, E., Sinninghe Damsté, J.S., 2002. Distributional variations in marine crenarchaeotal membrane lipids: a new tool for reconstructing ancient sea water temperatures? Earth and Planetary Science Letters 204, 265–274.

Sicre, M.A., Labeyrie, L., Ezat, U., Duprat, J., Turon, J.L., Schmidt, S., 2005. Mid-latitude Southern Indian Ocean response to Northern Hemisphere Heinrich events. Earth and Planetary Science Letters 240, 724–731.

Simon, A., Poulicek, M., Velimirov, B., MacKenzie, F.T., 1994. Comparison of anaerobic and aerobic biodegradation of mineralized skeletal structures in marine and estuarine conditions. Biogeochemistry 25, 167–195.

Solignac, S., Grøsfjeld, K., Giraudeau, J., de Vernal, A., 2009. Distribution of recent dinocyst assemblages in the western Barents Sea. Norwegian Journal of Geology 89, 109–119.

Spielhagen, R.F., Baumann, K.-H., Erlenkeuser, H., Nowaczyk, N.R., Nørgaard-Pedersen, N., Vogt, C., Weiel, D., 2004. Arctic Ocean deep-sea record of northern Eurasian ice sheet history. Quaternary Science Reviews 23, 1455–1483.

Stein, R., Grobe, H., Wahsner, M., 1994. Organic carbon, carbonate and clay mineral distributions in eastern central Arctic Ocean surface sediments. Marine Geology 119, 269–285.

Stein, R., Fahl, K., Müller, J., 2012. Proxy reconstruction of Arctic Ocean sea ice history: from IRD to IP_{25}. Polarforschung 82, 37–71.

Stoynova, V., Shanahan, T.M., Hughen, K.A., de Vernal, A., 2013. Insights into circum-Arctic sea ice variability from molecular geochemistry. Quaternary Science Reviews 79, 63–73.

Thomas, D.N., 2012. Sea ice. In: Bell, M.E. (Ed.), Life in Extremes: Environments, Organisms and Strategies for Survival. Oxford, U.K (Chapter 4).

Thomsen, C., Blaume, F., Fohrmann, H., Peeken, I., Zeller, U., 2001. Particle transport processes at slope environments—event driven flux across the Barents Sea continental margin. Marine Geology 175, 237–250.

Thorsnes, T., 2009. MAREANO – an introduction. Norwegian Journal of Geology 89, 3.

Vare, L.L., Massé, G., Gregory, T.R., Smart, C.W., Belt, S.T., 2009. Sea ice variations in the central Canadian Arctic Archipelago during the Holocene. Quaternary Science Reviews 28, 1354–1366.

Vare, L.L., Massé, G., Belt, S.T., 2010. A biomarker-based reconstruction of sea ice conditions for the Barents Sea in recent centuries. The Holocene 20, 637–643.

Vinje, T., 2001. Anomalies and trends of sea-ice extent and atmospheric circulation in the Nordic seas during the period 1864–1998. Journal of Climate 14, 255–267.

Vogt, C., Knies, J., 2009. Sediment pathways in the western Barents Sea inferred from clay mineral assemblages in surface sediments. Norwegian Journal of Geology 89, 41–55.

Vogt, C., Knies, J., Spielhagen, R.F., Stein, R., 2001. Detailed mineralogical evidence for two nearly identical glacial/deglacial cycles and Atlantic water advection to the Arctic Ocean during the last 90,000 years. Global and Planetary Change 31, 23–44.

Volkman, J.K., 1986. A review of sterol markers for marine and terrigenous organic matter. Organic Geochemistry 9, 83–99.

Volkman, J.K., Barrett, S.M., Blackburn, S.I., Mansour, M.P., Sikes, E.L., Gelin, F., 1998. Microalgal biomarkers: a review of recent research developments. Organic Geochemistry 29, 1163–1179.

Wassmann, P., Reigstad, M., Haug, T., Rudels, B., Carroll, M.L., Hop, H., Wing Gabrielsen, G., Falk-Petersen, S., Denisenko, S.G., Arashkevich, E., Slagstad, D., Pavlova, O., 2006. Food webs and carbon flux in the Barents Sea. Progress In Oceanography 71, 232–287.

Wassmann, P., Duarte, C.M., Agusti, S., Sejr, M.K., 2011. Footprints of climate change in the Arctic marine ecosystem. Global Change Biology 17, 1235–1249.

Werner, K., Spielhagen, R.F., Bauch, D., Hass, H.C., Kandiano, E., Zamelczyk, K., 2011. Atlantic Water advection to the eastern Fram Strait—Multiproxy evidence for late Holocene variability. Palaeogeography, Palaeoclimatology, Palaeoecology 308, 264–276.

Wexel Riser, C., Wassmann, P., Reigstad, M., Seuthe, L., 2008. Vertical flux regulation by zooplankton in the northern Barents Sea during Arctic spring. Deep Sea Research II 55, 2320–2329.

Xiao, X., Stein, R., Fahl, K., 2013. Biomarker distributions in surface sediments from the Kara and Laptev Seas (Arctic Ocean): indicators for organic-carbon sources and sea ice coverage. Quaternary Science Reviews 79, 40–52.

Zaborska, A., Carroll, J., Papucci, C., Torricelli, L., Carroll, M.L., Walkusz-Miotk, J., Pempkowiak, J., 2008. Recent sediment accumulation rates for the Western margin of the Barents Sea. Deep Sea Research Part II: Topical Studies in Oceanography 55, 2352–2360.

Zonneveld, K.A.F., Versteegh, G.J.M., Kasten, S., Eglinton, T.I., Emeis, K.-C., Huguet, C., Koch, B.P., de Lange, G.J., de Leeuw, J.W., Middelburg, J.J., Mollenhauer, G., Prahl, F.G., Rethemeyer, J., Wakeham, S.G., 2010. Selective preservation of organic matter in marine environments; processes and impact on the sedimentary record. Biogeosciences 7, 483–511.